

210P.

NE-15-020-420

99

# THREE-DIMENSIONAL TURBULENT BOUNDARY LAYERS— AN ASSESSMENT OF PREDICTION METHODS

By

A. J. Wheeler and J. P. Johnston

N93-71741

Unclass

29/34 0150728

Prepared from work sponsored by  
NASA-NGL-05-020-420



Report MD-30

NASA LIBRARY  
NASA RESEARCH CENTER  
MOORE FIELD, CALIF.

JUL 13 1972

COPY	
NO.	1

Thermosciences Division  
Department of Mechanical Engineering  
Stanford University  
Stanford, California

July 1971

(NASA-CR-192373) THREE-DIMENSIONAL  
TURBULENT BOUNDARY LAYERS: AN  
ASSESSMENT OF PREDICTION METHODS  
(Stanford Univ.) 210 p



THREE-DIMENSIONAL TURBULENT BOUNDARY LAYERS -  
AN ASSESSMENT OF PREDICTION METHODS

By

A. J. Wheeler and J. P. Johnston

Prepared from work sponsored by

NASA-NgL-05-020-420

Report MD-30

Thermosciences Division  
Department of Mechanical Engineering  
Stanford University  
Stanford, California

July 1971



#### ACKNOWLEDGMENTS

The sponsorship of Ames Research Center under the Stanford-NASA Cooperative Research Program in Computational Aspects of Fluid Mechanics (Grant No. NASA NgL-05-020-420) is gratefully acknowledged.

Professors S. J. Kline, W. C. Reynolds and W. M. Kays are thanked for their helpful discussions and advice.

The authors also appreciate the assistance of Miss Patrice Christensen who did the plotting and drafting, Miss Jan Elliott who typed the figures and the rough draft and Mrs. Nancy Weaver who typed the final draft.

## ABSTRACT

Three turbulent shear stress models for use in prediction schemes for three-dimensional turbulent boundary layers were studied. These three models were evaluated primarily by comparison of numerical calculations to experimental data.

A significant fraction of the existing three-dimensional turbulent boundary layer data was examined, reorganized, partially recomputed and tabulated in a consistent format.

A numerical procedure, suitable for all three shear stress closure models was prepared. This procedure is an explicit forward difference method that permits solution of the partial differential equations of the boundary layer.

All three turbulent shear stress closure models are extensions of current two-dimensional models:

1. The eddy viscosity model is based on the assumption that the shear stress profile is a prescribed function of the mean velocity profile. A two-dimensional prescription (Mellor 1967) is assumed for shear stress magnitude. The shear stress direction is computed by assuming that the eddy viscosity is isotropic (scalar).
2. In the Nash model the shear stress magnitude is computed from a rate equation based on an approximation of the turbulence kinetic energy equation. This rate equation is a simple extension of the two-dimensional equation of Bradshaw et. al.

(1967). The direction of the shear stress is computed by assuming an isotropic eddy viscosity (scalar).

3. In the Bradshaw model the shear stress magnitude is computed by the same equation as the Nash method. However a rate equation, including a turbulence diffusion term is used to compute the shear stress direction.

In general, it was found that all three methods predict the mean velocity fields of a wide sample of available experimental results to within our estimates of the uncertainty of the data. When compared with each other, the three shear stress models produce almost identical results for most flows. However at momentum thickness Reynolds numbers,  $R_\theta$ , below 2000, in cases with strong adverse pressure gradients, the three methods differ significantly. Direct shear stress measurements were made in only two of the available experimental flows. For one of these flows, Johnston (1970), the Nash and Bradshaw models give predictions of the shear stress magnitude which are significantly better than those of the eddy viscosity model. For this same flow the Bradshaw method predicts the shear stress direction slightly better than the other two models which used the isotropic eddy viscosity assumption although no model predicts the direction very well.

# CONTENTS

	Page
ACKNOWLEDGMENTS . . . . .	iii
ABSTRACT . . . . .	iv
TABLE OF CONTENTS . . . . .	vi
LIST OF FIGURES . . . . .	viii
LIST OF TABLES . . . . .	xii
NOMENCLATURE . . . . .	xiii
CHAPTER 1 INTRODUCTION . . . . .	1
A. General Considerations . . . . .	1
B. Experimental Data . . . . .	4
C. Separation in Three Dimensions . . . . .	6
D. Governing Equations . . . . .	7
E. Methods of Solution . . . . .	9
F. Integral Prediction Methods . . . . .	10
G. Objectives . . . . .	17
CHAPTER 2 SHEAR STRESS MODELS . . . . .	38
A. General Considerations . . . . .	38
B. Shear Stress Closure Assumptions . . . . .	39
C. Boundary Conditions . . . . .	46
D. Summary . . . . .	50
CHAPTER 3 NUMERICAL METHOD . . . . .	54
A. General Considerations . . . . .	54
B. Numerical Procedure (Overview) . . . . .	56
C. Numerical Procedure (Details) . . . . .	58
D. Verification of the Computer Program . . . . .	63

	Page
CHAPTER 4 EXPERIMENTAL COMPARISONS . . . . .	72
A. General Considerations . . . . .	72
B. The Flow at the Plane of Symmetry . . . . .	73
C. Infinite Swept Wing Flows . . . . .	78
D. Vaneless Diffuser Flows . . . . .	85
E. Summary of Comparisons with Experiment . . . . .	96
CHAPTER 5 CALCULATION OF IDEALIZED FLOWS . . . . .	133
A. Introduction . . . . .	133
B. Cumpsty and Head Infinite Swept Wing Demonstration Cases . . . . .	133
C. Vaneless Diffuser Demonstration Cases . . . . .	136
D. Summary . . . . .	141
CHAPTER 6 SUMMARY . . . . .	151
A. Summary of Conclusions . . . . .	151
B. Recommendations for Future Work . . . . .	154
REFERENCES . . . . .	156
APPENDIX A THE COMPUTER PROGRAM . . . . .	161
APPENDIX B METHODS FOR ESTIMATING THE WALL SHEAR STRESS DIRECTION . . . . .	185
APPENDIX C ATTEMPTS TO COMPUTE ROTATING DISC FLOWS . . . . .	192
APPENDIX D SUGGESTED IMPROVEMENTS IN COMPUTER PROGRAM . . . . .	193

# LIST OF FIGURES

Figure		Page
1.1	Three-dimensional wall-parallel velocity components . .	21
1.2	Experimental geometries for three-dimensional turbulent boundary layers . . . . .	22
1.3	Ordinary separation on a swept, infinite wing . . . . .	25
1.4	x-y-z coordinate system . . . . .	26
1.5	Crossflow profiles in Prandtl form (data of Gardow (1958) and Bradshaw and Terrell (1969)) . . . . .	27
1.6	Crossflow profiles in Prandtl form (data of Cham (1968)) . . . . .	28
1.7	Polar plots of Gardow (1958) . . . . .	29
1.8a	Polar plots of Gruschwitz (1935) with Eichelbrenner 5th degree polynomials . . . . .	30
1.8b	Polar plots of Johnston (1957) with Eichelbrenner 5th degree polynomials . . . . .	31
1.9	Polar plots of Bradshaw and Terrell and Klinksiek and Pierce with Eichelbrenner 5th degree polynomial . .	32
1.10	Crossover profiles of Klinksiek and Pierce (1968) . . .	33
1.11	Wake function component of Gardow and Bradshaw and Terrell profiles . . . . .	34
1.12	Wake function component for Hornung and Joubert (1963).	35
1.13	Wake function component for East and Hoxey (1969) . . .	36
1.14	Entrainment functions from Cham (1968) . . . . .	37
2.1	Bradshaw L and G functions . . . . .	52
2.2	Polar plot showing variation of direction of velocity and velocity gradient near wall . . . . .	53
3.1	y grids . . . . .	68
3.2	Fitting of parabolas for interpolation . . . . .	69
3.3	Ludwig and Tillman strong adverse pressure gradient .	70

Figure		Page
3.4	Comparison of present Nash calculations to those of Nash (1969) on Cumpsty and Head (1970) infinite swept wing . . . . .	71
4.1	Configuration of Johnston plane of symmetry flow . . .	99
4.2	$(\partial W / \partial z)_{\infty}$ vs. $x$ , Johnston plane of symmetry . . . . .	100
4.3	Johnston plane of symmetry, integral parameter results.	101
4.4	Predicted results, East and Hoxey plane of symmetry . .	102
4.5	Shear stress distributions for East and Hoxey plane of symmetry, $x = 0.585$ feet . . . . .	103
4.6	Sketch of Johnson infinite step . . . . .	104
4.7	Experimental pressure distribution, Johnston infinite step . . . . .	105
4.8	Integral parameter results, Johnston infinite step . .	106
4.9	Mean velocity profiles, $x = 0.75$ feet, Johnston infinite step . . . . .	108
4.10	Normal velocity, $V$ , Johnston infinite step . . . . .	109
4.11	Shear stress magnitude, $x = 0.75$ feet, Johnston infinite step . . . . .	110
4.12	Velocity and shear stress directions, $x = 0.75$ feet, Johnston infinite step . . . . .	111
4.13	Bradshaw and Terrell (1969) integral parameter results.	112
4.14	Bradshaw and Terrell velocity profiles at $x = 1.18$ feet . . . . .	114
4.15	Bradshaw and Terrell streamwise shear stress magnitude, $x = 1.18$ feet . . . . .	115
4.16	Bradshaw and Terrell mean velocity gradient $(\frac{\partial W}{\partial U})$ and shear stress $(\tau)$ directions relative to external velocity direction . . . . .	116
4.17	Cumpsty and Head integral parameter results . . . . .	117
4.18	Typical Gardow (1958) velocity profile . . . . .	119

Figure		Page
4.19	Gardow A-45.2 vaneless diffuser integral parameter results . . . . .	120
4.20	Gardow A-45.2 shear stress distributions (no data available) . . . . .	122
4.21	Gardow B-50.6 vaneless diffuser integral parameter results . . . . .	123
4.22	Gardow B-52.1 vaneless diffuser, integral parameter results . . . . .	125
4.23	Gardow B-54.5 vaneless diffuser, integral parameter results . . . . .	127
4.24	Integral parameter results, Jansen 47° vaneless diffuser . . . . .	129
4.25	Effect of $\pm 5\%$ change of $dP/dx$ on free stream velocity, Gardow A-45.2 vaneless diffuser . . . . .	131
4.26	Effect of $\pm 5\%$ change of $dP/dx$ on predictions for Gardow A-45.2. All curves are Bradshaw method calculations . . . . .	132
5.1	Separation point vs. sweep angle, Cumpsty and Head (1967) infinite wing demonstration cases . . . . .	142
5.2	Integral parameter results at $x = 1.0$ feet, Cumpsty and Head (1967) infinite wing demonstration cases . . . . .	143
5.3	Separation point vs. swirl angle, vaneless diffuser demonstration cases, Bradshaw method . . . . .	144
5.4	Separation point vs. swirl angle, vaneless diffuser demonstration cases, eddy viscosity method . . . . .	145
5.5	$\delta_{995}/R_i$ vs. sweep angle, vaneless diffuser demonstration cases, Bradshaw method . . . . .	146
5.6	$\delta_{995}/R_i$ vs. swirl angle, vaneless diffuser demonstration cases, eddy viscosity method . . . . .	147
5.7	$\delta_r^*/R_i$ vs. swirl angle, vaneless diffuser demonstration cases, Bradshaw method . . . . .	148
5.8	$\delta_r^*/R_i$ vs. swirl angle, vaneless diffuser demonstration cases, eddy viscosity method . . . . .	149

Figure		Page
5.9	H vs. $\lambda_\theta$ , vaneless diffuser demonstration cases, swirl angle = 0 (two-dimensional flow) . . . . .	150
B.1	Extrapolation of $\beta_w$ . . . . .	190
B.2	$\beta$ vs. $y$ near wall . . . . .	191

# LIST OF TABLES

	Page
1.1 Summary of Data Sources . . . . .	18
1.2 Key to Symbols and Remarks in Table 1.1 . . . . .	20
2.1 Shear Stress Models . . . . .	51
4.1 Effect of $\pm 5\%$ change of $\frac{dP}{dx}$ on Vaneless Diffuser Flows. .	97
4.2 Effect of Initial Shear Stress on Bradshaw Method Prediction of Vaneless Diffuser Flows . . . . .	98

## NOMENCLATURE

A	Constant in law of the wall, general constant where defined
a	Bradshaw empirical function $\tau/\overline{q^2}$
$C_E$	Head entrainment function
$C_f$	Normalized wall shear stress, $\tau_w/(\rho Q_\infty^2/2)$
$C_{fs}$	Normalized wall shear stress component in direction of external streamline, $\tau_{ws}/(\rho Q_\infty^2/2)$
dx, dy	Computation steps in x and y directions respectively
G	Bradshaw empirical diffusion function
H	Shape factor
$h_1, h_2$	Metric coefficients in momentum integral equations in streamline coordinate system
$H_{\delta-\delta_1}$	Shape factor in head entrainment equation
$\ell$	Mixing length
L	Dissipation length
LHS	Left hand side of momentum integral equation in x direction Eq. 3.16
P	Static pressure
Q	Wall parallel velocity magnitude
$\vec{Q}$	Wall parallel velocity vector
$\overline{Q}$	Volume flow rate through a vaneless diffuser
$Q_\tau$	Shear velocity
$\overline{q^2}$	Turbulence kinetic energy
r	Radial coordinate in r- $\theta$ -z cylindrical coordinate system
R	Local radius in radial vaneless diffuser

RHS	Right hand side of momentum integral equation in $x$ direction Eq. 3.16
$R_\theta$	Momentum thickness Reynolds number, Eq. 4.10
$R_{\delta_1}$	Displacement thickness Reynolds number, Eq. 4.13
$U$	Component of velocity in $x$ direction
$U_s$	Wall parallel component of velocity in direction of external streamline
$U_\tau$	Shear velocity in two-dimensional flow
$U_{\tau s}$	Streamwise shear velocity = $Q_\tau \sqrt{\cos \beta_w}$
$-\overline{u'v'}$	Reynolds stress in $x$ direction
$V$	Component of velocity normal to wall
$-\overline{v'w'}$	Reynolds stress in $z$ direction
$W$	Component of velocity in $z$ direction
$W_s$	Wall parallel component of velocity normal to external streamline
$x$	Surface coordinate in direction of pressure gradient
$\tilde{x}$	Generalized independent variable
$y$	Coordinate normal to wall
$\tilde{y}$	Generalized dependent variable
$y^+$	$= y Q_\tau / \nu$
$z$	Surface coordinate normal to $x$

#### Greek Letters

$\alpha$	Angle of characteristic line
$\beta$	Angle of $\vec{Q}$ relative to external streamline

$\beta_w$	Angle of limiting wall streamline and wall shear stress relative to external flow direction
$\gamma$	Angle of $\vec{Q}$ relative to $x$ axis
$\delta$	Boundary layer thickness in Coles' law of wake and also width of computing grid in $y$ direction
$\delta_{995}$	Value of $y$ where $Q/Q_\infty = 0.995$
$\delta_1$	Two-dimensional displacement thickness, Eq. 1.15
$\delta_2$	Integral parameter, Eq. 1.15
$\epsilon$	Eddy viscosity
$\zeta$	Surface coordinate normal to $\eta$
$\eta$	Surface coordinate in direction of external streamline
$\theta$	Coordinate in $r$ - $\theta$ - $z$ cylindrical coordinate system
$\theta_{11}$	Momentum thickness in two dimensions, Eq. 1.15
$\theta_{12}$	Integral parameter, Eq. 1.15
$\theta_{22}$	Integral parameter, Eq. 1.15
$\kappa$	Karman constant, 0.4 in present work
$\lambda_\theta$	Sandborn separation parameter, Eq. 5.8b
$\nu$	Kinematic viscosity
$\Pi$	Parameter in Coles law of the wake
$\rho$	Density
$\tau_c$	Shear stress in $\zeta$ direction
$\tau_s$	Shear stress in $\eta$ direction
$\tau_{max}$	Maximum shear stress at a given $x$
$\tau_x$	Shear stress in $x$ direction
$\tau_z$	Shear stress in $y$ direction
$\psi$	Direction of external streamline relative to $x$ axis

$w$  Wake function

$\frac{\partial \hat{\theta}}{\partial x} \frac{1}{2}$  Cross flow integral parameter on plane of symmetry, Eq. 4.11

Subscripts

$i$  Inlet

$s$  At separation point or in streamwise direction

$\infty$  In free stream

$w$  At wall

## CHAPTER 1

### INTRODUCTION

#### A. General Considerations

The fluid dynamic performance of a diverse group of fluid machines, e.g. aircraft wings, centrifugal compressors and ships hulls, is controlled by the three-dimensional, turbulent boundary layers at the solid boundaries of the devices. The behavior of the boundary layers is itself dependent on the pressure field imposed by the outer inviscid regions of the flow. Although in some cases, particularly when flow separation occurs, there is a strong interaction between the boundary layers and the outer flow, in the present work, the outer flow has been presumed given or known.

The boundary layers in most practical flows are in general exceedingly complex. The flow is unsteady on a large scale, turbulent, compressible and three-dimensional (three velocity components and three independent space coordinates needed to define the flow field). Nevertheless most of the research to date has concerned the simplest class of turbulent flows: turbulent layers that are steady in the large, incompressible and two-dimensional (two space coordinates and two velocity components needed to define velocity field). In 1968, a conference was held at Stanford (Kline et.al. 1969) on prediction methods for this simplest class of turbulent flows. The predictions of most methods known in 1968 were compared to a carefully screened set of the available data. A large number of the two-dimensional methods predicted the mean flow well, even though none of those presented at the conference

included any but the most rudimentary physics of the turbulent structure. The best of the two-dimensional methods thus became logical candidates for extension to more complicated problems, i.e. those involving large scale unsteadiness, compressibility and three-dimensionality. Although considerable effort had been expended on such advanced problems prior to 1968, much of it involved extensions of early methods which were proven to be second rate or simply unsatisfactory at the Stanford conference. For example, we worked on a three-dimensional momentum integral type method based on the Von Doenhoff and Tetervin shape factor equation. This shape factor equation was shown at the Stanford Conference to be unsatisfactory, even for two-dimensional flows.

This report documents our research into the extension of some of the better prediction methods of two-dimensional, incompressible, steady turbulent boundary layers into three dimensions.

It is useful to consider briefly the basic ideas underlying three-dimensional turbulent boundary layer theory. The most general type of three-dimensional boundary layers are characterized by skewed velocity profiles, see Figure 1.1. Skewed profiles are distinguished from collateral profiles in which all the velocity vectors from the wall outward lie in one plane i.e.  $W_s = 0$  in Fig. 1.1. Two-dimensional layers and limited classes of three-dimensional layers have collateral velocity profiles. It is common to describe three-dimensional boundary layer profiles in terms of two wall-parallel velocity components - one in the direction of the outer inviscid flow, the streamwise component  $U_s$ , and another perpendicular to this direction, the crossflow component,  $W_s$ .

The wall-parallel velocity vector has magnitude  $\sqrt{W_s^2 + U_s^2}$  and its angle relative to the inviscid external streamline is  $\beta = \tan^{-1} W_s / U_s$ .

The angle of the limiting wall streamline\* is

$$\beta_w = \tan^{-1}(\lim_{y \rightarrow 0} W_s / U_s) \quad (1.1)$$

Skewing (non-zero  $\beta_w$  or  $W_s$ ) of the boundary layer is commonly caused by three effects. (i) It may result from an external free stream pressure gradient with a component normal to the local free stream direction. The pressure gradient's normal component causes acceleration of the low inertia, inner layer fluid such that the fluid tends to turn with a smaller radius of curvature than that of the external flow. This mechanism is responsible for the boundary layer crossflows on yawed wings and on the walls of curved ducts where it is often referred to as secondary flow. (ii) Another cause of skewing is the transverse motion of a wall under a boundary layer in a direction perpendicular to the main flow. This results in crossflows being formed purely by transverse shear stresses. End wall boundary layers in axial flow compressors in part fall in this class. (iii) Finally, skewing may be caused by a combination of the above effects when the moving wall follows a curved path and induces, by drag action, the inner layer fluid particles to follow curved paths. This fluid motion in turn creates a pressure gradient normal to the wall velocity which tends to give the inner fluid layers a component of velocity perpendicular to the wall velocity. Flow over a disc rotating in a stationary

---

\*See Maskell (1955), Johnston (1960a) for concept of limiting wall stream-line.

fluid is the most common example of this class of flow. In summary whenever a pressure gradient or shear force exists perpendicular to the external free stream velocity direction, the potential for crossflow exists.

#### B. Experimental Data

Although almost all flow geometries lead to three-dimensional boundary layers which are turbulent at high Reynolds numbers, only a limited number of geometries and flow conditions have been tested that have produced data suitable for developing and evaluating prediction methods. Figure 1.2 shows the most common experimental configurations which are:

- (a) Wing-Body junctions (boundary layers on the body wall)
- (b) Swept wings, finite and infinite in length
- (c) Curved ducts (boundary layers on the flat walls)
- (d) Radial vaneless diffusers with axisymmetric, swirling flow at inlet
- (e) Rotating discs

As part of this research program, a high percentage of available data sources were gathered and examined for content, completeness and usefulness as a basis for testing prediction methods. A summary of the results of this data study are presented in Table 1.1. As can be seen, only two flows include direct measurement of the shear stress profiles and several flows are missing vital data such as the external pressure field. In fact, of the total of 68 flows shown in Table I, only 34 are complete enough to be usable and only 18 are expected to be of significant value.

There exists a subset of these data which are particularly useful because while the velocity field must be described with three velocity components, only two independent space coordinates need be used to predict the boundary layer development. This two-space coordinate subset includes:

1. Plane of symmetry flows on flat walls upstream of symmetrical wing-body junctions.<sup>+</sup>
2. Infinite swept wing flows where the external pressure is constant in the spanwise direction.
3. Axially symmetric flows in vaneless diffusers.
4. Rotating discs and bodies in axially symmetric free stream flows.

Flows of this type can be used as a first test of a prediction method for three-dimensional turbulent boundary layers without necessitating the development of a computer program using a three-dimensional grid and without the necessity of handling difficult boundary conditions at the transverse edges of the computed flow field. Most of the flows of the two-space coordinate subset, denoted by a \* in Table 1.1, have been examined by us more closely than the other flows. The pressure gradients in the free stream have been extracted from the free stream velocity data and the wall shear stresses have been estimated by assuming two different fits of the velocity profiles to the "law of the wall."<sup>++</sup> In

---

<sup>+</sup>In these flows, only two velocity components are needed but a gradient of the third component is required.

<sup>++</sup>None of the data selected from Table 1.1 had direct measurements of the wall shear stress. Recently, Pierce and his coworkers have been developing instrumentation for the direct measurement of the wall shear stress in three dimensions (Kromenhoek and Pierce, 1968).

addition, momentum and displacement integral parameters have been calculated for each velocity profile and all the results have been tabulated and plotted in a consistent format. The results of this work to codify the data are used later on in this report and are presented and discussed in their entirety elsewhere (Wheeler and Johnston, 1971).

### C. Separation in Three Dimensions

In several of the flow geometries discussed above and in many practical applications, the flowing fluid separates from the surface. Since it is desirable that prediction methods be capable of predicting this phenomenon a brief discussion of flow separation is useful.

A unique and most important characteristic of a three-dimensional boundary layer is that the flow can separate from the surface without the mean surface shear stress becoming zero. This type of three-dimensional separation, known as ordinary separation,<sup>+</sup> is distinguishable from singular separation whose principal characteristic is that the local, mean wall shear stress is zero at the separation point. Separation in two-dimensional flows is singular.

The infinite swept wing flow, shown in Figure 1.3, serves to illustrate the occurrence of ordinary separation. When the pressure gradient force on the fluid (which has a component only in the chordwise direction) is very strong relative to the shear stress force, the chordwise component of velocity in the boundary layer will continuously decrease as the flow approaches the trailing edge. Since the fluid at the same point feels no spanwise pressure gradient forces, it will appear as one

---

<sup>+</sup>See Maskell (1955) for a more complete discussion of separation in three dimensions.

views the boundary layer velocity profile along the  $y$  axis that the local velocity vector is rotating toward the spanwise direction as the flow proceeds downstream. The only forces that can resist this rotation are shear stresses. Since we have assumed a pressure gradient sufficient to overcome the chordwise shear stress effect, the velocity vector near the wall will eventually have rotated as we follow the flow downstream until it is directed parallel to the leading edge (see the limiting wall streamline in Figure 1.3). With no flow in the chordwise direction, the fluid at a slightly larger chord must have come from somewhere other than upstream, i.e. a backflow at the surface from the trailing edge is required. Since the spanwise velocity is non-zero except at the surface, there exists a finite wall shear stress along the separation line. If the infinite wing had no sweep and no initial crossflow, singular separation would occur.

Singular separation can occur at a point on a line of ordinary separation. This occurs at the symmetry plane when the flow leaves the body in a symmetrical wing-body junction flow. In the case of axially symmetric flows such as radial vaneless diffusers ordinary separation occurs when the limiting wall streamlines become tangent to a circle about the axis of symmetry.

#### D. Governing Equations

When boundary layer approximations are applied to the Navier-Stokes Equation in the cartesian coordinate system shown in Figure 1.4 and the assumptions are made that the flow is over flat surfaces, steady in the mean, incompressible and has constant properties, the equations for the mean motion in inertial coordinates are:

continuity

$$\frac{\partial U}{\partial x} + \frac{\partial V}{\partial y} + \frac{\partial W}{\partial z} = 0 \quad (1.3)$$

x-momentum

$$U \frac{\partial U}{\partial x} + V \frac{\partial U}{\partial y} + W \frac{\partial U}{\partial z} = - \frac{1}{\rho} \frac{\partial P}{\partial x} + \frac{1}{\rho} \frac{\partial \tau_x}{\partial y} \quad (1.4)$$

z-momentum

$$U \frac{\partial W}{\partial x} + V \frac{\partial W}{\partial y} + W \frac{\partial W}{\partial z} = - \frac{1}{\rho} \frac{\partial P}{\partial z} + \frac{1}{\rho} \frac{\partial \tau_z}{\partial y} \quad (1.5)$$

Euler's equations apply to the free stream, i.e.

$$- \frac{1}{\rho} \frac{\partial P}{\partial x} = U_{\infty} \frac{\partial U_{\infty}}{\partial x} + W_{\infty} \frac{\partial W_{\infty}}{\partial x} \quad (1.6)$$

$$- \frac{1}{\rho} \frac{\partial P}{\partial z} = U_{\infty} \frac{\partial U_{\infty}}{\partial z} + W_{\infty} \frac{\partial W_{\infty}}{\partial z} \quad (1.7)$$

In the present work, the assumption of zero  $z$  derivatives ( $\partial(\ )/\partial z = 0$ ) has been made for infinite swept wings. In an  $r, \theta$  and  $z$  cylindrical coordinate system  $(r, \theta, z)$  applicable to the vaneless diffuser and rotating disc flows, (see Figure 1.2d) derivatives with respect to  $\theta$  are assumed to be zero ( $\partial(\ )/\partial \theta = 0$ ). A combined form of the equations valid in both coordinate systems is obtained if in the cylindrical coordinate system,  $z$  is replaced by  $y$ ,  $x + r_i$  rather than  $r$  is the radial coordinate where  $r_i$  is the inside or initial radius.  $R$  is the local radius curvature of the transverse,  $\theta$  coordinate axis. In the present work  $R = r = x + r_i$  but in general,  $R$  could be a function of  $x$ ,  $R(x)$ .

continuity

$$\frac{\partial U}{\partial x} + \left\{ \frac{U}{R} \right\} + \frac{\partial V}{\partial y} = 0 \quad (1.8)$$

#### x-momentum

$$U \frac{\partial U}{\partial x} + V \frac{\partial U}{\partial y} - \left\{ \frac{W^2}{R} \right\} = - \frac{1}{\rho} \frac{dP}{dx} + \frac{1}{\rho} \frac{\partial \tau_x}{\partial y} \quad (1.9)$$

#### z-momentum

$$U \frac{\partial W}{\partial x} + V \frac{\partial W}{\partial y} + \left\{ \frac{UW}{R} \right\} = - \frac{1}{\rho} \frac{\partial \tau_z}{\partial y} \quad (1.10)$$

The terms in brackets  $\left\{ \right\}$  are applicable only for the axisymmetric cases. For infinite wings,  $R$  is effectively infinite.

These equations are valid for laminar flow in which case the shear stresses are evaluated from:

$$\tau_x / \rho = \nu \partial U / \partial y \quad (1.11a)$$

$$\tau_z / \rho = \nu \partial W / \partial y \quad (1.11b)$$

For turbulent flows, equations 1.3 to 1.10 are valid for the mean motion, and the shear stresses are a combination of the viscous stresses and the turbulent, or Reynold's stresses:

$$\tau_x / \rho = - \overline{u'v'} + \nu \partial U / \partial y \quad (1.12a)$$

$$\tau_z / \rho = - \overline{v'w'} + \nu \partial W / \partial y \quad (1.12b)$$

Approximate closure equations to be discussed in Chapter 2 are necessary to approximate the Reynolds' stresses and to solve the set of equations for turbulent flows.

#### E. Methods of Solution

Since there exists no general analytic solution to the turbulent boundary layer equations in two or three dimensions, it is necessary to use numerical techniques. There are two general numerical methods for solving the turbulent boundary layer equations: (i) the differential approach in which equations 1.8 to 1.10 (together with the shear stress closure assumptions) are approximated by finite differences - finite

differences being required in both the  $x$  and  $y$  directions. (ii) The integral approach in which equations 1.8 to 1.10 are first integrated with respect to  $y$  and the resulting differential equations solved by finite differences in the  $x$  direction. These integrated equations, known as the momentum integral equations are generally used with a streamline coordinate system (Figure 1.1) where one momentum equation is obtained along an external streamline direction and the other normal to that direction. Thus, if the external streamline is curved, the coordinate system will rotate as the computations proceed. In differential methods, it is most common to use a coordinate system which is fixed in space or has some simple well defined motion, e.g. a coordinate system fixed to the surface of a rotating disc.

Due to difficulties in developing satisfactory integral methods (discussed in the following section) only differential methods have been treated in detail in the present program. In the following section, integral methods are briefly outlined and some of their difficulties emphasized.

#### F. Integral Prediction Methods

The momentum integral equations in three dimensions can take the form (see Cooke and Hall (1962))

$$\begin{aligned} & \frac{1}{h_1 Q_\infty^2} \frac{\partial}{\partial \eta} (\theta_{11} Q_\infty^2) + \frac{1}{h_2 Q_\infty^2} \frac{\partial}{\partial \zeta} (\theta_{12} Q_\infty^2) + \frac{\delta_1}{h_1 Q_\infty} \frac{\partial Q_\infty}{\partial \eta} \\ & + \frac{\delta_2}{h_2 Q_\infty} \frac{\partial Q_\infty}{\partial \zeta} + \frac{(\theta_{11} - \theta_{22})}{h_1 h_2} \frac{\partial h_2}{\partial \eta} + \frac{(2\theta_{12} + 2\delta_2)}{h_1 h_2} \frac{\partial h_1}{\partial \zeta} = \frac{C_{fs}}{2} \end{aligned} \quad (1.13)$$

in the streamwise direction (see Figure 1.1) and the form

$$\begin{aligned}
& \frac{1}{h_1 Q_\infty^2} \frac{\partial}{\partial \eta} (Q_\infty^2 [\theta_{12} - 2\delta_2]) + \frac{1}{h_2 Q_\infty^2} \frac{\partial}{\partial \zeta} (\theta_{22} Q_\infty^2) \\
& + \frac{(2\theta_{12} + 2\delta_2)}{h_1 h_2} \frac{\partial h_2}{\partial \zeta} + \frac{(\theta_{22} - \theta_{11} - \delta_1)}{h_1 h_2} \frac{\partial h_1}{\partial \zeta} = \tan \beta_w \frac{C_{fs}}{2}
\end{aligned} \tag{1.14}$$

in the crossflow direction.

$h_1$  and  $h_2$  are the metric coefficients defined so that an element of distance,  $ds$ , is given by  $ds^2 = h_1^2 d\eta^2 + h_2^2 d\zeta^2 + dy^2$ .  $h_1$  and  $h_2$  depend on the external streamline shape only and are presumed to be known function of  $\eta$  and  $\zeta$  once the external pressure field is established.  $\beta_w$  is the angle of the limiting wall streamline and  $C_{fs}$  is the dimensionless streamwise component of the wall shear stress

$$C_{fs} = \tau_{sw} / \frac{1}{2} \rho Q_\infty^2$$

The remaining dependent variables in equations 1.13 and 1.14 are known as integral parameters and are defined as:

$$\begin{aligned}
\delta_1 &= \frac{1}{Q_\infty} \int_0^\delta (Q_\infty - U_s) dy & \theta_{11} &= \frac{1}{Q_\infty^2} \int_0^\delta U_s (Q_\infty - U_s) dy \\
\delta_2 &= \frac{1}{Q_\infty} \int_0^\delta W_s dy & \theta_{22} &= \frac{1}{Q_\infty^2} \int_0^\delta W_s^2 dy \\
\theta_{12} &= \frac{1}{Q_\infty^2} \int_0^\delta (Q_\infty - U_s) W_s dy & H &= \delta_1 / \theta_{11}
\end{aligned} \tag{1.15}$$

The momentum integral equations represent two equations in seven unknown dependent variables. Thus a considerable amount of additional information is required in order to effect a solution. The various closure assumptions used in two dimensions are well illustrated in Kline et al. (1969). This additional information is usually supplied in two forms. The first form is that of auxiliary equations which in some way

directly relate the variables appearing in equations 1.13 and 1.14 to each other. For example, in three dimensions it has been found that the streamwise component of the velocity often has a profile which is very similar in shape to a known two-dimensional form. Thus, two-dimensional wall shear stress laws have met with some success when applied in three-dimensional prediction methods. Perhaps the most famous of these wall shear stress laws is that of Ludwig and Tillman which when carried over to three-dimensional has the form

$$C_{fs} = 0.246 [e^{-1.561H}] R_{\theta_{11}}^{-0.268} \quad (1.16)$$

The second manner in which the problem is closed is by the direct use of assumed functional forms for the velocity profiles, both in the streamwise and crossflow directions. Universal functions of the form  $U/U_{\infty} = f(y/\delta)$  have met with very little success in prediction of two-dimensional flows and there is no reason to believe that they would be more successful in three-dimensional flows. However, one parameter velocity profiles are a considerable improvement and one by Ling (see Hirst and Reynolds, 1969) performed satisfactorily in an integral method submitted at 1968 Stanford conference. He used

$$\frac{U_{\infty} - U}{U_{\tau}} = a(\eta) (1 - y/\delta)^2 \quad (1.17)$$

Such a velocity profile could be used in a three-dimensional prediction scheme if it were assumed that it represented the streamwise component of the velocity. Coles (1956) and others have proposed two parameter representations for two-dimensional velocity profiles which will generally fit data much better than equation 1.17. With these profiles, a

skin friction law is generally implied and an equation such as equation 1.16 is not needed.

Crossflow velocity profiles have proven much more difficult to describe with a functional form than streamwise profiles. Prandtl (1946) proposed that crossflow velocities could be represented by the form

$$\frac{W_s}{U_s} = \tan \beta_w g(y/\delta) \quad (1.18)$$

where  $g(y/\delta)$  is a universal function, and Mager (1952) suggested

$$g(y/\delta) = (1 - y/\delta)^2 \quad (1.19)$$

This profile model is simple - it requires only one parameter,  $\beta_w$ . Figure 1.5 shows some data of Gardow (1958) and Bradshaw and Terrell (1969) plotted in the form of equation 1.18. The data is too high relative to the Mager profile for the most part but does appear to approximately follow one functional form. The profile data of Cham (1968) in Figure 1.6 shows a somewhat different behavior and could not be fitted by a simple function of  $y/\delta$ . Nevertheless, the Mager profile is at least a fair approximation to the data and may work satisfactorily in some cases.

Another method of crossflow profile description is the polar profile method. Figure 1.7 shows some typical crossflow data plotted in this form. In this approach, it is assumed that the crossflow can be expressed in the form:

$$\frac{W_s}{Q_\infty} = f\left(\frac{U_s}{Q_\infty}, \text{Parameters}\right) \quad (1.20)$$

Johnston (1957) proposed a two region form of this function - an inner region where

$$\frac{W_s}{Q_\infty} = \frac{U_s}{Q_\infty} \tan \beta_w \quad (1.21a)$$

and an outer region where

$$\frac{W_s}{Q_\infty} = A \left( 1 - \frac{U_s}{Q_\infty} \right) \quad (1.21b)$$

A is now a second parameter. This model is also shown on Figure 1.7 and coincides with the data well except in the region of the peak. Cham (1968) demonstrates another limitation of this method - that the cross-flow cannot generally be straight all the way to the wall. For integral methods however, this is probably not a practical limitation. In order to improve the fit of the polar model to the data in the region of the peak, Eichelbrenner (1963) proposed using polynomial fits of the form

$$\frac{W_s}{Q_\infty} = \sum_{i=1}^n A_i \frac{U_s}{Q_\infty} \quad (1.22)$$

where  $A_i (i = 1, 2, \dots, n)$  are constants. Figure 1.8 shows the fit of a fifth order polynomial to the data of Gruschwitz (1935) and Johnston (1957). In some cases the fit is very good but in others a definite discrepancy appears in the outer part of the layer. This latter problem can be quite severe as shown by the data of Bradshaw and Terrell (1969) and Klinksiek and Pierce (1968) in Figure 1.9. The Eichelbrenner profiles use the position of the peak as a parameter to determine one of the  $A_i$  and Klinksiek and Pierce (1968) found that for all orders of  $n$  less than six, the Eichelbrenner profiles could not match the data when the peak was at large values of  $U_s/Q_\infty$ . Klinksiek and Pierce also found

that some other polynomial suggestions of Eichelbrenner (1966) and Shanebrook (1966) met with various difficulties. Figure 1.10 shows some of Klinksiek and Pierce' "crossover" profiles which would challenge any designer of crossflow velocity profile models.

Coles (1956) proposed a three dimensional form of the law of the wall-law of the wake

$$\vec{Q} = \vec{Q}_\tau \left[ \frac{1}{\kappa} \ln \frac{y |\vec{Q}_\tau|}{\nu} + C + \frac{\Pi}{\kappa} \omega(y/\delta) \right] \quad (1.23)$$

where  $\vec{Q}_\tau$  is a vector in the direction of the wall shear stress that has a magnitude  $\sqrt{\tau_w/\rho}$ .  $\Pi \vec{Q}_\tau$  is a wake vector whose direction is set so that the free stream velocity vector is in the correct direction.  $\Pi$  is thus a tensor whose magnitude sets the wake fraction of the profile. Components of the velocity in a direction perpendicular to the wall shear stress are proportional only to the wake function  $\omega(y/\delta)$ . Figure 1.11 shows some data that show approximate agreement with Coles' model, but Figures 1.12 and 1.13 present data which shows very poor agreement. Pierce (1966) argues that the plane of symmetry flows which were used to test the Coles model (Figures 1.12 and 1.13) were special cases in that the flows move toward separation too rapidly and the profiles do not reach an "asymptotic" or equilibrium form. He shows that the wake component of the collateral flow on the plane of symmetry of the Johnston (1957) data does not develop a wake function form ( $\omega(y/\delta)$  above) either. However, this argument can be turned into a criticism of integral methods for both two and three-dimensional cases because rapidly separating flows are often of practical interest.

If one were to consider the Mager crossflow profile to be satisfactory, and were to use a one parameter streamwise velocity profile, the

problem would be reduced to three equations (two momentum, one skin-friction) in four dependent variables. Thus, for closure an additional relationship is needed. Head, and his co-workers at Cambridge (see Cham, 1968) have completed a similar set of equations by using an entrainment relation

$$\frac{\partial}{\partial \eta} (\delta - \delta_1) = C_E (H_{\delta - \delta_1}) \quad (1.24)$$

where  $C_E$  is a function of a new shape parameter  $H_{\delta - \delta_1}$  and  $\delta$  is the boundary layer thickness. Cham, (1968) found however that  $C_E$  was geometry dependent as shown in Figure 1.14. It should be noted however that the entrainment approach, in various forms, works well in two dimensions. Recently Crabbe (1971) and Townsend (1970) have worked on entrainment models which may lead to a more satisfactory form.

It can be seen that the extension of integral methods to three dimensions is far from simple. To date, three-dimensional turbulent prediction methods using integral methods have been unsatisfactory in that they have been unable to provide predictions agreeing with a wide variety range of experimental data. The extension of differential methods to three-dimensional turbulent boundary layers, as will be seen in Chapter 2, is easy by comparison. As a result, it was decided to study only three-dimensional extensions of differential methods in the present research program. The development in the later 1950's of modern high speed digital computers has made one disadvantage of differential methods, substantially longer computer run times, much less significant.

#### G. Objectives

In summary, the objectives of this research program were:

1. To collect and organize available data on three-dimensional turbulent boundary layers
2. To develop a numerical technique and computer program to solve the differential equations of the boundary layer such that various three-dimensional prediction methods based on different models for the turbulent shear stress could be evaluated without introduction of ambiguity due to differences in numerical technique used with each model.
3. To critically examine the selected prediction methods, both in relation to each other and in relation to existing experimental data.

Number	AUTHOR (REPORT DATE)	Reference Velocity (ft/sec)	Typical Initial Reynolds Number (10 <sup>-1</sup> )	Initial (fractional) boundary layer thickness (in.)	T <sub>90</sub> /V <sub>90</sub> range of values	Free Stream Pressure Ratio	HEAD ON DATA										T. W. DATA				Number of Flows or Runs	Remarks	
							Reynolds Number	Angle of Incidence	Angle of Attack	Angle of Incidence	Angle of Attack	Angle of Incidence	Angle of Attack	Angle of Incidence	Angle of Attack	Angle of Incidence	Angle of Attack	Angle of Incidence	Angle of Attack	Angle of Incidence			Angle of Attack
I.A. Swept Wing, Plate or Poly (Finite)																							
20	Kuestle, A.M. et al. [1959]	74	4.6x10 <sup>4</sup>	0.2	1000	GA	GA	GA	GA	GA	GA	GA	GA	GA	GA	GA	GA	GA	GA	GA	GA	1	
3	Bretherton, G.C. and Kyatt, L.A. [1960]	200	1.3x10 <sup>4</sup>	0.1	NC	GA	TA	TA	TA	TA	TA	TA	TA	TA	TA	TA	TA	TA	TA	TA	TA	7	
I.B. Swept Wing, Plate or Body (Infinite or approx. Infinite span)																							
	Altman, J.M. and Hoggarth, R. [1958]	150	1x10 <sup>4</sup>	0.125	1000	GA	GA	GA	GA	GA	GA	GA	GA	GA	GA	GA	GA	GA	GA	GA	GA	1	
1	Altman, J.M. and Hoggarth, R. [1958]	150	1x10 <sup>4</sup>	0.1	1000	GA	GA	GA	GA	GA	GA	GA	GA	GA	GA	GA	GA	GA	GA	GA	GA	1	
2	Altman, J.M. and Hoggarth, R. [1958]	150	1x10 <sup>4</sup>	0.1	1000	GA	GA	GA	GA	GA	GA	GA	GA	GA	GA	GA	GA	GA	GA	GA	GA	1	
3	Altman, J.M. and Hoggarth, R. [1958]	150	1x10 <sup>4</sup>	0.1	1000	GA	GA	GA	GA	GA	GA	GA	GA	GA	GA	GA	GA	GA	GA	GA	GA	1	
4	Altman, J.M. and Hoggarth, R. [1958]	150	1x10 <sup>4</sup>	0.1	1000	GA	GA	GA	GA	GA	GA	GA	GA	GA	GA	GA	GA	GA	GA	GA	GA	1	
5	Altman, J.M. and Hoggarth, R. [1958]	150	1x10 <sup>4</sup>	0.1	1000	GA	GA	GA	GA	GA	GA	GA	GA	GA	GA	GA	GA	GA	GA	GA	GA	1	
6	Altman, J.M. and Hoggarth, R. [1958]	150	1x10 <sup>4</sup>	0.1	1000	GA	GA	GA	GA	GA	GA	GA	GA	GA	GA	GA	GA	GA	GA	GA	GA	1	
7	Altman, J.M. and Hoggarth, R. [1958]	150	1x10 <sup>4</sup>	0.1	1000	GA	GA	GA	GA	GA	GA	GA	GA	GA	GA	GA	GA	GA	GA	GA	GA	1	
8	Altman, J.M. and Hoggarth, R. [1958]	150	1x10 <sup>4</sup>	0.1	1000	GA	GA	GA	GA	GA	GA	GA	GA	GA	GA	GA	GA	GA	GA	GA	GA	1	
9	Altman, J.M. and Hoggarth, R. [1958]	150	1x10 <sup>4</sup>	0.1	1000	GA	GA	GA	GA	GA	GA	GA	GA	GA	GA	GA	GA	GA	GA	GA	GA	1	
II. Wing-Pan Junction (Infinite span)																							
10	John, J.P. [1957]	101	6x10 <sup>4</sup>	1.1	1000	TA	TA	TA	TA	TA	TA	TA	TA	TA	TA	TA	TA	TA	TA	TA	TA	1	
11	John, J.P. [1957]	101	6x10 <sup>4</sup>	1.1	1000	GA	TA	TA	TA	TA	TA	TA	TA	TA	TA	TA	TA	TA	TA	TA	TA	1	
12	John, J.P. [1957]	101	6x10 <sup>4</sup>	1.1	1000	TA	TA	TA	TA	TA	TA	TA	TA	TA	TA	TA	TA	TA	TA	TA	TA	1	
13	John, J.P. [1957]	101	6x10 <sup>4</sup>	1.1	1000	TA	TA	TA	TA	TA	TA	TA	TA	TA	TA	TA	TA	TA	TA	TA	TA	1	
14	John, J.P. [1957]	101	6x10 <sup>4</sup>	1.1	1000	TA	TA	TA	TA	TA	TA	TA	TA	TA	TA	TA	TA	TA	TA	TA	TA	1	
15	John, J.P. [1957]	101	6x10 <sup>4</sup>	1.1	1000	TA	TA	TA	TA	TA	TA	TA	TA	TA	TA	TA	TA	TA	TA	TA	TA	1	
16	John, J.P. [1957]	101	6x10 <sup>4</sup>	1.1	1000	TA	TA	TA	TA	TA	TA	TA	TA	TA	TA	TA	TA	TA	TA	TA	TA	1	
17	John, J.P. [1957]	101	6x10 <sup>4</sup>	1.1	1000	TA	TA	TA	TA	TA	TA	TA	TA	TA	TA	TA	TA	TA	TA	TA	TA	1	
18	John, J.P. [1957]	101	6x10 <sup>4</sup>	1.1	1000	TA	TA	TA	TA	TA	TA	TA	TA	TA	TA	TA	TA	TA	TA	TA	TA	1	
19	John, J.P. [1957]	101	6x10 <sup>4</sup>	1.1	1000	TA	TA	TA	TA	TA	TA	TA	TA	TA	TA	TA	TA	TA	TA	TA	TA	1	
20	John, J.P. [1957]	101	6x10 <sup>4</sup>	1.1	1000	TA	TA	TA	TA	TA	TA	TA	TA	TA	TA	TA	TA	TA	TA	TA	TA	1	

Table I.1 - Summary of Data Sources

Index	AUTHOR(S) (REPORT DATE)	Reference or Free Stream Velocity (ft/sec)	Typical Initial Reynolds Number ( $10^{-1}$ )	Initial (Qualit.) Boundary Layer Thickness (in.)	$U_{11}/V$ , range or Characteristic Value	Free Stream Pressure Field	NEAR FLOW DATA										TOLERANCE DATA				Number of Flows or Runs	Remarks See Table 1.2																																																																																																																																																																																																																																																							
							Velocity Profiles		Limiting Angle at Wall	Integral Thickness Parameters	Profile Coefficients	Profile Coefficients	Profile Coefficients	Profile Coefficients	Profile Coefficients	Profile Coefficients	Profile Coefficients	Profile Coefficients	Profile Coefficients	Profile Coefficients			Profile Coefficients	Profile Coefficients	Profile Coefficients	Profile Coefficients	Profile Coefficients	Profile Coefficients	Profile Coefficients	Profile Coefficients	Profile Coefficients	Profile Coefficients	Profile Coefficients	Profile Coefficients	Profile Coefficients	Profile Coefficients	Profile Coefficients	Profile Coefficients	Profile Coefficients	Profile Coefficients	Profile Coefficients	Profile Coefficients	Profile Coefficients	Profile Coefficients	Profile Coefficients	Profile Coefficients	Profile Coefficients	Profile Coefficients	Profile Coefficients	Profile Coefficients	Profile Coefficients	Profile Coefficients	Profile Coefficients	Profile Coefficients	Profile Coefficients	Profile Coefficients	Profile Coefficients	Profile Coefficients	Profile Coefficients	Profile Coefficients	Profile Coefficients	Profile Coefficients	Profile Coefficients	Profile Coefficients	Profile Coefficients	Profile Coefficients	Profile Coefficients	Profile Coefficients	Profile Coefficients	Profile Coefficients	Profile Coefficients	Profile Coefficients	Profile Coefficients	Profile Coefficients	Profile Coefficients	Profile Coefficients	Profile Coefficients	Profile Coefficients	Profile Coefficients	Profile Coefficients	Profile Coefficients	Profile Coefficients	Profile Coefficients	Profile Coefficients	Profile Coefficients	Profile Coefficients	Profile Coefficients	Profile Coefficients	Profile Coefficients	Profile Coefficients	Profile Coefficients	Profile Coefficients	Profile Coefficients	Profile Coefficients	Profile Coefficients	Profile Coefficients	Profile Coefficients	Profile Coefficients	Profile Coefficients	Profile Coefficients	Profile Coefficients	Profile Coefficients	Profile Coefficients	Profile Coefficients	Profile Coefficients	Profile Coefficients	Profile Coefficients	Profile Coefficients	Profile Coefficients	Profile Coefficients	Profile Coefficients	Profile Coefficients	Profile Coefficients	Profile Coefficients	Profile Coefficients	Profile Coefficients	Profile Coefficients	Profile Coefficients	Profile Coefficients	Profile Coefficients	Profile Coefficients	Profile Coefficients	Profile Coefficients	Profile Coefficients	Profile Coefficients	Profile Coefficients	Profile Coefficients	Profile Coefficients	Profile Coefficients	Profile Coefficients	Profile Coefficients	Profile Coefficients	Profile Coefficients	Profile Coefficients	Profile Coefficients	Profile Coefficients	Profile Coefficients	Profile Coefficients	Profile Coefficients	Profile Coefficients	Profile Coefficients	Profile Coefficients	Profile Coefficients	Profile Coefficients	Profile Coefficients	Profile Coefficients	Profile Coefficients	Profile Coefficients	Profile Coefficients	Profile Coefficients	Profile Coefficients	Profile Coefficients	Profile Coefficients	Profile Coefficients	Profile Coefficients	Profile Coefficients	Profile Coefficients	Profile Coefficients	Profile Coefficients	Profile Coefficients	Profile Coefficients	Profile Coefficients	Profile Coefficients	Profile Coefficients	Profile Coefficients	Profile Coefficients	Profile Coefficients	Profile Coefficients	Profile Coefficients	Profile Coefficients	Profile Coefficients	Profile Coefficients	Profile Coefficients	Profile Coefficients	Profile Coefficients	Profile Coefficients	Profile Coefficients	Profile Coefficients	Profile Coefficients	Profile Coefficients	Profile Coefficients	Profile Coefficients	Profile Coefficients	Profile Coefficients	Profile Coefficients	Profile Coefficients	Profile Coefficients	Profile Coefficients	Profile Coefficients	Profile Coefficients	Profile Coefficients	Profile Coefficients	Profile Coefficients	Profile Coefficients	Profile Coefficients	Profile Coefficients	Profile Coefficients	Profile Coefficients	Profile Coefficients	Profile Coefficients	Profile Coefficients	Profile Coefficients	Profile Coefficients	Profile Coefficients	Profile Coefficients	Profile Coefficients	Profile Coefficients	Profile Coefficients	Profile Coefficients	Profile Coefficients	Profile Coefficients	Profile Coefficients	Profile Coefficients	Profile Coefficients	Profile Coefficients	Profile Coefficients	Profile Coefficients	Profile Coefficients	Profile Coefficients	Profile Coefficients	Profile Coefficients	Profile Coefficients	Profile Coefficients	Profile Coefficients	Profile Coefficients	Profile Coefficients	Profile Coefficients	Profile Coefficients	Profile Coefficients	Profile Coefficients	Profile Coefficients	Profile Coefficients	Profile Coefficients	Profile Coefficients	Profile Coefficients	Profile Coefficients	Profile Coefficients	Profile Coefficients	Profile Coefficients	Profile Coefficients	Profile Coefficients	Profile Coefficients	Profile Coefficients	Profile Coefficients	Profile Coefficients	Profile Coefficients	Profile Coefficients	Profile Coefficients	Profile Coefficients	Profile Coefficients	Profile Coefficients	Profile Coefficients	Profile Coefficients	Profile Coefficients	Profile Coefficients	Profile Coefficients	Profile Coefficients	Profile Coefficients	Profile Coefficients	Profile Coefficients	Profile Coefficients	Profile Coefficients	Profile Coefficients	Profile Coefficients	Profile Coefficients	Profile Coefficients	Profile Coefficients	Profile Coefficients	Profile

Table 1.1 (Cont'd)

\*

\*

\*

Table 1.2 - Key to Symbols and Remarks in Table 1.1

[A] Definition of Symbols

AZ - Assumed zero  
 GA - Graphical values given - all runs and/or profiles  
 GS - " " " " - some " " " "  
 IA - May be inferred from given data - all runs and/or profiles  
 IS - " " " " - some " " " "  
 NC - Not calculated  
 NM - Not measured  
 NR - Not reported, may have been measured  
 TA - Tabulated values - all runs and/or profiles  
 TS - " " " " - some " " " "  
 ? - No information, or considerable uncertainty indicated

[B] Numbered Remarks

1. Report suggests that complete data will be published at a later date.
2. Unpublished report obtained from authors.
3. Graphical Profiles may be of limited value since the layer thickness not reported.
4. Only one profile given. Other integral data might be extracted with much effort. Source of moderate cross flows not clear.
5. Given integral parameters inaccurate, see Cham [1968].
6. Although flow at moderate subsonic Mach number, variations were small and density changes thought not to be important.
7. Value of  $\nu$  for air at normal (room) pressure and temperature will probably suffice.
8. One-dimensional turbulence intensity measured along local mean flow direction.
9. Some question of completeness here as original data source not in hand.
10. Initial and normalizing conditions not given directly.

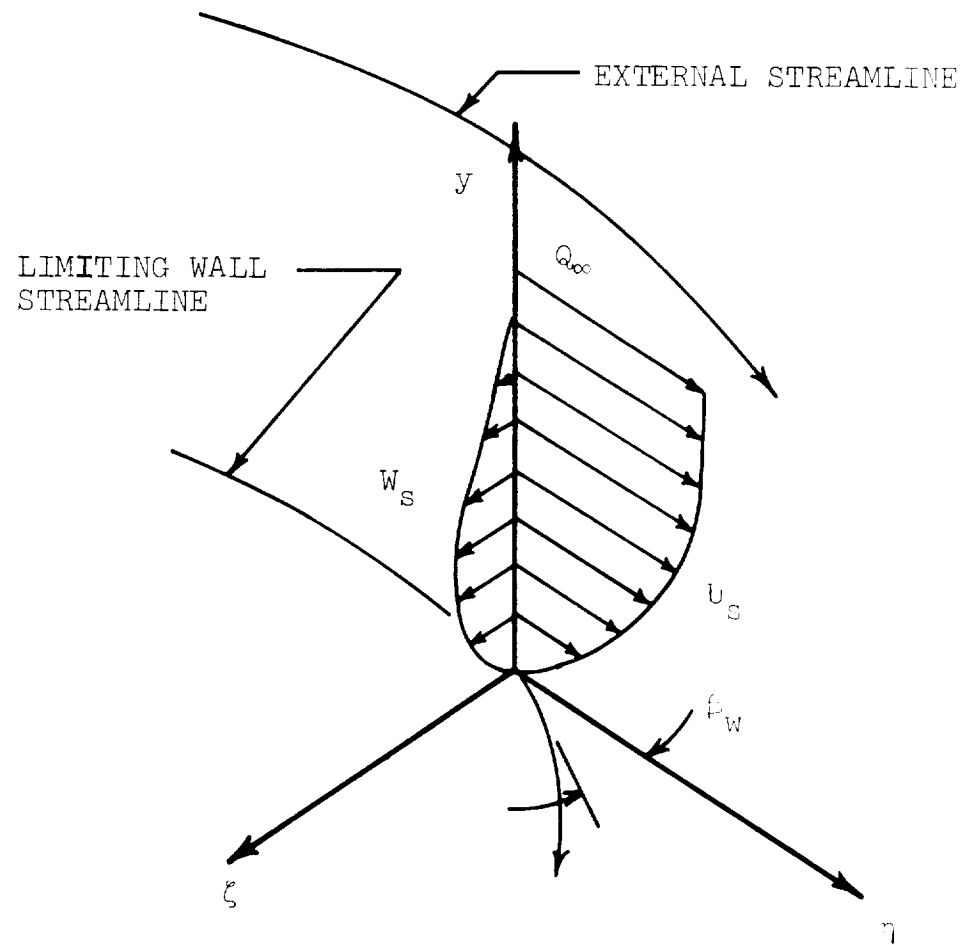
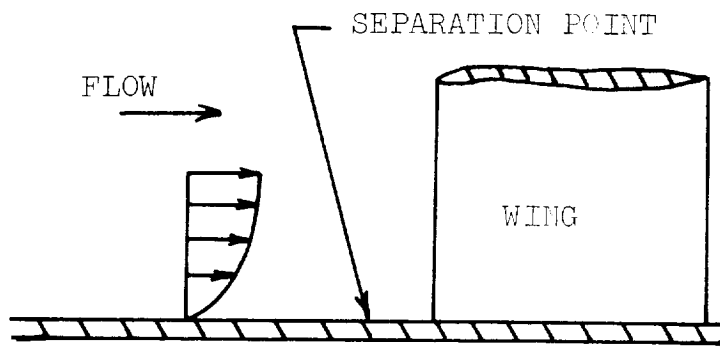
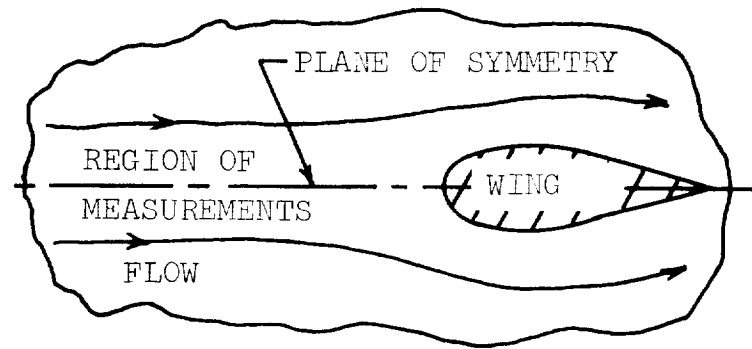
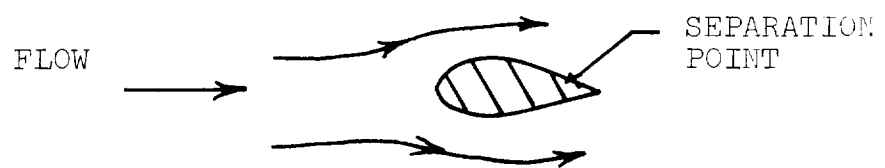
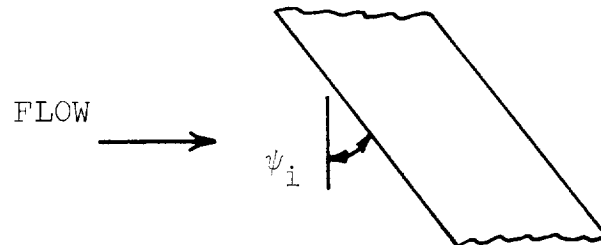


Figure 1.1 Three-Dimensional Wall-Parallel Velocity Components

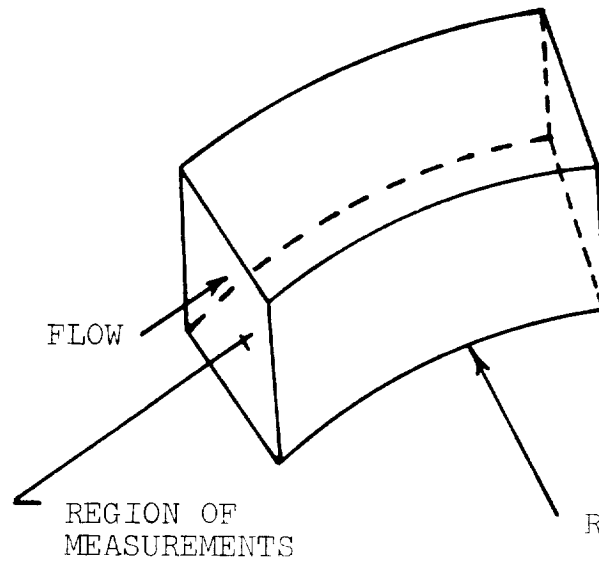


(a) WING-BODY JUNCTION

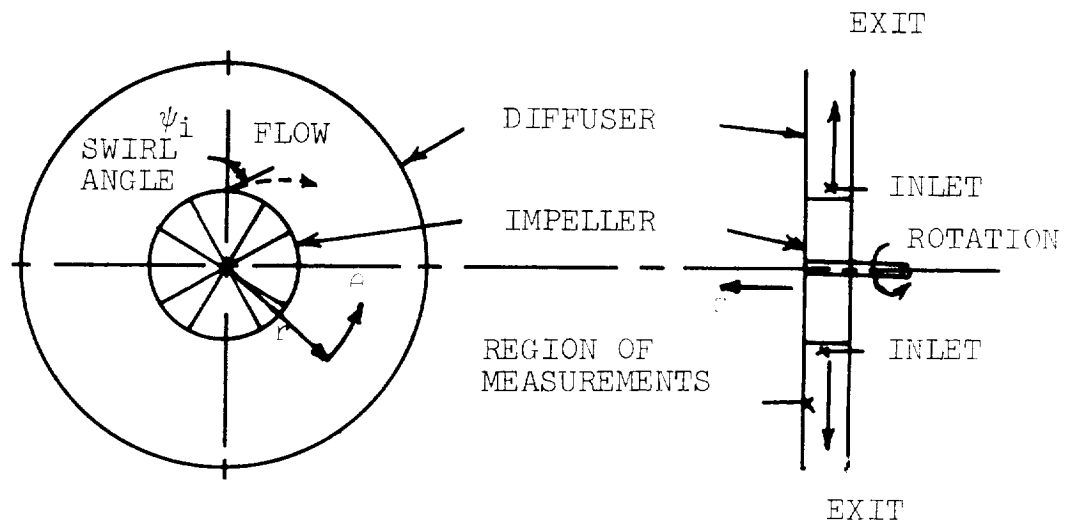


(b) SWEPT WING

Figure 1.2 Experimental Geometries for Three-Dimensional Turbulent Boundary Layers

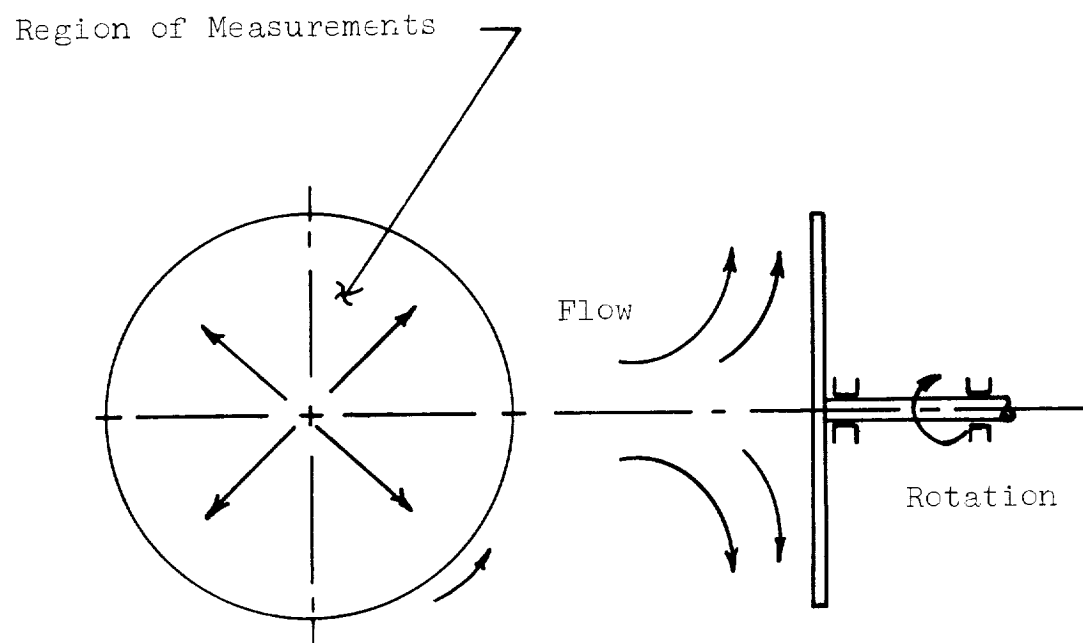


(c) CURVED DUCT



(d) VANELESS DIFFUSER

Figure 1.2 (Cont'd)



(e) Rotating Disc

Figure 1.2 (Cont'd)

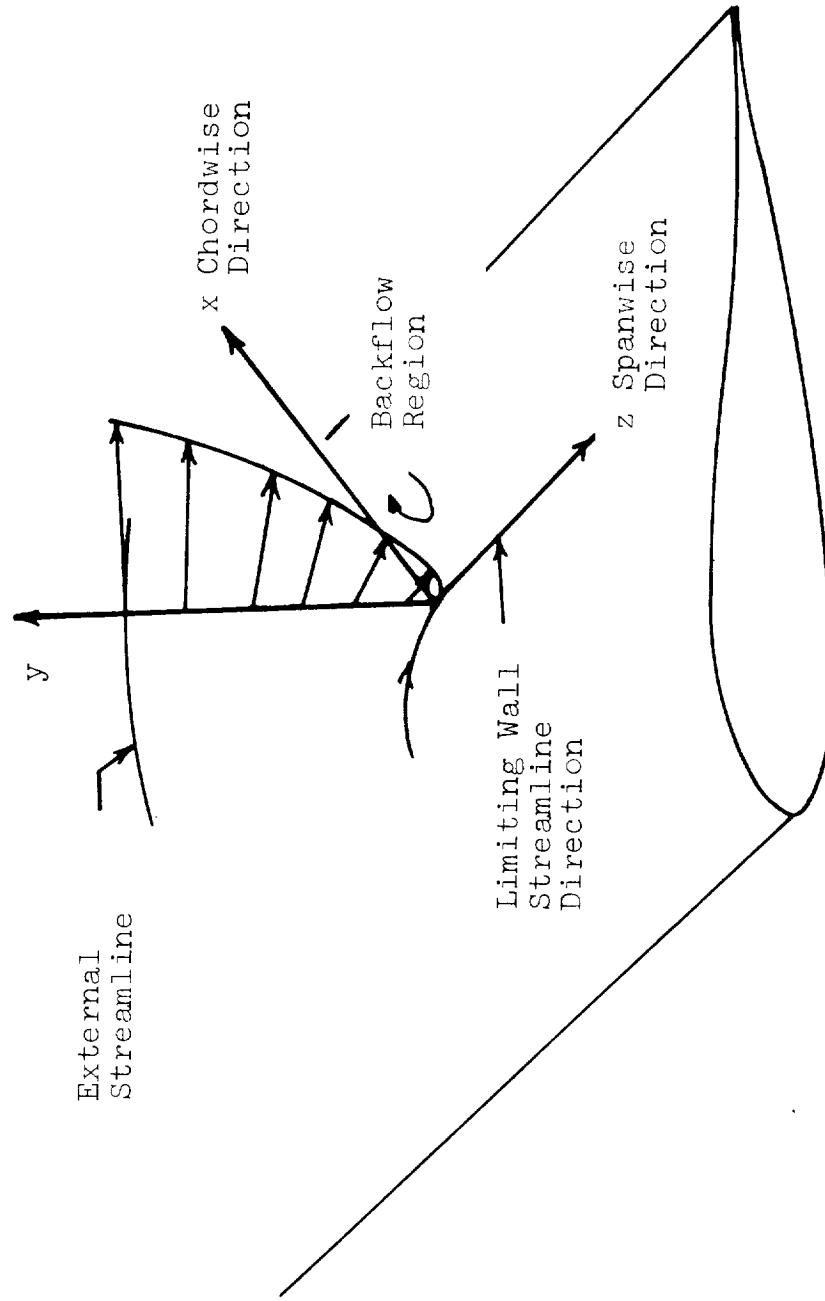


Figure 1.3 Ordinary Separation on a Swept, Infinite Wing

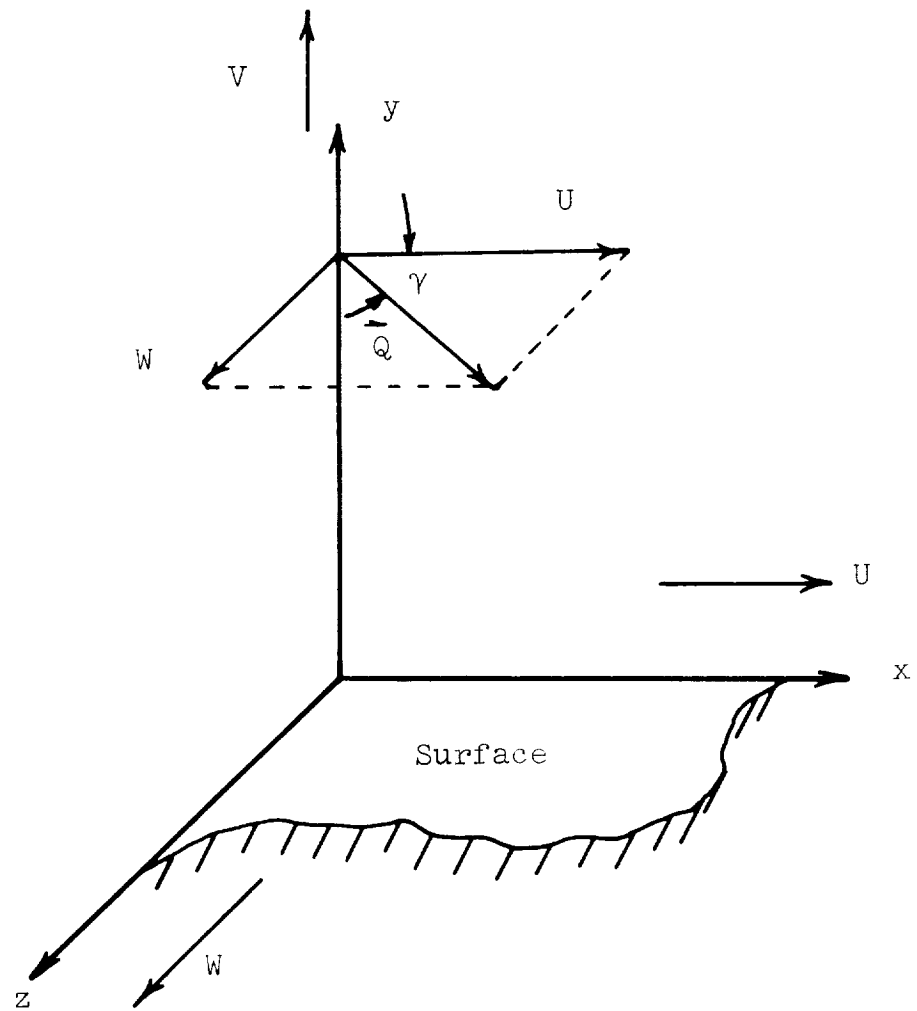


Figure 1.4 - x-y-z Coordinate System

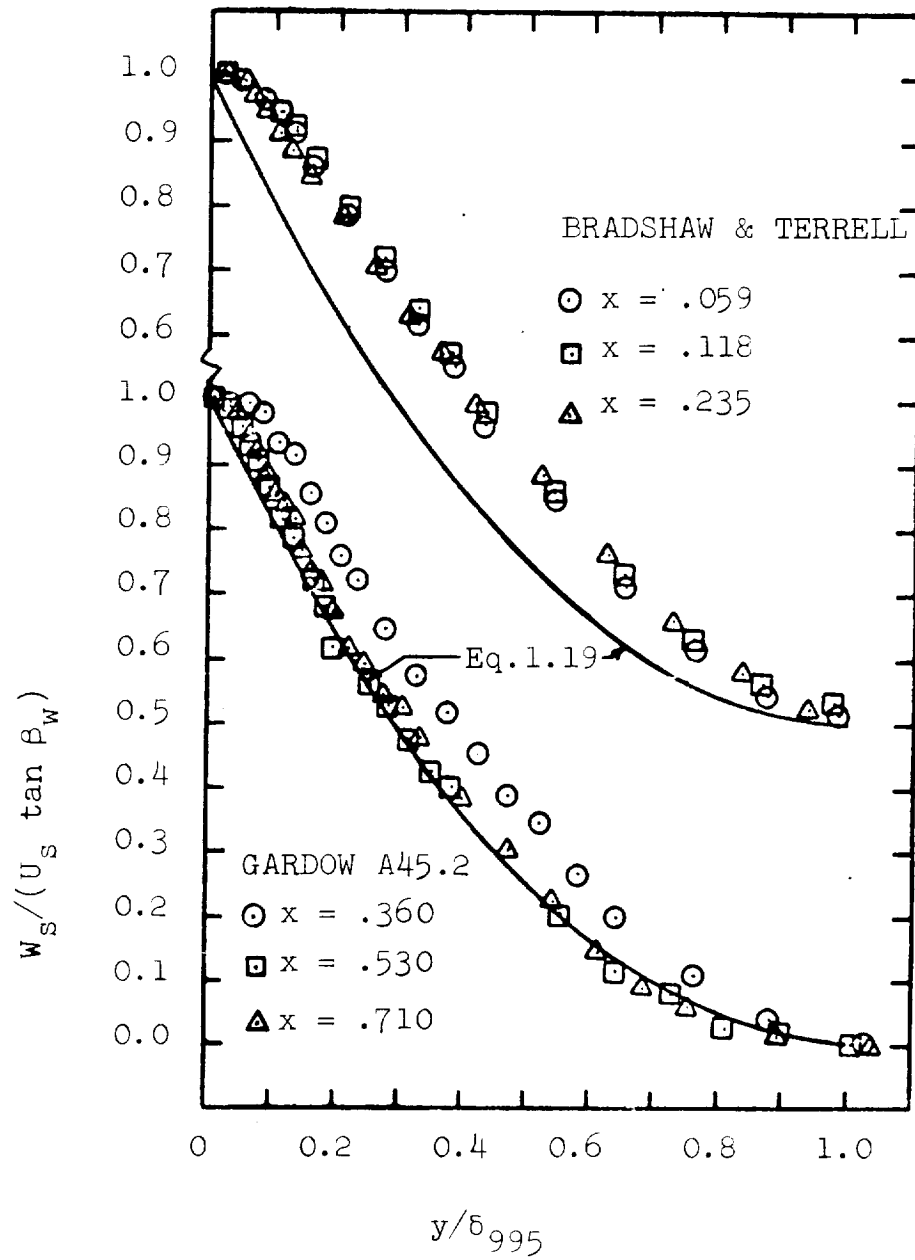


Figure 1.5 - Crossflow Profiles in Prandtl Form  
(Data of Gardow (1958) and  
Bradshaw and Terrell (1969) )

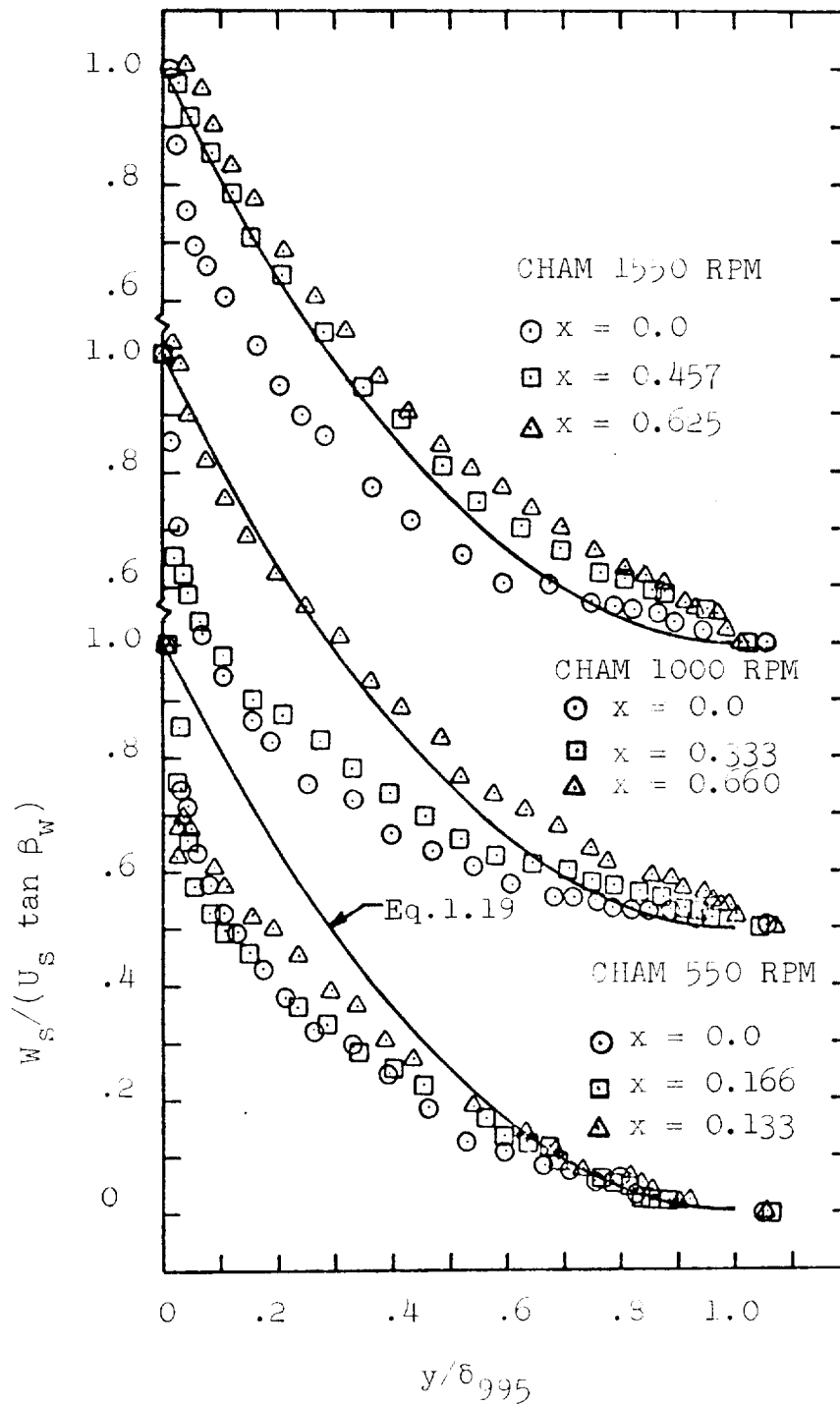


Figure 1.6 - Crossflow Profiles in Prandtl Form  
(Data of Cham (1968))

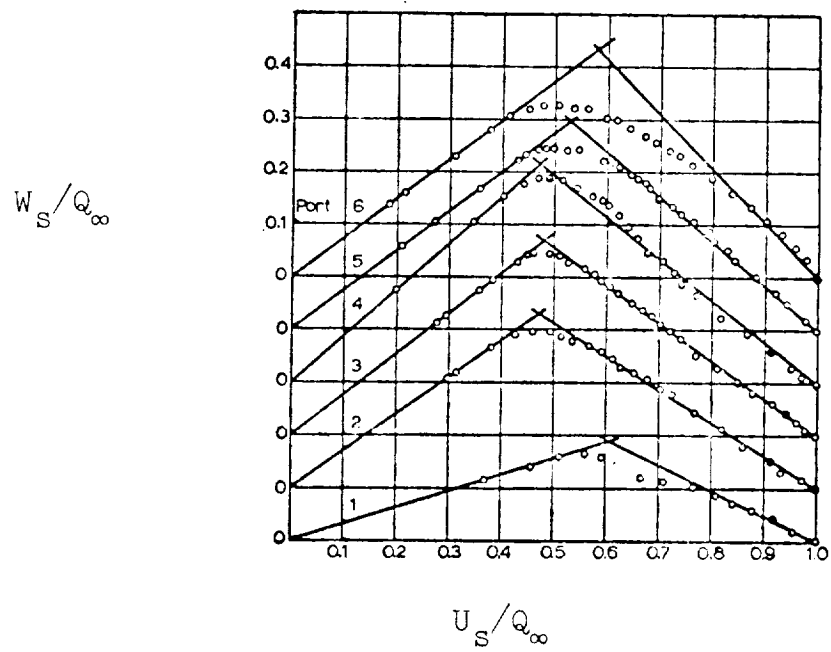


Figure 1.7 - Polar Plots of Gardow (1958)

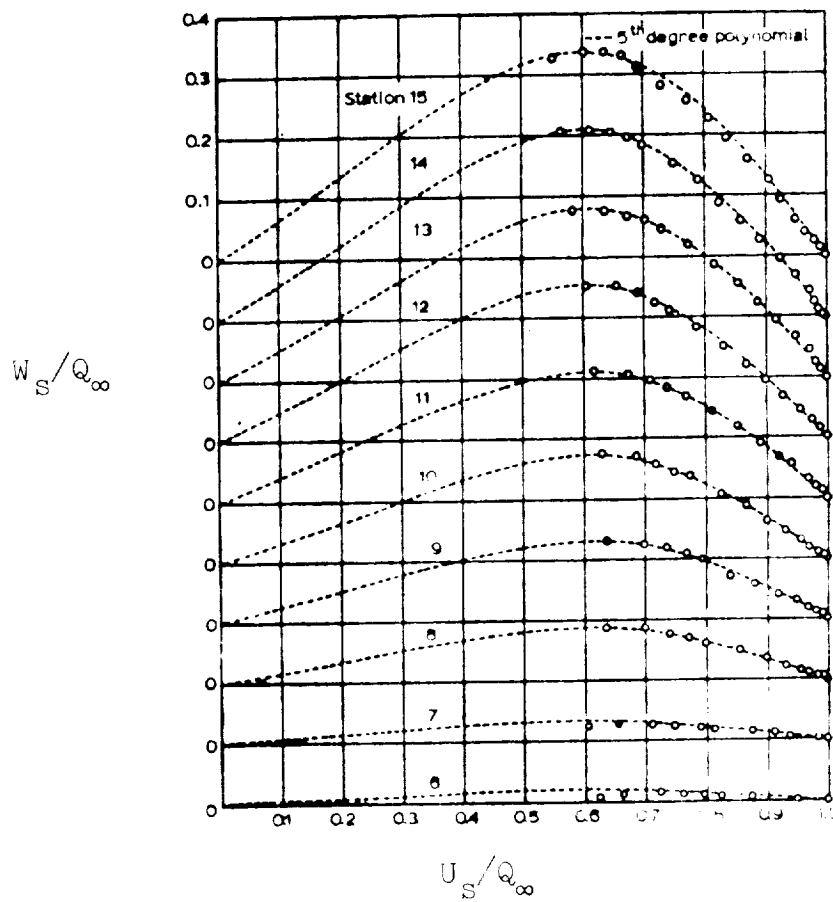


Figure 1.8a - Polar Plots of Gruschwitz (1935) with Eichelbrenner 5th Degree Polynomials

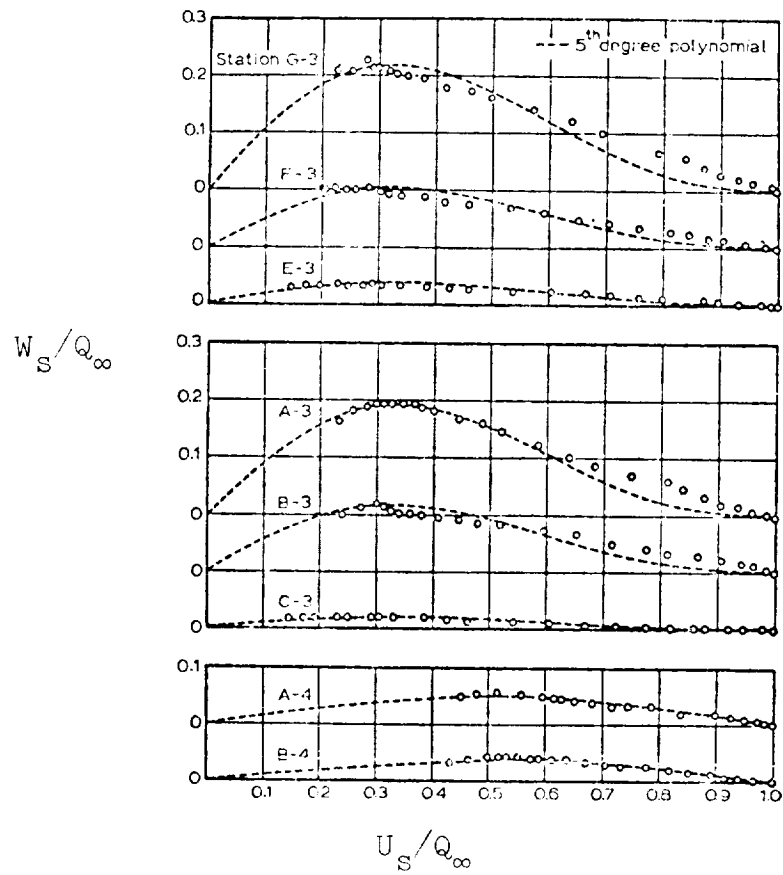


Figure 1.8b - Polar Plots of Johnston (1957) with Eichelbrenner 5th Degree Polynomials

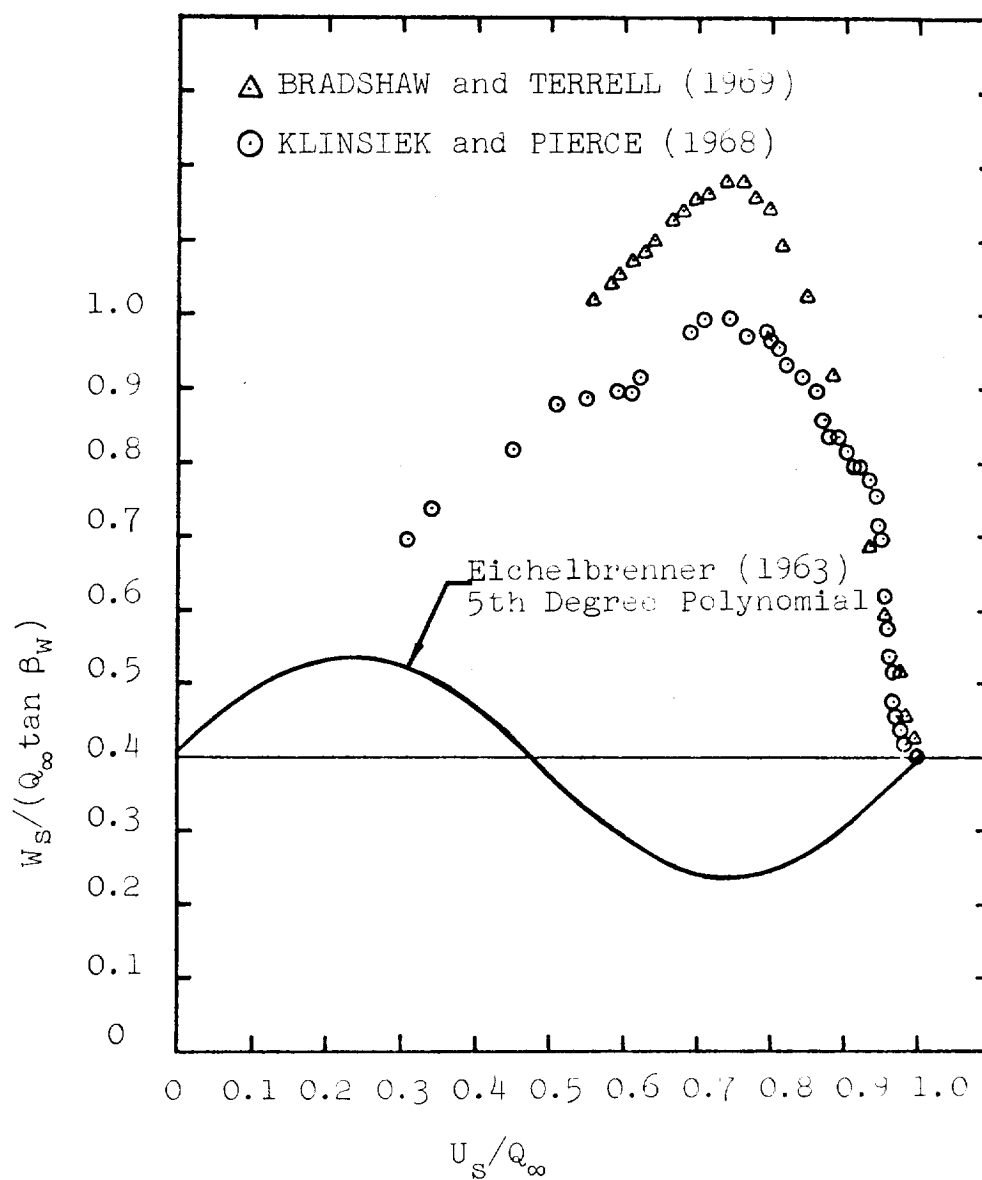


Figure 1.9 - Polar Plots of Bradshaw and Terrell and Klinknsiek and Pierce with Eichelbrenner 5th Degree Polynomial

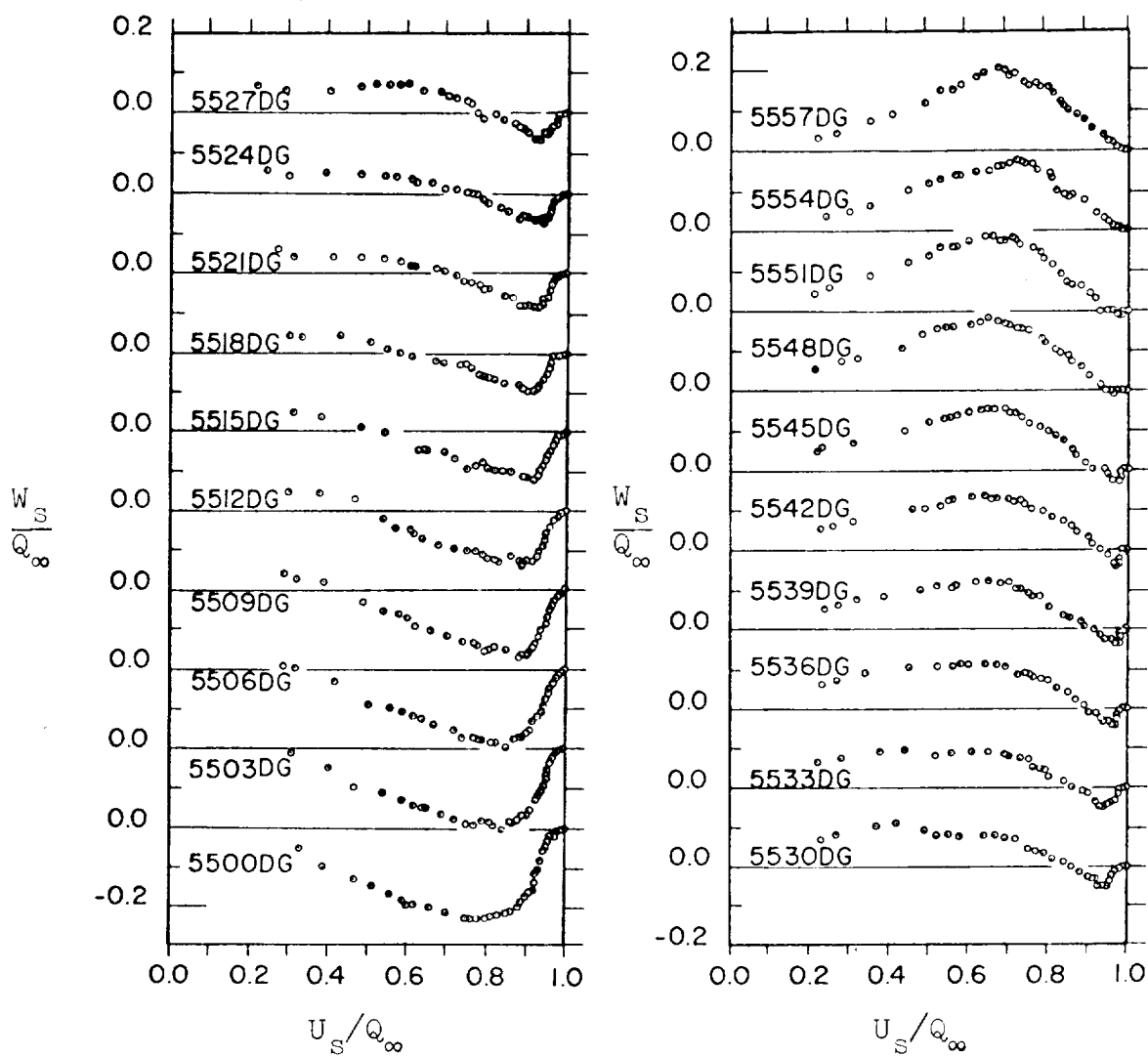


Figure 1.10 - Crossover Profiles of  
Klinksieck and Pierce (1968)

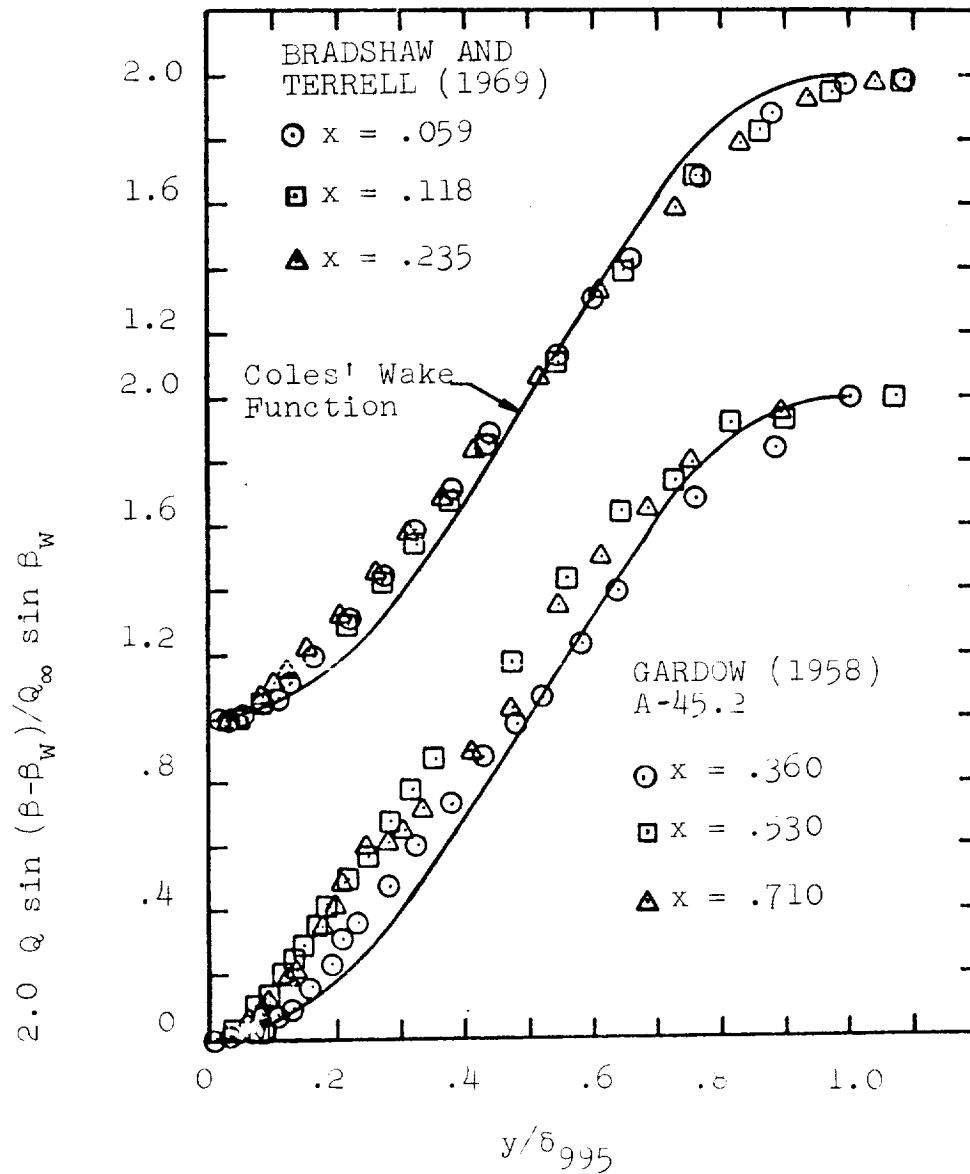


Figure 1.11 - Wake Function Component of Gardow and Bradshaw and Terrell Profiles

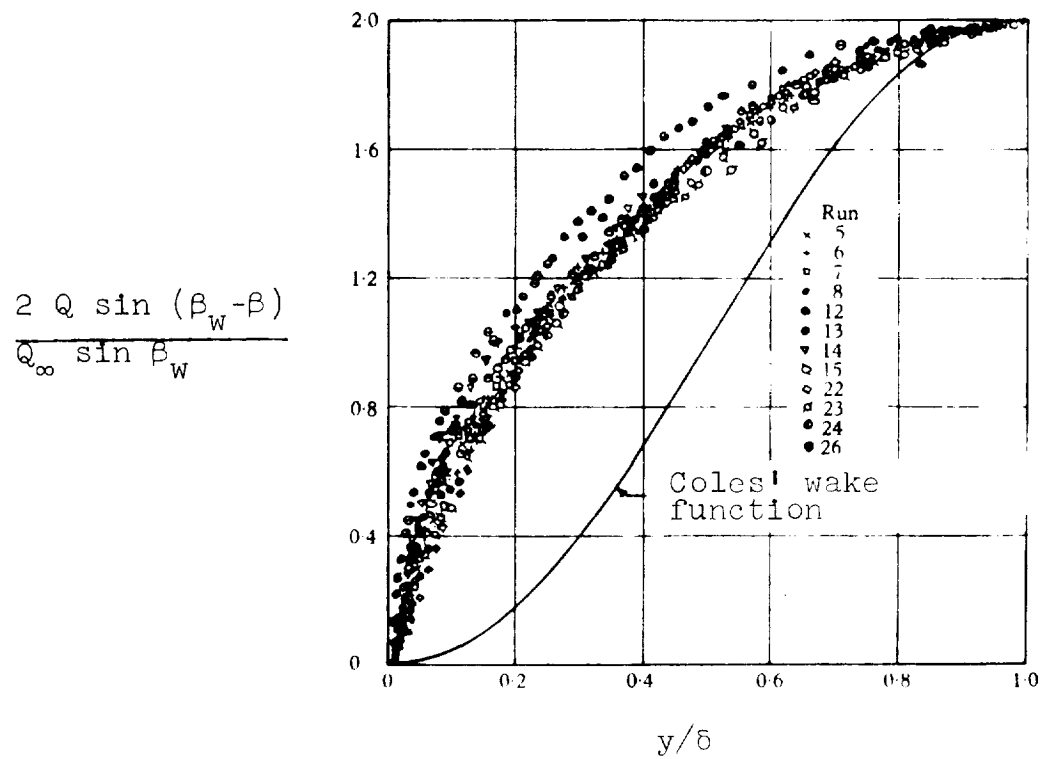


Figure 1.12 - Wake Function Component for Hornung and Joubert (1963)

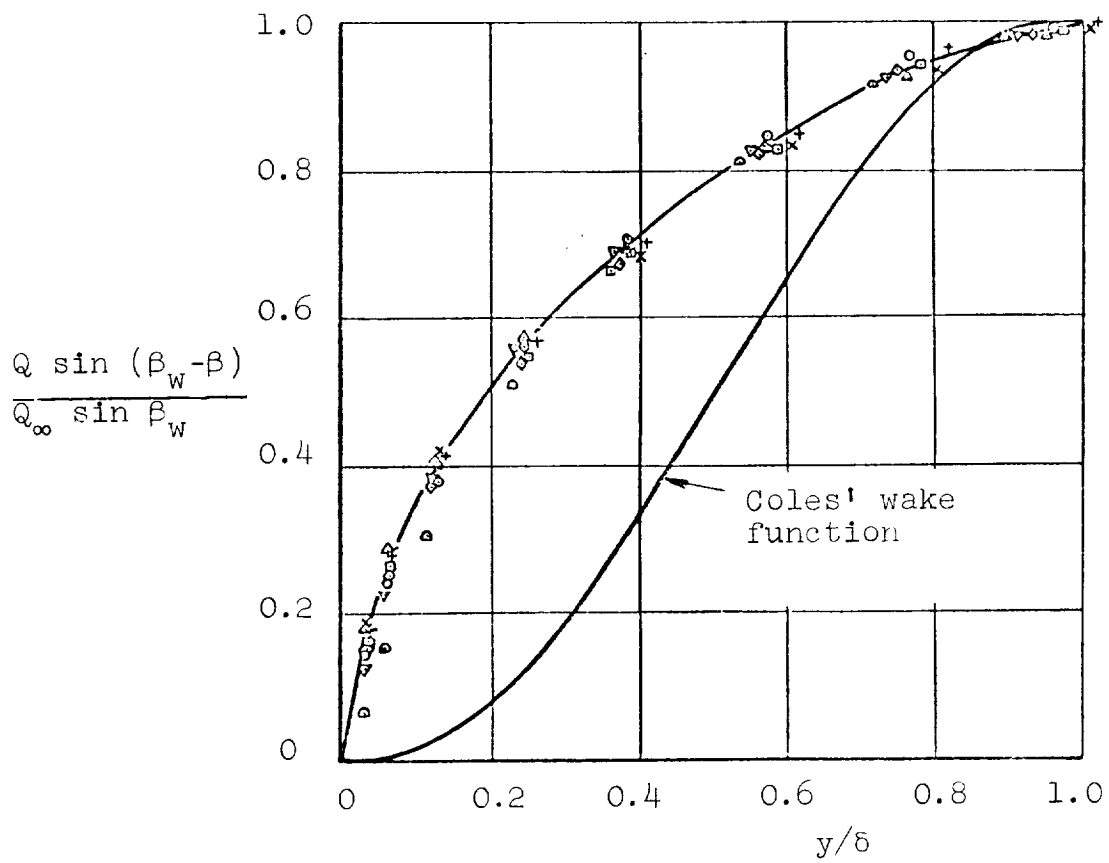


Figure 1.13 - Wake Function Component for East and Hoxey (1969)

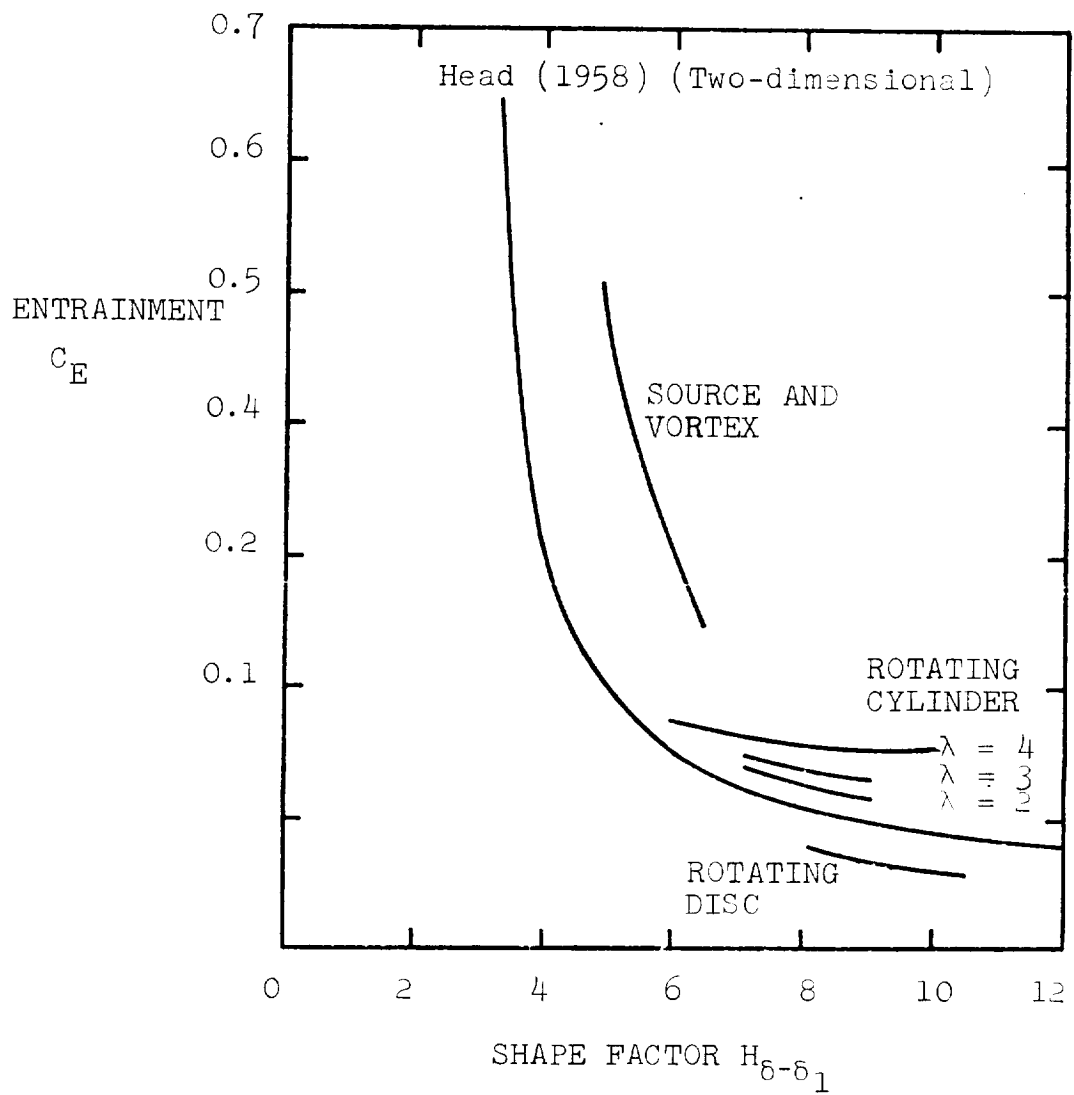


Figure 1.14 - Entrainment Functions from Cham (1968)



## CHAPTER 2

### SHEAR STRESS MODELS

#### A. General Considerations

As mentioned in Chapter 1, a differential prediction method requires closure assumptions for the turbulent shear stresses. Since the mechanisms of turbulence production in three dimensions are not expected to be essentially different from those in two dimensions, logical extensions of two dimensional closure models are expected to be appropriate. At the 1968 Stanford Conference (Kline et. al. 1969) differential methods with closure assumptions based on an eddy viscosity and differential methods with closure assumptions based the turbulence kinetic energy equation placed in the top third, according to the evaluation committee. Differential methods using a third assumption, the mixing length model, placed in the middle third. In the present work, three-dimensional methods using extensions of all three types of closure assumptions above have been studied and compared to the data.

For purposes of discussing fluid stresses, turbulent boundary layers can be considered to have two principal regions, an inner region or viscous sublayer in which the effects of molecular viscosity predominate and an outer turbulent region in which the turbulent or Reynolds stresses are dominant. For the present work, calculations are only made in the fully turbulent region and empirical functions are used to bridge the gap that links the turbulent region to the sublayer and the wall. Thus, for example, the "no slip" condition at the wall is not satisfied explicitly but the "law of the wall" is used in its place. Experimental data indicates that at  $y^+ = 30$  the velocity profile has deviated very

little from what would be expected in a fully turbulent flow near a wall. Thus  $y^+ = 30$  has been selected for the innermost mesh point in the calculation scheme where  $y^+ = yQ_\tau/\nu$  and  $Q_\tau$  is  $\sqrt{\tau_w}/\rho$ . Extrapolation to obtain wall stress and the angle  $\beta_w$  are thus important parts of the methods developed.

## B. Shear Stress Closure Assumptions

In this chapter, only those closure assumptions which we have actually used for computations are described. A more complete summary and discussion of closure assumptions is given by Reynolds (1970).

### B.1 Mixing Length Closure

The oldest of the shear stress closure assumptions is the mixing length hypothesis. Spalding used such a model in the work he did for the 1968 Stanford conference (Kline et. al. 1969). In the present work, some computations of experimental flows have been made using the mixing length and it has also been used extensively to generate starting shear stress profiles. In two-dimensional flows the mixing length  $\ell$  is defined by

$$\tau = \rho \ell^2 \left| \frac{\partial u}{\partial y} \right| \frac{\partial u}{\partial y} \quad (2.1a)$$

By analogy to laminar flow, an eddy viscosity can be defined as

$$\tau = \rho \epsilon \frac{\partial u}{\partial y} \quad (2.1b)$$

so the eddy viscosity is

$$\epsilon = \ell^2 \frac{\partial u}{\partial y} \quad (2.1c)$$

$\ell$  must be selected to produce shear stresses which agree with available data. This has been done on a number of occasions (e.g. Spalding at the Stanford conference) and a useful formulation is

$$\begin{aligned}
\ell &= \kappa y & y/\delta_{995} &< \frac{0.079}{\kappa} \\
\ell &= 0.079\delta_{995} & y/\delta_{995} &> \frac{0.079}{\kappa} \\
\kappa &= 0.40
\end{aligned} \tag{2.2}$$

where  $\delta_{995}$  is defined as the value of  $y$  where  $Q/Q_\infty$  is 0.995.

A possible extension of this model to three dimensions is to take

$$\epsilon = \ell^2 \left| \frac{\partial \vec{Q}}{\partial y} \right| \tag{2.3}$$

where  $\vec{Q}$  is the velocity vector parallel to the wall

$$\vec{Q} = \vec{i}U + \vec{j}W \tag{2.4}$$

so

$$\frac{\partial \vec{Q}}{\partial y} = \vec{i} \frac{\partial U}{\partial y} + \vec{j} \frac{\partial W}{\partial y} \tag{2.5}$$

or

$$\left| \frac{\partial \vec{Q}}{\partial y} \right| = \sqrt{\left( \frac{\partial U}{\partial y} \right)^2 + \left( \frac{\partial W}{\partial y} \right)^2} \tag{2.6}$$

$\ell$  is assumed to be a scalar and to have the same form as that used for two dimensions, e.g. Equation 2.2.

The shear stress direction can be calculated by assuming that the eddy viscosity  $\epsilon$  is a simple isotropic scalar. That is,  $\epsilon$  is assumed to behave like a molecular viscosity in a sheared fluid except that the eddy viscosity is much larger. Thus, by analogy with equation 1.11a and 1.11b

$$\tau_x = \rho \epsilon \frac{\partial U}{\partial y} \tag{2.7a}$$

$$\tau_z = \rho \epsilon \frac{\partial W}{\partial y} \tag{2.7b}$$

This would be a good assumption if boundary layer turbulence were a random, disoriented type of motion such as occurs behind a grid. However, boundary layer turbulence appears to have a vorticity with favored directions and so the isotropic eddy viscosity is at best a crude approximation.

The mixing length model used here then consists of eqs. (2.2), (2.3), (2.6) and (2.7a and b).

## B.2 Eddy Viscosity Model

Mellor (1967) and others have used a variation of the mixing length hypothesis called the eddy viscosity model. Both Mellor and Cebeci used such methods successfully at the 1968 conference. The two-dimensional form of Mellor formulation\* is the same as the mixing length model in the inner portion of the fully turbulent part of the layer:

$$\epsilon_{\text{inner}} = (\kappa y)^2 \left| \frac{\partial U}{\partial y} \right| \quad (2.8a)$$

In the outer portion, Mellor suggests use of a constant eddy viscosity

$$\epsilon_{\text{outer}} = (0.016) \delta_1 U_{\infty} \quad (2.8b)$$

This model can be extended to three dimensions using the same idea discussed for the mixing length model, i.e.

$$\epsilon_{\text{inner}} = (0.4y)^2 \sqrt{\left( \frac{\partial U}{\partial y} \right)^2 + \left( \frac{\partial W}{\partial y} \right)^2} \quad (2.9a)$$

$$\epsilon_{\text{outer}} = 0.016 \delta_1 Q_{\infty} \quad (2.9b)$$

The shear stresses in Mellor (1967) are also computed on the basis of an isotropic eddy viscosity so equations 2.7a and 2.7b also apply to the eddy viscosity model used in this study.

## B.3 Two-Dimensional Bradshaw Model (Turbulent Energy Equation)

Bradshaw (1967) proposed a two-dimensional shear stress model following earlier work of Townsend (1960). It is based on the turbulence kinetic energy equation (see Reynolds morphology (Kline et. al. 1969)).

---

\*Mellor uses  $\kappa = 0.41$  but 0.4 has been used in the present work.

$$\frac{1}{2} \rho \left[ U \frac{\partial \overline{q^2}}{\partial x} + V \frac{\partial \overline{q^2}}{\partial y} \right] = \overbrace{\tau \frac{\partial U}{\partial y}}^{\text{production}} - \overbrace{\frac{\partial}{\partial y} \left[ \overline{p'v'} + \frac{1}{2} \rho \overline{q^2 v'} \right]}^{\text{diffusion}} \quad (2.10)$$

$$\underbrace{+ \rho \epsilon}_{\text{dissipation}}$$

Bradshaw made a number of assumptions in order to make this equation useful for computations. First he assumed that the turbulent shear stress is roughly proportional to the turbulent kinetic energy

$$\tau = a \overline{q^2} \quad (2.11)$$

As a first approximation, Bradshaw concluded that a constant value of 0.15 for  $a$  would be satisfactory but said that  $a$  could be made a function of  $y$  if necessary. The dissipation term is approximated by

$$\epsilon = \frac{(\tau/\rho)^{3/2}}{L} \quad (2.12)$$

where  $L$  is the dissipation length, a function of  $y$ . Finally, Bradshaw made a large eddy transport assumption for the diffusion term and postulated

$$\frac{\overline{p'v'}}{\rho} + \frac{1}{2} \overline{q^2 v'} = G \tau_{\max}^{1/2} \tau/\rho^{3/2} \quad (2.13)$$

where  $G$  is a universal function of  $y$ . Bradshaw suggests functional forms for  $L$  and  $G$  based on his examinations of data (Figure 2.1).

The resulting equation for the shear stress is:

$$U \frac{\partial}{\partial x} \left( \frac{\tau}{2a\rho} \right) + V \frac{\partial}{\partial y} \left( \frac{\tau}{2a\rho} \right) = \frac{\tau}{\rho} \frac{\partial U}{\partial y} - \frac{1}{L} \left( \frac{\tau}{\rho} \right)^{3/2} - \frac{\tau_{\max}^{1/2}}{\rho} \frac{\partial}{\partial y} \left( \frac{G\tau}{\rho} \right) \quad (2.14)$$

In the remainder of this report,  $\tau/\rho$  will be replaced by  $\tau$  for simplicity.

Bradshaw's prediction method performed well at the 1968 Stanford conference. One feature which makes it significantly different from the mixing length and eddy viscosity models treated in this report is that

it allows for a "shear lag". That is, a given mean velocity profile can have different shear stress profiles depending on the past history of the flow. In the mixing length and eddy viscosity models used in this report, the shear stress is a unique function of the mean velocity profile.

Another interesting feature of the Bradshaw method is that with the large eddy assumption for the diffusion, the equation system is hyperbolic. Bradshaw and his coworkers (Bradshaw 1967) proved this point by deriving the direction of the characteristic lines and the appropriate ordinary differential equations valid along the characteristics. In fact, Bradshaw's computer programs for both two and three-dimensional calculations uses the method of characteristics. The mixing length and eddy viscosity assumptions discussed here produce parabolic equations as do the laminar flow shear stresses and are thus not solvable by the method of characteristics.

Experiments show that for flows not too near separation,  $\tau$  varies slowly (by factors of 2 at the most) as the wall is approached. In addition,  $U$  and  $V$  decrease as the wall is approached. Thus, to first approximation, the mean convective terms on the left of Equation 2.14 do not change order as the wall is approached. Since near the wall,  $G$  and  $L$  are small and  $\frac{\partial U}{\partial y}$  is large, the dominant terms in Equation 2.14 are the production and dissipation terms. Thus

$$\tau \frac{\partial U}{\partial y} = \frac{\tau^{3/2}}{L} \quad (2.15)$$

or

$$\tau = L^2 \left( \frac{\partial U}{\partial y} \right)^2 \quad (2.16)$$

Since Bradshaw has proposed that  $L = \ell = 0.4y$  in the inner part of the turbulent region of the flow, it can be seen that near the wall, the Bradshaw method reduces to a mixing length method. In some cases however, the shear stress will lag the equilibrium (mixing length) value which Equation 2.16 would predict.

#### B.4 Nash Method (Turbulent Energy Equation)

Nash (1969) proposed a three-dimensional extension of the Bradshaw model. The equation for the shear stress magnitude proposed by Nash (an approximation of the three-dimensional turbulence kinetic energy equation) is

$$U \frac{\partial \tau}{\partial x} + V \frac{\partial \tau}{\partial y} = 2a \left[ \tau_x \frac{\partial U}{\partial y} + \tau_z \frac{\partial W}{\partial y} - \frac{\tau^{3/2}}{L} - \frac{\partial}{\partial y} \left( G \tau_{\max}^{1/2} \right) \right] \quad (2.17)$$

To find the direction of the shear stress, Nash used the isotropic eddy viscosity formulation which may be written

$$\frac{\tau_x}{\tau_z} = \frac{\partial U / \partial y}{\partial W / \partial y} \quad (2.18)$$

Nash also proposed slightly different values of  $L$  and  $G$  than given by Bradshaw. In the present work, predictions which are labeled Nash use the Bradshaw functions for  $L$  and  $G$ , but equations 2.17 and 2.18 to compute the shear stress.

#### B.5 Three-Dimensional Bradshaw Method (Turbulent Energy Equation)

When Bradshaw himself approached the three-dimensional problem, he took a different approach from that of Nash. Bradshaw started with the exact equations for the mean  $x$  and  $y$  components of the Reynolds stress,  $-\rho \overline{u'v'}$  and  $-\rho \overline{v'w'}$ . With some approximations and the requirement that the results be compatible with his two-dimensional result, he suggested the following equations:

$$U \frac{\partial \tau_x}{\partial x} + V \frac{\partial \tau_x}{\partial y} = 2a \left[ \tau \frac{\partial U}{\partial y} - \frac{\tau_x \tau^{1/2}}{L} - \frac{\partial}{\partial y} \left( G \tau_{\max}^{1/2} \tau_x \right) \right] \quad (2.19)$$

$$U \frac{\partial \tau_z}{\partial x} + V \frac{\partial \tau_z}{\partial y} = 2a \left[ \tau \frac{\partial W}{\partial y} - \frac{\tau_z \tau^{1/2}}{L} - \frac{\partial}{\partial y} \left( G \tau_{\max}^{1/2} \tau_z \right) \right] \quad (2.20)$$

Alternatively, these equations can be expressed as Equation 2.17 for the shear stress magnitude and an equation for the shear stress direction,

$(\tau_z/\tau_x)$ :

$$U \frac{\partial \tau_z/\tau_x}{\partial x} + V \frac{\partial \tau_z/\tau_x}{\partial y} = 2a \left[ \frac{\tau}{\tau_x^2} \left( \tau_x \frac{\partial W}{\partial y} - \tau_z \frac{\partial U}{\partial y} \right) - G \tau_{\max}^{1/2} \frac{\partial}{\partial y} \left( \frac{\tau_z}{\tau_x} \right) \right] \quad (2.21)$$

This equation differs from the isotropic eddy viscosity model in two important respects. First, the addition of the diffusion term means that in the outer part of the layer, the equilibrium shear stress direction can be different from the direction of the mean velocity gradient. Secondly, the shear stress vector direction can lag the equilibrium value.

A total of four three-dimensional shear stress models have been presented here. They are summarized in Table 2.1. The mixing length and eddy viscosity models are similar in most respects and thus extensive calculations have been done only with the eddy viscosity model. Any one of these shear stress models, together with the momentum and continuity equations (equations 1.8 to 1.10) form a closed set. The only additional requirement needed to perform calculations are the boundary conditions, both at the wall and at the outer edge of the boundary layer.

## C. Boundary Conditions

### C.1 Outside Edge Boundary Conditions

For infinite wing flows, the boundary layer velocity is forced to be the prescribed free stream velocity by allowing

$$\lim_{y \rightarrow \infty} U \frac{\partial U}{\partial x} = - \frac{dP}{dx} \quad (2.22)$$

Since  $\frac{\partial P}{\partial z}$  is zero,

$$\lim_{y \rightarrow \infty} U \frac{\partial W}{\partial x} = 0 \quad (2.23a)$$

so

$$W_{\infty} = \text{constant} \quad (2.23b)$$

For the axisymmetric vaneless diffuser cases, the outer conditions are:

$$\lim_{y \rightarrow \infty} \left( U \frac{\partial U}{\partial x} - \frac{W^2}{R} \right) = - \frac{dP}{dx} \quad (2.24)$$

and

$$\lim_{y \rightarrow \infty} \left( U \frac{\partial W}{\partial x} + \frac{UW}{R} \right) = 0 \quad (2.25)$$

As the edge of the boundary layer is approached,  $\frac{\partial U}{\partial y}$  and  $\frac{\partial W}{\partial y}$  become zero and the shear stresses also approach zero. In the computations, the grid is expanded in the  $y$  direction so that these conditions are satisfied by increasing the distance between the mesh points. In some cases, this has required that the computing grid be extended to 1.88<sub>995</sub>.

### C.2 Wall Boundary Conditions

The general boundary conditions which must be satisfied at solid walls are the "no flow" (conservation of mass) and "no slip" conditions which specify that the  $y$ ,  $x$  and  $z$  components of velocity are zero at the surface. However, in the region close to the wall ( $y^+ \approx 30$ ), the fluid velocity changes very rapidly with increasing  $y$  - in fact,

it is common for the velocity to reach 50% of the free stream velocity in only 5% of the boundary layer thickness. This large  $y$  gradient of velocity, which would require a large number of grid points for computation, combined with the necessity of considering both turbulent and viscous shear stresses in the wall regions makes it desirable to use empirical functions to pass over this region. This approach does not satisfy the no-slip, no flow conditions directly. These conditions are implicit in the empirical functions.

In two-dimensional flows, a function known as the "law of the wall" describes the velocity profile in the wall region

$$\frac{Q}{Q_\tau} = f(yQ_\tau/\nu) \quad (2.26)$$

In the fully turbulent part of the flow, the law of the wall takes the form

$$\frac{Q}{Q_\tau} = \frac{1}{\kappa} \ln \frac{yQ_\tau}{\nu} + A \quad (2.27)$$

This expression can be derived from the mixing length formula if it is assumed that the shear stress is constant, and equal to the wall value. Equation 2.27 also applies to three-dimensional flows if the assumption

$$\left| \frac{\partial \vec{Q}}{\partial y} \right| = \frac{\partial Q}{\partial y} \quad (2.28)$$

can be made; an assumption which is quite good in most cases. In fact if the velocity direction has a linear variation of 4 degrees (which is high) between the wall and  $y^+ = 30$ ,  $\left| \frac{\partial \vec{Q}}{\partial y} \right|$  deviates from  $\partial Q / \partial y$  by less than 5% at a  $y^+$  of 30. The deviation is less at lower values of  $y^+$ . A somewhat more general form of Equation 2.27 is found if it is assumed that the shear stress magnitude varies linearly between the wall

and the point in question. The resulting expression, which was first derived by Townsend for two-dimensional flow (in a slightly more sophisticated form) is:

$$\frac{Q}{Q_\tau} = \frac{1}{\kappa} \ln \frac{yQ_\tau}{\nu} + A + \frac{1}{\kappa} \left[ 2 \ln \frac{2}{(1+x)^{1/2} + 1} + 2(1+x)^{1/2} - 1 \right] \quad (2.29)$$

where

$$x = \tau/\tau_w - 1$$

In our computations, this expression is used to compute the wall shear stress magnitude by substitution of the value of the computed velocity,  $Q$ , and shear stress  $\tau$  at the first mesh point out from the wall and iterating to get  $Q_\tau$ .  $\kappa$  is taken to be 0.4 and  $A$  to be 5.0. The wall shear stress thus obtained reenters the calculations because it is used to calculate the shear stress gradients  $\partial\tau_x/\partial y$  and  $\partial\tau_z/\partial y$ , which appear in equations 1.9 and 1.10, at the first mesh point.

To calculate the shear stress gradients, it is also necessary to know the direction of the wall shear stress. The direction of the shear stress vector changes much more rapidly than the direction of the velocity vector in the wall region. This can be seen by examining the polar plot shown in Figure 2.2 and noting that if the isotropic eddy viscosity assumption is valid it follows that

$$\frac{\tau_z}{\tau_x} = \left( \frac{\partial w / \partial y}{\partial u / \partial y} \right) = \left( \frac{\partial w}{\partial u} \right) \quad (2.30)$$

Between the origin and the peak of the polar plots, the shear stress direction has varied from  $\beta_w^+$  to zero whereas the direction of the

---

<sup>+</sup>At the wall, the shear stress and the limiting wall streamline must have the same direction.

velocity has changed only slightly. Several methods were tried to find the direction of the wall shear stress (Appendix B) but difficulties were found with most of them. The most satisfactory method appeared to be extrapolating to the wall from the first point away from the wall by a Taylor series where the derivatives  $\frac{\partial \gamma}{\partial y}$  and  $\frac{\partial^2 \gamma}{\partial y^2}$  are estimated from the first three mesh points in the  $y$  direction.

$$\gamma_w = \gamma_1 - \frac{\partial \gamma}{\partial y} y_1 + 0.5 \frac{\partial^2 \gamma}{\partial y^2} y_1^2 \quad (2.31)$$

This is a slight improvement over simple linear extrapolation from the first two mesh points away from the wall.

The final boundary condition is the specification of the normal velocity at the first mesh point,  $V_1$ .  $V_1$  can be found from an integration of continuity (equation 1.8)

$$V_1 = \int_0^{y_1} \left( \frac{\partial U}{\partial x} + \frac{U}{R} \right) dy \quad (2.32)$$

If it is assumed that the flow is collateral between the wall and the first mesh point

$$U = Q \cos \gamma_1 \quad (2.33)$$

and

$$\frac{\partial U}{\partial x} = \frac{\partial Q}{\partial x} \cos \gamma_1 - Q \sin \gamma_1 \frac{\partial \gamma_1}{\partial x} \quad (2.34)$$

The velocity  $Q$  was assumed to be represented by Equation 2.27 between  $y^+ = 11$  and  $y^+ = 30$  and by

$$\frac{Q}{Q_\tau} = y Q_\tau / \nu \quad (2.35)$$

from the wall to  $y^+ = 11$ . If the differentiation of Equations 2.27 and 2.35 and subsequent integration of Equation 2.32 are performed, the following expression is obtained for  $V$  at  $y^+ = 30$ :

$$v_{y^+=30} = \cos \gamma_1 \left( 405v \frac{\partial Q_\tau}{\partial x} / Q_\tau + 298v/R \right) + 296.5 \sin \gamma_1 \frac{\partial \gamma_1}{\partial x} v \quad (2.36)$$

$\frac{\partial Q_\tau}{\partial x}$  and  $\frac{\partial \gamma_1}{\partial x}$  are evaluated by differencing from previously computed profiles. In most cases, the first mesh point is very close to the wall and  $V_1 = 0$  is a satisfactory approximation. This assumption ( $V_1 = 0$ ) has been made in the plane of symmetry flows but expression 2.36 above has been used for the other flows.

#### D. Summary

The basic idea pursued in this report is that until each of the ideas presented here for shear-stress closure of the three-dimensional boundary layer problem is tested, it is futile and perhaps unnecessary to develop new and potentially more complex schemes. In the following chapter a numerical computing scheme into which each of these shear stress models can be tested is developed. The computing method is not intended to be the ultimate in efficiency, but rather to allow a proper test of the closure models outlined here. The computed results are compared with actual data and to each other in chapters 4 and 5. Without proof at this point, it is worth stating one of our principal conclusions: the current shear-stress closure models are sufficiently accurate to deal with all problems (except possibly those of the rotating disk type which was not tested) on which data are currently available. Thus, on a practical level we do not recommend major theoretical efforts on closure schemes for this kind of problem at the present time.

Table 2.1 SHEAR STRESS MODELS

1. MIXING LENGTH

$$\tau_x = \ell^2 \left( \frac{\partial U}{\partial y}^2 + \frac{\partial U}{\partial y}^2 \right)^{1/2} \frac{\partial U}{\partial y}$$

$$\tau_z = \ell^2 \left( \frac{\partial U}{\partial y}^2 + \frac{\partial W}{\partial y}^2 \right)^{1/2} \frac{\partial W}{\partial y}$$

$$\ell = 0.4y \quad y/\delta_{995} = < 0.198$$

$$\ell = 0.079\delta_{995} \quad y/\delta_{995} = > 0.198$$

2. EDDY VISCOSITY

$$\tau_x = \epsilon \frac{\partial U}{\partial y}$$

$$\tau_z = \epsilon \frac{\partial W}{\partial y}$$

$$\epsilon_{\text{inner}} = (0.4y)^2 \left( \frac{\partial U}{\partial y}^2 + \frac{\partial W}{\partial y}^2 \right)^{1/2}$$

$$\epsilon_{\text{outer}} = 0.016\delta_1 Q_\infty$$

3. TURBULENCE KINETIC ENERGY

$$U \frac{\partial \tau}{\partial x} + V \frac{\partial \tau}{\partial y} = 0.3 \left( \tau_x \frac{\partial U}{\partial y} + \tau_z \frac{\partial W}{\partial y} - \frac{\tau^{3/2}}{L} - \frac{\partial}{\partial y} G \tau_{\text{max}}^{1/2} \right)$$

3a. NASH

$$\tau_z/\tau_x = (\partial W/\partial y)/(\partial U/\partial y)$$

3b. BRADSHAW

$$U \frac{\partial \tau_z/\tau_x}{\partial x} + V \frac{\partial \tau_z/\tau_x}{\partial y} = 0.3 \left[ \frac{\tau}{\tau_x} \left( \frac{\partial W}{\partial y} - \tau_z \frac{\partial U}{\partial y} \right) - G \tau_{\text{max}}^{1/2} \frac{\partial (\tau_z/\tau_x)}{\partial y} \right]$$

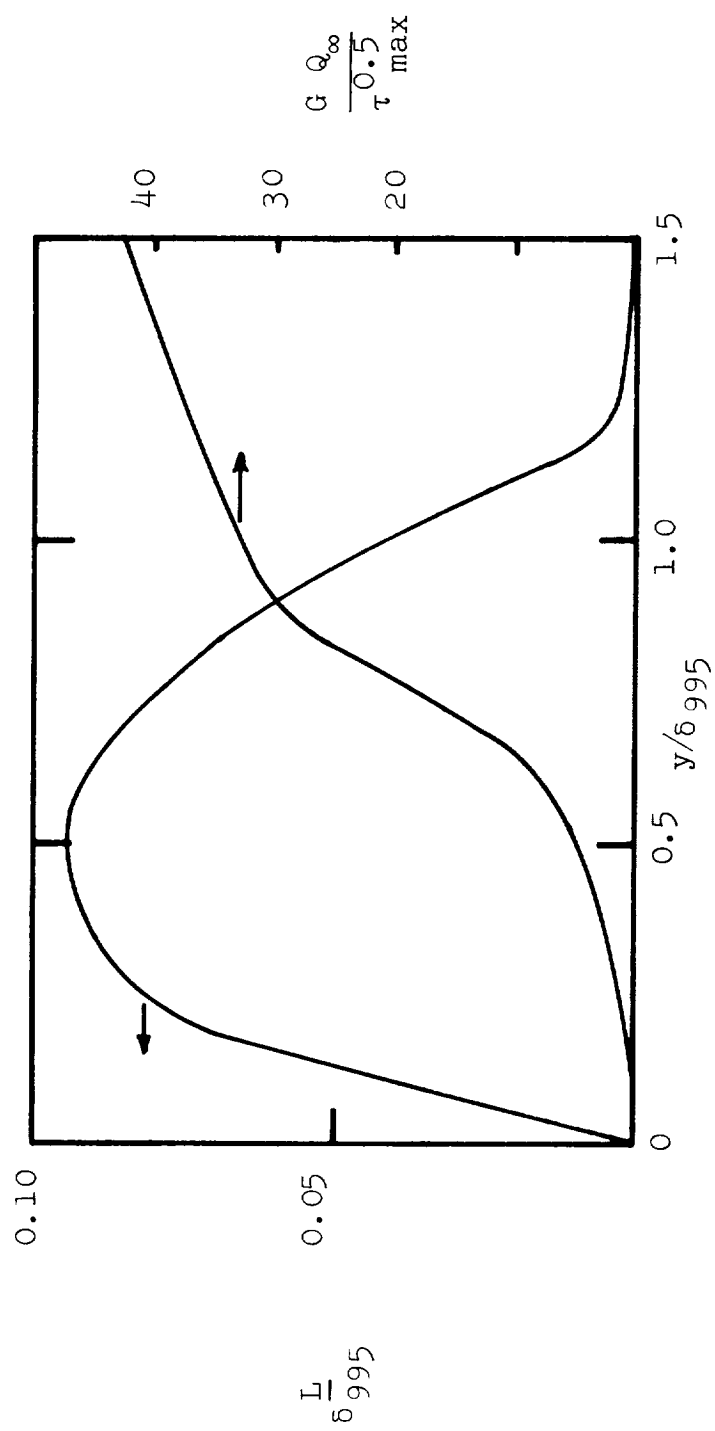


Figure 2.1 Bradshaw L and G Functions

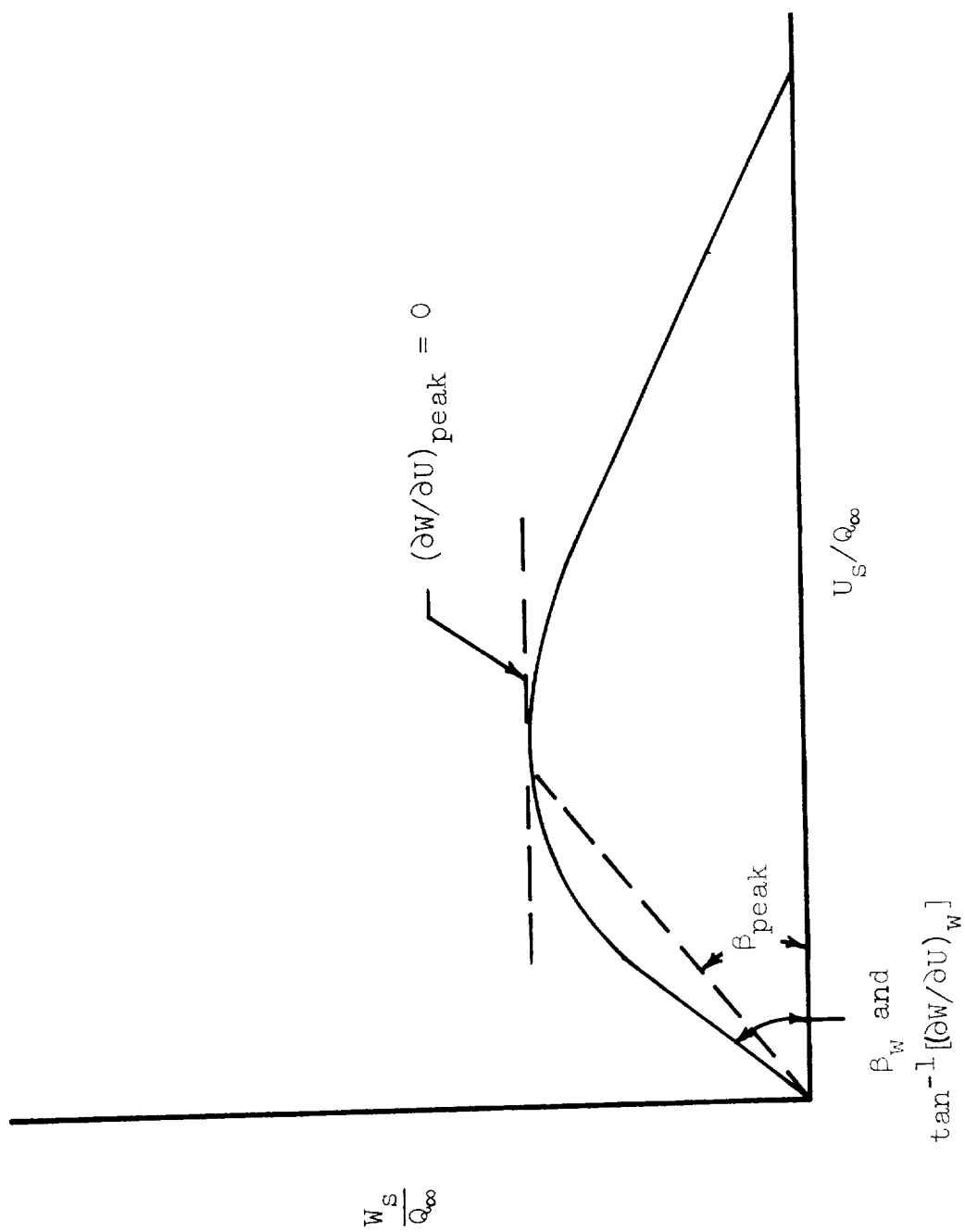


Figure 2.2 Polar Plot Showing Variation of Direction of Velocity and Velocity Gradient Near Wall

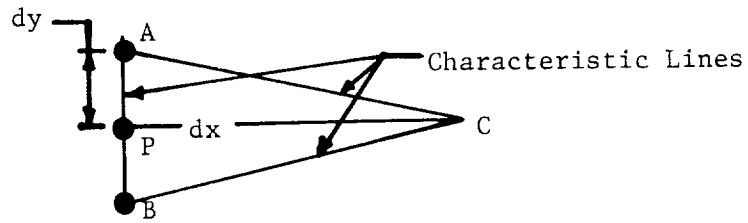
## CHAPTER 3

### NUMERICAL METHOD

#### A. General Considerations

The numerical method adopted here is similar to that used by Nash (1968, 1969). Although the general approach and some specific details are due to Nash, the actual computer program and fine points of the numerics were developed independently. Very recently Nash (1971) developed a more sophisticated numerical technique but this has not been used in the present work. The procedure can best be described as an explicit forward difference method. Explicit methods are often criticized because they require a large number of steps in the  $x$  direction - in fact it can be demonstrated that explicit methods become unstable in many problems if the  $x$ -step is too long. Implicit methods, on the other hand, can often take as long a step as is desired, numerical accuracy providing the upper limit on step length. Nevertheless, the explicit method used seems well suited to the present application for a number of reasons:

1. The sets of equations formed with two of the proposed shear stress models being tested (Nash and Bradshaw) are hyperbolic, not parabolic as are the laminar boundary layer equations and turbulent boundary layer equations using an eddy viscosity closure assumption. This means that there exist real characteristic lines and regions of dependence and independence.



In the sketch, the region within the triangle contains flow which is entirely determined by information on the line AB. This information in a finite difference approximation consists of the values of, and derivatives of, the dependent variables at point P. An attempt to extrapolate from point P to a point beyond point C would require information from outside the interval AB. The net effect is an upper limit on the x-step,  $dx$ , which is proportional to the y-step,  $dy^*$ . This limited x-step is in fact considerably shorter than would be required by an implicit method simply for accuracy and thus an important advantage of the implicit method is lost.

2. To use the numerical method described here, it is not necessary to transform the momentum or shear stress equation from the forms in which they are normally presented in the literature - only a minor rearrangement is required. This is particularly useful when, as in the present study, it is required that several possible equations be used.
3. Although a large number of x-steps are required, the computations at each step are less complicated than in most implicit methods

---

\*If one were to carry computations all the way to the wall the minimum y-step would be very small and would require an extremely short x-step. This fact is the main reason the region close to the wall is passed over with empirical functions.

and the computation times for complete flows are not increased in proportion to the number of  $x$ -steps. For example, the present method requires about ten times as many  $x$ -steps as the method used by Mellor and Herring at the 1968 Stanford Conference (Kline et. al. 1969) but requires only about two to three times the computer time. Using 20 mesh points in the  $y$ -direction and Fortran IV, level G on an IBM 360/67, the program executes three to four  $x$ -steps per second. Each step moves a distance of 0.2 to 0.58<sub>995</sub>.

#### B. Numerical Procedure (Overview)

Consider Figure 3.1 on which are shown two successive  $x$  stations and their respective grids in the  $y$  direction. If the values of all variables are known at  $x$  then it is possible by Taylor's series expansion to extrapolate to  $x + dx$  by

$$U_{i,x+dx} = U_{i,x} + dx \left( \frac{\partial U}{\partial x} \right)_{i,x} + O(dx^2) \quad (3.1)$$

where the  $x$ -component of velocity  $U$  is used as an example.  $\left( \frac{\partial U}{\partial x} \right)_{i,x}$  can be obtained from the  $x$ -momentum equation (Equation 1.9).

$$\left( \frac{\partial U}{\partial x} \right)_{i,x} = \frac{1}{U_{i,x}} \left[ - \left( \frac{dP}{dx} \right)_x + \left( \frac{\partial \tau_x}{\partial x} \right)_{i,x} - v_{i,x} \left( \frac{\partial U}{\partial y} \right)_{i,x} \right] \quad (3.2)$$

Of course, some care is required in evaluating the derivatives on the right side of equation and expression 3.1 is an approximation valid only to order  $dx^2$  if  $dx$  is finite. The approximation is improved by first extrapolating to  $(x + dx/2)$ , evaluating  $\left( \frac{\partial U}{\partial x} \right)_{i,x+\frac{dx}{2}}$  at  $(x + dx/2)$  and then extrapolating from  $x$  to  $x + dx$  using

$$U_{i,x+dx} = U_{i,x} + dx \left( \frac{\partial U}{\partial x} \right)_{i,x+\frac{dx}{2}} \quad (3.3)$$

This approach is considered accurate enough for our purposes. For example, in early work, Equation 3.1 was used and was found to produce appreciable errors when  $\frac{dP}{dx}$  was integrated to produce the experimental free-stream velocity in cases with strong adverse pressure gradients. These errors were eliminated when equation 3.3 was used.

Each variable except the normal velocity  $V$  can be forward extrapolated in this way. The general procedure (Equation 3.3) is used for  $U$  and  $W$  in the eddy viscosity and mixing length methods,  $U$ ,  $W$ , and  $\tau$  in the Nash method and  $U$ ,  $W$ ,  $\tau_x$  and  $\tau_z$  in the Bradshaw method. The appropriate momentum or shear stress equation is used in each case to evaluate the  $x$ -derivatives as shown by example in Equation (3.2).

$V$ , the normal velocity, need not be extrapolated but can be calculated at the new  $x$  station directly. This is done by eliminating  $\partial U / \partial x$  between the continuity (Equation 1.8) and  $x$ -momentum (Equation 1.9) equation to obtain

$$V = \int_0^y \left[ -\frac{\partial \tau_x}{\partial x} + \frac{\partial P}{\partial x} - \left\{ \frac{U^2 + W^2}{R} \right\} / U^2 \right] dy \quad (3.4)$$

$V_1$  is estimated by the method of Chapter 2 at the first mesh point and then  $V$  at the remaining points is evaluated by a numerical integration of Equation 3.4 from  $y_1$  to the outer mesh point.

The wall shear stress is determined by an iterative process that leads to satisfaction of the law of wall, Equation 2.29. This procedure normally converges in two or three iterations.

The wall shear stress angle,  $\gamma_w$ , is calculated by a Taylor series expansion in  $y$  about the first mesh point.  $\gamma$  is the angle between the projection of local velocity vector in the plane of the wall and the

x axis. Thus the wall value of  $\gamma$ ,  $\gamma_w$ , is found by

$$\gamma_w = \gamma_1 - y_1(\gamma_2 - \gamma_1)/(y_2 - y_1) + 0.5y_1^2[(\gamma_3 - \gamma_2)/(y_3 - y_2) - (\gamma_2 - \gamma_1)/(y_2 - y_1)]/[0.5(y_3 - y_1)] \quad (3.5)$$

Nash (1968) found that an interpolation procedure was necessary at each x-station in order to damp out irregularities in computed profiles which led to numerical instabilities. Our procedure uses alternating meshes at adjacent x-stations. All variables are transferred from one mesh to the other by interpolation after each forward extrapolation. The process of interpolation has the added advantage of enabling the y mesh step size to be adjusted so that the y-mesh always just fills the boundary layer, when the number of y mesh points (usually twenty in our calculation) is fixed.

### C. Numerical Procedure (Details)

#### C.1 Differentiation in y-Direction

Differentiation of all dependent variables except Q, the velocity magnitude, is accomplished by a three point procedure which fits parabolas of the general form

$$\tilde{y} = A + B\tilde{x} + C\tilde{x}^2 \quad (3.6a)$$

to the tabular profiles. In Equation (3.6a)  $\tilde{x}$  is the independent variable (y) and  $\tilde{y}$  is the dependent variable. The coefficients at a point k are found from

$$C = [\xi + (\tilde{y}_k - \tilde{y}_{k-1})/(\tilde{x}_{k+1} - \tilde{x}_k)]/(\tilde{x}_{k-1} - \tilde{x}_{k+1}) \quad (3.6b)$$

$$B = \xi - C(\tilde{x}_{k-1} + \tilde{x}_k) \quad (3.6c)$$

$$A = \tilde{y}_{k-1} - (B + C\tilde{x}_{k-1})\tilde{x}_{k-1}$$

where

$$\xi = (\tilde{y}_k - \tilde{y}_{k-1}) / (\tilde{x}_k - \tilde{x}_{k-1}) \quad (3.6d)$$

The derivative of a dependent variable at the point  $k$  is thus

$$\frac{\partial \tilde{y}}{\partial \tilde{x}_k} = B + 2C\tilde{x}_k \quad (3.7)$$

The velocity magnitude presents greater difficulty. In the inner regions, because the solution behaves like the law of the wall, it is close to logarithmic in form. This is not the case in the outer parts of the layer. Simple, parabolic fitting does not produce accurate derivatives in the logarithmic region. In early stages of the work, a logarithmic fitting procedure was used in the inner region and parabolic in the outer region but a suitable, general cross-over point proved difficult to find. Finally, it was decided to subtract from the velocity magnitude profile the value which would be computed by Equation 2.27. The difference,  $\hat{Q}$  was then differentiated by the parabolic method and the desired result found from

$$\frac{\partial Q}{\partial y} = \frac{\partial \hat{Q}}{\partial y} + 2.5Q_\tau / y \quad (3.8)$$

At the first mesh point,  $y_1$ , a two point rather than a three point method was used to differentiate  $\hat{Q}$ .

## C.2 Integration in $y$ -Direction

Integration is also performed by fitting parabolas. If an integral from  $\tilde{x}_{i-1}$  to  $\tilde{x}_i$  is desired, the coefficients are found by use of equation 3.6 and the result is

$$\begin{aligned} \int_{\tilde{x}_{i-1}}^{\tilde{x}_i} \tilde{y} dy &= A(\tilde{x}_i - \tilde{x}_{i-1}) + \frac{1}{2} B(\tilde{x}_i^2 - \tilde{x}_{i-1}^2) \\ &+ \frac{1}{3} C(\tilde{x}_i^3 - \tilde{x}_{i-1}^3) \end{aligned} \quad (3.9)$$

### C.3 Interpolation

The grid points are distributed in the  $y$  direction so their spacing is small near the wall and larger toward the edge of the layer. The form chosen to obtain such a spacing is

$$y_i = \delta[\varphi i/N + (1-\varphi)(i/N)^2] + C \quad (3.10)$$

where  $N$  is the number of points in the  $y$  direction;  $i$  is the point number (1, 2 etc.); and  $\varphi$  takes on a value of either 0.2 or 0.4. The constant  $C$  is adjusted so that the first mesh point occurs at a desired value of  $y^+$ , usually 30.  $\delta$  is an arbitrary multiple of  $\delta_{995}$ . The multiple is usually set at 1.6 but values from 1.4 to 2.2 have been used for various flows.  $\delta/\delta_{995}$  is selected so that the profiles do not become "clipped" at the outer edge (see section C.1 in Chapter 2).

At alternate  $x$ -stations two different grids computed by Equation 3.10 are used. This is accomplished by alternating  $\varphi$  between 0.2 and 0.4. Variables are transferred from one grid to the other by interpolation. Interpolation at each  $x$ -station can cause problems. If only a very small error is made at each step and if it is always in the same direction, after many steps, the accumulated error can be large. A parabolic fitting procedure was found to be adequate for all variables except the velocity magnitude. Four points are used for each fit as shown in Figure 3.3. The average value of the two fitted parabolas is accepted as the result.

The velocity magnitude presents much the same problems for interpolate as it does for differentiation. It is even more critical to interpolate accurately particularly as good performance is required near the outer edge of the boundary layer so that  $\delta_{995}$  can be determined with

precision. A number of things were tried but ultimately the two-dimensional law of the wall-wake was found to work very well. The two-dimensional law of the wall-wake (Coles 1956) is assumed to approximate the velocity magnitude, i.e.

$$Q = Q_{\tau} [2.5 \ln y Q_{\tau} / \nu + 5 + 2.5 \Pi (1 - \cos(\pi y / \delta))] \quad y < \delta \quad (3.11a)$$

$$Q = Q_{\infty} \quad y > \delta \quad (3.11b)$$

where the wake function is approximated by a cosine form. In this application  $\delta$  was taken as  $\delta_{995}$ .  $\Pi$  was then evaluated so that Equation 3.11 matched the known value of  $Q_{\infty}$  at  $y = \delta_{995}$ . The value of  $Q$  computed by Equation 3.11 was then subtracted from the tabular  $Q$  profile. Parabolic interpolation was performed on the difference between the tabular profile and the result of Equation (3.11) and a value computed by Equation 3.11 added to obtain the final result.

#### C.4 Length of x-Step

As mentioned previously, the Nash and Bradshaw methods result in hyperbolic equation sets. If too large an x-step is taken, the methods become unstable and diverge very rapidly. Setting the x-step as a simple fixed fraction of  $\delta_{995}$  was tried but instability resulted in some cases. It was reasoned that although the method of characteristics is not being used explicitly, the same stability criterion should be applicable to the present approach to the problem. Regions of dependence and independence will be the same. Thus it was decided to use the criterion for the step length used by Bradshaw (1967).

$$dx = (dy / \tan \alpha)_{\min} \quad (3.12)$$

where  $\alpha$  is the angle of the characteristic lines. From Bradshaw (1967) the characteristic angles are computed from

$$\alpha = V + aG\tau_{\max}^{1/2} \pm (a^2 G^2 \tau_{\max}^2 + 2a\tau)^{1/2}/U \quad (3.13)$$

No problems with instability were encountered when this approach was used. This criterion is also used for the eddy viscosity and mixing length calculations, although not needed, in order to maintain approximately the same  $x$ -step and thus eliminate possible differences in accuracy of the respective results due to  $x$ -step differences.

### C.5 Integral Parameters

In order to compare data to computed results all the integral parameters defined in Chapter 1 are calculated at each  $x$ -station where printout is required. The integration procedure of section C.2 is used for this purpose. The portion of the integrals between the wall and the first mesh point are evaluated in much the same way as the normal velocity  $V$  is calculated - by assuming that Equation 2.35 is valid to  $y^+ = 11$  and Equation 2.27 from  $y^+ = 11$  to the first point. For this calculation the flow is assumed collateral in this region.

### C.6 Starting Profiles

In order to start calculations, it is necessary to have profiles of  $U$  and  $W$  at the first  $x$ -station. The Nash and Bradshaw methods also require starting shear stress profiles. It is possible to input these profiles or to generate them from integral parameters given at the starting value of  $x$ . The streamwise velocity profile is generated here by using Equation 3.11 with  $U_s$  substituted for  $Q$  and the streamwise component of the shear stress used for  $Q_\tau$

$$U_{\tau s} = Q_\tau \sqrt{\cos \beta_w} \quad (3.14)$$

$U_{\tau s}$ , and  $\Pi$  are evaluated by inputing values of  $H$ ,  $\theta_{11}$  and  $Q_{\infty}$  at the start. The following equations (Coles 1956)

$$\frac{Q_{\infty}}{U_{\tau s}} = \frac{1}{\kappa} \ln \frac{\delta U_{\tau s}}{\nu} + 5.0 + \frac{2\Pi}{\kappa} \quad (3.15a)$$

$$\kappa \frac{(\delta_1 - \theta_{11})}{\delta U_{\tau s}} = 1 + \Pi \quad (3.15b)$$

$$2\kappa \frac{(\delta_1 - \theta_{11})}{\delta} \frac{Q_{\infty}^2}{U_{\tau s}} = 1. + 1.6\Pi + 0.76\Pi^2 \quad (3.15c)$$

are solved simultaneously by an iterative scheme for  $U_{\tau s}$  and  $\Pi$ . The crossflow velocity profile is then generated by the triangular polar profile of Johnston (1957) (Equation 1.21) with given  $\tan\beta_w$  and  $A$  as input to the program.

#### D. Verification of the Computer Program

When results of a three-dimensional turbulent boundary prediction method layer are compared with data, discrepancies will be noted which are due to three distinct causes - (i) numerical errors or inaccuracies, (ii) inadequacies of the physical equations and (iii) errors or inaccuracies of the experimental data. The objective of the present research program is to examine the merits of the physical equations and it is thus desirable to minimize (i) and (iii) above. Unfortunately, nothing can be done about item (iii) directly but it is hoped that the influence of experimental errors on the general conclusions will be minimized by making comparisons to several sets of experimental data. To verify that numerical errors, (i), were not significant, comparisons of the results calculated by the present computer program have been made to the computed results of other workers. In addition internal momentum integral checks were made on the computations.

## D.1 Momentum Integral Checks

Although we are solving the differential equations of motion (Equations 1.9 and 1.10) by finite differences in the  $y$  direction, the computed results should satisfy the momentum integral equations which consist of integrating Equations 1.9 and 1.10 with respect to  $y$  (using Equation 1.8 also). In the  $x$  direction, the momentum integral equation has the form

$$\begin{aligned} & \frac{\partial}{\partial x} [Q_{\infty}^2 \{ -C^2\theta_{11} - 2CS\theta_{21} + S^2\theta_{22} + CS\delta_2 \}] \\ & + \frac{1}{R} [Q_{\infty}^2 \{ (S^2-C^2)\theta_{11} - 4CS\theta_{21} + (S^2-C^2)\theta_{22} + CS\delta_2 + S^2\delta_2 \}] \\ & - \frac{\partial Q_{\infty} C}{\partial x} [CQ_{\infty}\delta_1 + SQ_{\infty}\delta_2] = 0.5Q_{\infty}^2 C_f \cos\gamma_w \end{aligned} \quad (3.16a)$$

where

$$C = \cos \psi = \cos \gamma_{\infty} \quad (3.16b)$$

$$S = \sin \psi = \sin \gamma_{\infty} \quad (3.16c)$$

In the present computer program, the left (LHS) and right (RHS) hand sides of this equation have been integrated by the trapezoidal rule from the start of the computations to each value of  $x$ . If the computations had no numerical errors, the integrated left and right hand sides should be identical.<sup>+</sup> Momentum integral unbalance is defined as

$$\text{Unbalance (\%)} = \frac{\int_0^x \text{LHS} dx - \int_0^x \text{RHS} dx}{\int_0^x \text{RHS} dx} \times 100 \quad (3.17)$$

In most of the flows studied in the present study, the momentum integral unbalance has been kept under 10%. The exceptions are the adverse

---

<sup>+</sup>The effect of a poor shear stress closure model would not be reflected in this test.

pressure gradient flows at low Reynolds numbers (the vaneless diffuser flows) where due to the large distance between the wall and the first mesh point (order of  $0.1\delta_{995}$ ) the empirical functions are put to a severe test. Unbalance for the separating vaneless diffuser flows of up to 100% have been observed. This is not as bad as it may appear however and can be clarified by examining the simpler form of Equation 3.16, the momentum integral equation for two dimensions.

$$\frac{d\theta_{11}}{dx} + \frac{(2\theta_{11} + \delta_1)}{Q_\infty} \frac{dQ_\infty}{dx} = \frac{C_f}{2} \quad (3.18)$$

In an adverse pressure gradient, the first term on the left side of Equation 3.18, is always positive whereas the second on the left hand side is negative. The momentum unbalance is based on an error in the difference of these two terms. In many of the vaneless diffuser flows, this difference is only about 5% of the magnitude of either term and thus a 5% error in one term would cause a 100% momentum integral unbalance. The momentum integral check, when applied in the form of Equation (3.16) is thus a very sensitive test. In the moderate Reynolds number flows, the 10% maximum unbalance indicates good performance of the numerical scheme. While better numerical schemes might produce even smaller momentum integral unbalances, it is doubtful if the improvement would show in comparisons to the data. Momentum integral balance checks are not, however, sufficient to verify the adequacy of the computing scheme. The possibility of compensating errors is not eliminated. Thus, it is desirable to compare predictions to those made with other numerical schemes using the same physics.

## D.2 Comparisons to Other Predictors

In Figure 3.3, predictions using the eddy viscosity model are compared to the predictions of Mellor from the 1968 Stanford conference for the Ludwig and Tillman strong adverse pressure gradient flow (flow 1200). As can be seen, the agreement between the predicted results is good. Both predictions show poor agreement with the data because neither allowed for the streamwise convergence of the flow, which was substantial in this experiment. Also shown in Figure 3.3 are the results of Cebeci from the 1968 conference for the same flow. His results are slightly different but not significantly so. Cebeci uses a slightly different model for the eddy viscosity but the differences are probably mostly numerical.

The predictions of the present method shown in Figure 3.3 were calculated using 20 mesh points. When calculated using 30 mesh points, no appreciable change in results was seen (e.g.  $R_\theta$  only changed from 24,010 to 23,851 at  $x = 3.5$  feet).

The present method uses a more than adequate number of  $x$  steps for good accuracy. The large number of  $x$ -steps is a requirement of Equation 3.12. Further reduction in the  $x$ -step can produce a deterioration in the computed results. In the above Ludwig and Tillman flow, halving the  $x$ -step with 20  $y$  points increased the average momentum integral unbalance from 3% to over 20%. This effect is primarily due to increased errors due to interpolation.

Figure 3.4 presents results of the Nash method calculations compared to the results of Nash himself (1969) for the Cumpsty and Head Infinite swept wing flow. The velocity profile shown is for the largest

value of  $x$ . The agreement between predictions is quite good and the differences which are apparent are probably the result of different interpretations of the external pressure gradient. Most attempts by predictors show poor agreement with the data for this flow; the cause is not known.

In the present work, all prediction methods use essentially the same numerical method and it is thus expected that while comparisons of predictions to data will show some effects of numerical inaccuracies, comparisons of methods to each other should be more accurate. However, the results shown by Figures 3.4 and 3.5 indicate that numerical errors should be small in most cases.

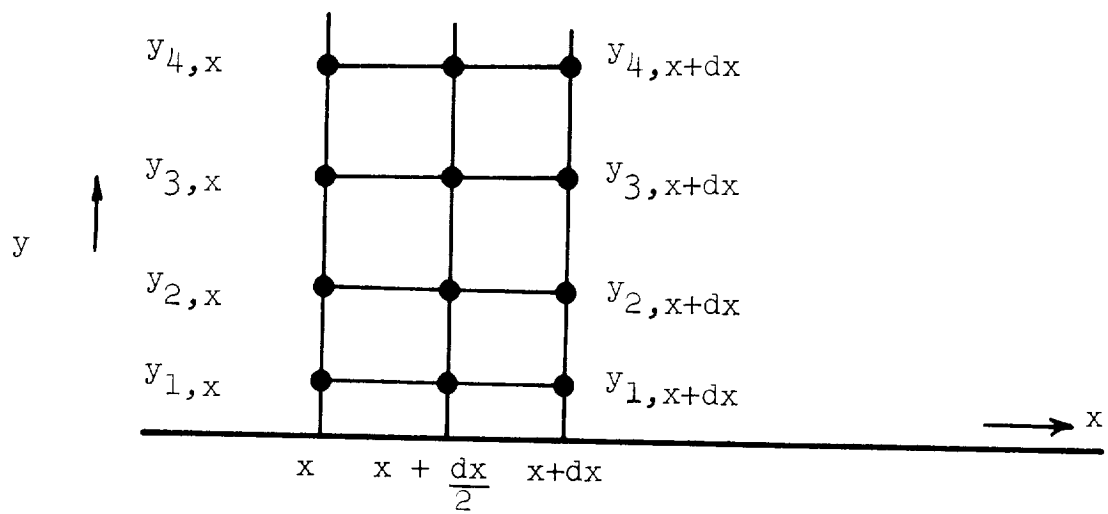


Figure 3.1 - y Grids

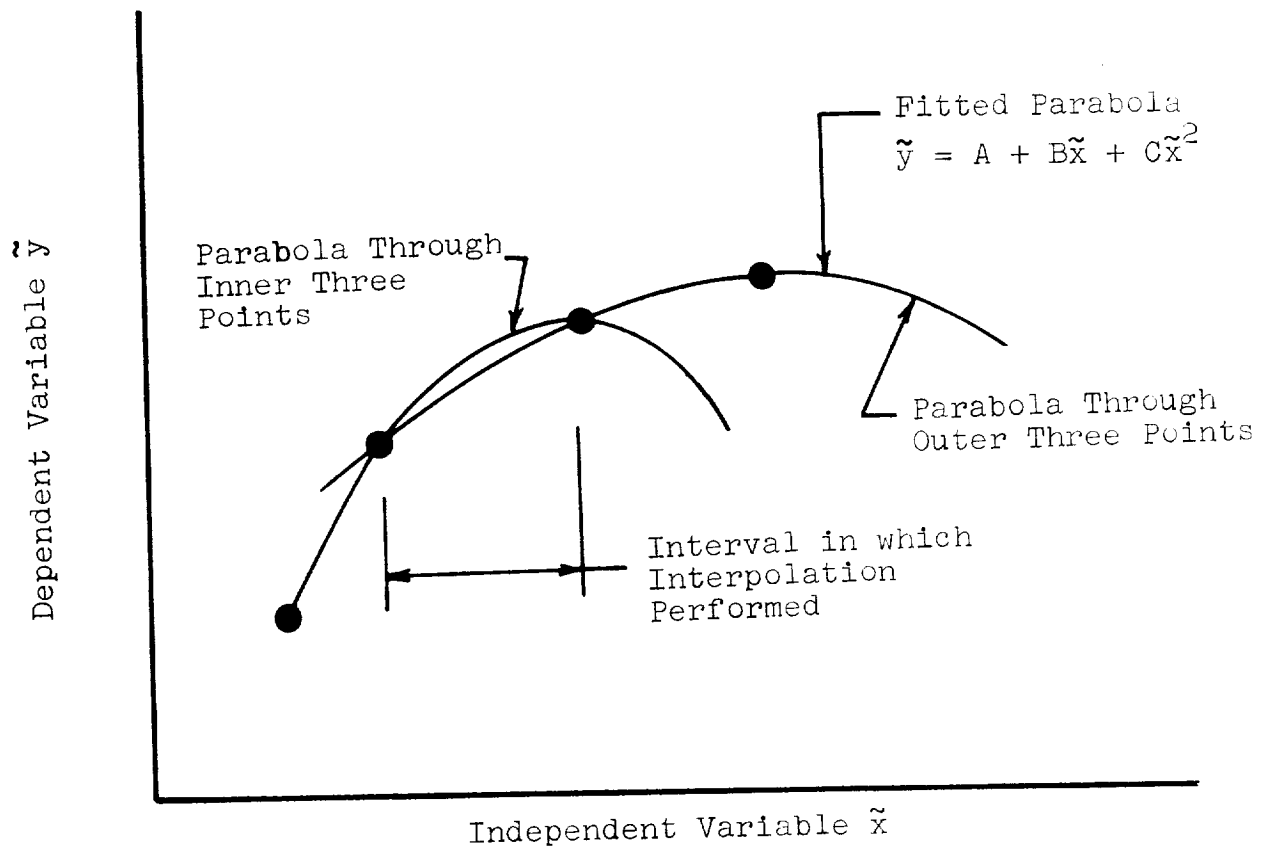


Figure 3.2 - Fitting of Parabolas for Interpolation

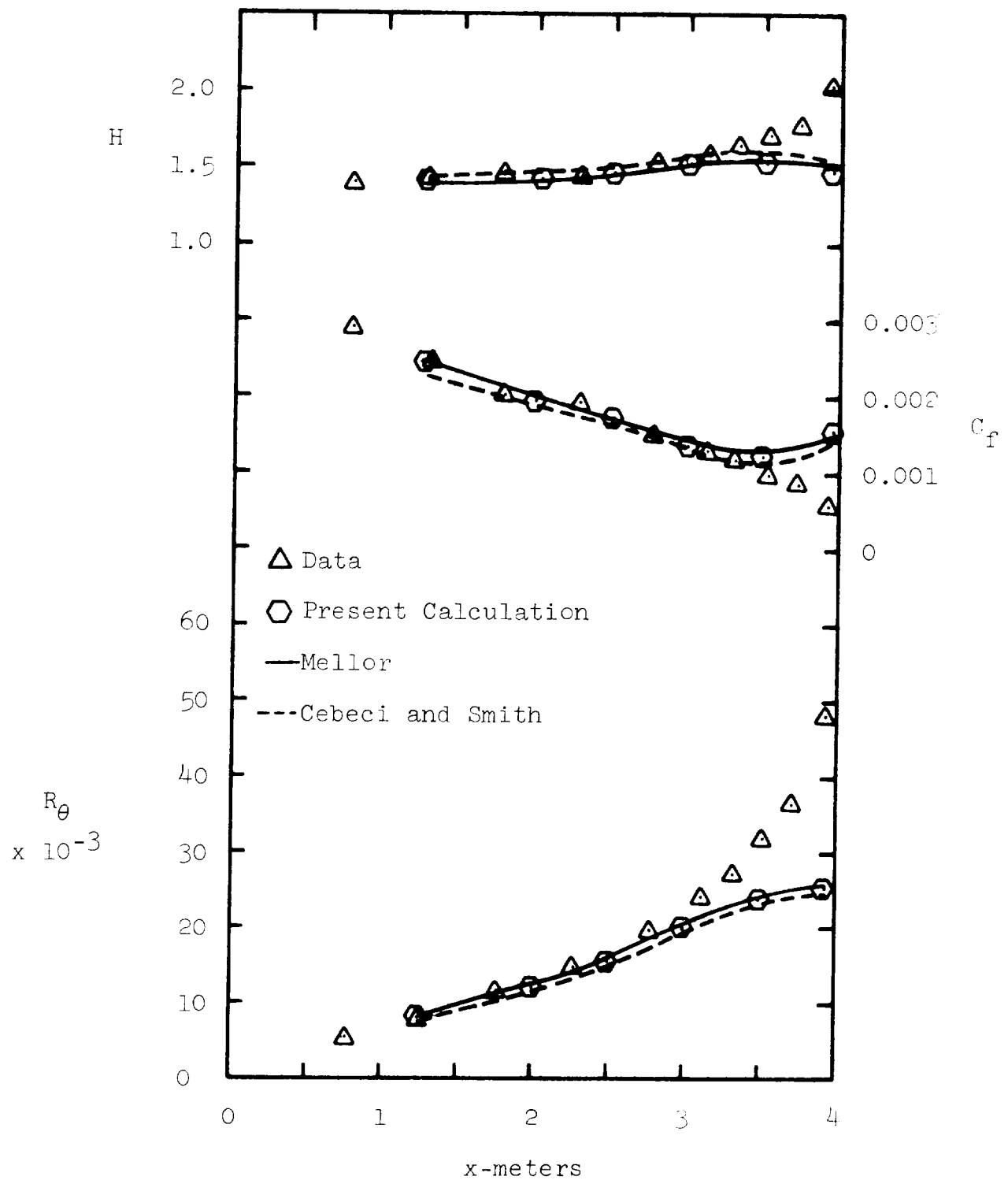


Figure 3.3 Ludwig and Tillman Strong Adverse Pressure Gradient

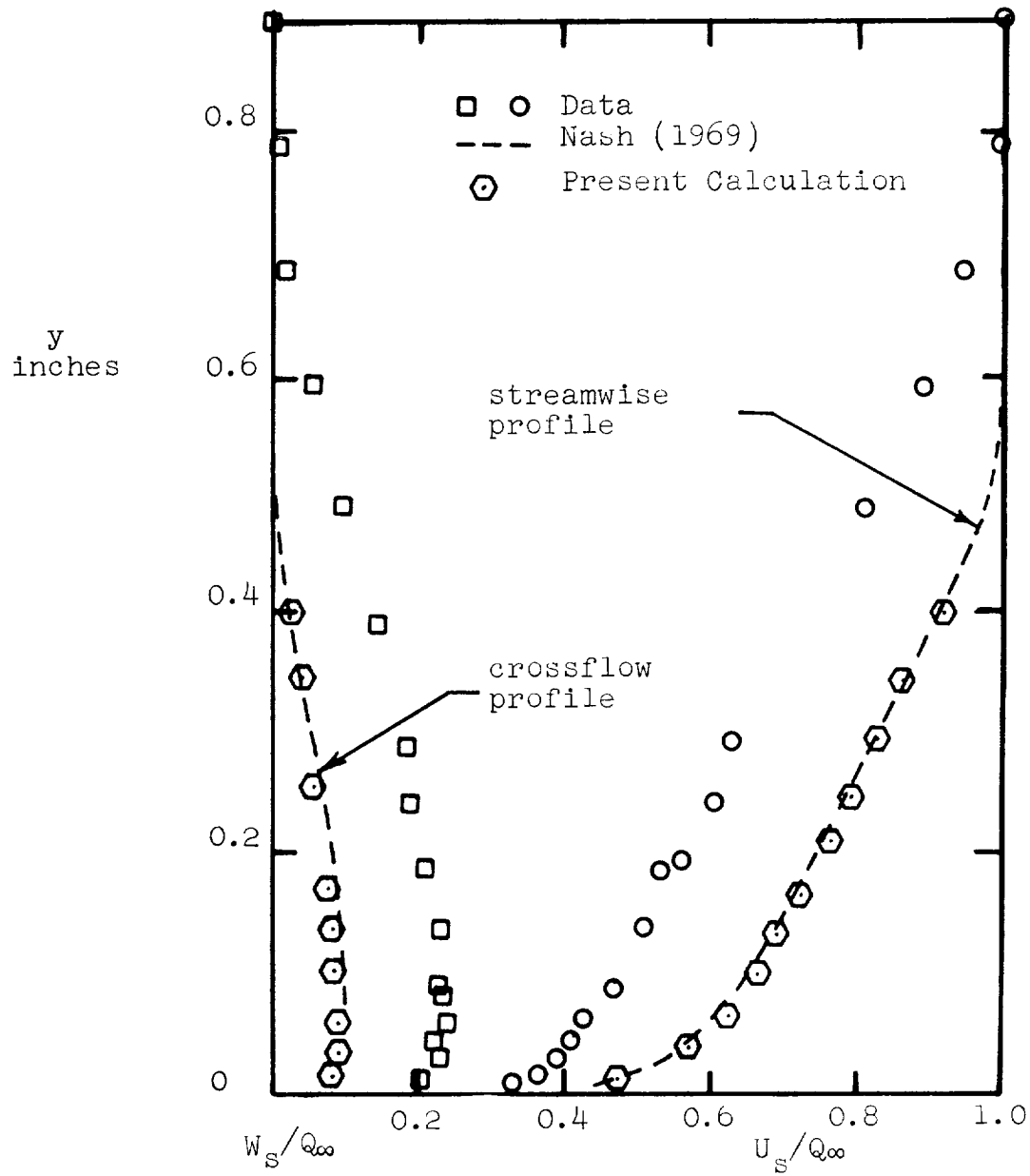


Figure 3.4 - Comparison of Present Nash Calculations to those of Nash (1969) on Cumpsty and Head (1970) Infinite Swept Wing

## CHAPTER 4

### COMPARISONS WITH EXPERIMENT

#### A. General Considerations

The worth of any prediction scheme for turbulent boundary layers can be fully assessed only when it has been compared with a wide variety of experimental data. Although the selection of good three-dimensional turbulent boundary layer data is not extensive, some good data do exist (see Chapter 1). In this chapter, predictions have been attempted for ten experimental flows using three prediction methods (Nash, Bradshaw and eddy viscosity). In addition, a fourth method, the mixing length method, has been tried on some flows.

The experimental flows fall into three general geometric classes:<sup>+</sup> (i) plane of symmetry flows at the plane of symmetry of wing-body junctions, (ii) infinite swept wing flows, and (iii) radial vaneless diffuser flows. Each of these flows requires the use of only two independent space variables. Hence, to the limit that the data satisfy this assumption, the entire boundary layer flow field is calculated for the infinite wing and vaneless diffuser flows. On the other hand, in the plane of symmetry flows, only the flow at the plane of symmetry is calculated. For general information about each experiment which is discussed, the reader should consult Table 1.1.

In this chapter, a convention has been used for the curves representing the predictions of the various methods. Except as noted, this convention is:

---

<sup>+</sup>A fourth class of flows, the flow on a rotating disc was not successfully predicted. The attempt to compute this class of flows is discussed in Appendix C.

_____	Bradshaw method
- - - - -	Eddy viscosity method
_____	Nash method
_____ - - - _____	Mixing length
_____ - _____	Eddy viscosity with low Reynolds number correction (discussed later).

## B. The Flow at a Plane of Symmetry

Plane of symmetry flows fall into the general class of three-dimensional flows which can be predicted using only two independent space variables as discussed in Chapter 1. On the symmetry plane, however, three-dimensionality enters not as a crossflow but as a gradient of the crossflow in the direction perpendicular to the symmetry plane. Thus, the crossflow velocity  $W$  is zero while  $\frac{\partial W}{\partial z}$  is non-zero. Rather simple modifications of the equations presented in Chapter 1 are thus required to predict the flow on the plane of symmetry. Since  $\frac{\partial W}{\partial z}$  is non-zero, the continuity equation (Equation 1.3) takes the general form:

$$\frac{\partial U}{\partial x} + \frac{\partial V}{\partial y} + \frac{\partial W}{\partial z} = 0 \quad (4.1)$$

rather than the restricted form (Equation 1.8) used for all the other predictions in this report. Since  $W$  is zero, the  $x$ -momentum equation (Equation 1.4) reduces to Equation 1.9 as for the infinite swept wing, but Equation 1.5 becomes a  $0 = 0$  identity. However, the appearance of  $\frac{\partial W}{\partial z}$  in Equation 4.1 requires a new equation which can be obtained by differentiating  $z$ -momentum, Equation 1.5, with respect to  $z$  and noting that symmetry requires that  $W = \frac{\partial U}{\partial z} = \frac{\partial W}{\partial y} = 0$ . The resulting equation is:

$$U \frac{\partial}{\partial x} \left( \frac{\partial W}{\partial z} \right) + V \frac{\partial}{\partial y} \left( \frac{\partial W}{\partial z} \right) + \left( \frac{\partial W}{\partial z} \right)^2 = U_{\infty} \left( \frac{\partial^2 U_{\infty}}{\partial z^2} \right) + \left( \frac{\partial W_{\infty}}{\partial z} \right)^2 + \frac{\partial}{\partial y} \left( \frac{\partial \tau_z}{\partial z} \right) \quad (4.2)$$

By assuming that the free stream is irrotational

$$\frac{\partial U_{\infty}}{\partial z} = \frac{\partial W_{\infty}}{\partial x} \quad (4.3)$$

then in the free stream

$$U_{\infty} \left( \frac{\partial^2 U_{\infty}}{\partial z^2} \right) = U_{\infty} \frac{\partial}{\partial x} \left( \frac{\partial W_{\infty}}{\partial z} \right) \quad (4.4)$$

The right hand side of Equation 4.4, which can be obtained from the data more readily than the left hand side, is used to evaluate the term  $U_{\infty} \left( \frac{\partial^2 U_{\infty}}{\partial z^2} \right)$  which appears in Equation 4.2.

Equation 4.2 introduces another stress variable  $\frac{\partial \tau_z}{\partial z}$ . In the models which use the isotropic eddy viscosity assumption to compute the shear stress direction,  $\frac{\partial \tau_z}{\partial z}$  can be obtained by differentiating Equation 2.18 with respect to  $z$  to obtain the following expression:

$$\frac{\partial \tau_z}{\partial z} = \tau_x \frac{\partial}{\partial y} \left( \frac{\partial W}{\partial z} \right) / \left( \frac{\partial U}{\partial y} \right) \quad (4.5)$$

In the Bradshaw method,  $\frac{\partial \tau_z}{\partial z}$  can be obtained by differentiating Equation 2.20 with respect to  $z$  to obtain

$$U \frac{\partial}{\partial x} \left( \frac{\partial \tau_z}{\partial z} \right) + V \frac{\partial}{\partial y} \left( \frac{\partial \tau_z}{\partial z} \right) = 0.3 \left[ \tau \frac{\partial}{\partial y} \left( \frac{\partial W}{\partial z} \right) - \frac{\tau^{1/2}}{L} \frac{\partial \tau_z}{\partial z} - \tau_{\max} \frac{\partial}{\partial y} \left( G \frac{\partial \tau_z}{\partial z} \right) \right] \quad (4.6)$$

Thus, with a few minor changes, a set of equations is obtained which are similar to those of the infinite swept wing except that  $\frac{\partial W}{\partial z}$  and  $\frac{\partial \tau_z}{\partial z}$  are used as dependent variables instead of  $W$  and  $\tau_z$ .

#### B.1 Johnston Plane of Symmetry

The geometry of this flow is sketched in Figure 4.1. Johnston (1957, 1960b) measured mean velocity profiles at many points all along the

plane of symmetry from  $x = 0$  to  $x = 2.5$  feet (see Figure 4.1) and at points off the symmetry plane from  $x = 2$  to  $x = 2.5$  feet. Examination of Equations 4.2 and 4.4 shows that  $(\partial W / \partial z)_{\infty}$  is needed in order to make predictions. Since Johnston did not measure velocities off the plane of symmetry for  $x$  less than 2.0 feet,  $(\partial W / \partial z)_{\infty}$  had to be obtained indirectly. This was done by assuming that  $\frac{\partial v}{\partial y}$  was zero on the centerline of the flow so the continuity equation yields

$$\frac{\partial W_{\infty}}{\partial z} = - \frac{\partial U_{\infty}}{\partial x} \quad (4.7)$$

This result cannot be justified directly from the data but the results so obtained fair in smoothly with the direct measurements at  $x = 2.0$  feet (Figure 4.2).

The calculated results of integral parameters are shown in Figure 4.3.  $H$  is the two-dimensional shape factor

$$H = \frac{\delta_1}{\theta_{11}} \quad (4.8)$$

$C_f$  is the normalized wall shear stress

$$C_f = \tau_w / \frac{1}{2} \rho Q_{\infty}^2 \quad (4.9)$$

and  $R_{\theta}$  is the momentum Reynolds number

$$R_{\theta} = Q_{\infty} \theta_{11} / \nu \quad (4.10)$$

$\frac{\partial \hat{\theta}_{12}}{\partial z}$ , the remaining parameter shown in Figure 4.3 is defined as

$$\frac{\partial \hat{\theta}_{12}}{\partial z} = \frac{1}{Q_{\infty}^2} \int_0^{\delta} [(Q_{\infty} - Q) \frac{\partial W}{\partial z}] dy \quad (4.11)$$

$\frac{\partial \hat{\theta}_{12}}{\partial z}$  is the only cross flow term appearing in the momentum integral equation on the plane of symmetry (see Johnston 1960b):

$$\frac{\partial \theta_{11}}{\partial x} + (2\theta_{11} + \delta_1) \frac{1}{Q_{\infty}} \frac{\partial Q_{\infty}}{\partial x} + \frac{\partial \hat{\theta}_{12}}{\partial z} = \frac{C_f}{2} \quad (4.12)$$

With the exception of the last data point, the agreement between the predictions and the data is good for all methods. The Nash and Bradshaw results are indistinguishable. Unfortunately, the freestream pressure gradient is uncertain at the last data point due to a discrepancy between tabulated and graphical results in Johnston's report.

A major factor which causes the results to be essentially the same is the short length of the flow (about ten times the upstream boundary layer thickness) and the strong adverse pressure gradient which causes the pressure terms to dominate the shear stress terms in the momentum equations. For example, at  $x = 2.33$ , the shear stress gradient is only about 25% of the right hand side of the  $x$ -momentum equation (Equation 1.4). Thus only a weak dependence of the predictions on the shear stress model is expected for this flow.

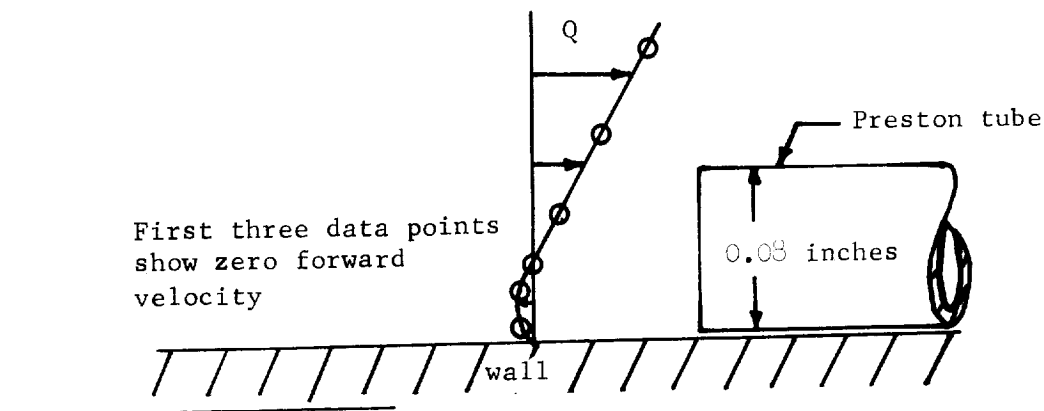
## B.2 East and Hoxey Plane of Symmetry

The geometry of this flow (East and Hoxey 1969) closely resembles a real wing-body junction as shown in Figure 1.2 (a). Since mean velocity profiles were measured at many locations both on and off the plane of symmetry, we computed  $\left(\frac{\partial w}{\partial z}\right)_{\infty}$  directly from the data. Indirect wall shear stress measurements were made by East and Hoxey using a Preston tube and a related technique using a razor blade to supplement their mean profile data.

The results of integral parameters, shown in Figure 4.4, are in good agreement with the data except for  $C_f$  which appears to be under-predicted by all methods. This discrepancy in  $C_f$  may result from the use of the Townsend form of the law of the wall (Equation 2.29) in the prediction methods whereas the data points shown in Figure 4.4 were

obtained from the experimental velocity profiles using a fit to the conventional law of the wall, Equation 2.27. The Townsend form yields a lower  $\tau_w$  when  $\frac{\partial \tau}{\partial y}$  is high in the wall region. In fact, when the flow was recomputed, using the Nash method, with the conventional law of the wall, the computed  $C_f$  was in much better agreement with the "law of the wall" data and the Preston tube estimates.

These difficulties with the data for  $C_f$  are further emphasized if one considers flow separation, which is singular ( $\tau_w = 0$ ) at the plane of symmetry. The evidence indicates that the flow separates at about  $x = 0.666$ . At  $x = 0.666$ ,  $C_f$  by the razor blade technique is zero, the inner part of the measured velocity shows no forward velocity and an examination of the oil flow photograph shows separation close to this value of  $x$ . The predictions (using Equation 2.29) also show separation at about this value of  $x$ . However the Preston tube estimate of  $C_f$  is non-zero at  $x = 0.666$  and if one were to extrapolate  $C_f$  determined from the conventional law of the wall (Equation 2.27) to  $x = 0.666$  it appears that  $C_f$  would be greater than zero.<sup>+</sup> The



<sup>+</sup>In fact, an examination of Equation 2.27 indicates that it cannot predict a zero wall shear stress unless the velocity at the first mesh point is zero whereas with a high  $\partial \tau / \partial y$ , Equation 2.29 can predict zero wall shear stress with a finite velocity at the first mesh point.

Preston tube however does not give a very reliable indication of the wall shear stress since it responds to the flow some distance from the wall.

The conclusion reached is that the predictions using the Townsend form of the law of the wall (Equation 2.29) are more reliable than the data points based on the conventional law of the wall (Equation 2.27) or the Preston tube measurements.

This adverse pressure gradient flow develops even more rapidly than the Johnston flow ( $x = 0$  to separation in approximately  $1.08_{995}$ ). Again the choice of stress model is not critical so all the prediction methods produce nearly identical results. A noticeable but small difference between methods is seen in the shape factor,  $H$ , results. The eddy viscosity method gives a somewhat lower  $H$  near the end of the flow (Figure 4.4). This effect appears to be a consequence of the higher shear stress which this method predicts (Figure 4.5). The Nash and Bradshaw methods give lower shear stress values because the shear stress lags the equilibrium value due to the rapid flow development. The higher shear stress of the eddy viscosity model prevents the fluid layers near to the wall from decelerating as much as the Nash and Bradshaw models and produces as a result a "squarer" velocity profile (lower  $H$ ).

### C. Infinite Swept Wing Flows

Infinite swept wing flows are described in cartesian coordinates where  $x$  is measured along a chord and gradients in the  $z$ , or spanwise, direction are zero. Since there is no spanwise pressure gradient,

$W_\infty$  the component of free stream velocity parallel to the leading edge\* is everywhere constant. These flows are computed using Equations 1.8, 1.9 and 1.10 and the various shear stress model equations presented in Chapter 2.

### C.1 Johnston Infinite Step

Johnston (1970) took some rather detailed measurements on the geometry shown in Figure 4.6. The measurements were made on the floor of the wind tunnel immediately upstream of a long, forward-facing step oriented 45 degrees to the tunnel centerline. The step produces an extremely abrupt change in the flow field and in fact, the streamlines are curved in the  $y$  direction so that the usual boundary layer approximation of  $\partial P / \partial y = 0$  is not valid. Fortunately, Johnston measured the  $y$  profiles of static pressure in the flow at various values of  $x$  (Figure 4.7). Thus, in this special case, the prediction methods were modified to take advantage of this additional data and  $\partial P / \partial x$  replaced  $dP/dx$  in the  $x$ -momentum equation (Equation 1.9).  $\partial P / \partial x$  calculated from the data in Figure 4.7 was supplied as input to the prediction methods as a function of  $x$  and  $y$ . Since Johnston measured turbulent shear stresses as well as mean velocity profiles, an experimental shear stress profile is used as well as an experimental velocity profile to start the calculations for this flow.

The results of integral parameters for this flow are presented in Figure 4.8. The parameters not used in the discussion of the plane of symmetry flows,  $\theta_{12}$ ,  $\theta_{22}$ ,  $\delta_2$  and  $\beta_w$  are defined in Chapter 1. The

---

\*In practice infinite swept wing flow need not be over an airfoil hence the use of the terminology of airfoil flow is purely illustrative.

results of all the methods are almost the same and they agree quite well with the data. Figure 4.9 shows the mean velocity profiles at  $x = 0.75$  feet. No differences are apparent between the methods and the agreement with the profile data is good. Johnston measured the pitch of the flow so that experimental data is also available for the normal velocity  $V$ . Predictions of this variable at  $x = 0.75$  shown in Figure 4.10 are not as good as the wall-parallel velocities.  $V$  depends entirely on the accuracy of the local calculation of  $\partial U / \partial x$  since it can be evaluated from continuity (Equation 1.8) by  $V = \int_0^y \left( \frac{\partial U}{\partial x} \right) dy$ . Thus, the results for  $V$  indicate that the calculations are starting to deteriorate at  $x = 0.75$ . This may in part result from rapid change of pressure gradient in a region, see Figure 4.7, where it is not accurately known.

The predicted and experimental shear stress profiles shown in Figure 4.11 for  $x = 0.75$  are quite striking. The Nash and the Bradshaw methods agree well with the data but the eddy viscosity model gives shear stresses which are too high. This discrepancy is a consequence of the lack of shear stress rate equation in the eddy viscosity model. In the Johnston step flow, the turbulence field does not have time to develop to an equilibrium state and therefore the equilibrium stresses computed using an eddy viscosity method are too high. This high shear stress of the eddy viscosity model has another significant effect - it reduced the skewing of the flow so that separation (which is predicted by Nash and Bradshaw methods to occur at  $x = 0.89$  feet) never occurs. The Nash and the Bradshaw methods predict a separation point in the location where Johnston observed it experimentally.

Another result of interest is the direction of the shear stress, since assumptions concerning this direction constitute the difference between the Nash and the Bradshaw methods. As can be seen in Figure 4.12, the Nash shear stress is approximately aligned with the mean velocity gradient direction from the data and the Bradshaw shear stress direction is closer to the shear stress data direction.<sup>+</sup> However, the Bradshaw method does not correctly predict the shear stress direction but appears to be at best only an improvement over the Nash method. It should be emphasized that the Nash and Bradshaw methods produce virtually identical results for the mean velocities. This experiment was especially designed to emphasize the difference between the direction of the shear stress and the mean velocity gradient and since the difference in assumptions between the Nash and Bradshaw method makes no difference in prediction of the mean flow it may well be that the isotropic eddy viscosity assumption for shear stress direction, while not generally valid, is quite adequate for many practical calculations.

## C.2 Bradshaw and Terrell Swept Plate

The Bradshaw and Terrell flow (Bradshaw and Terrell 1969) is a zero pressure gradient flow on a flat plate which is attached to the trailing edge of an infinite swept wing. The fluid was air at atmospheric pressure and temperature flowing at about 130 ft/sec. The flow relaxes from a modestly skewed form ( $\beta_w = 8^\circ$  at  $x = 0$ ) toward a simple, two-dimensional flat plate form. Shear stress profiles were

---

<sup>+</sup>The measurements of shear stress direction were quite difficult and are recognized to be of relatively high uncertainty, e.g. the bars on the points represent a significant fixed error. However, in the region close to  $y = 0.5''$  the uncertainty is not believed to exceed 2 degrees.

taken in addition to mean velocity profiles at each measuring station. Experimental shear stress and velocity profiles were used at  $x = 0$  to start the computations.


The results of integral parameters are shown in Figure 4.13. The data shows scatter which is caused by the test arrangement where profiles were taken at various spanwise,  $z$ , positions. There was a small variation of the flow conditions along the span. The points shown by  are directly downstream from the first point and do show somewhat less scatter. The general agreement between predictions and data is good (note that most of the plotting scales are quite expanded). In both streamwise and crossflow parameters the differences between the various methods appear to be no larger than the scatter of the data.

Figure 4.14 shows the mean velocity profiles at  $x = 1.18$  feet. Moderate differences are apparent in the crossflow velocity profile predictions. However, considering the effect of a 0.5 degree measurement error of the velocity direction on the data (see Figure 4.14), it would be difficult to say which method produces best agreement to the data.

Figure 4.15 shows the computed and experimental shear stress profiles at  $x = 1.18$  feet. The agreement is not as good as expected. In fact, when the eddy viscosity model was used to calculate a shear stress from the experimental mean velocity profile at the  $x = 1.18$  station, it produces values of  $\tau_s/Q_\infty^2$  of 0.00095 and 0.00048 at  $y = 0.0416$  and 0.08333 feet respectively compared to experimental values of .00155 at  $y = 0.0416$  and 0.00078 at  $y = 0.08333$ . These results raise questions concerning the accuracy of these stress data. If the

data are later demonstrated to be  $\pm 10\%$  uncertain, then a re-examination of all shear stress models for two-dimensional flow is warranted.

In Figure 4.16 are plotted the shear stress and mean velocity directions for this flow at  $x = 1.18$ . The data does show a difference between the directions of the shear stress and mean velocity gradient and this trend is also seen in profiles at other values of  $x$ . In the inner parts of the layer, this difference is small but becomes appreciable near the edge of the boundary layer. Near the layer edge however, the mean velocity gradients and shear stresses are small and hence the predicted and experiment directions have a high uncertainty. The Nash and eddy viscosity methods predict shear stresses in the direction of the mean velocity gradient (by assumption) and are in acceptable agreement with the experimental velocity gradient direction. The Bradshaw method shear stress and mean velocity gradient directions are different from each other but in the inner part of the layer the trend is reversed from the data. For  $y$  greater than 0.073 feet, the data and predictions show the same trends; however, the shear stresses are becoming small and of little importance in the ultimate prediction of mean velocity profiles.

In summary, it appears that all the shear stress assumptions including the eddy viscosity method tried on this flow produced results which agree quite well with the mean velocity data.

### C.3 Cumpsty and Head Infinite Swept Wing

Cumpsty and Head (1970) measured the development of the boundary layer in the adverse pressure gradient on the rear of a wing with a sweep angle of 61.0 degrees (see Figure 1.2(b)). Free stream velocity

in the atmospheric temperature and pressure air flow was 133 ft/sec. The experimenters experienced difficulty with flow interference effects from their first traverse gear which caused the separation point to move about but they finally minimized the problem by use of a slender traverse gear. It is the latter data (slendergear) that is used here. Only mean velocity profiles were measured in this flow.

The predicted results of integral parameters, shown in Figure 4.17, are in poor agreement with the data. The predictions of Cumpsty and Head (1970), who used an integral method, and Bradshaw (1969), whose basic method is the same as ours but whose numerical method was quite different are also in poor agreement with each other and the data. As mentioned in Chapter 3, Nash also got poor agreement when he calculated this flow. The Cumpsty and Head and Bradshaw's own results for  $\beta_w$  are also shown in Figure 4.17. Nash does not present results for  $\beta_w$  but it is estimated from the velocity profile that his computations gave values no more than 10% higher than the present work. Thus, it appears either that the data is questionable or in some way fails to meet the assumptions. The fact that the Cumpsty and Head calculations do not agree with the present calculations is not surprising since he used a significantly different prediction method (an integral method). That the Bradshaw's own results do not agree with the present results is puzzling. It is surmized that he may have computed the pressure gradient differently, and as is pointed out later in discussion of the Gardow (1958) flows, accurate input for  $dP/dx$  is essential in adverse pressure gradient cases.

In order to improve the predictions, the various authors have tried different things. Bradshaw obtained improvement by assuming a

surface curvature correction for the shear stress. Cumpsty and Head modified the external velocity angle at the start and obtained an improvement. Nash, who has a program which allows variations in the  $z$  direction improved his predictions by assuming a spanwise pressure gradient. It is felt that the data from this flow is not complete enough to adequately determine the difficulty and it is not felt that corrections are really of much merit. What is demonstrated by this flow is the need for a better infinite swept wing experiment. The sweep angle selected ( $61^\circ$ ) is very high (it was governed by an available apparatus) and it is suggested that an experiment be performed in the future on a wing with a sweep angle of about 45 degrees so that the assumption of "infinite" span can be better approximated.

#### D. Vaneless Diffuser Flows

Two sets of three-dimensional turbulent boundary layer data were obtained on a radial vaneless diffuser rig (see Figure 1.2d) in the late 1950's. One of these was by Gardow (1958) and the other by Jansen (1959). Gardow ran seven flows and took measurements on one wall of the diffuser. Jansen ran three flows but took measurements on both walls. Both authors measured only mean velocity profiles. In the present work, calculations are presented for four of the Gardow flows and one of the Jansen flows. In both cases the test fluid was air at atmospheric temperature and pressure and the inlet free stream velocity levels low (30 - 55 feet/sec).

Unfortunately, all of the vaneless diffuser flows were run at low momentum thickness Reynolds numbers ( $R_\theta$ ) and most of the useful data has  $R_\theta$  under 2000. This fact complicates the numerical method and

also extends the shear stress assumptions into a Reynolds number regime for which they were not originally developed.

The numerical difficulty arises because of the restriction that the first mesh point occur at a  $y^+ = 30$ . At an  $R_\theta$  of 1000, such a value of  $y^+$  occurs at a  $y/\delta_{995}$  of about 0.1, which is quite far from the wall. This means that the empirical functions for  $\tau_w$ ,  $\beta_w$  and  $V_1$  are put to a severe test. In addition, since the second mesh point is much closer to the first mesh point than the first mesh point is to the wall, numerical instabilities appear. In his two-dimensional method, Bradshaw doesn't use the restriction that the first mesh point fall in what is experimentally observed to be the log-law region. Hence if  $y^+$  at the first mesh point is less than 30, an artificially high velocity is computed. Since the first mesh point is used to compute the wall shear stress and the differential equations give a logarithmic solution in the inner layer (all the way to the wall if allowed), the value of the wall shear stress extracted from the computed log-law is the same. However, it is not clear that an artificially high velocity value near the wall will have no effect in a three-dimensional boundary layer. The higher apparent inertia of the fluid may cause it to resist skewing and cause errors in the estimation of the wall shear stress angle (see Chapter 2). Thus, it was elected to always require that  $y^+ = 30$  at the first mesh point and bear the resultant inaccuracies. It is possible that allowing the first mesh point to be closer to the wall as was done in the two-dimensional Bradshaw method would not have produced any greater inaccuracies.

The second problem at low Reynolds numbers, extension of the theory to an untested regime, is well known to the originators of the various shear stress models. In his paper for the 1968 Stanford conference, Bradshaw notes that his method does not include the viscous shear stresses which may be as high as 10% of the total shear stress at an  $R_\theta = 500$ . He notes that simply adding this effect into the calculations is not necessarily meaningful because the empirical functions (L etc.) may also change. Herring and Mellor (1968) also make note of the low Reynolds number problem and suggest a correction to their eddy viscosity model. They suggest that the outer eddy viscosity be modified from the usual form Equation 2.9b ( $\epsilon_{outer} = 0.016\delta_1 Q_\infty$ ) to

$$\epsilon_{outer} = 0.016 \delta_1 Q_\infty \left[ 1 + \left( \frac{1100}{R_{\delta_1}} \right)^2 \right] \quad (4.13a)$$

where

$$R_{\delta_1} = Q_\infty \delta_1 / \nu \quad (4.13b)$$

In the present work, all of the vaneless diffuser flows have been computed using the eddy viscosity model with and without this low Reynolds number correction. For brevity, these methods have been denoted EVLR and EV respectively.

Since the available vaneless diffuser flows indicated a significant difference between results from the Bradshaw and the EV predictions (Nash is very similar to Bradshaw) it was considered to be of interest here to try the mixing length model also. It was found that the mixing length model produced essentially the same results as the eddy viscosity model for the infinite wing flows of Bradshaw and Terrell and Cumpsty and Head. In fact, the outer mixing length was adjusted for best

agreement ( $\ell/\delta_{995} = 0.79$ ) in these cases.

The data for the vaneless diffuser flows appears to be of appreciably lower quality than the other experimental flows discussed so far. Figure 4.18 shows a typical velocity profile by Gardow which shows the scatter of the data points to be substantial. The difficulty is probably caused by the low velocity levels used in the vaneless diffuser experiments. In none of the flows presented in his report does the free stream velocity exceed 55 feet per second and the average velocity level is closer to 35 feet per second. Such low velocities produced low total to static pressure differences (0.2 - 0.4 inches of water column) and high uncertainties in the resulting measured velocities. The scatter in the velocity profiles led to concern about the accuracy of the pressure gradient data. Minor errors in the measurement of the pressure gradient were thought to have a major effect on the predictions. As a result, a set of runs on each of the vaneless diffuser flows was taken with the best estimate of the local pressure gradient uniformly increased by 5% and uniformly decreased by 5% at each value of  $x$ . The results of this study are presented after the presentation of the predictions using our best estimate of the experimental pressure gradient.

The Bradshaw and the Nash methods require that a starting shear stress profile be supplied. In all of the calculations for the vaneless diffusers, the mixing length<sup>+</sup> (see Chapter 2) has been used to

---

<sup>+</sup>The mixing length used for starting shear stress profiles has been rounded slightly in the region where the two straight line portion of the  $\ell(y)$  function intersect. This procedure eliminates a slight spike in the starting shear stress profile.

generate a starting profile from the starting velocity profile. Since it is possible that the selection of a starting shear stress could appreciably alter the calculations, a set of calculations were done with the starting shear stress profiles arbitrarily altered by plus or by minus 10% at all values of  $y$ .

The vaneless diffuser flows are denoted by the authors name and a number which is the free stream swirl angle ( $\psi_i$ ) at the inlet to the diffuser (see Figure 1.2(d)).

#### D.1 Gardow A-45.2 Vaneless Diffuser Flow

The predictions of integral parameters for this flow are presented in Figure 4.19. At the last two values of  $x$  for which data is given, the experimental boundary layer thicknesses are 0.991 and 1.008 inches - values large compared to a passage half width of 1.000 inches. Assuming that the unmeasured boundary layer on the other diffuser wall is about the same thickness, the inviscid core of the flow had disappeared. If this is the case, the predictions at these last two points should not be compared to the data.

The prediction methods produce a wide range of results in Figure 4.19 which completely span the range of data points. Rather surprisingly, the mixing length model predicts this flow very well. The Nash and Bradshaw methods give identical results as in previous cases.

The Nash, Bradshaw, and eddy viscosity methods all tend to overpredict the crossflow. If one were to believe the data, this excessive crossflow would indicate that these methods are predicting an average shear stress across the layer which is too low. A low shear stress decreases the resistance to skewing. Mellor, in his correction for the

low Reynolds numbers (Equation 4.13) increases the outer eddy viscosity when his method is used at low Reynolds numbers. It is difficult to demonstrate precisely how the different shear models modify the flow since as the computations proceed, the mean velocity profiles tend to adjust so that the shear stress profiles for all methods are much the same. This is demonstrated by Figure 4.20 which shows the shear stress profiles at the start of the flow ( $x = 0.18$  ft) and downstream at  $x = 0.36$  ft. Note particularly that the immense difference between the EV and EVLR shear profiles at  $x = 0.18$  ft has almost completely disappeared at  $x = 0.36$  ft. Of course, as Figure 4.19 shows, to achieve this similarity of shear stress profiles, the velocity profiles have different shapes as evidenced by the different values of  $H$ , the streamwise shape factor. The important point is that the strong interaction between the mean flow and the shear stress makes it difficult to pinpoint which characteristics of the shear stress models are responsible for the differences in mean flow predictions.

A superficial evaluation of the predictions for this flow indicated that the mixing length model does best, followed by the EV, EVLR and Nash-Bradshaw results. The discussion in the paragraph above illustrates some of the difficulties of proceeding beyond this level of evaluation.

#### D.2 Gardow B-50.6 Vaneless Diffuser Flow

In this flow, the Nash, Bradshaw and EV methods indicate ordinary separation well upstream of the last  $x$  station. The mixing length and EVLR methods provide greater resistance to skewing and predict unseparated flow for the entire diffuser. The data show no evidence

of separation anywhere. As in the Gardow A-45.2 flow, the boundary layer appears to fill the passage at the last two data points and thus comparisons to data should not be made in this region. In general, it appears that the mixing length and EVLR methods both predict the flow well. However, these predictions are very sensitive to the pressure gradient as will be shown later.

The oscillations of  $C_f$  and  $\beta_w$  near the start of the computations with the Nash and Bradshaw methods are a consequence of a numerical instability in the wall region which results from an incompatibility of the initial conditions. In all the vaneless diffuser flows, the irregular experimental velocity profiles (Figure 4.18) required us to use synthetic starting velocity profiles. These synthetic profiles were evidently somewhat different from those which the computational methods required. With the shear lag of the Nash and Bradshaw methods, the adjustment was somewhat unstable. The instability disappears however and is not thought to be significant in the prediction of the downstream growth of the boundary layer. The eddy viscosity and mixing length models, which do not use a rate equation for the shear stress, remain stable.

#### D.3 Gardow B52.1 Vaneless Diffuser Flow

The results of integral parameter for this flow are shown in Figure 4.22. The mixing length results are not shown but are very similar to the EV results. As in the Gardow B50.6 flow, the Nash, Bradshaw and EV methods all predict ordinary separation. Again, the data does not indicate separation. However, the data comes close to separation ( $\beta_w + \psi = 82^\circ$ ) and it may be that experimental errors mask

actual separation. The boundary layer appears to fill the passage for the last two data points. The EVLR method predictions compare well to the valid data points. If experimental separation does in fact occur, then the Nash, Bradshaw and EV methods also perform fairly well since they do not deviate drastically from the valid data.

#### D.4 Gardow B-54.5 Vaneless Diffuser Flow

The results of integral parameters for this flow, shown in Figure 4.23 indicate that all methods predict separation very near to  $x = 0.3$  ft, close to the start of computation. The experimental results show a long region in which  $\beta_w + \psi$  is very close to 90 degrees and it is probable that the experimental flow is actually separated. The mixing length results are not shown, but are virtually the same as the EV results. The experimental boundary layer appears to fill the passage for the last three values of  $x$ .

#### D.5 Jansen 47 Degree Vaneless Diffuser Flow

The results of the Jansen 47 degree flow are presented in Figure 4.24. Jansen did not present any tabulations of his data, only tracings of his original plots which were then multilithed into a report. Thus, there may be a considerable loss of accuracy from the original results to the results shown in Figure 4.24. The Nash and Bradshaw method prediction, which are virtually the same, agree quite well with all the data except shape factor  $H$ . The EVLR method agrees even better with the streamwise data but leads to serious underestimation of the cross-flow parameters. The EV method gives somewhat poorer agreement with the data than the Nash and Bradshaw methods; it overestimates  $R_\theta$  and underestimates  $C_f$ . Considering the questionable quality of the data, it is surprising that any of the methods agree well with the data.

#### D.6 Variable Pressure Gradient Effects

It was suspected that the predicted results for the various methods are very sensitive to the free stream pressure gradient. Therefore a series of calculations on the vaneless diffuser flows were carried out in which the pressure gradient was deliberately varied from the best estimate. The pressure gradient was varied according to

$$\frac{dP}{dx} = a \frac{dP}{dx} \text{ best estimate}$$

where  $a$  was taken as 1.05 for the 5% high pressure gradient calculation and 0.95 for the 5% low pressure gradient calculations. The results of these changes of  $dP/dx$  on the computed free stream velocity, for the Gardow A-45.2 flow are shown in Figure 4.25. Note that over the range of  $x$  considered, a 5% change in the pressure gradient produces at most a 2% deviation in the computed velocity. In Gardow's tests, the uncertainty of the pressure transducer readings varied from  $\pm .75\%$  to about  $\pm 1.5\%$ . Other errors, such as fluctuating readings could have increased this uncertainty significantly. While it is difficult to guess what the actual uncertainty of the velocity readings were, the  $\pm 5\%$  changes of the pressure gradient do not produce changes in free stream velocity which are outside the uncertainty of the data.

Figure 4.26 shows the effect of this variation on the best fit pressure gradient on some of the integral parameters for the Gardow A-45.2 flow. As can be seen, the effects are substantial. The 5% high pressure gradient causes the prediction of separation and significantly increases the crossflow parameter  $\theta_{12}$ . The 5% low pressure gradient on the other hand reduces the maximum Reynolds number by 16% and the

maximum change in Reynolds number ( $R_{\theta\text{final}} - R_{\theta\text{initial}}$ ) is reduced by 25%. These results make it difficult to draw strong conclusions about the prediction methods for the vaneless diffuser flows since the real pressure gradient is clearly not known to sufficient precision.

The presentation of the results of the variation of the pressure gradient on all the vaneless diffuser flows are summarized in Table 4.1 which gives the most pertinent results. The pressure gradient was varied for three of the methods, Bradshaw, EV and EVLR for all of the vaneless diffuser flows. For each flow the dimensionless separation point location is listed at  $x_s/x_{\text{last}}$ . In addition, values of  $R_\theta$ ,  $C_f$  and  $\beta_w$  are given. These values of  $R_\theta$ ,  $C_f$  and  $\beta_w$  correspond to the last value of  $x$  if the flow does not separate when the 5% high  $\frac{dP}{dx}$  is applied. If the flow separates with the 5% high  $\frac{dP}{dx}$  these values  $R_\theta$ ,  $C_f$  and  $\beta_w$  obtain at the value of  $x$  where the 5% high  $\frac{dP}{dx}$  calculation separates. Comparison of the three  $\frac{dP}{dx}$  cases for a given flow shows clearly, because of the large differences obtained, the importance of very accurate measurement or representation of the pressure gradient in strong adverse pressure gradient flows.

#### D.7 Variable Initial Shear Stress Effects

Since none of the vaneless diffuser flows had measured shear stress profiles at the start, the Nash and Bradshaw methods, which require a starting shear stress profile, were started using the mixing length model. It was thus of interest to see how sensitive the calculations were to this selection. The Bradshaw calculations for the vaneless diffusers were all recomputed using an initial shear stress distribution which was uniformly changed by plus and minus 10% at each values of  $y$ .

The results of these calculations are summarized in Table 4.2. For the flows, in which separation is not predicted, Gardow A-45.2 and Jansen 47 degrees, it is seen that the changes in the predicted results were not significant. On the other hand, the separation points of the separating flows were significantly altered by the changes in shear stress at the start. It is possible then, that in some flows the initial shear stress distribution could make the difference between a prediction of separation and no separation. It is thus concluded that knowledge of the initial shear stress distribution is important in the prediction of flows with very strong adverse pressure gradients.

#### D.8 Summary of Vaneless Diffuser Flows

When the effects of the uncertainty in the pressure gradient is taken into account, it appears that all tested methods predict the flows to within the uncertainty of the data. However, no method was significantly superior in predictive ability. What is demonstrated is the need for a better vaneless diffuser experiment in which the uncertainties in the measured quantities can be reduced and the shear stresses measured directly. This may necessitate using higher fluid velocities and higher Reynolds numbers than were used by Gardow and Jansen. Although selection of "best" shear stress model cannot be made on the basis of the vaneless diffuser calculations here, the fact that the different methods produce such different results indicates that there may indeed be one method which is preferable at the low Reynolds numbers studied here. Much more precise low Reynolds number flow data than is today available is required however to pinpoint the best method if one exists.

#### E. Summary of Comparisons with Experiments

In summary, it appears that all closure assumptions tested here for three-dimensional turbulent boundary layers gave predicted mean velocity profiles within the accuracy of the data. Prediction of the shear stress profiles was not so accurate. In the Johnston step flow, the eddy viscosity model failed to predict the shear stress magnitude accurately while the Nash and Bradshaw methods were in good agreement with the data. In this same flow, no method accurately predicted the direction of the shear stress, but the Bradshaw method was closer to the data than either the Nash or eddy viscosity methods. In the Bradshaw and Terrell flow, the only other flow in which shear stresses were measured, no method was successful in accurately predicting the shear stress magnitude. For this same flow when experimental uncertainty is considered, no method was significantly superior in predicting the magnitude or the direction of the shear stress. Since in most engineering applications, it is the prediction of the mean velocity field which is important, no fully rational basis is available for selection of the best of the differential prediction schemes considered in this study. This is not to say that one method is not preferable - just that a preference cannot be distinguished on the basis of the present data. More experiments are needed to fully differentiate the merits of the various proposed methods. It should be kept in mind that the methods tried in the present study all work well in two dimension at moderate (5-50 thousand) momentum Reynolds numbers and thus their good performance in three dimension was considered an expected possibility.

Table 4.1 - Effect of  $\pm 5\%$  Change of  $\frac{dp}{dx}$  on Vaneless Diffuser Flows

	a	Eddy Viscosity					Bradshaw					Eddy Viscosity, Low $R_\theta$ Correction				
		$x_s/x_\ell$	$R_\theta$	$C_f$	$\beta + \psi$	$x_s/x_\ell$	$R_\theta$	$C_f$	$\beta + \psi$	$x_s/x_\ell$	$R_\theta$	$C_f$	$\beta + \psi$			
GARDOW A-45.2	1.05	0.715	2076	.00208	90	0.563	1871	.00202	90.	NS	1752	.00264	66.2			
	1.00	NS	1538	.00251	71	NS	1428	.00257	72.	NS	1548	.00293	57.7			
	0.95	NS	1320	.00268	64.	NS	1257	.00281	65.	NS	1380	.00322	51.9			
GARDOW B-50.6	1.05	0.440	1883	.00228	90.	0.420	1890	.00226	90	0.60	2151	.00230	90.			
	1.00	0.555	1581	.00265	79.	0.505	1580	.00263	79.	NS	1690	.00277	76.			
	0.95	NS	1450	.00283	75.	NS	1440	.00286	74.	NS	1500	.00300	70.			
GARDOW B-52.1	1.05	0.44	2070	.00237	90.	0.445	2101	.00227	90.	0.525	2207	.00243	90.			
	1.00	0.52	1780	.00270	82.	0.505	1750	.00268	81.	NS	1850	.00278	80.			
	0.95	NS	1640	.00285	78.	NS	1650	.00285	79.	NS	1660	.00301	75.			
GARDOW B-54.5	1.05	0.235	2002	.00245	90.	0.260	2078	.00245	90	0.25	2000	.00255	90.			
	1.00	0.255	1875	.00264	87.	0.283	1870	.00283	84.	0.293	1870	.00272	86.			
	0.95	0.316	1750	.00278	84.	NS	1740	.00300	79.	NS	1750	.00290	84.			
JANSEN 47°	1.05	NS	857	.00237	66.	NS	783	.00353	61.	NS	739	.00464	54.			
	1.00	NS	877	.00273	63.	NS	745	.00369	58.	NS	715	.00473	53.			
	0.95	NS	844	.00281	62.	NS	720	.00380	57.	NS	698	.00483	52.			

NS - Separation not predicted

Table 4.2 - Effect of Initial Shear Stress on Bradshaw Method  
Prediction of Vaneless Diffuser Flows

		$x_s/x_d$	$R_0$	$C_f$	$\beta + \psi$
GARDOW A - 45.2	+10	NS	1813	.00256	66
	0	NS	1801	.00259	65
	-10	NS	1795	.00262	65
GARDOW B - 50.6	+10	.530	1750	.00256	81
	0	.505	1801	.00244	84
	-10	.480	1953	.00221	90
GARDOW B - 52.1	+10	.538	1840	.00265	82
	0	.505	1950	.00250	85
	-10	.480	2075	.00233	90
GARDOW B - 54.5	+10	.316	1828	.00288	83
	0	.263	1880	.00280	85
	-10	.265	2055	.00241	90
JANSEN 47°	+10	NS	743	.00372	58.3
	0	NS	745	.00369	58.4
	-10	NS	747	.00366	58.7

NS - Not Separated

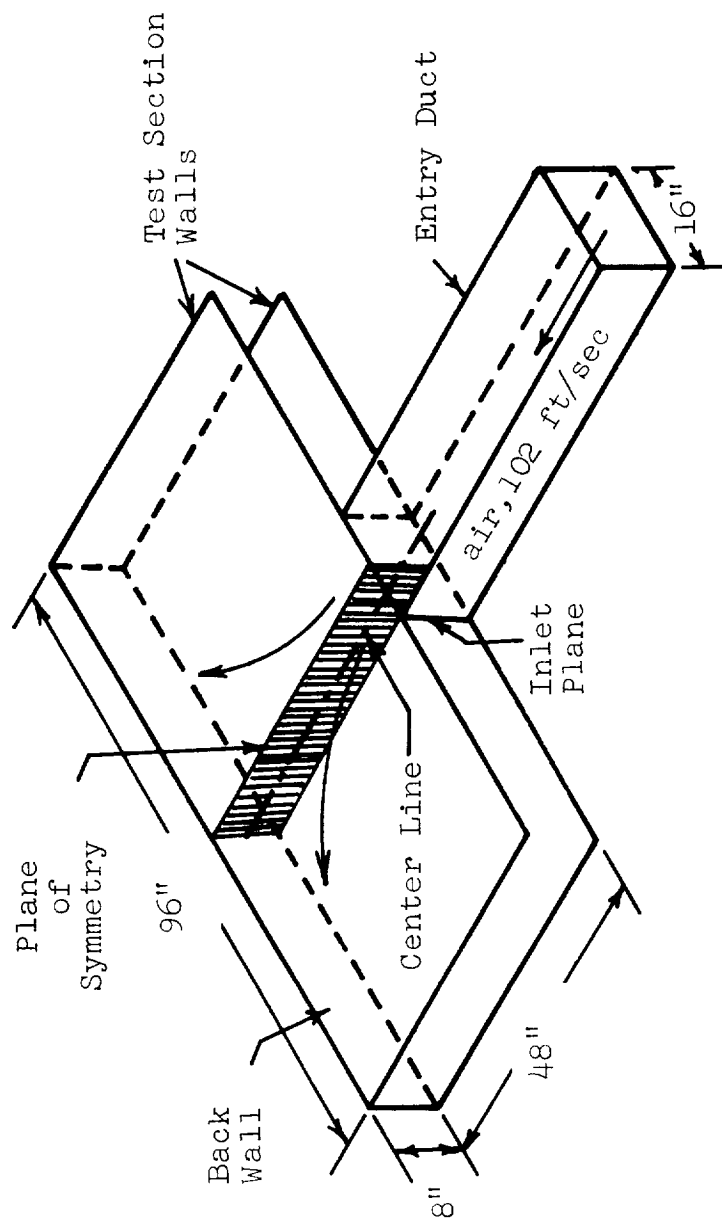


Figure 4.1 - Configuration of Johnston Plane of Symmetry Flow

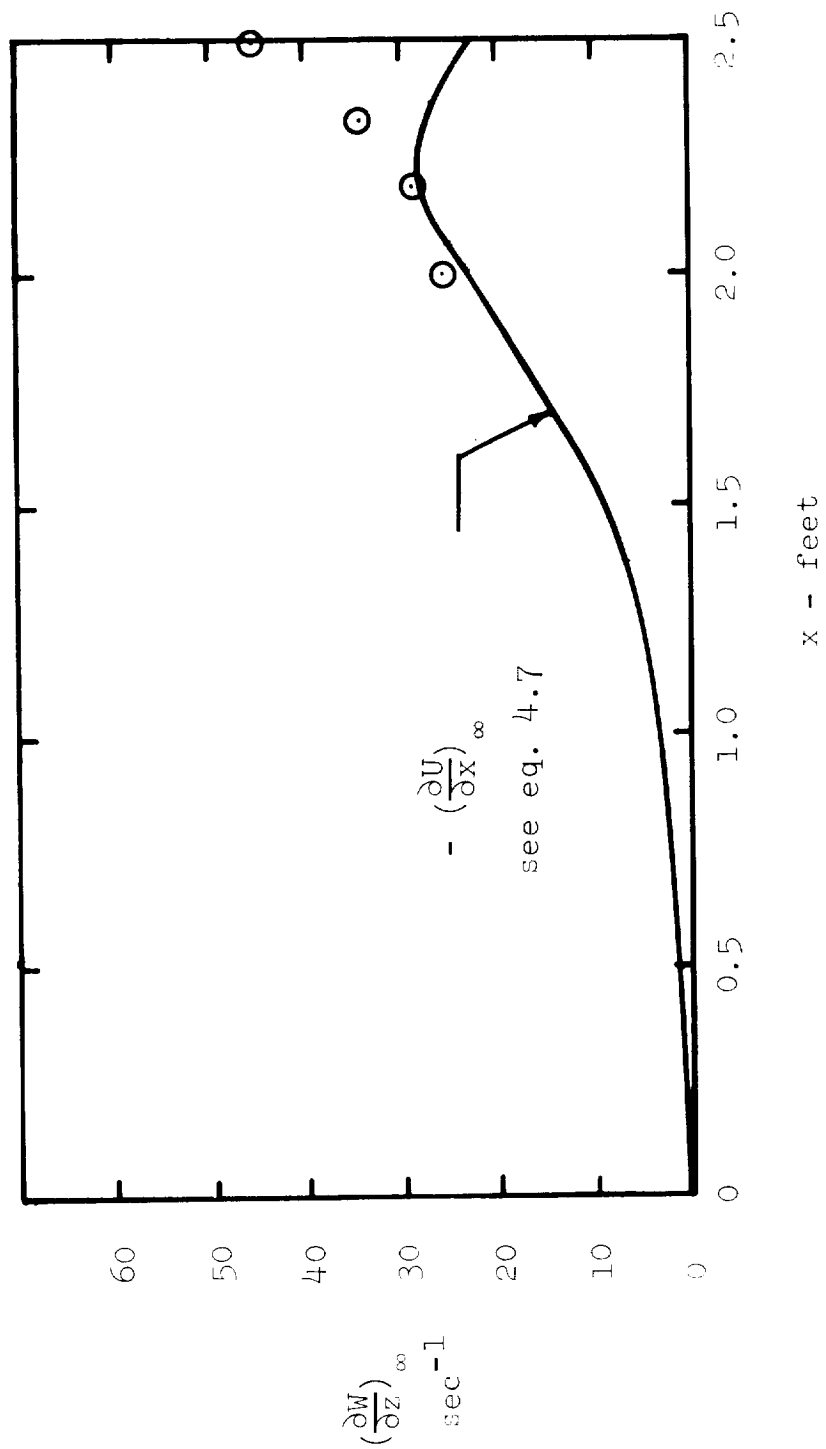


Figure 4.2  $(\frac{\partial W}{\partial z})_{\infty}$  vs.  $x$ , Johnston Plane of Symmetry

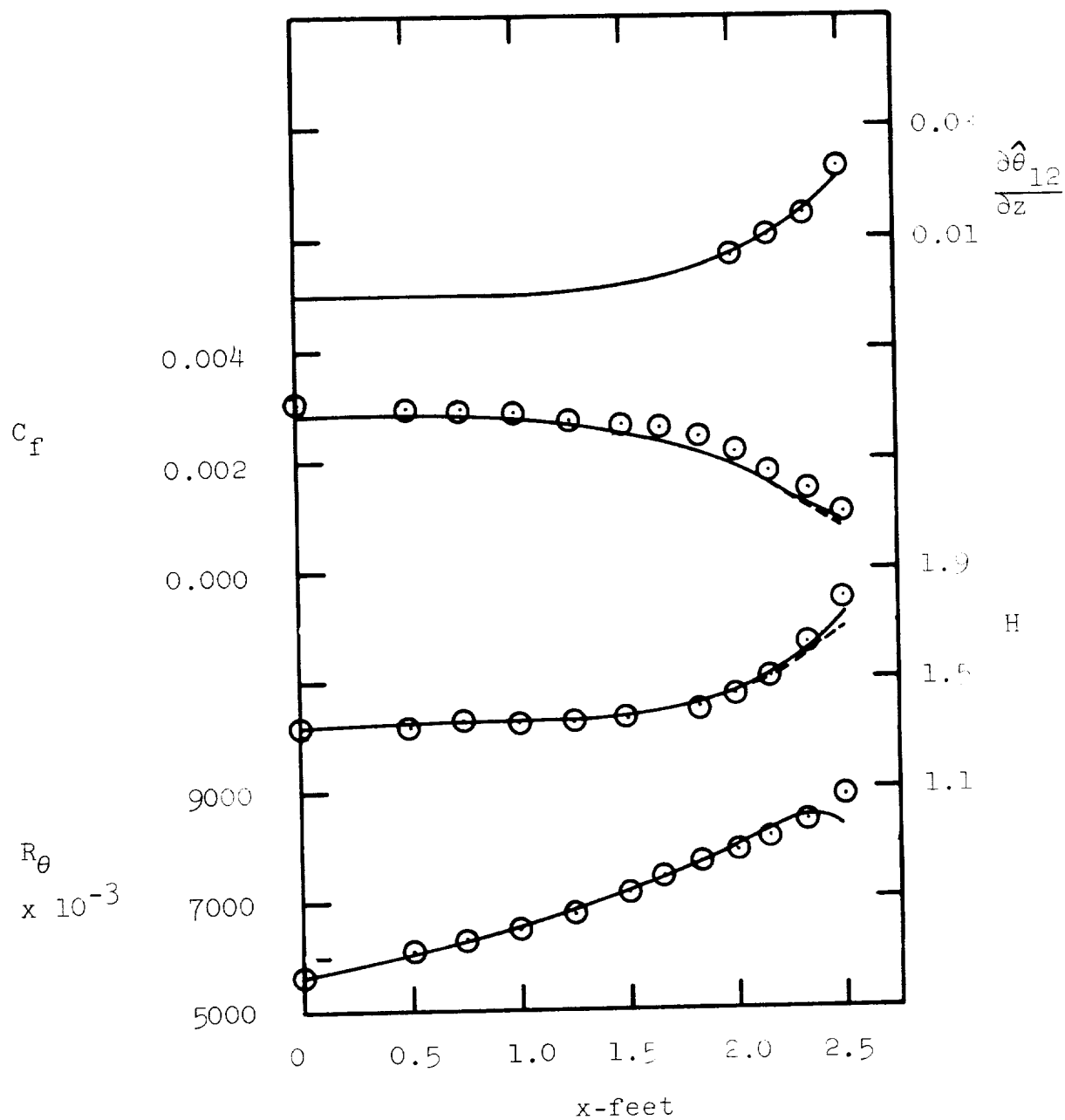


Figure 4.3 Johnston Plane of Symmetry, Integral Parameter Results

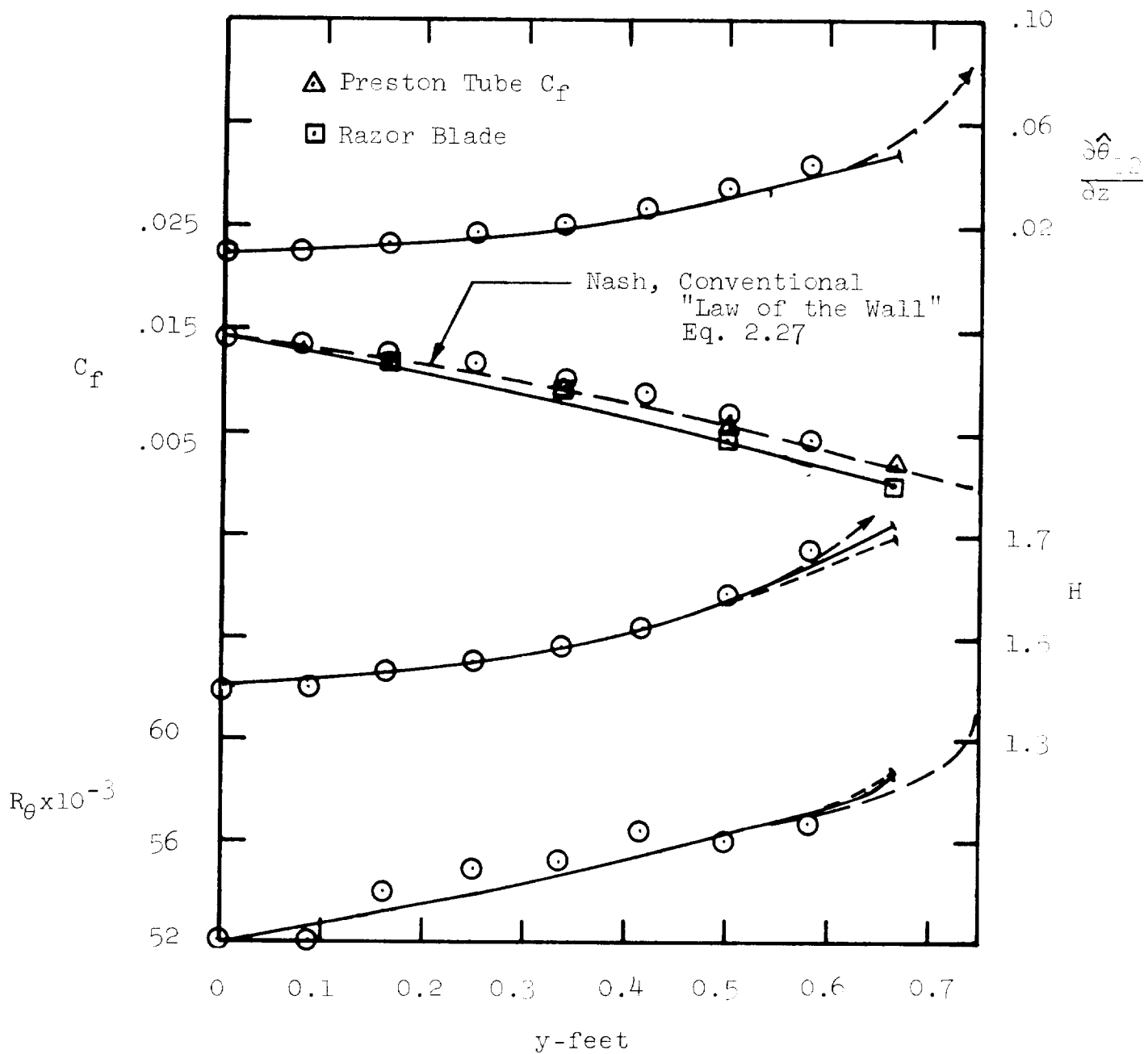


Figure 4.4 Predicted Results, East and Hoxey Plane of Symmetry

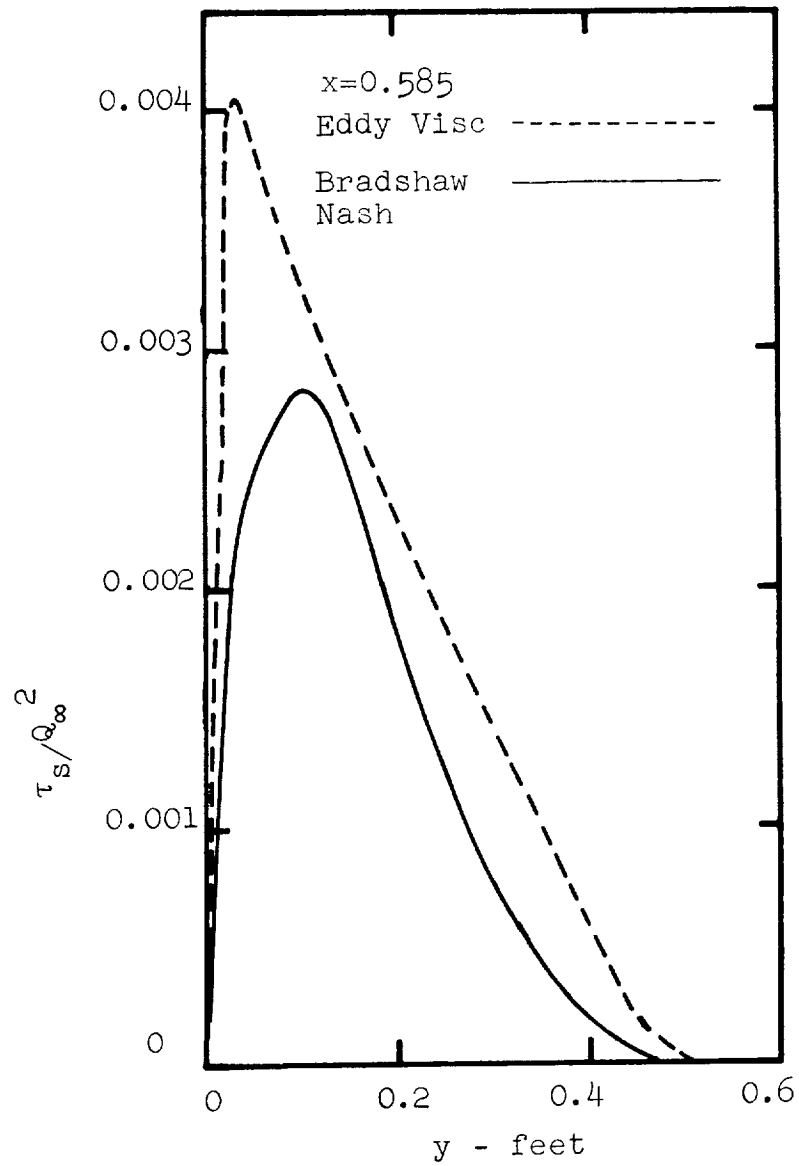


Figure 4.5 - Shear Stress Distributions For East and Hoxey Plane of Symmetry,  $x = 0.585$  feet

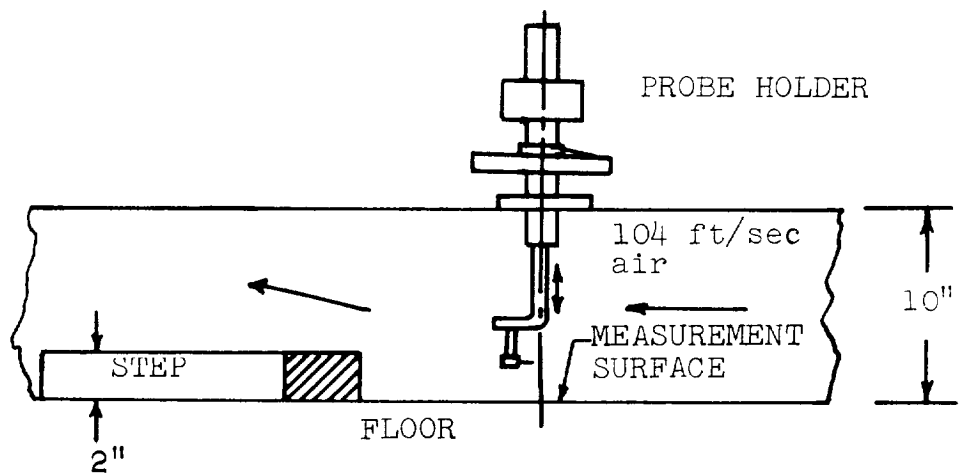
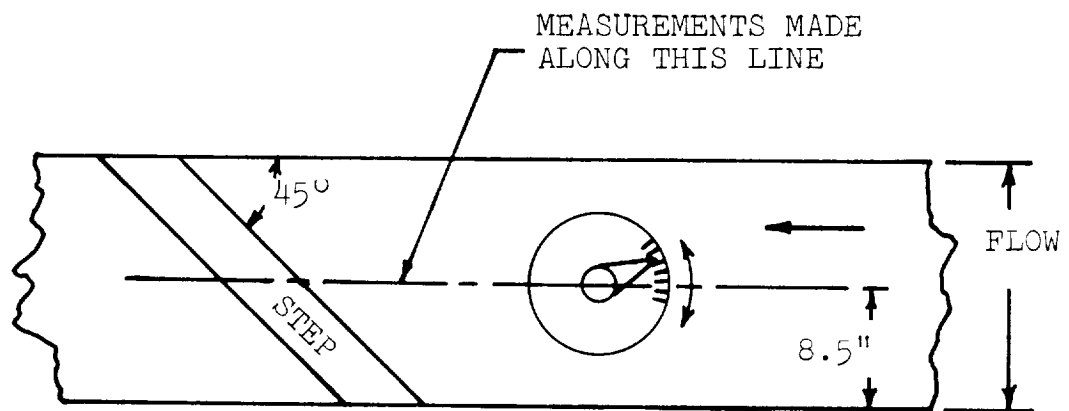


Figure 4.6 - Sketch of Johnstone Infinite Step

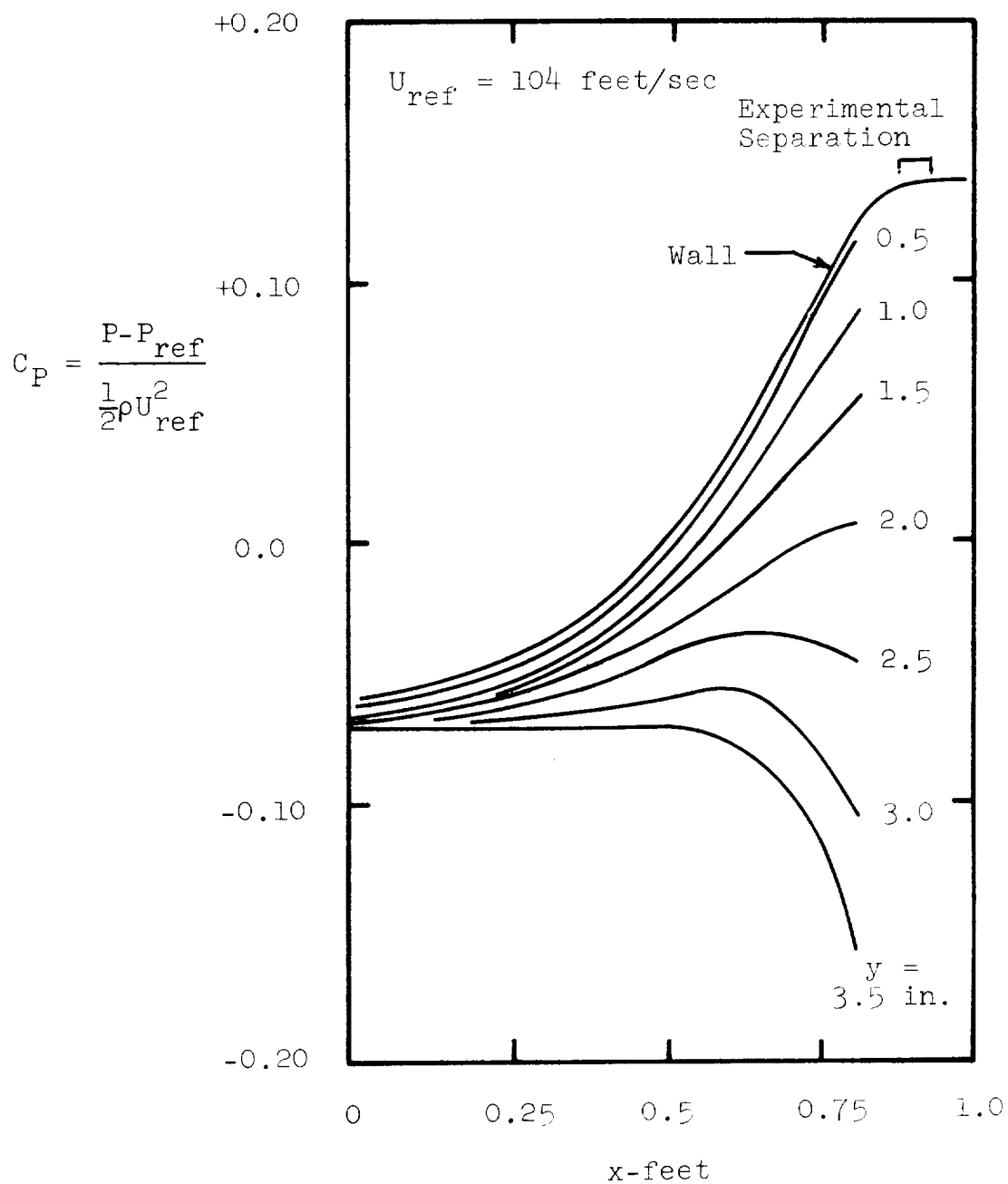


Figure 4.7 Experimental Pressure Distribution, Johnston Infinite Step

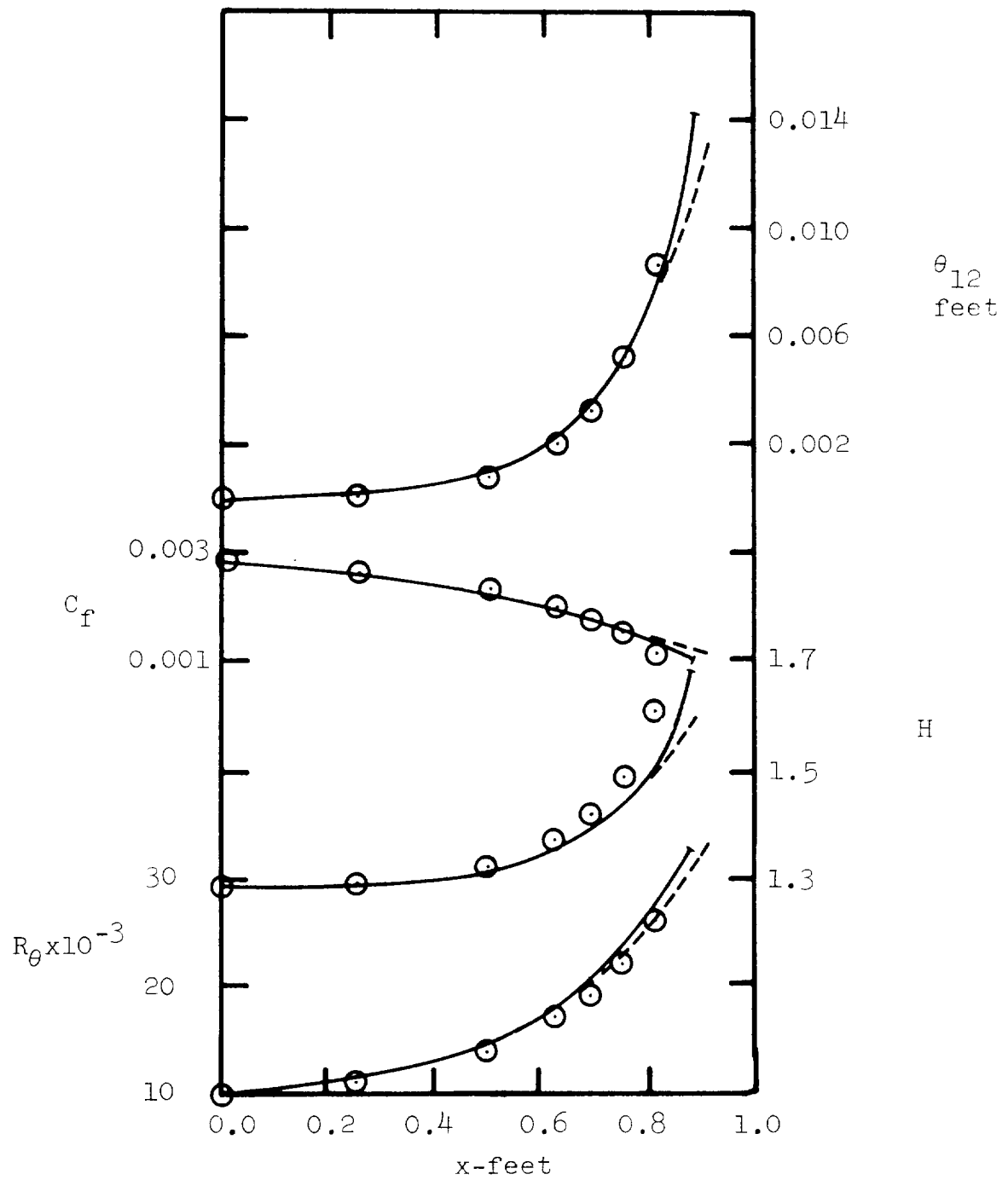


Figure 4.8 Integral Parameter Results,  
Johnston Infinite Step

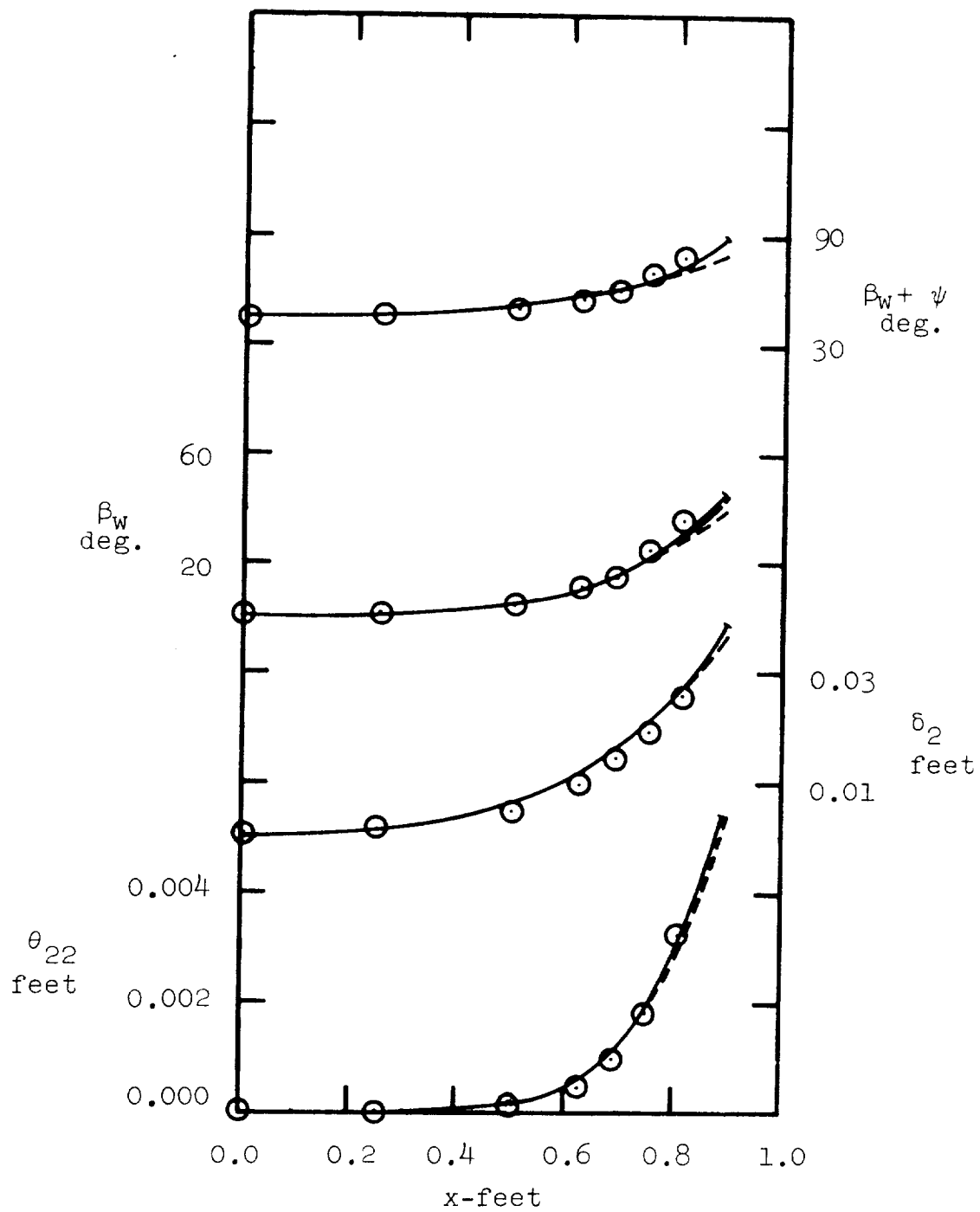


Figure 4.8 (cont'd)

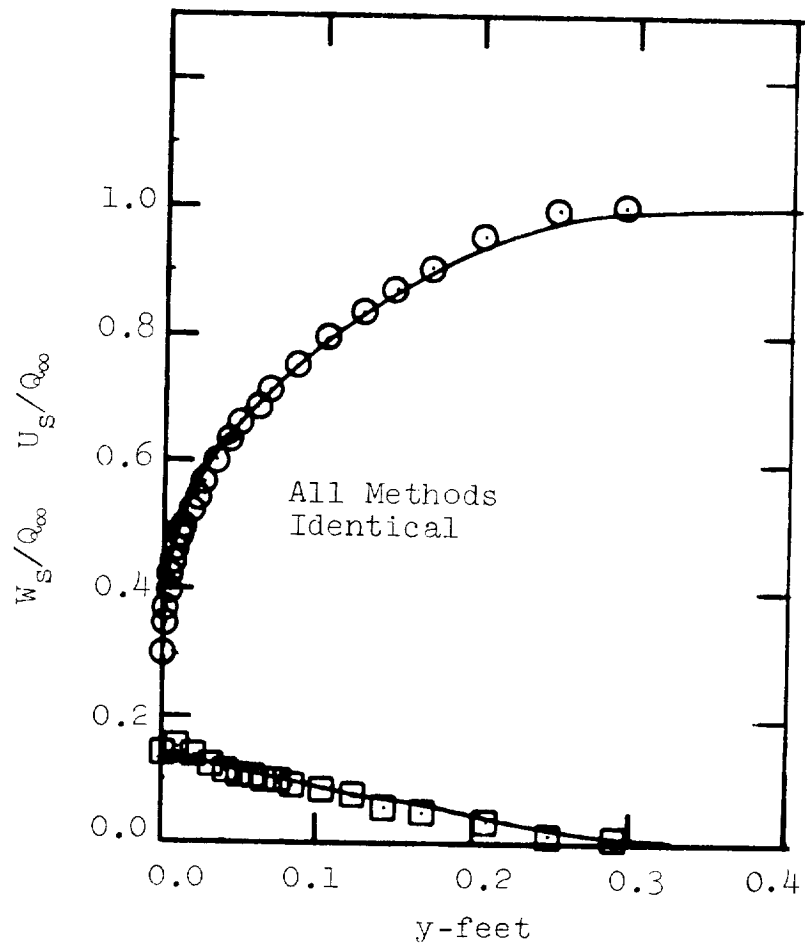


Figure 4.9 Mean Velocity Profiles,  $x = 0.75$  Feet, Johnston Infinite Step

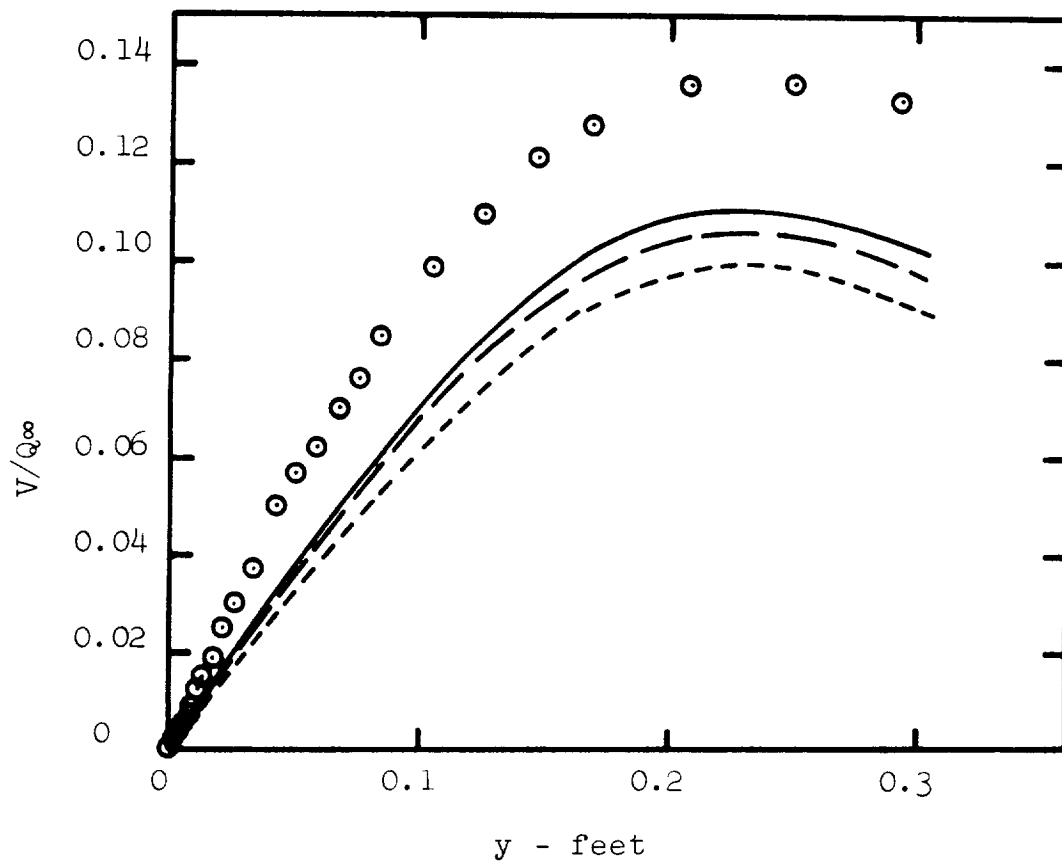


Figure 4.10 - Normal Velocity,  $V$ ,  
Johnston Infinite Step

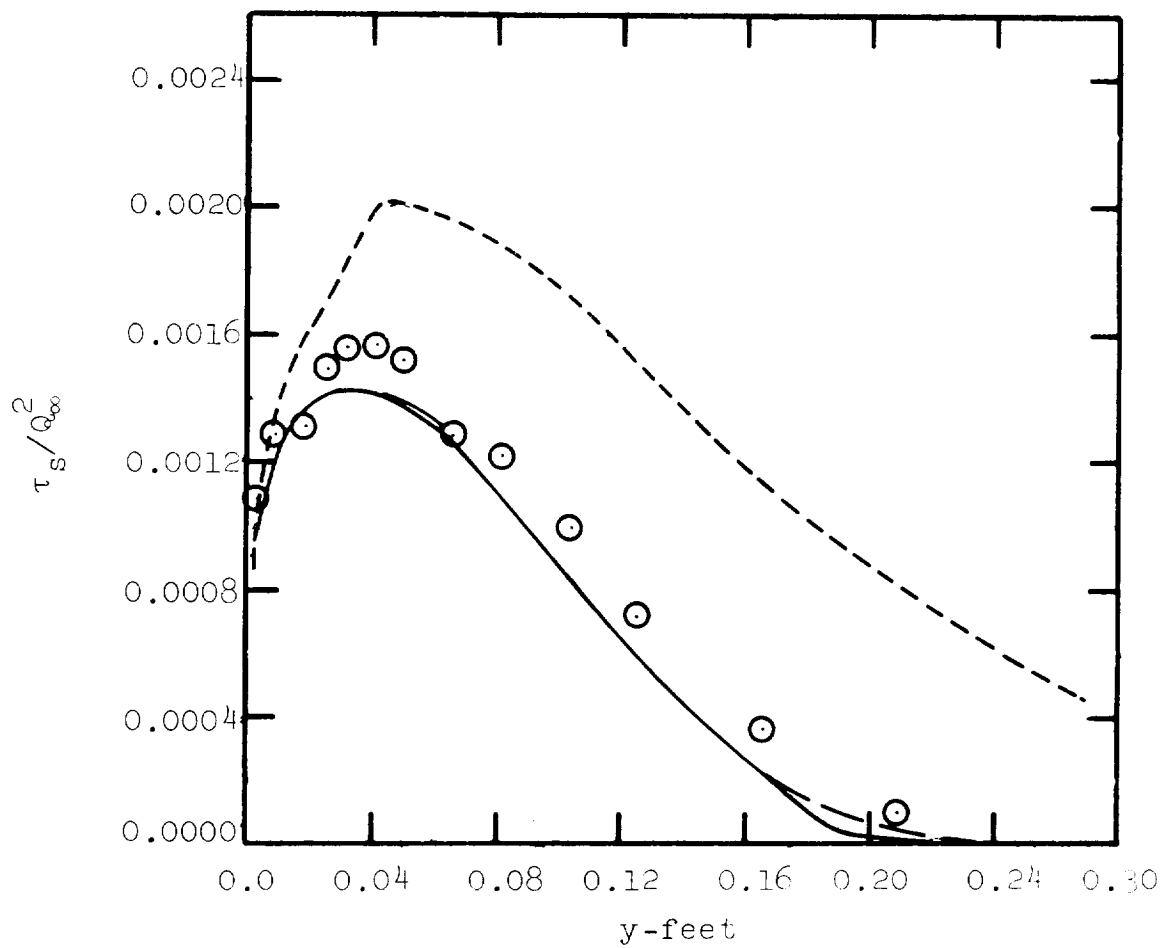


Figure 4.11 Shear Stress Magnitude,  $x = 0.75$  Feet, Johnston Infinite Step

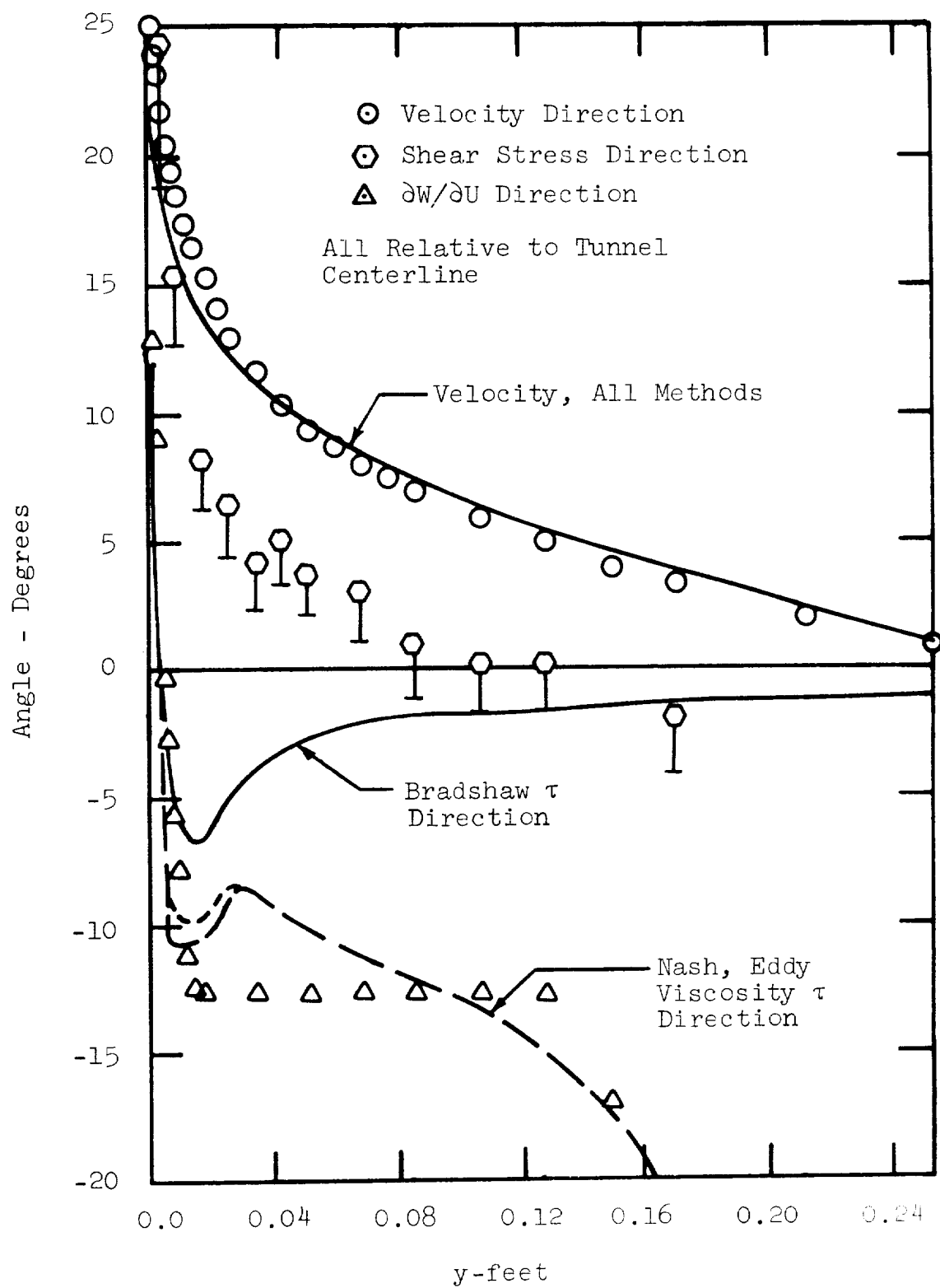


Figure 4.12 Velocity and Shear Stress Directions,  
 $x = 0.75$  Feet, Johnston Infinite Step

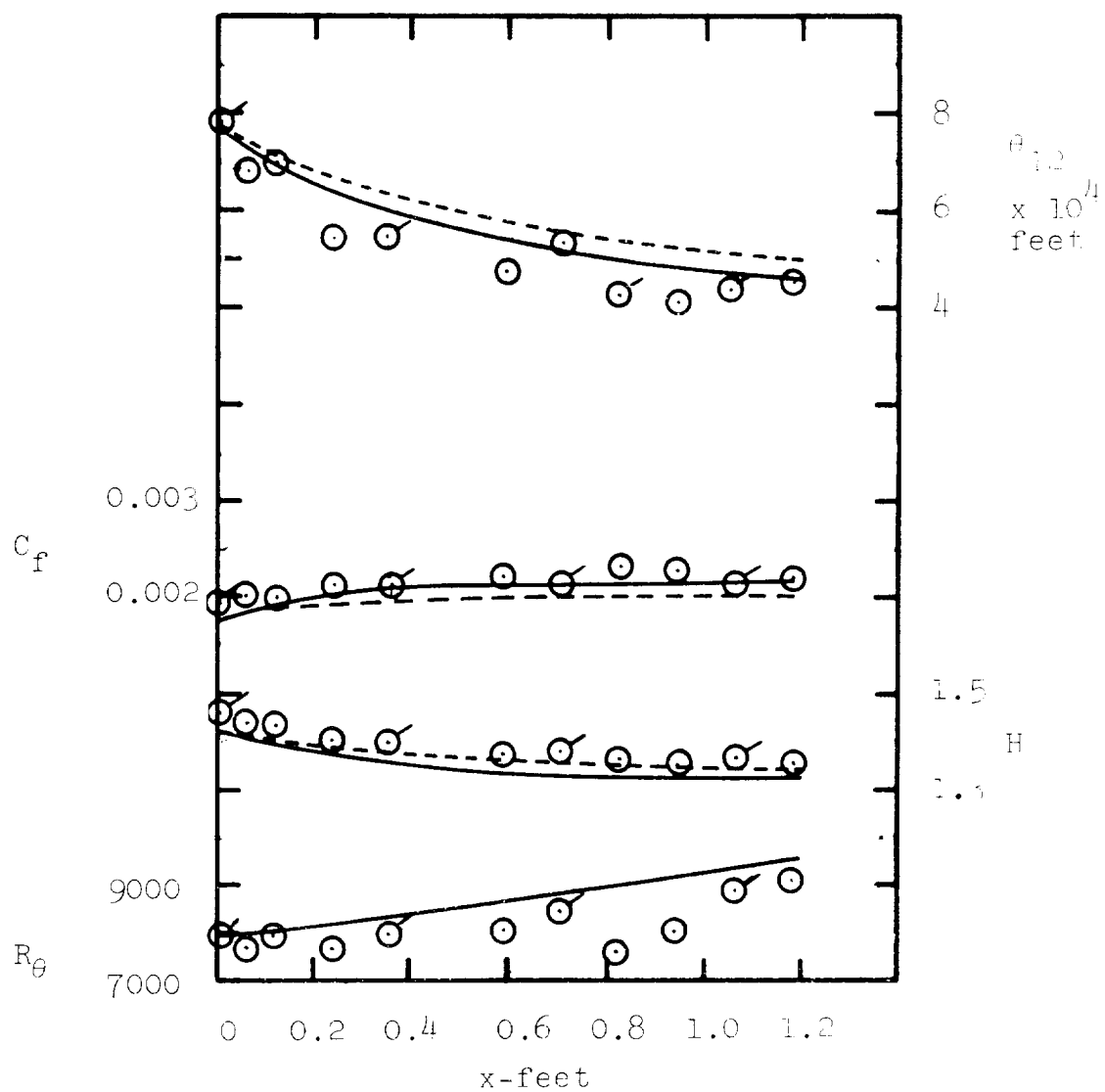


Figure 4.13 Bradshaw and Terrell (1969) Integral Parameter Results

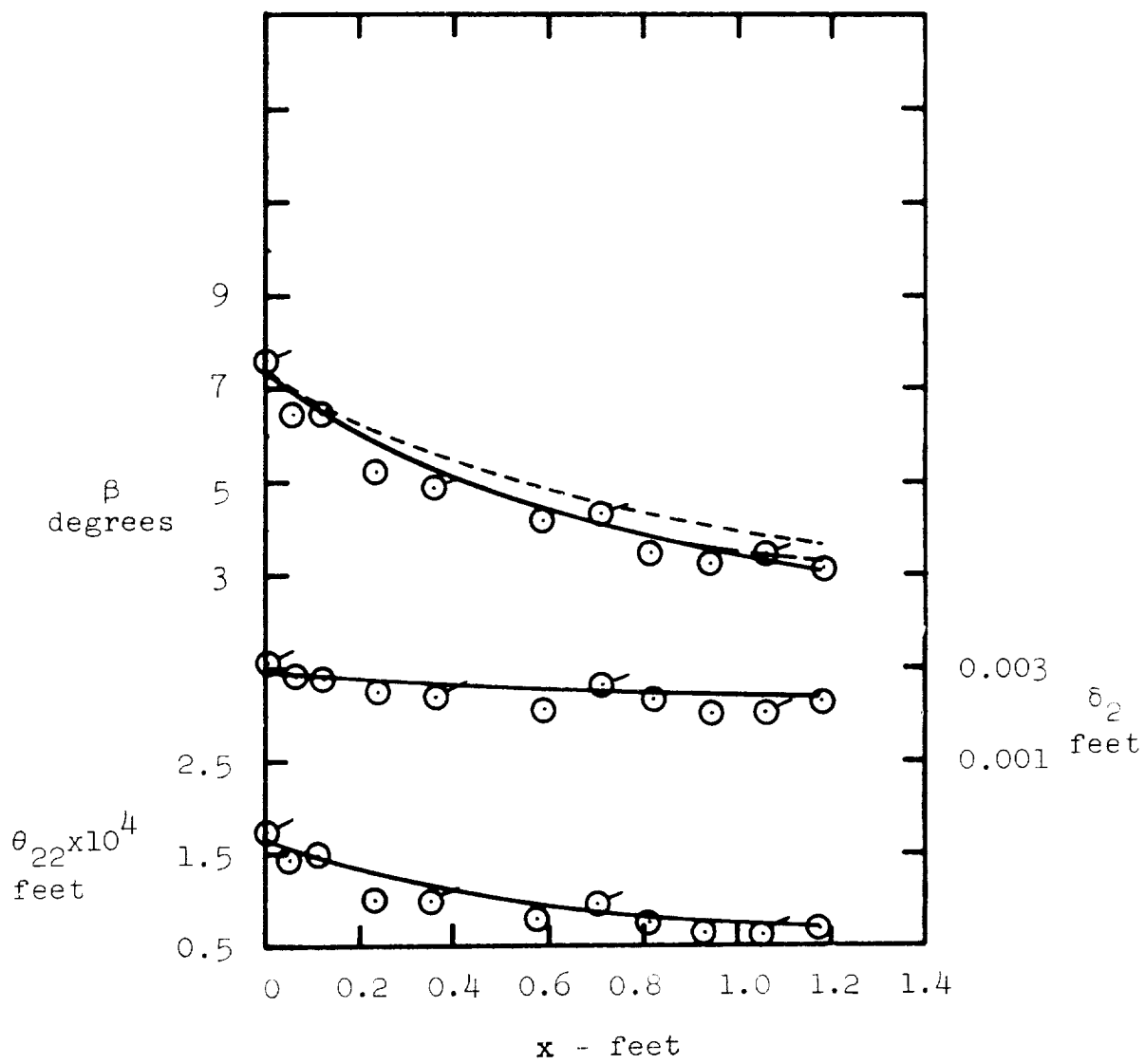


Figure 4.13 - (Cont'd)

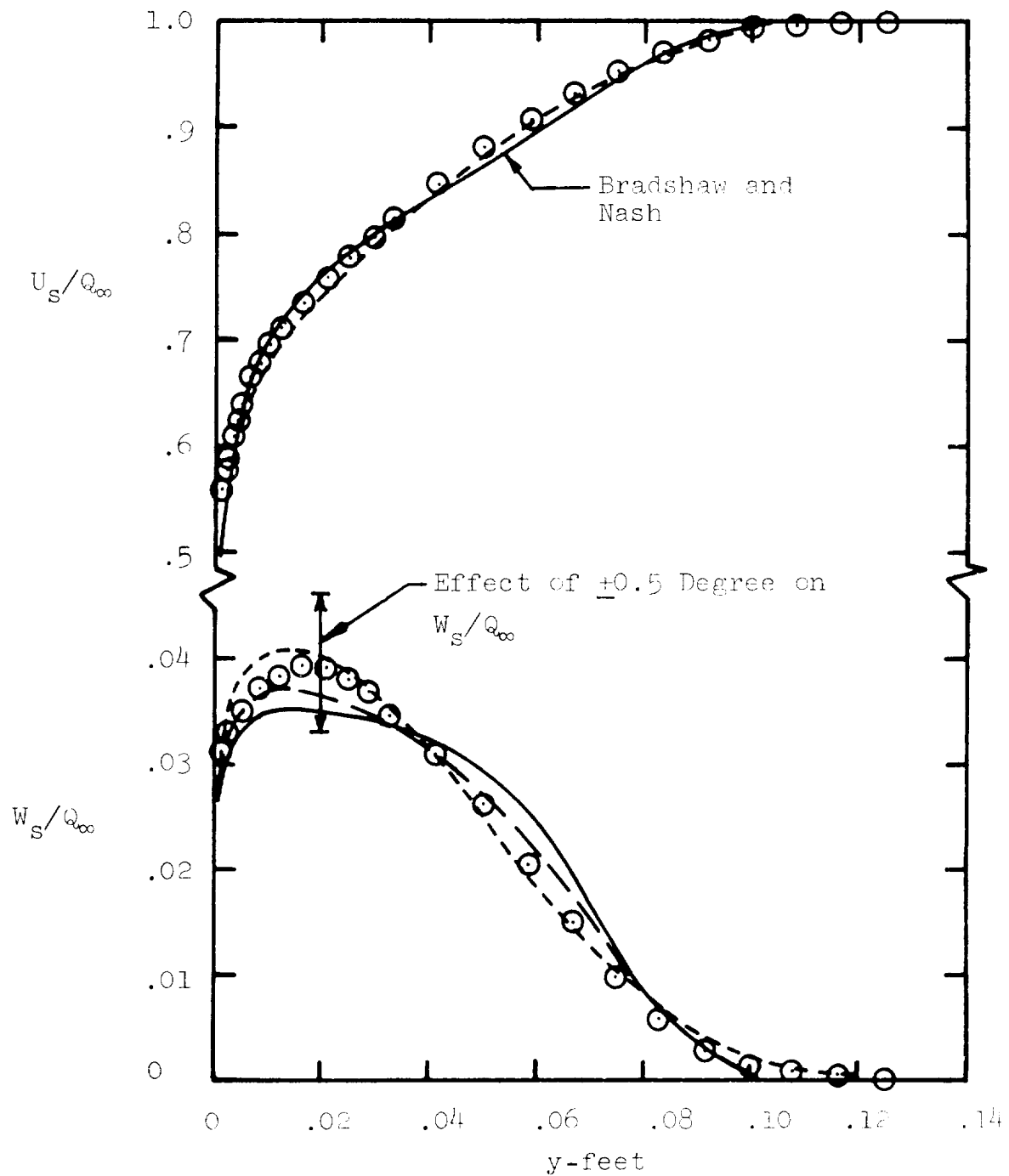


Figure 4.14 Bradshaw and Terrell Velocity Profiles  
at  $x = 1.18$  Feet

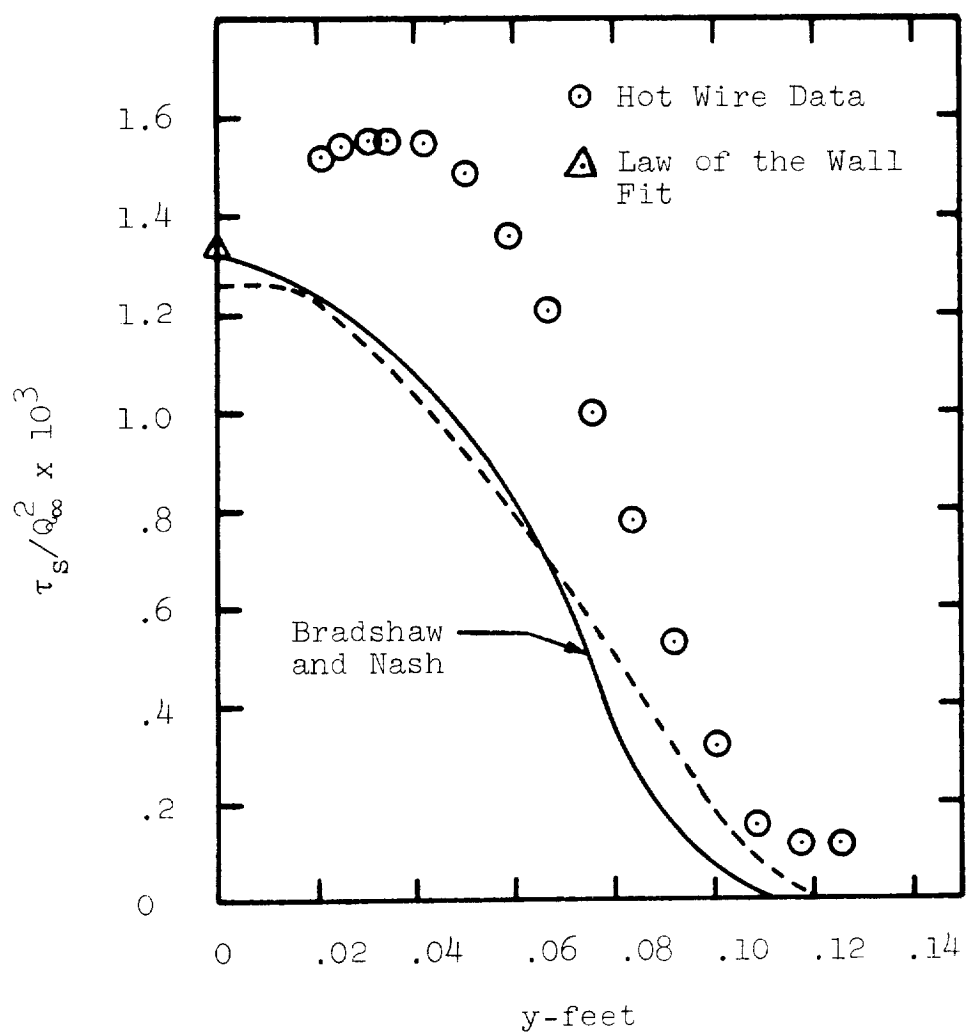


Figure 4.15 Bradshaw and Terrell Streamwise Shear Stress Magnitude,  $x = 1.18$  Feet

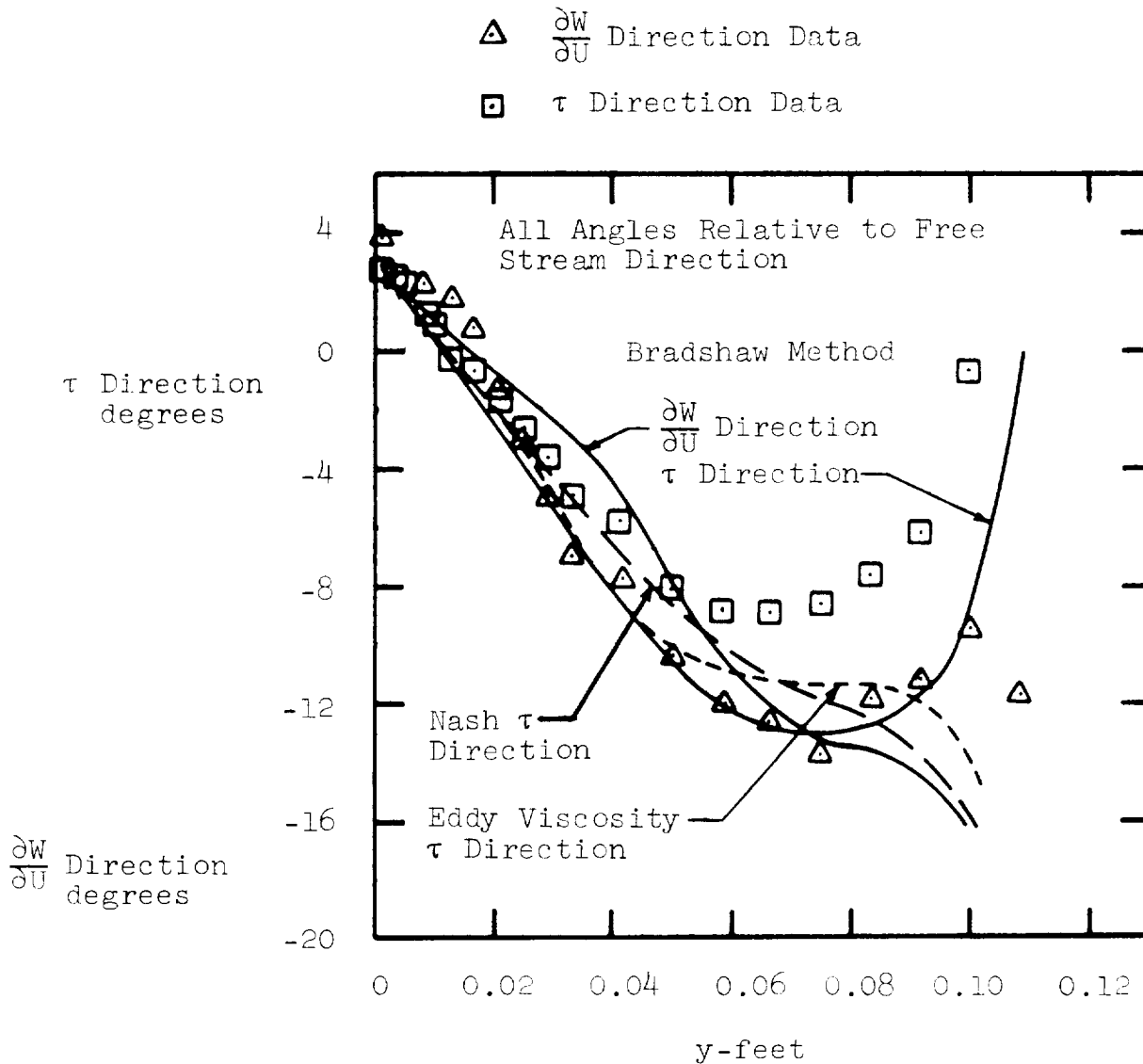


Figure 4.16 Bradshaw and Terrell Mean Velocity Gradient ( $\frac{\partial W}{\partial U}$ ) and Shear Stress ( $\tau$ ) Directions Relative to External Velocity Direction

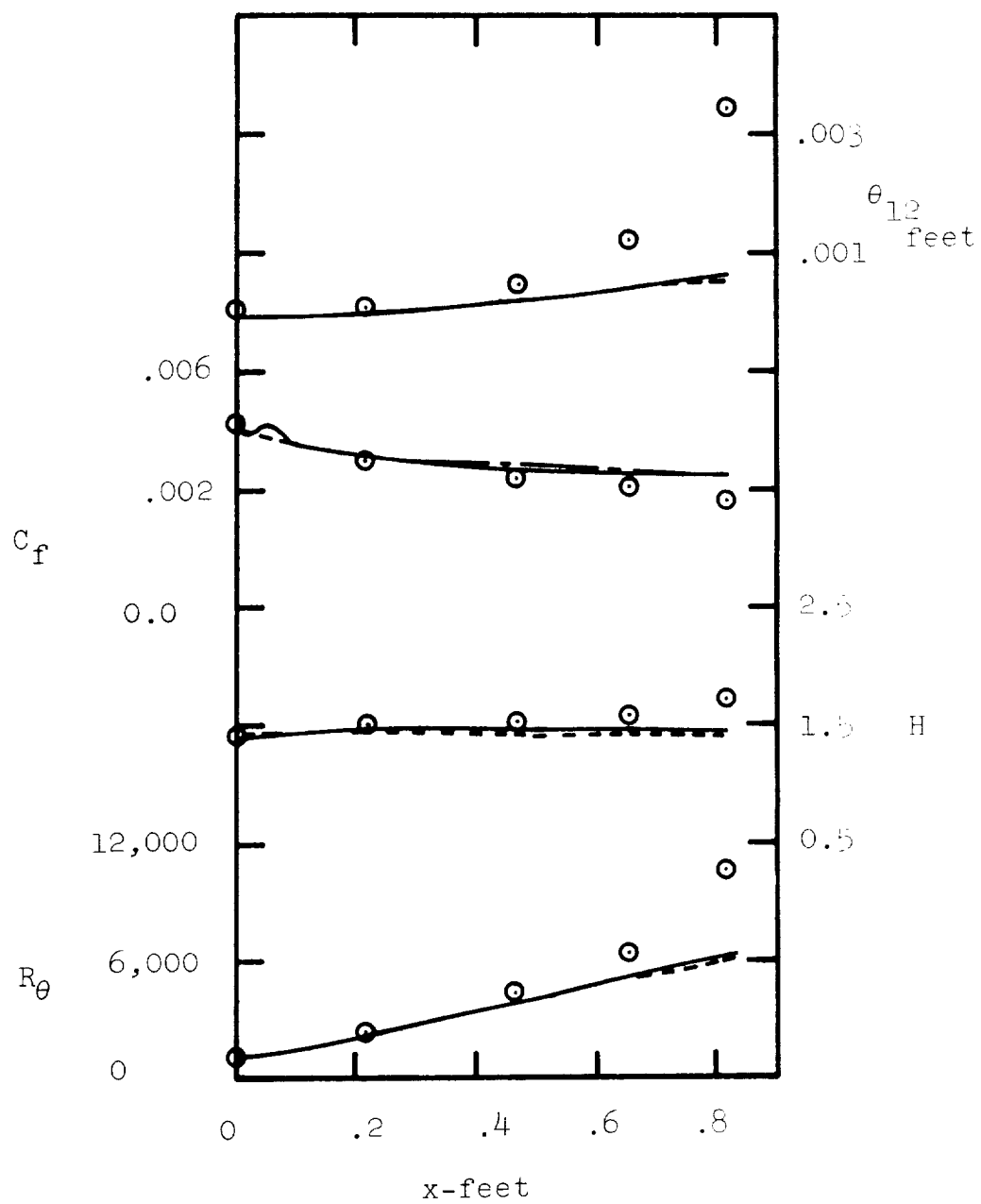


Figure 4.17 Cumpsty and Head Integral Parameter Results

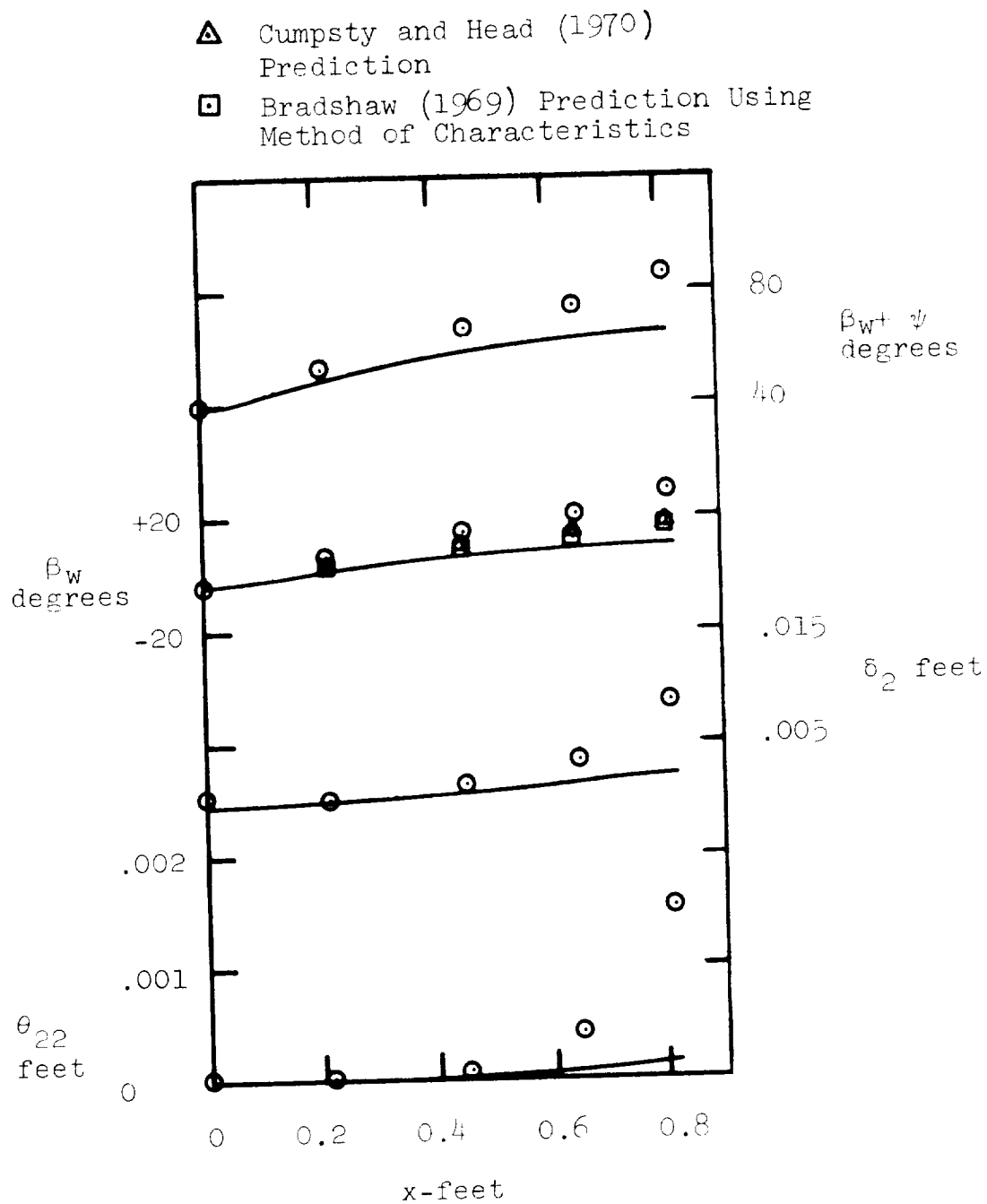


Figure 4.17 (Cont'd)

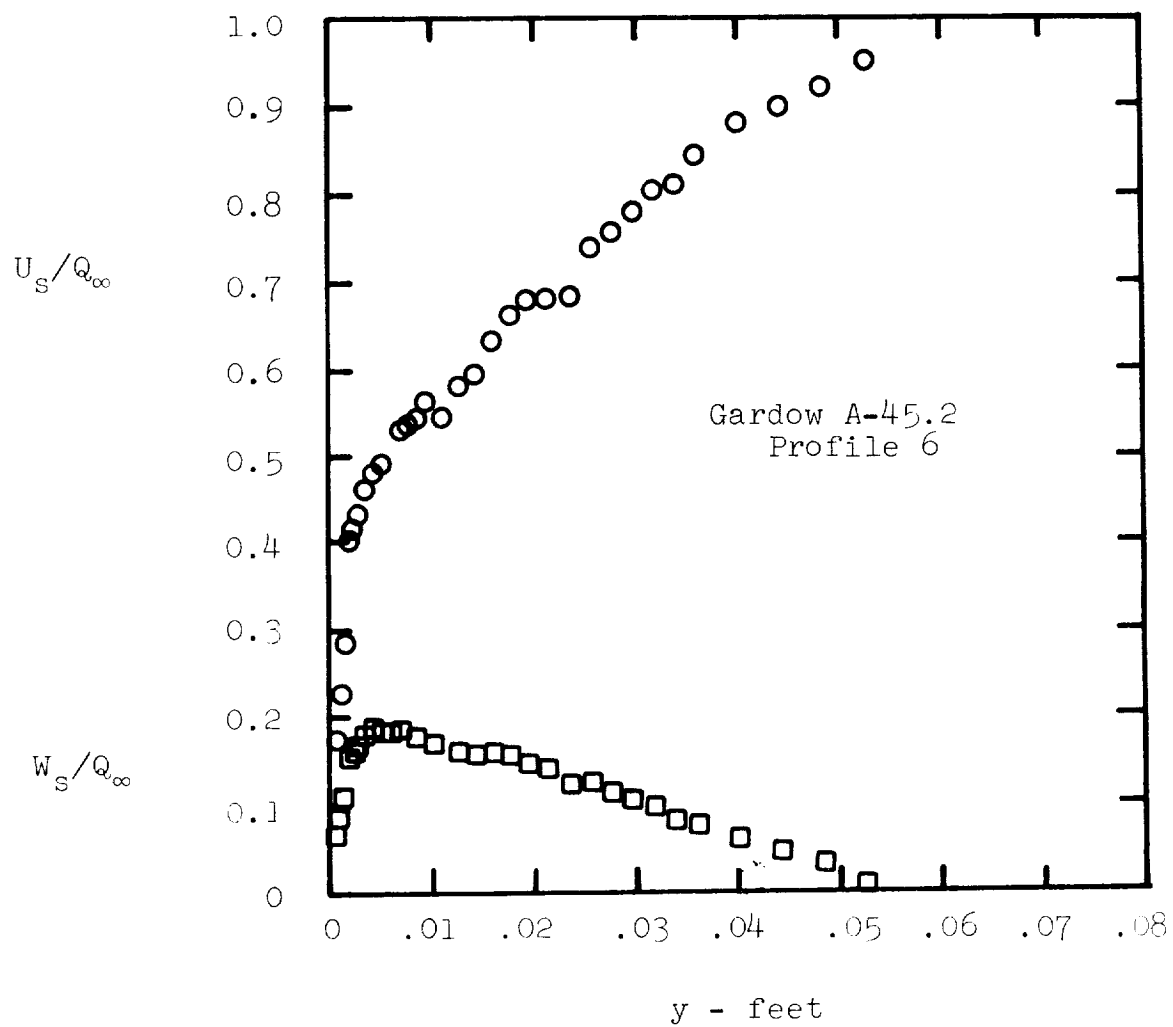


Figure 4.18 Typical Gardow (1958) Velocity Profile

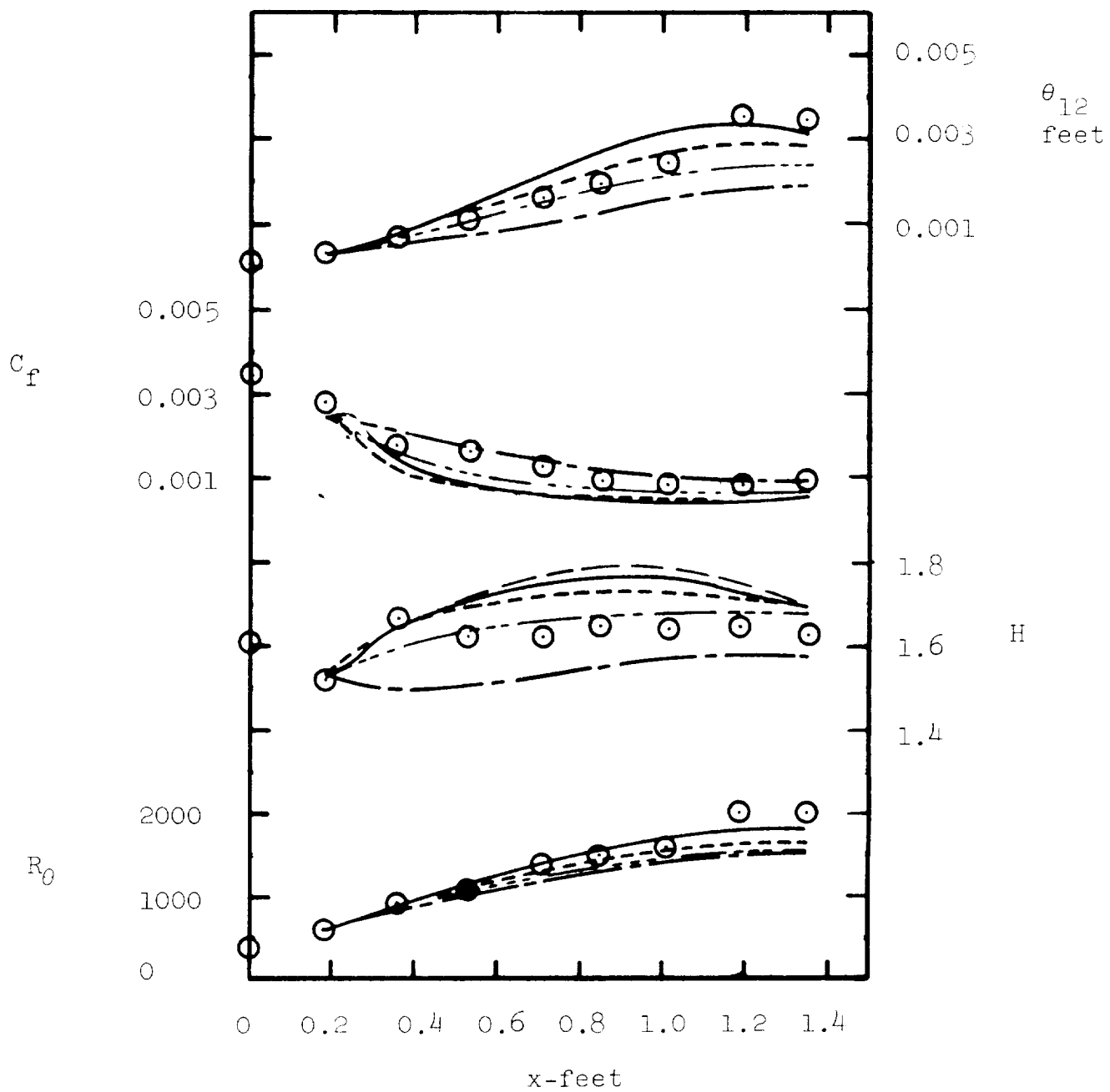


Figure 4.19 Gardow A-45.2 Vaneless Diffuser Integral Parameter Results

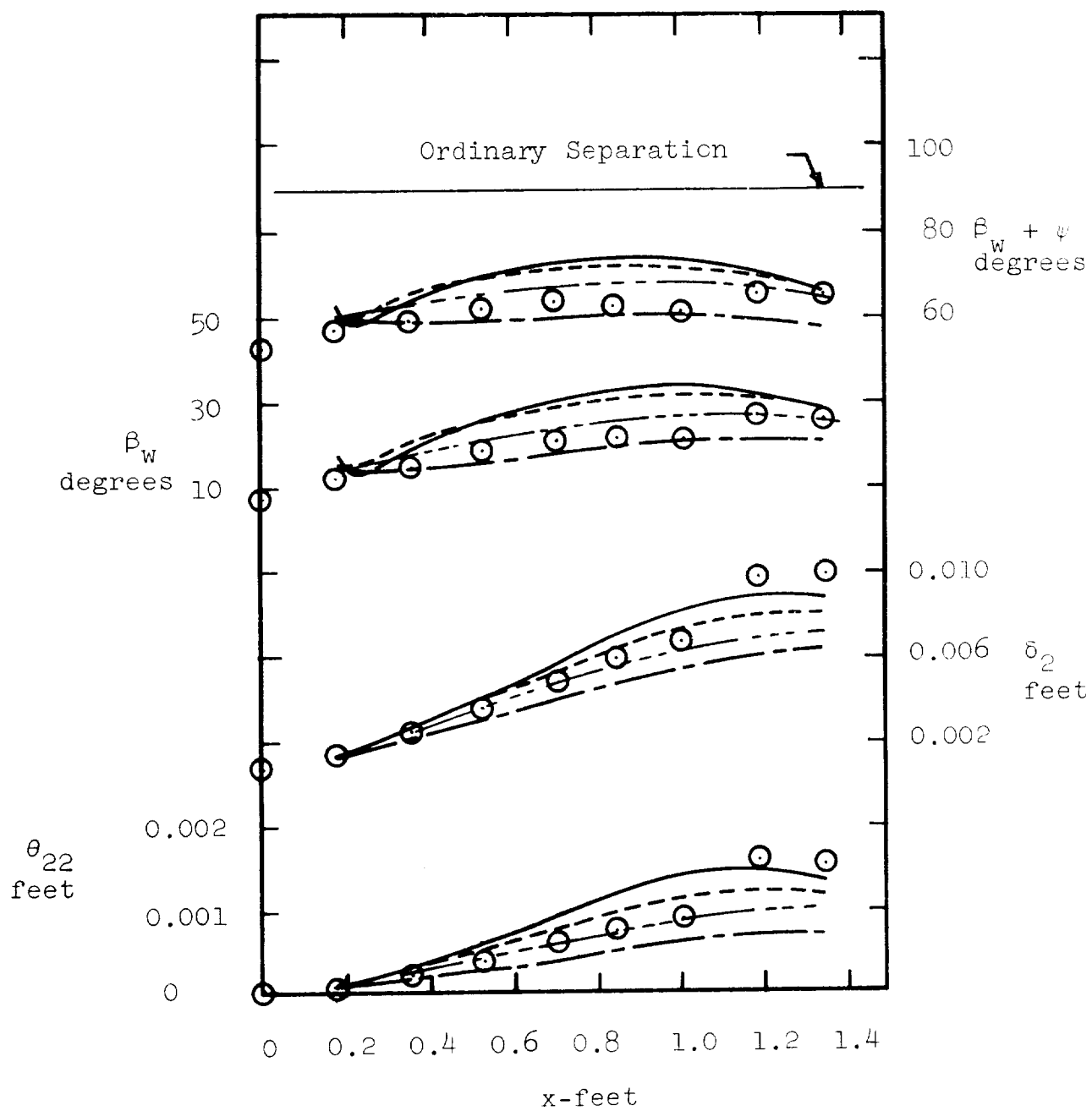


Figure 4.19 (Cont'd)

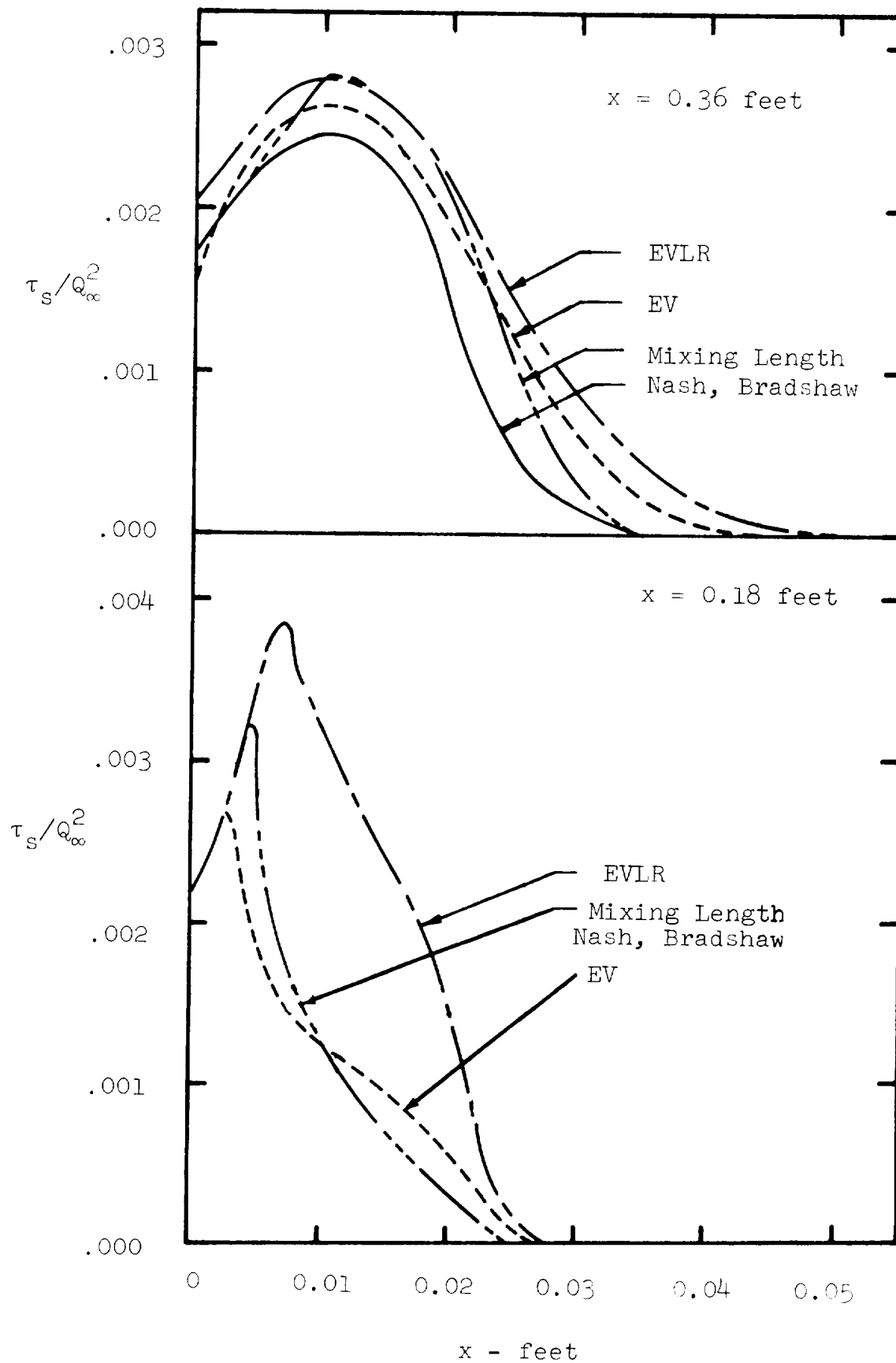


Figure 4.20 Gardow A-45.2 Shear Stress Distributions (No Data Available)

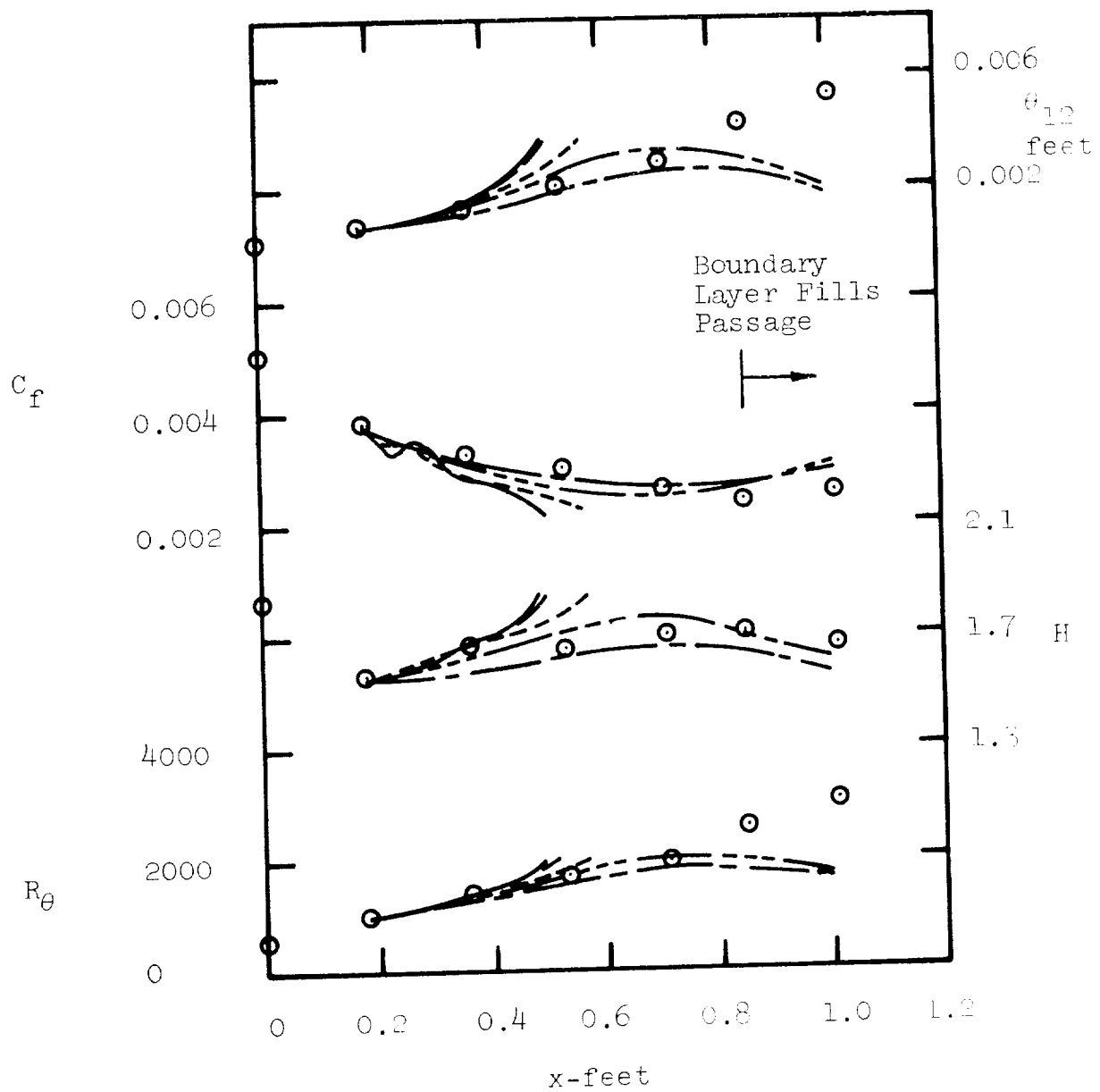


Figure 4.21 Gardow B-50.6 Vaneless Diffuser Integral Parameter Results

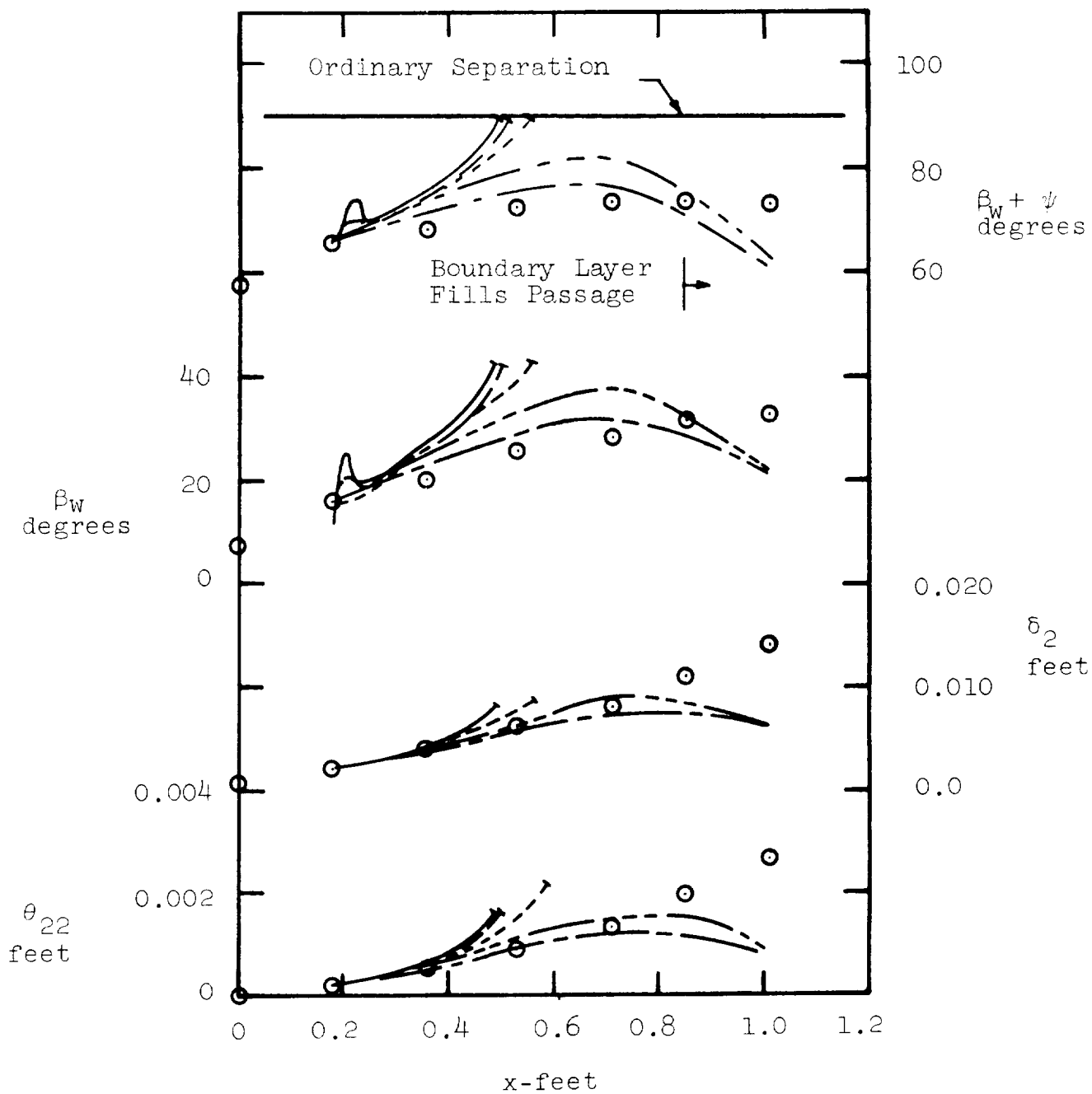


Figure 4.21 (Cont'd)

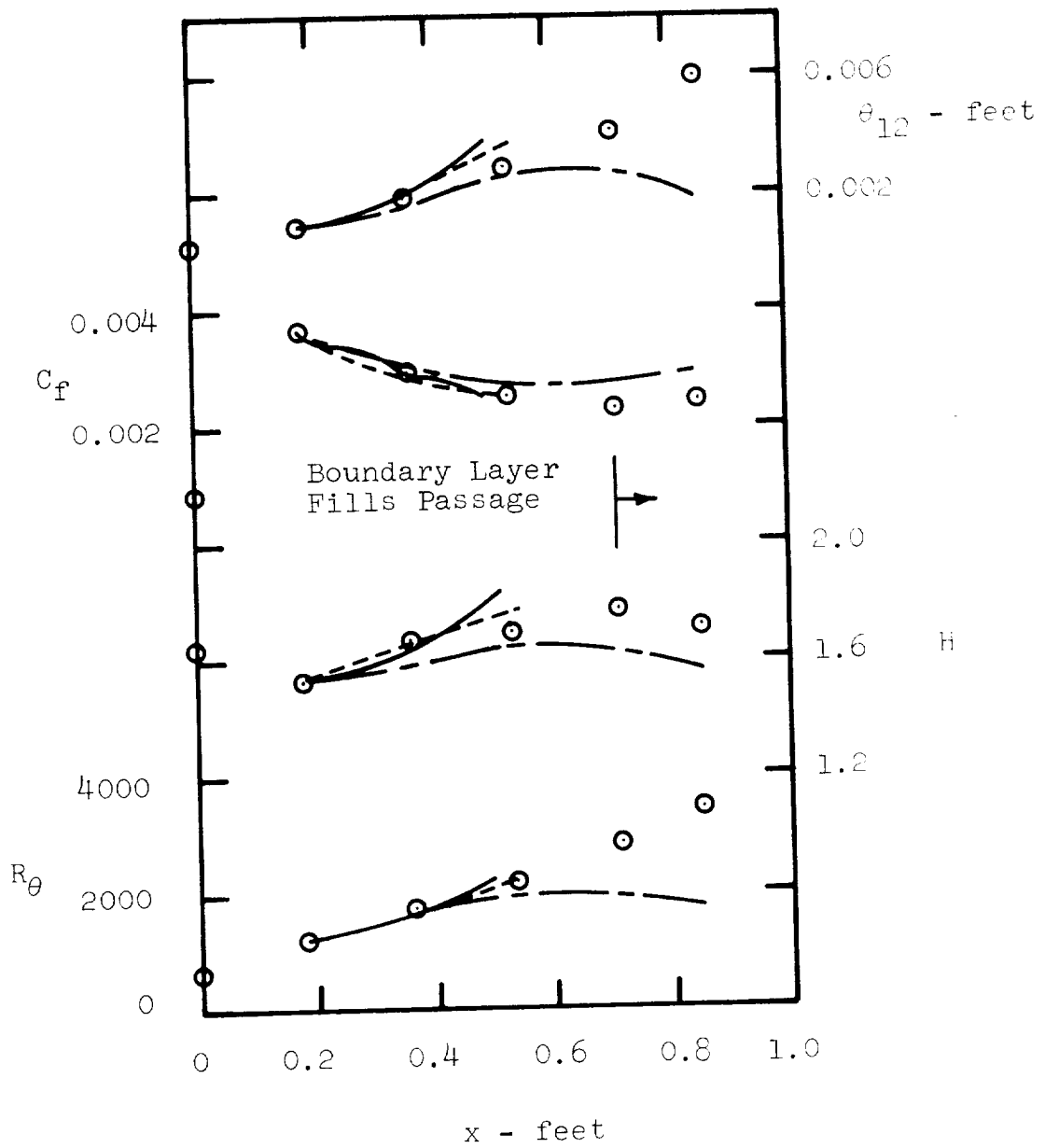


Figure 4.22 Gardow B-52.1 Vaneless Diffuser, Integral Parameter Results

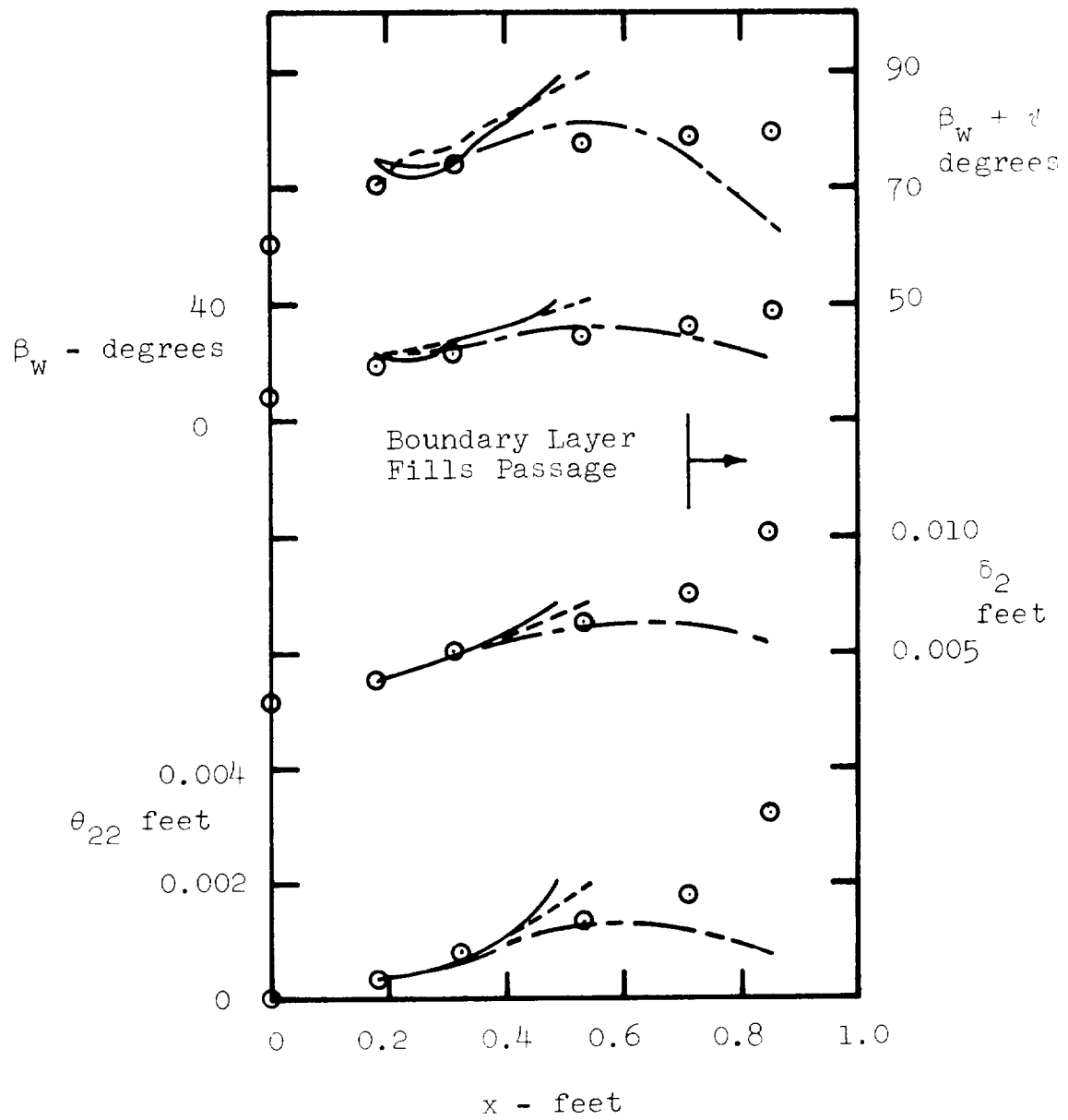


Figure 4.22 (continued)

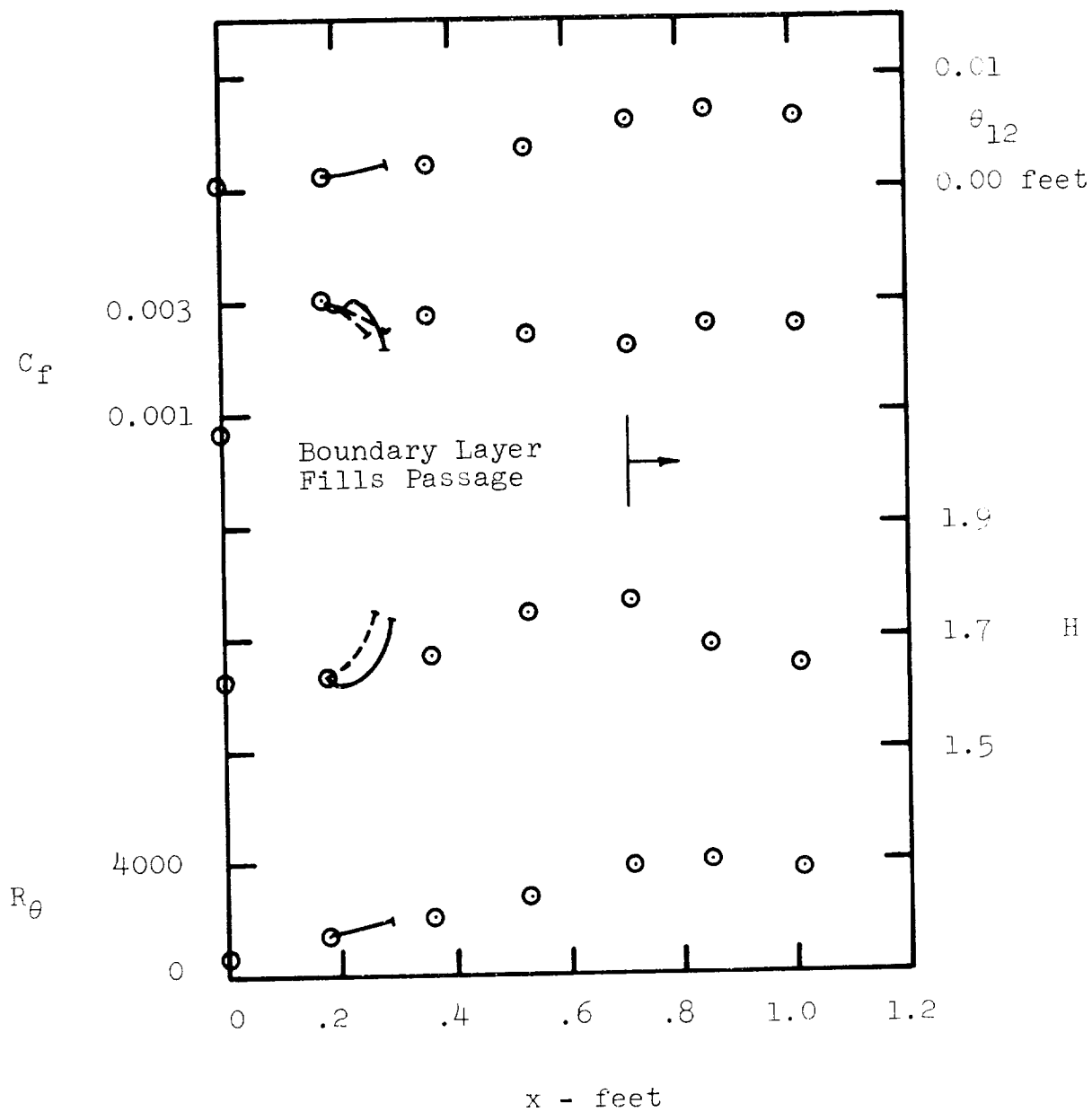


Figure 4.23 Gardow B-54.5 Vaneless Diffuser, Integral Parameter Results

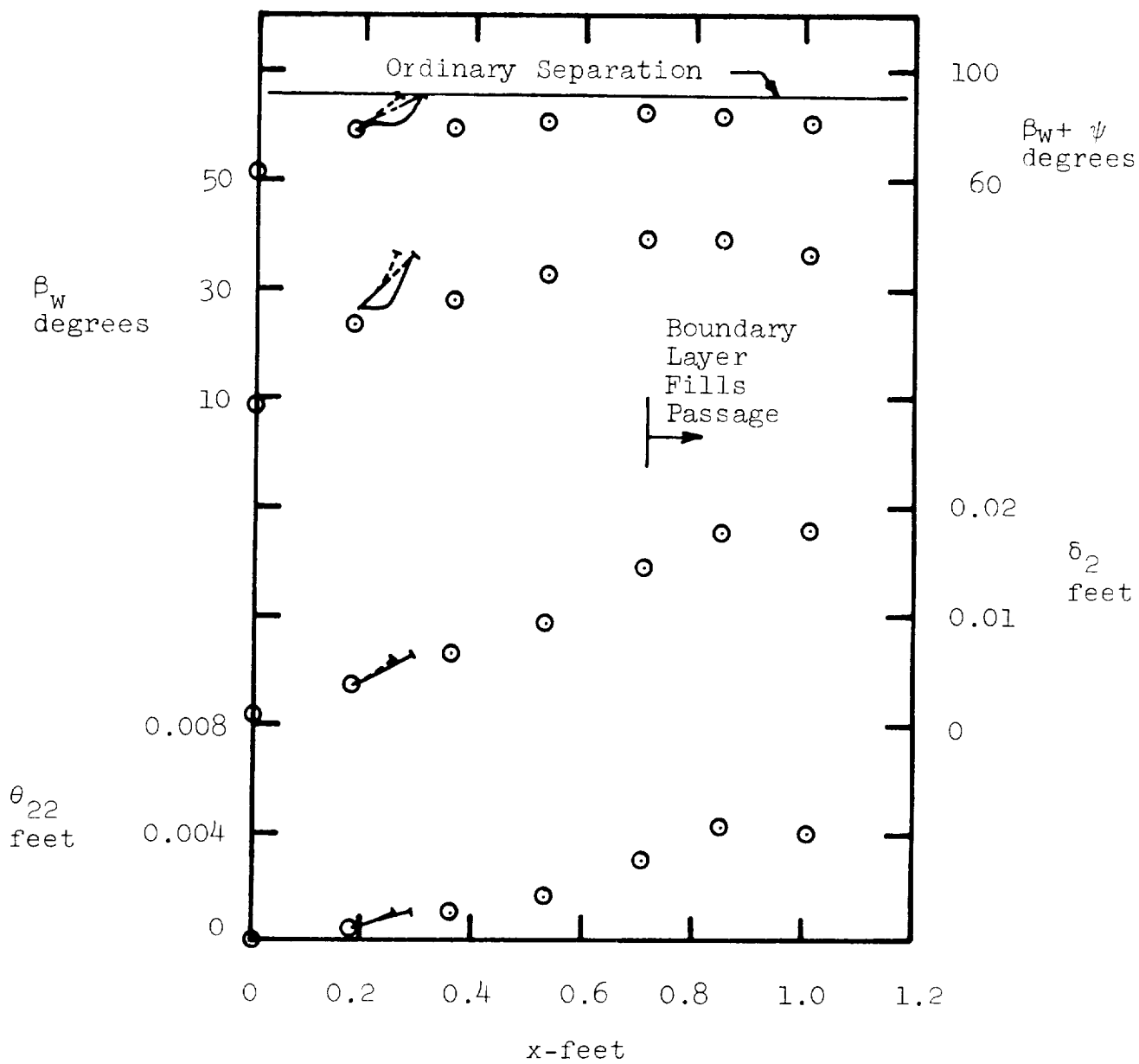


Figure 4.23 (Cont'd)

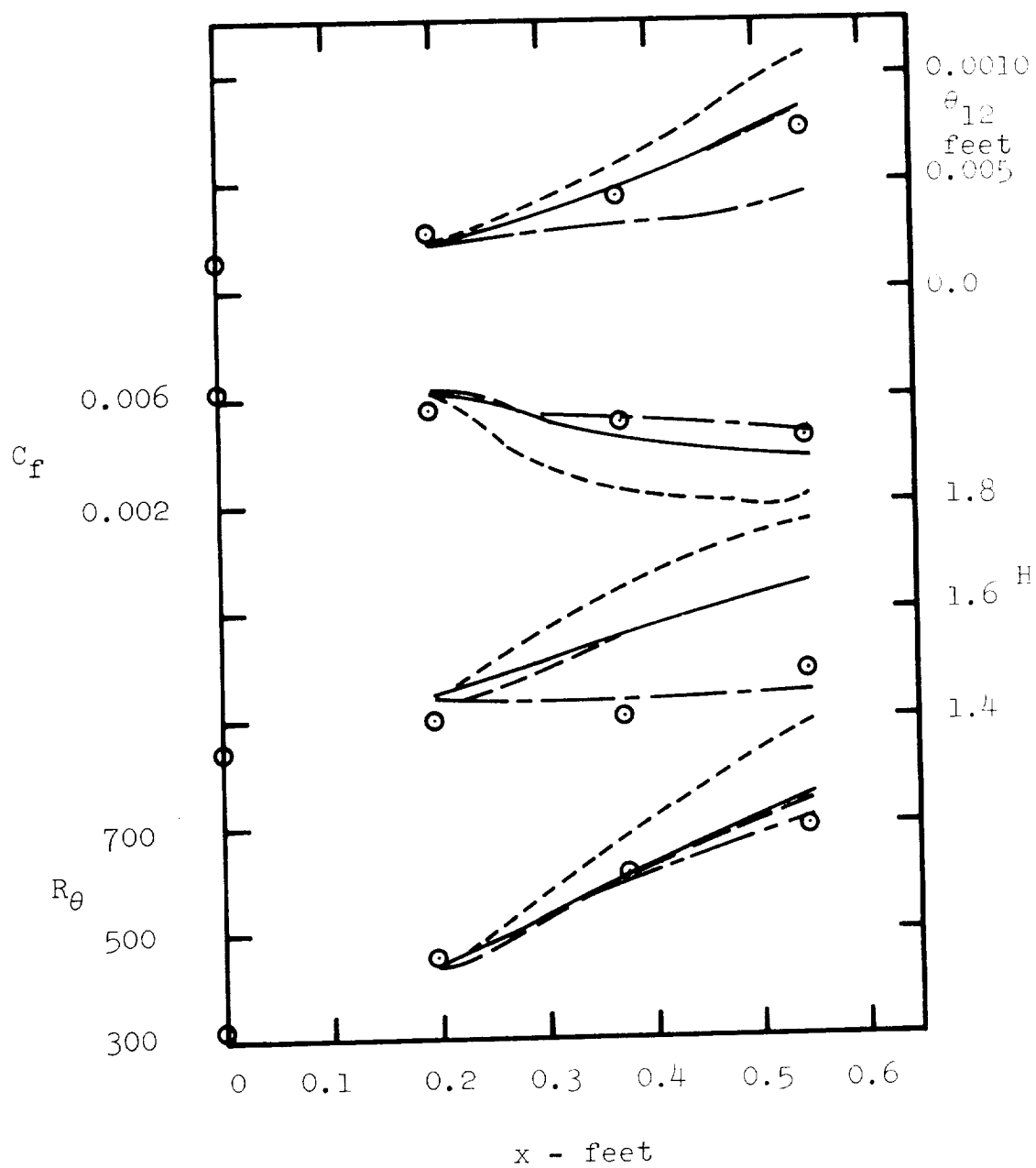


Figure 4.24 Integral Parameter Results, Jansen 47° Vaneless Diffuser

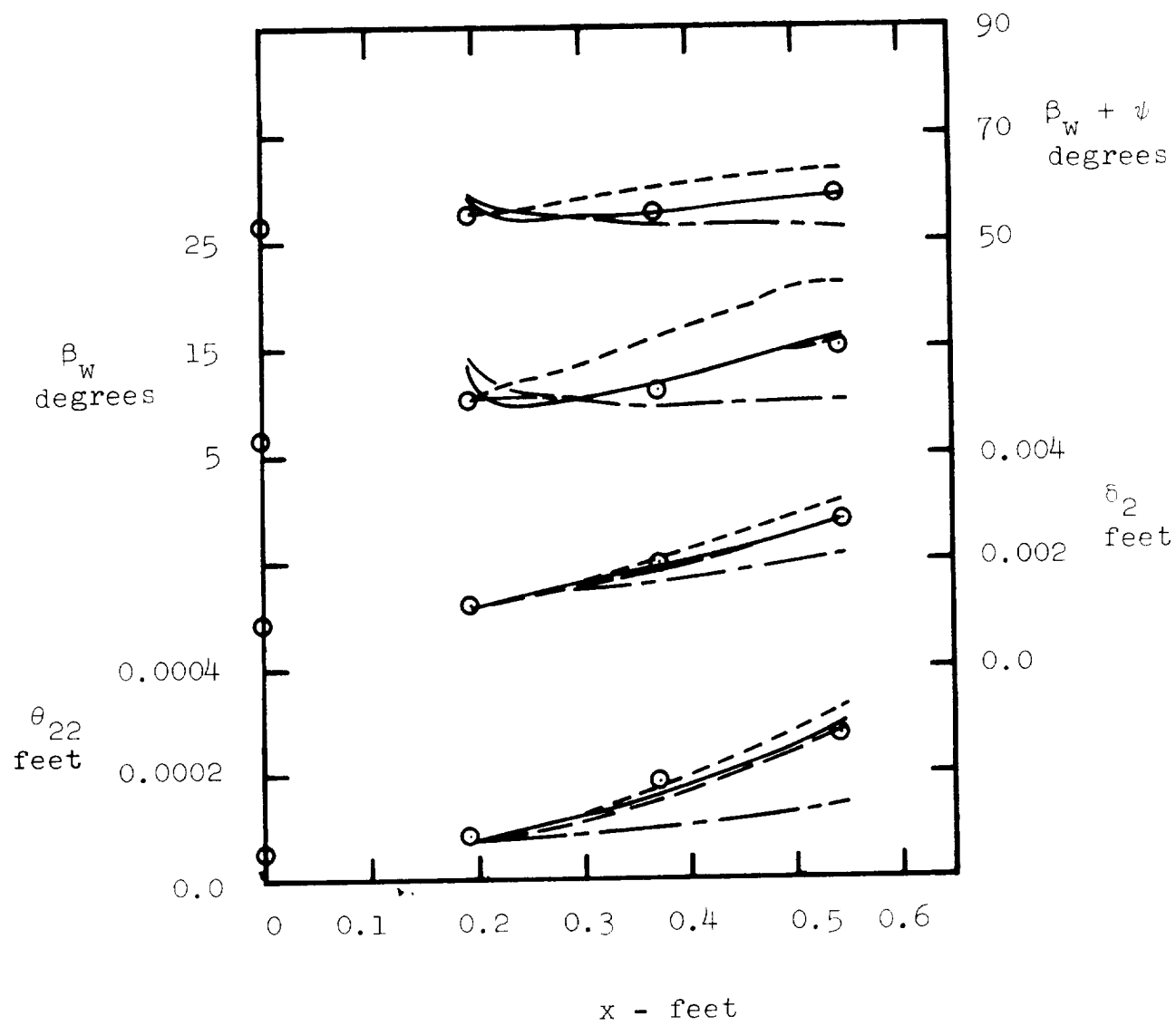


Figure 4.26 (continued)

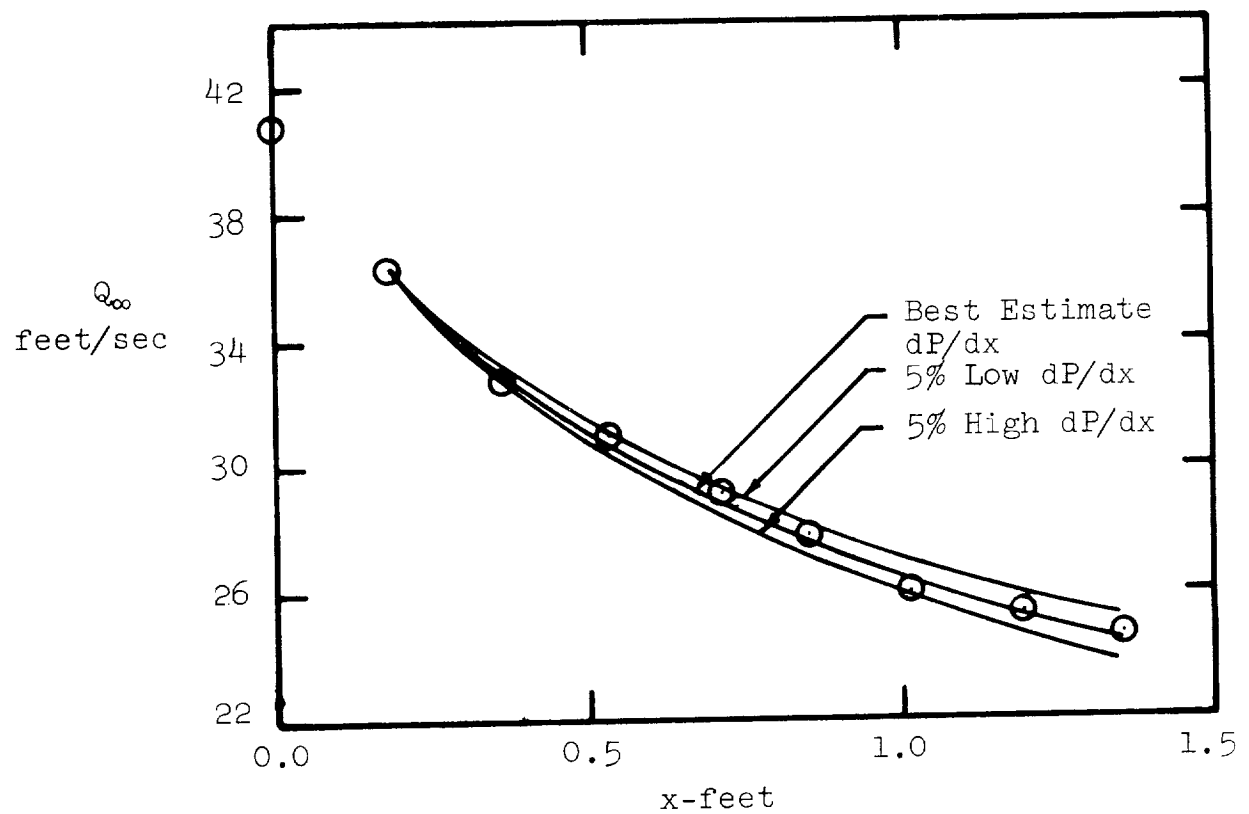


Figure 4.25 Effect of  $\pm 5\%$  Change of  $dP/dx$  on Free Stream Velocity, Gardow A-45.2 Vaneless Diffuser

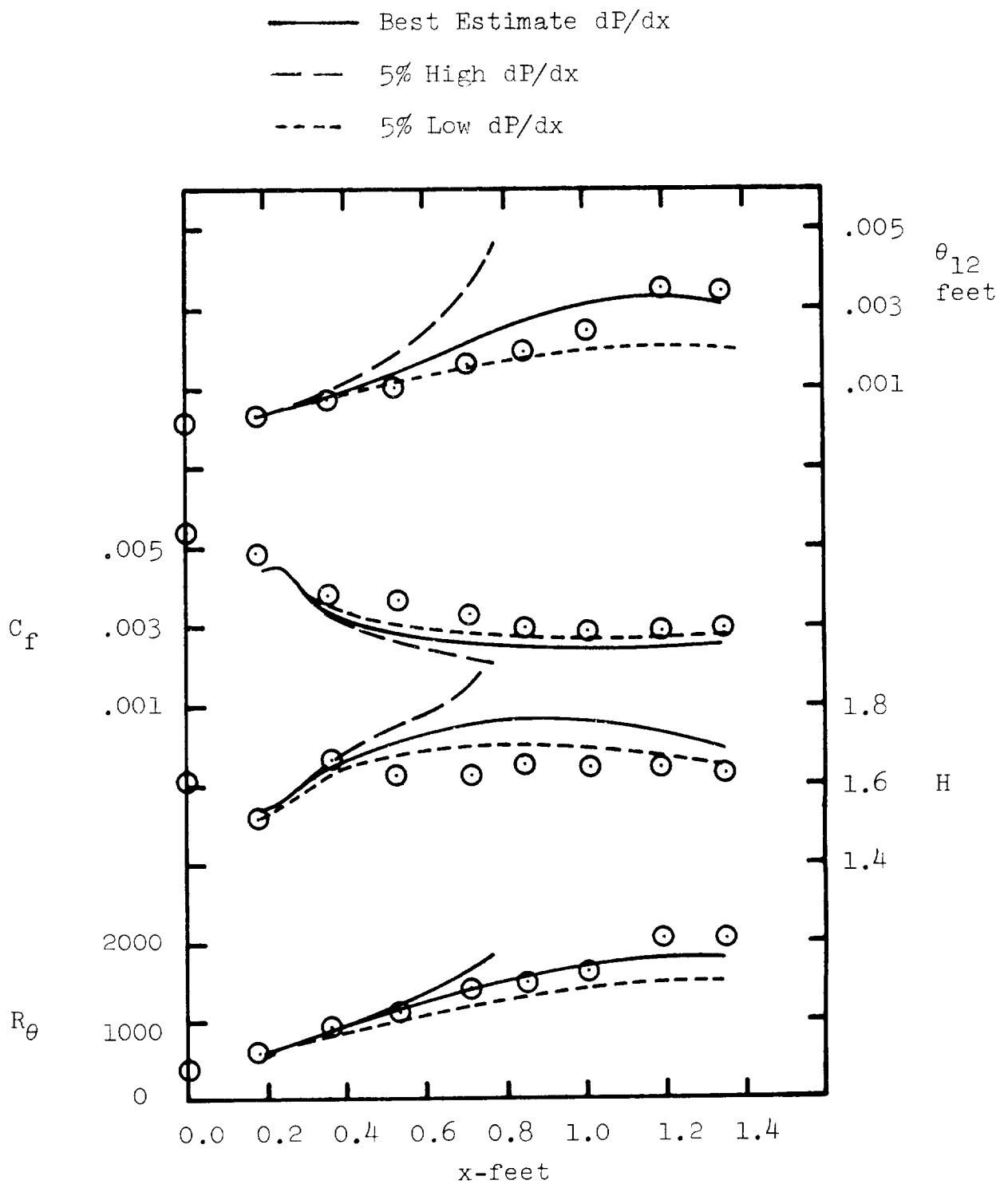


Figure 4.26 Effect of  $\pm 5\%$  Change of  $dP/dx$  on Predictions for Gardow A-45.2. All Curves are Bradshaw Method Calculations



## CHAPTER 5

### CALCULATION OF IDEALIZED FLOWS

#### A. Introduction

Frequently it is of interest to perform predictions of the boundary layer growth in configurations for which there is no data. Of course, the ultimate purpose of any boundary layer prediction method is to predict and optimize the performance of fluid mechanical machines in the design stage. With the extremely complex flow fields present in most real devices however, insight into the actual fluid behavior is the most that can be expected from present day boundary prediction methods. In addition although the best method to evaluate the performance of a prediction method is to compare its predictions to experimental data, predictions of purely theoretical flows can give insight into the relative performance of prediction methods.

An example of purely theoretical predictions of three-dimensional turbulent boundary layers is the work of Cumpsty and Head (1967). They performed predictions using their integral entrainment method on a series of idealized infinite swept wing flows with a variable sweep angle ( $\psi_1$ ). We have also predicted the Cumpsty and Head swept wing flows. In addition, we have performed calculations for a series of vaneless diffuser flows with various inlet conditions.

#### B. Cumpsty and Head Infinite Swept Wing Demonstration Cases

Cumpsty and Head (1967) proposed a set of infinite wings in which the free stream velocity over the rear (adverse pressure gradient region) is given by

$$U_{\infty} = Q_{\infty} \cos \psi_i (1 - kx) \quad (5.1a)$$

$$W_{\infty} = Q_{\infty} \sin \psi_i \quad (5.1b)$$

where  $x$  is measured in the chordwise direction,  $\psi_i$  is the effective sweep angle (Figure 1.2b) at the start of the adverse pressure gradient and  $k$  is a constant determining the strength of the pressure gradient. Both Bradshaw (1969) and Cumpsty and Head (1967) performed prediction using a value of  $k$  of 0.25, the value that has been used in the present work. The boundary layer was assumed to be collateral at the start of the flow ( $x = 0$ ) and to have the parameters

$$\theta_{1li} = 0.00234 \text{ feet} \quad (5.2a)$$

$$Q_{\infty} = 1.00 \text{ ft/sec}$$

$$R_{\theta_{1li}} = \frac{Q_{\infty} \theta_{1li}}{\nu} = 2690 \quad (5.2b)$$

$$H_i = 1.41 \quad (5.2c)$$

Calculations were performed at values of  $\psi_i$  of 0, 17.5, 35, and 52.5 degrees. Only the Bradshaw model and the eddy viscosity model (without the low Reynolds number correction) were tried in these calculations. For brevity, only certain key characteristics of the results have been presented.

In Figure 5.1 are presented the results for the position of the separation point as a function of sweep angle. This figure shows that there exists a difference between our predictions using Bradshaw's method and the predictions made by Bradshaw himself. This difference appears to be a consequence of the different methods of handling the wall boundary conditions in flows with large crossflows. For two-dimensional flows, our wall condition and that used by Bradshaw are very similar

and consequently the two methods produce the same results for zero sweep angle.

The Cumpsty and Head prediction has a rather different character than the other predictions shown on Figure 5.1. For large sweep angles, Cumpsty and Head predict that the separation value of  $x$  will decrease rather than increase with increasing sweep. The Cumpsty and Head results are, of course, an integral method and it is probable that they are not as reliable as the differential methods, particularly near separation.

Difficulty was encountered with the eddy viscosity model in predicting the separation point for zero sweep angle, which is a case of singular separation (ordinary separation occurs for all other values of sweep for all methods). As mentioned in Chapter 4 in the section on the East and Hoxey plane of symmetry flow, successful prediction of singular separation using the Townsend form of law of the wall as part of the wall conditions is dependent upon a high shear stress gradient between the wall and the first mesh point away from the wall. Without this shear gradient effect, the conventional law of the wall (Equation 2.27) predicts separation too far downstream. As separation is approached, the velocity profile becomes inflected and the  $y$  gradient of velocity ( $\partial \bar{Q} / \partial y$ ), near the wall is reduced. With its shear stress rate equation, the Bradshaw method continues to predict a high shear stress at the first mesh point despite the decrease in  $y$  gradient of velocity. Since the wall shear stress is dropping rapidly as separation is approached,  $\frac{\partial \tau}{\partial y}$  remains high. On the other hand, with the eddy viscosity model the shear stress at the first mesh point responds immediately to

the reduced  $\frac{\partial Q}{\partial y}$  and consequently,  $\frac{\partial \tau}{\partial y}$  also drops. When this low  $\frac{\partial \tau}{\partial y}$  is used in Equation 2.29, a high value of  $\tau_w$  results and prediction of separation is delayed. Evidently, in the East and Hoxey Flow, the adverse pressure gradient was so strong and the advent of separation so sudden that this difficulty with the eddy viscosity model was not apparent. In the Cumpsty and Head flow, using the eddy viscosity model, the wall shear stress drops to a low value but never reaches zero. Since singular separation was expected (based on the other prediction methods) for the wing with zero sweep, the estimate of the separation point zero sweep by the eddy viscosity model shown in Figure 5.1 was obtained by extrapolating to zero wall shear stress values in the vicinity of  $x = 1.0$  feet.

Figure 5.2 gives some representative predictions of dependent variables at a value of  $x$  which is not near separation,  $x = 1.0$  feet. With the exception of the Cumpsty and Head predictions, all the methods give close to the same results. By comparison, the large variations in the results for separation location, Figure 5.1, probably results from the different ways in which the various methods behave near separation. Although the methods presented in Figure 5.1 do have the capability of predicting separation, they were not designed using separating flows and thus when the various parameters start to change rapidly with  $x$  as separation is approached, they all behave in different ways.

### C. Vaneless Diffuser Demonstration Cases

In an ideal inviscid flow, the streamlines in a parallel walled radial vaneless diffuser (Figure 1.2d) follows a logarithmic spiral, and radial and tangential velocity components are given by:

$$U_{\infty} = U_{\infty i} \frac{R_i}{R} \quad (5.3a)$$

and

$$W_{\infty} = W_{\infty i} \frac{R_i}{R} \quad (5.3b)$$

Such a velocity variation would approximate that in the free-stream for a vaneless diffuser where the spacing between the walls is very large compared to the thickness of the boundary layers. This velocity distribution, produces a swirl angle  $\psi = \tan^{-1} \left( \frac{W_{\infty}}{U_{\infty}} \right)$  which is constant with radius. In actual diffusers, the boundary layers on the walls of the diffuser grow rapidly with radius and cause an apparent convergence of the diffuser walls which in turn causes the radial velocity component to be larger at a given  $R$  than the value obtained from Equation 5.3a.

$U_{\infty}$ , is in fact controlled by the displacement thickness parameter  $\delta_r^*$

$$\delta_r^* = \delta_1 + \delta_2 \tan \psi \quad (5.4)$$

and the conservation of mass equation written in the form

$$U_{\infty} = \bar{Q} / [2\pi R (B - 2\delta_r^*)] \quad (5.5)$$

where  $\bar{Q}$  is the volume flowrate through the diffuser and  $B$  is the distance between the parallel walls of the diffuser.

Calculations have been performed, using the eddy viscosity model and the Bradshaw model on a series of vaneless diffuser flows having simple logarithmic spiral streamlines with pressure distributions obtained from Eulers equation and Equations 5.3 (note: effects of  $\delta_r^*$  are neglected or  $\delta_r^* \ll B$  assumed)

$$\frac{dP}{dr} = - \frac{U_{\infty i}^2 + W_{\infty i}^2}{(R/R_i)^2 R_i} \quad (5.6)$$

The initial conditions at  $x = 0$  have been fixed as:

$$R_{\theta_{11i}} = 2000 . \quad (5.7a)$$

$$H_i = 1.50 \quad (5.7b)$$

and the flow assumed to be collateral. The only other significant inlet parameter (as long as  $\delta_r^* \gg B$ ) is the ratio of the inlet boundary layer thickness to the inlet radius. This parameter has been represented by  $R_i/\theta_{11i}$ . Three values (500, 1000 and 2500) for  $R_i/\theta_{11i}$  have been used in the computations.

It is worth noting that the flow situation being described here is highly idealized compared to the flow which one would expect in a real centrifugal blower or compressor. In real flows, the inlet to the diffuser consists of alternate wakes and jets coming off the impeller blades which makes the flow both unsteady and non-axisymmetric. In addition the inlet boundary layers would not necessarily be collateral.

The first computed result we shall examine is the separation point location. Figures 5.3 and 5.4 show the separation point radius as a function of swirl angle,  $\psi$ , for the Bradshaw and eddy viscosity models. It can be seen that for the range of the parameter  $R_i/\theta_{11i}$  examined, the flow always separates for all values of the swirl angle. There is a significant effect of the parameter  $R_i/\theta_{11i}$  because the pressure gradient computed by Equation 5.6 is inversely proportional to the inlet radius. Computations have also been performed for an inlet Reynolds number of 20,000 with  $R_i/\theta_{11i} = 500$ . No significant effect on separation point was noted.

For any value of  $R_i/\theta_{11i}$  the flow separates at very small radius

ratio,  $R_s/R_i$ , if the swirl angle is greater than about 70 degrees. The swirl angle becomes large as surge is approached in centrifugal compressors and it is possible that flow separation in the short vaneless space just downstream of the impeller is a factor contributing to the surge problem.

It is also of interest to examine the validity some of the assumptions used here as the separation condition is approached. For the log-spiral streamline pressure gradient and thus the present calculations to be valid, the boundary layer must not fill the passage (there must be an inviscid core) and the radial displacement thicknesses,  $\delta_r^*$ , must be small compared to the distance between the diffuser walls,  $B$ . In the present calculations,  $B$ , has been assumed to be infinite. In Figures 5.5 and 5.6 are presented the results for  $\delta_{995}/R_i$  versus swirl angle at a point upstream of separation where  $R/R_i = 0.9(R_s - R_i)/R_i$ . This radius was selected to avoid the region very close to separation where the calculations are uncertain due to numerical difficulties, but close enough to  $R_s$  so that an idea of the value attained by  $\delta_{995}$  when separation is imminent is obtained. Unfortunately, it was found that the parameter  $\delta_{995}/R_i$  is very sensitive to the computed location of the separation point, especially at small swirl angles. The error band shown in Figures 5.5 and 5.6 represents the approximate variation in  $\delta_{995}/R_i$  caused by an error in prediction of the separation point  $(R_s - R_i)/R_i$  of  $\pm 5\%$ . It is thus difficult to draw the curves for this result and only the calculated points are shown. The general trend is evident however. For example, for a diffuser with a radius to passage width ratio at inlet of  $R_i/B = 10$  and a swirl angle of 40 degrees, the

boundary layer on each wall would fill about 30% of the passage width as separation is approached. For the same diffuser with purely radial flow, the boundary layers would have completely filled the passage by separation.

Figures 5.7 and 5.8 present similar results for  $\delta_r^*/R_i$ . For the ratio  $R_i/B$  of 10 used in discussion above, the radial displacement thickness  $\delta_r^*$  on each wall would be about 10% of the passage width at a swirl angle of  $40^\circ$ , enough to have a 20% effect on the free-stream radial velocity component (Equation 5.5). The pressure gradient would thus be reduced from the value used in computation and consequently the tendency to separation slowed. The reduction of  $\frac{dP}{dr}$  is even more pronounced at lower swirl angle i.e. as  $\psi \rightarrow 0$  and it is probable that for geometries of high  $R_i/B$  separation will never occur for low swirl angles. High swirl angles are, however, the most common situation in centrifugal compressor diffusers and in such cases the results given here are probably more realistic.

A final result of some interest obtained from these vaneless diffuser studies concerns singular separation (at  $\psi = 0$ ). Sandborn (1970) found that for a variety of experimental data, a correlation of integral parameters produced a criterion for singular separation in two-dimensional turbulent boundary layers. Sandborn's empirical criterion for singular turbulent separation is that separation has occurred for values of  $H$  greater than

$$H = 2.12 + 0.306 \log_{10} \lambda_\theta \quad (5.8a)$$

$$\lambda_\theta = - \frac{\theta_{11}^2}{\nu} \frac{\partial u_\infty}{\partial x} \quad (5.8b)$$

The location of singular separation in the present methods is the point where a negative or zero value for the wall shear stress is predicted. The predicted singular separation results for the vaneless diffuser flows are shown in Figure 5.9 in terms of the correlating parameters  $H$  and  $\lambda_\theta$ . The point for the Cumpsty and Head unswept wing (Section B of this chapter) is also shown for the Bradshaw model. It is apparent that if Sandborn's criterion is proper,  $H$  is underpredicted at separation by all the present methods. The prediction of singular separation using the eddy viscosity model is not considered very reliable due to the difficulties discussed earlier.

#### D. Summary

Although it is not possible to use computer experiments of the type presented in this chapter to certify prediction methods, the results enable various predictors to compare their results and can also give insight into the performance of fluid machines. The flows presented here only represent simple examples of the potential for such calculation.

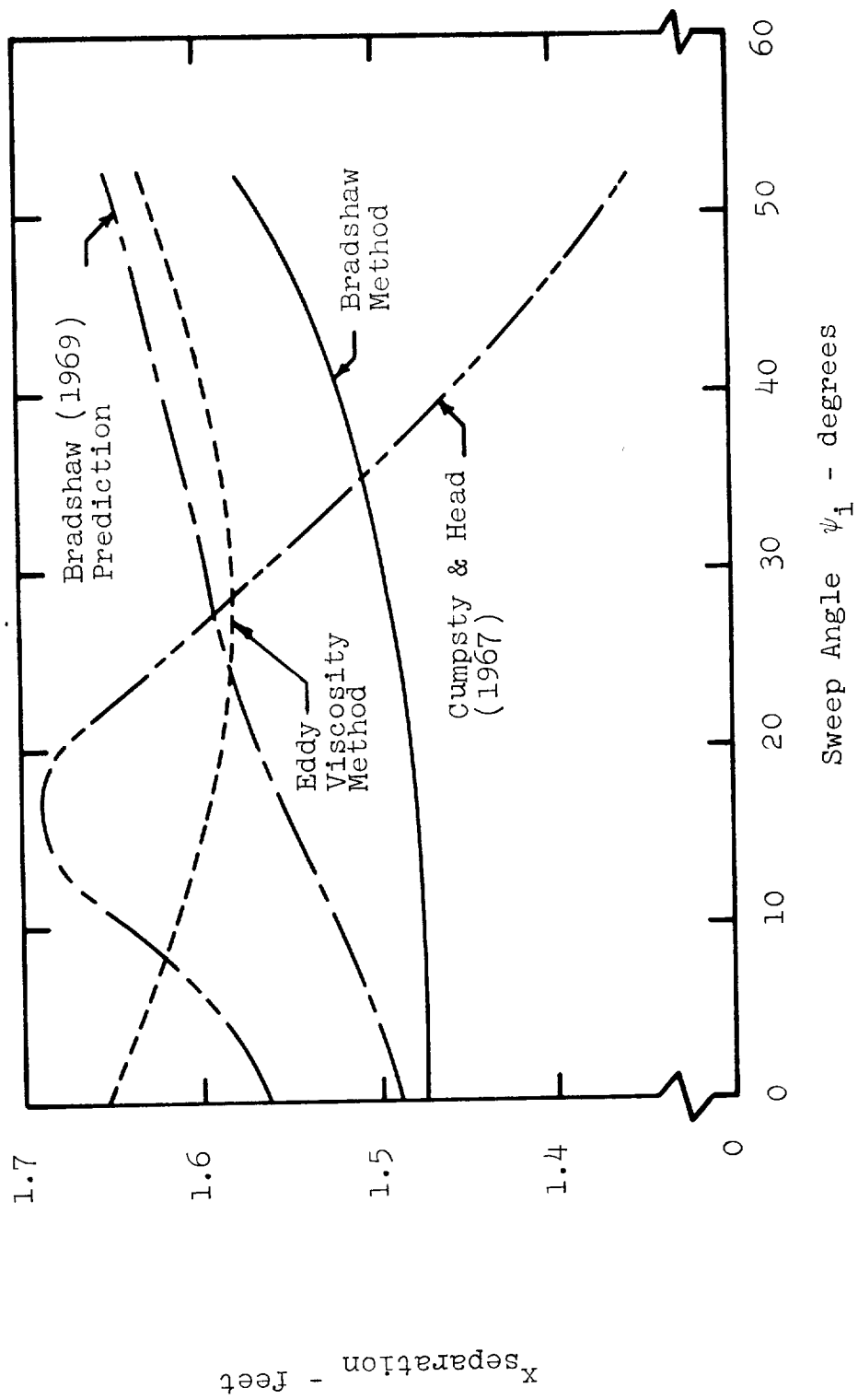


Figure 5.1 Separation Point vs. Sweep Angle, Cumpsty and Head (1967)  
Infinite Wing Demonstration Cases

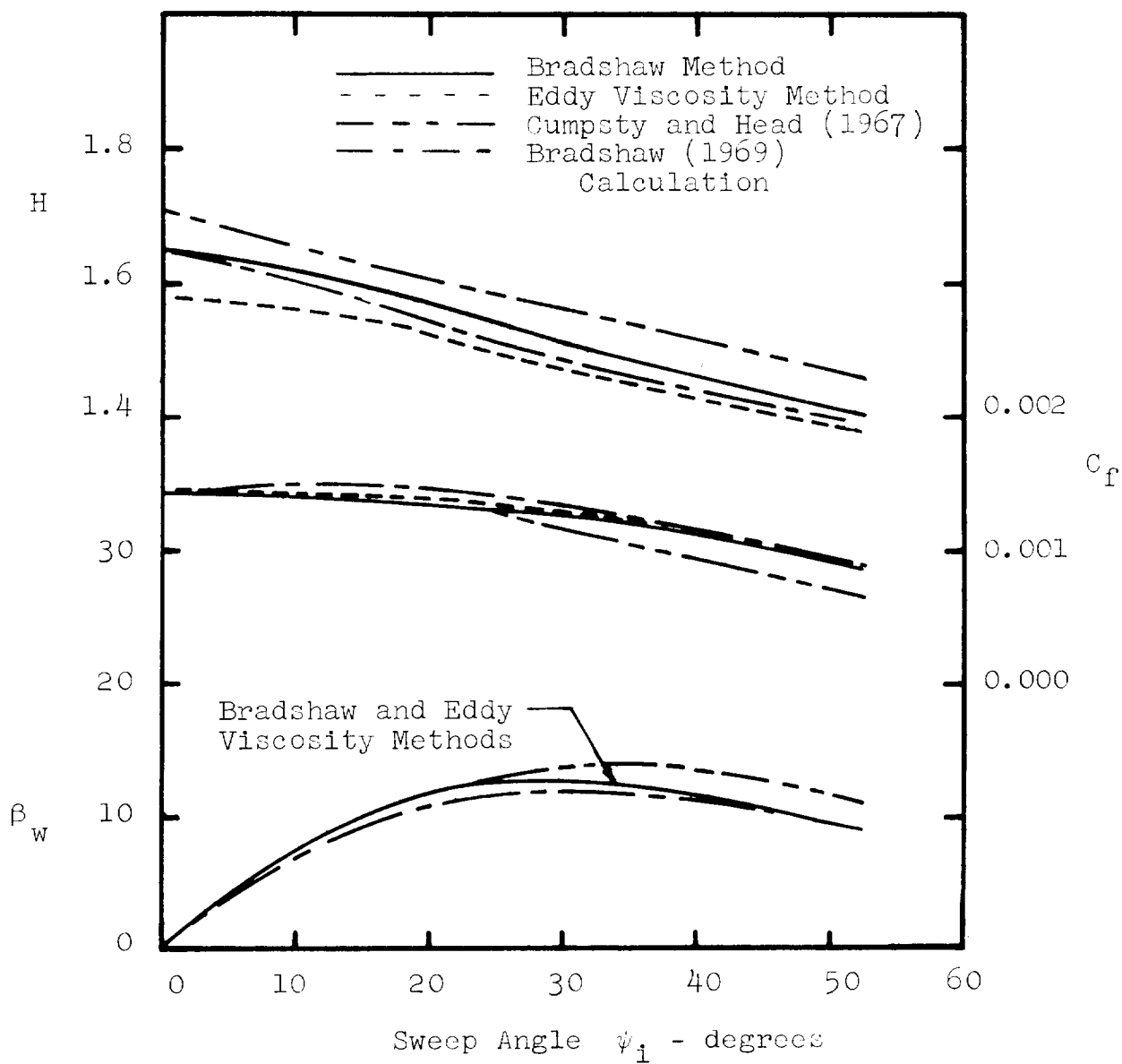


Figure 5.2 Integral Parameter Results at  $x = 1.0$  feet, Cumpsty and Head (1967) Infinite Wing Demonstration Cases

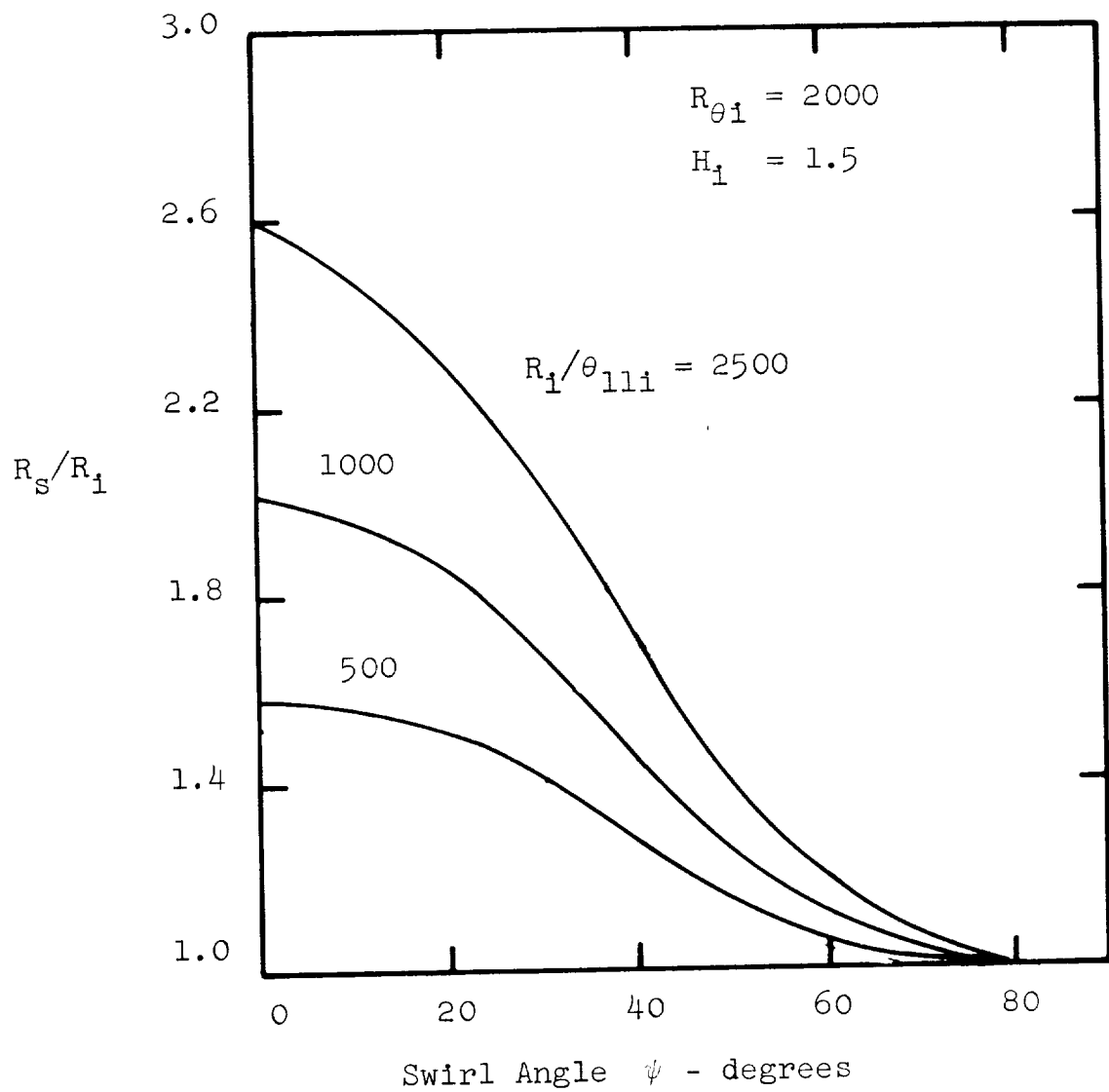


Figure 5.3 Separation Point vs. Swirl Angle, Vaneless  
 Diffuser Demonstration Cases, Bradshaw Method

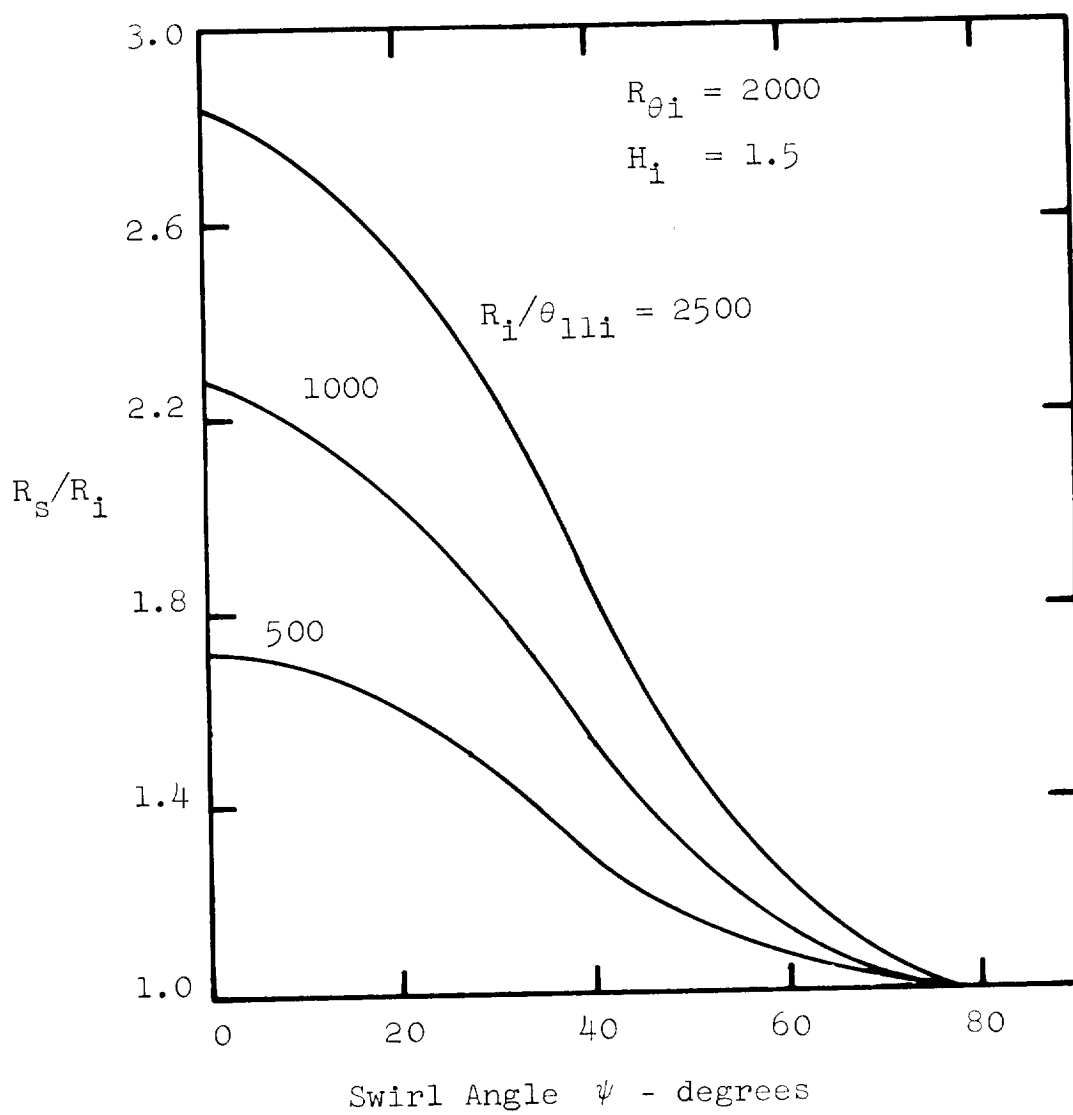


Figure 5.4 Separation Point vs. Swirl Angle, Vaneless  
 Diffuser Demonstration Cases, Eddy Viscosity Method

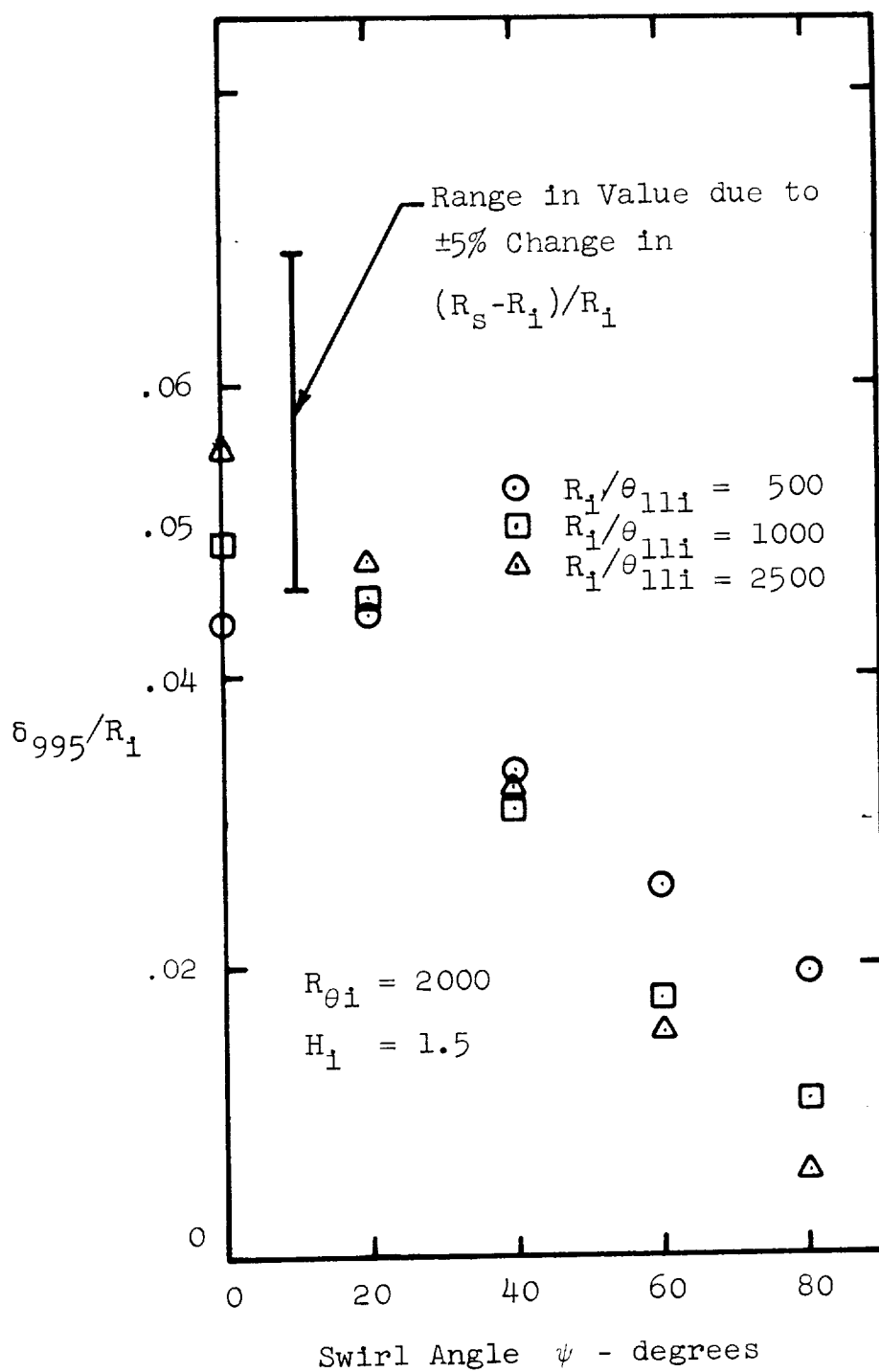


Figure 5.5  $\delta_{995}/R_1$  vs. Sweep Angle, Vaneless Diffuser Demonstration Cases, Bradshaw Method

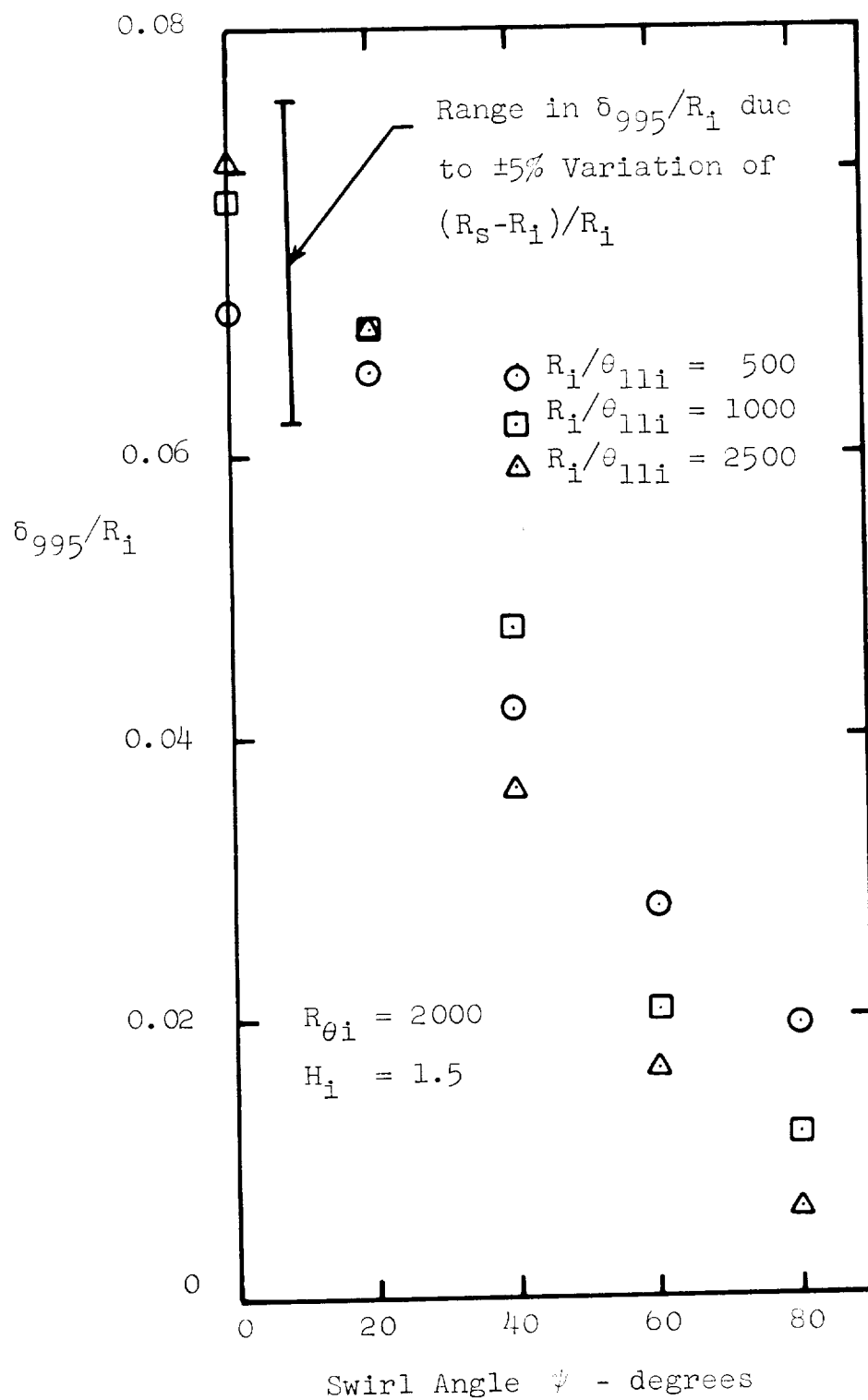


Figure 5.6  $\delta_{995}/R_i$  vs. Swirl Angle, Vaneless Diffuser Demonstration Cases, Eddy Viscosity Method

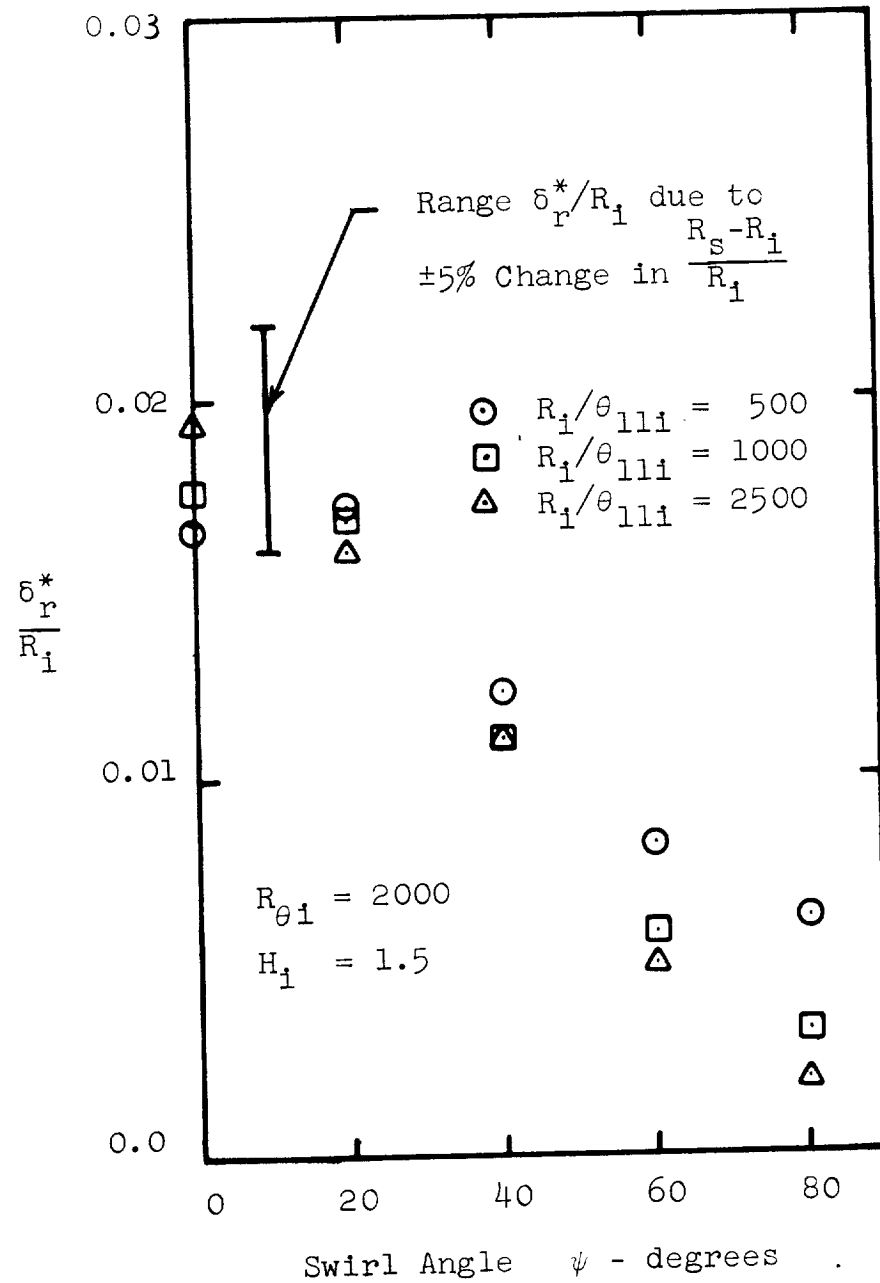


Figure 5.7  $\delta_r^*/R_1$  vs. Swirl Angle, Vaneless Diffuser Demonstration Cases, Bradshaw Method

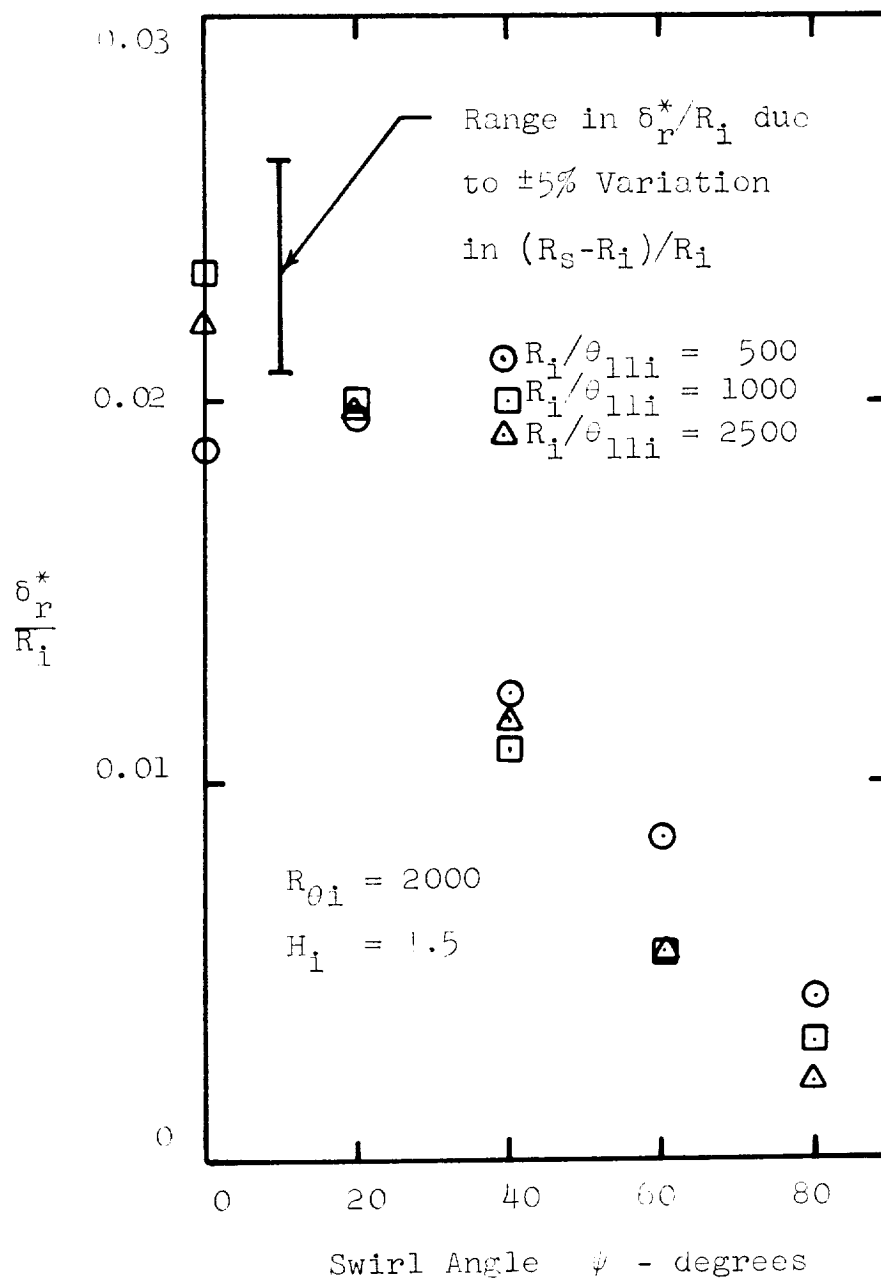
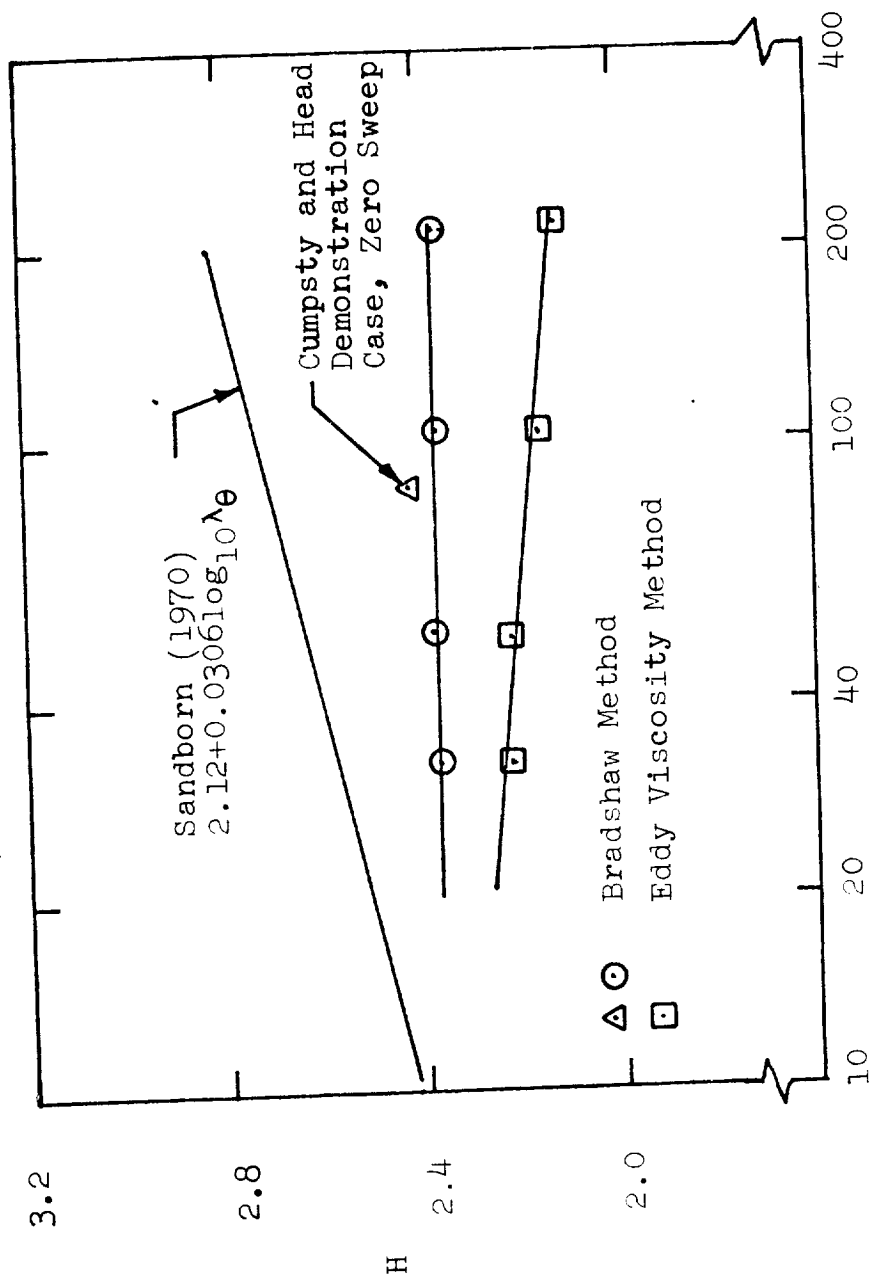


Figure 5.8  $\delta_r^*/R_i$  vs. Swirl Angle, Vaneless Diffuser  
Demonstration Cases, Eddy Viscosity Method



$$\lambda_\theta = \frac{\theta_{11}^2}{v} \frac{\partial Q_\infty}{\partial x}$$

Figure 5.9  $H$  vs.  $\lambda_\theta$ , Vaneless Diffuser Demonstration Cases, Swirl Angle = 0 (Two-Dimensional Flow)

## CHAPTER 6

### SUMMARY

#### A. Summary of Conclusions

In the course of the present research program, a number of significant conclusions have been reached:

1. All three shear stress closure models used in this study permit prediction of the mean velocity field to within the accuracy of the data. In addition, in flows with moderate Reynolds numbers ( $R_\theta = 5000-50,000$ ), all models produce results which are in good agreement with each other. At lower Reynolds numbers, ( $R_\theta$  less than 2000) the methods differ from each other to a greater extent and although it may be that one model is preferable, a preference cannot be determined with the available data.

2. There appears to be a large class of three-dimensional flows that can be predicted with differential methods in which the choice of shear stress closure assumption is not very important. This class includes the flow on a flat wall in the vicinity of wing-body junctions, large bumps and other obstructions. In general, this class of flows appears to encompass well developed nearly two-dimensional layers which suddenly encounter very strong adverse pressure gradients.

3. Direct measurements of the shear stress are available in only two experimental flows. Hence it is impossible to draw final conclusions with regard to the prediction of shear stress magnitude and direction.

In one flow, the Johnston infinite step, the predictions of shear stress magnitude using the Nash and Bradshaw models were much better

than the predictions using the present eddy viscosity model. The improvement due to the Nash and Bradshaw models can be attributed to the use of a rate equation to compute the shear stress magnitude. In this same flow, all models predicted the shear stress direction poorly although the prediction using the Bradshaw model were closer to the data. It should be noted that this flow was a very severe test of the shear stress assumptions but at the same time a flow (see conclusion 2) in which the shear stress model is not too important for the prediction of the mean velocity.

In the other flow where shear stresses were measured, the Bradshaw and Terrell swept plate, the shear stress terms dominate the development of the boundary layer, i.e. the pressure field is constant. No clear advantage was shown by any of the closure models either in prediction of the shear stress magnitude or direction.

4. It has been demonstrated in this study that the streamwise development of boundary layers in strong adverse pressure gradients is extremely sensitive to gradients of pressure imposed by the external pressure field. Thus, if an experimental flow of this type is to be useful for evaluation of prediction methods, the free stream pressure gradient must be measured with extreme accuracy, preferably to better than  $\pm 1\%$ . In the present study, an uncertainty in the pressure gradient of  $\pm 5\%$  was found, in a number of flows, to produce extremely wide variations in the predicted growth of the boundary layer when the adverse pressure gradient was strong.

5. In addition to the major conclusions above, a number of lesser conclusions were reached.

- a. With regard to the accuracy of the available data:
- i. Due to the low velocities of the vaneless diffuser flows and the consequent low, and difficult to measure, total to static pressures, the vaneless diffuser flows of Jansen and Gardow are of poorer quality than the other flows considered here. More scatter is apparent in the velocity profiles and the pressure gradients have a higher uncertainty (see conclusion 4).
  - ii. The Cumpsty and Head  $61^{\circ}$  swept wing flow probably does not meet the assumption of infinite span.
  - iii. Jansen does not provide tabulations of his data. This oversight seriously limits the usefulness of this data source.
  - iv. The accuracy of the shear stress magnitude data for the Bradshaw and Terrell flow is questioned. While it is essentially a two-dimensional flat plate flow with regard to the shear stress magnitude, the measured magnitude is 30% to 50% too high compared to results predicted with the shear stress models. Back checking, using the eddy viscosity model and the experimental mean velocity profiles, the same discrepancy was found.
- b. With regard to the numerical method:
- i. At low Reynolds numbers, the numerical method works poorly. The restriction that the first mesh point in the  $y$  direction fall at a  $y^{+}$  greater than 30 causes the first mesh point to be too far from the

wall, often at a  $y/\delta$  of greater than 0.1 .

- ii. The form of law of the wall based on the assumption that the shear stress is constant in the wall region significantly overestimates the wall shear stress in strong adverse pressure gradients. The Townsend form of the law of the wall, which allows for a linear shear stress variation in the wall region appears to have significant advantages in this regard when used as an inner boundary condition for a differential prediction method of the type used here.

#### B. Recommendations for Future Work

In the course of the present program, deficiencies in the available data became apparent and, in addition, extensions of the present work suggested themselves.

1. One class of three-dimensional turbulent flows for which data are needed are those in a moderate Reynolds number range (5,000-50,000) in which the development of the flow is governed by shear forces and pressure gradient forces of about the same magnitude. The Cumpsty and Head 61 degree infinite swept wing experiment is such a flow but appears to not meet the assumption of infinite span. It is recommended that a swept wing experiment with moderate sweep (about  $45^\circ$ ) be attempted and that the pressure gradient be mild enough so that the flow develops for an appreciable distance (20-50 boundary layer thicknesses) before separation occurs.

Since the predictions of the low Reynolds number vaneless diffusers showed a diversity of results, it is apparent that one or more of the prediction methods is breaking down in the low Reynolds number regime. Thus, a definitive low Reynolds number, adverse pressure gradient experiment would be desirable.

2. It is recommended that in future developments of numerical methods which can handle generalized geometries or solve complete flow fields, that the simplest of the models tested here, the eddy viscosity model, be used. It has demonstrated no serious deficiencies in computation of the mean velocity field and would be the most efficient in terms of computer time. Although not fully tested in the present program, the mixing length model is also probably quite adequate. Either of these methods work well in modern implicit numerical schemes which, because of their larger x-step, should be more economical with respect to computer time.

### C. Closure

It is hoped that the conclusions of the present work will give other researchers in turbulent boundary layers confidence in available three-dimensional turbulent boundary layer prediction schemes and encourage them to develop numerical schemes for the calculation of the flow on generalized geometries and perhaps complete, three-dimensional flow fields.



## REFERENCES

- Altman, J. M. and Hayter, Nora-Lee (1951) "A comparison of the turbulent boundary layer growth on an unswept and a swept wing," NACA Tech Note 2500.
- Ashkenas, H. (1958) "Turbulent shearing stress in the boundary layer on a yawed flat plate," NACA Tech Note 4140.
- Ashkenas, H. and Riddell, F. R. (1955) "Investigation of the turbulent boundary layer on a yawed flat plate," NACA Tech Note 3383.
- Bradshaw, P., Ferriss, D. and Atwell, N. (1967) "Calculation of boundary layer development using the turbulent energy equations," JFM 28, p. 593-616.
- Bradshaw, P. (1969) "Calculation of boundary-layer development using the turbulent energy equation, VII. three-dimensional flow," NPL Aero Report 1286. Also JFM 46, p. 417-445.
- Bradshaw, P. and Terrell M. (1969) "The response of a turbulent boundary layer on an 'infinite' swept wing to the sudden removal of pressure gradient," NPL Aero Report 1305.
- Brebner, G. G. and Wyatt, L. A. (1960) "Boundary layer measurements at low speed on two wings of  $45^\circ$  and  $55^\circ$  sweep," A.R.C., C.P. 554.
- Cham, T. (1968) "Turbulent boundary layers in rotating flows," PhD Thesis, Department of Engineering, Cambridge University. Also available in part in JFM, 37 p. 129-148.
- Coles, D. (1956) "The law of the wake in the turbulent boundary layer," JFM 1, p. 191-226.
- Cooke, J. and Hall, M. (1962) "Boundary layers in three dimensions," Progress in Aeronautical Sciences, Vol. 2, Pergamon Press, New York.
- Cooper, P. (1971) "Turbulent boundary layer on a rotating disc calculated with an effective viscosity," unpublished paper, Division of Fluid, Thermal and Aerospace Sciences, School of Engineering, Case Western Reserve University, Cleveland, Ohio.
- Crabbe, R. (1971) "Measurements in a laterally strained turbulent boundary layer," Mechanical Engineering Research Laboratories, McGill University, Montreal.
- Cumpsty, N. and Head, M. (1967) "The calculation of three-dimensional turbulent boundary layers, Part I: Flow over the rear of an infinite swept wing," The Aeronautical Quarterly, Vol. XVIII.

- Cumpsty, N. and Head, M. (1970) "The calculation of three-dimensional turbulent boundary layers, Part IV: Comparison of measurements with calculations on the rear of a swept wing," The Aeronautical Quarterly, Vol. XXI, May 1970, p. 121-132.
- East, L. and Hoxey, R. (1969) "Low speed three-dimensional turbulent boundary layer data," Royal Aircraft Establishment Technical Report 69041, Great Britain.
- Eichelbrenner, E. et. al. (1963) "Theoretical investigation and control by measuring tests on the behavior of the three-dimensional turbulent boundary layer on an annular wing at various incidences," Bureau Technique Zborowski, Brunoy (available as AD428 671).
- Eichelbrenner, E. et. al. (1966) "Theoretical and experimental investigation on three-dimensional (laminar and turbulent) boundary layers, in particular, problems of transition, separation and reattachment," Laboratory de Mechanique de Fluids, University de Poitier (available as AD 650 952).
- Francis, G. P. (1965) "Incompressible flow of the three-dimensional turbulent boundary layer on the flow of curved channels," Cornell University PhD Thesis, see also: Francis and Pierce, Trans. ASME, Ser. D, Vol. 89, pp. 597-608.
- Gardow, E. (1958) "The three-dimensional turbulent boundary layer in a free vortex diffuser," Gas Turbine Lab. Report 42, Massachusetts Institute of Technology.
- Gregory, N., Stuart, J. T. and Walker, W. S. (1955) "On the stability of three-dimensional boundary layers with application to the flow due to a rotating disc," Proc. Royal Soc. Phil. Trans. A, 248, p. 155.
- Gruschwitz, E. (1935) "Turbulente reibungsschichten mit secundarstromung" Ingenieur-Archiv., Bd. VI, S. 355-365.
- Herring, H. and Mellor, G. (1968) "A method of calculating compressible turbulent boundary layers," Paper at symposium "Compressible turbulent boundary layers," at Langley Research Center, Dec. 10-11, 1968.
- Hirst, E. and Reynolds, W. (1969) see Kline et. al. (1969) p. 213.
- Hornung, H. and Joubert, P. (1963) "The mean velocity profile in three-dimensional turbulent boundary layers," JFM, 15, Part 3.
- Jansen, W. (1959) "Incompressible fluid flow in a radial vaneless diffuser," Gas Turbine Lab. Report 52, Massachusetts Institute of Technology.
- Johnston, J. (1957) "Three-dimensional turbulent boundary layer," Gas Turbine Lab. Report 39, Massachusetts Institute of Technology.

- Johnston, J. (1960a) "On three-dimensional turbulent boundary layers generated by secondary flow," TASME, 82, Ser. D, p. 233-248.
- Johnston, J. (1960b) "The turbulent boundary layer at a plane of symmetry in a three-dimensional flow," TASME, 82, p. 622-628.
- Johnston, J. (1970) "Measurements in a three-dimensional turbulent boundary layer induced by a swept, forward facing step," JFM 42, p. 823-844.
- Kline, S. et. al. (1969) Proceedings, computation of turbulent boundary layers-1968 AFOSR - IFP - Stanford conference, Department of Mechanical Engineering, Stanford University.
- Klinksiek, W. and Pierce, F. (1968) "Secondary flow reversal and velocity profile models in a three-dimensional turbulent boundary layer," Mechanical Engrg. Dept., Virginia Polytechnic Institute.
- Klinksiek, W. and Pierce, F. (1969) "Simultaneous lateral skewing in a three-dimensional turbulent boundary-layer flow," ASME Paper 69-FE-24.
- Kromenhoek, D. and Pierce, F. (1968) "Wall shear stress diagnostics in three-dimensional turbulent boundary layer," Virginia Polytechnic Institute, Dept. of Mechanical Engrg., Interim Technical Report No. 2.
- Kuethe, A. M., McKee, P. B. and Curry, W. H. (1949) "Measurements in the boundary layer of a yawed wing" NACA Tech. Note 1946.
- Lewkowicz, A. K. (1965) "Two- and three-dimensional incompressible turbulent boundary layers," PhD Thesis, University of Liverpool, UK.
- Mager, A. (1952) "Generalization of boundary layer momentum integral equations to three-dimensional flows including those of rotating systems," NACA Report 1067.
- Maskell, E. (1955) "Flow separation in three dimensions," Royal Aircraft Establishment, Farnborough, Report No. Aero 2565.
- Mellor, G. (1967) "Incompressible, turbulent boundary layers with arbitrary pressure gradients and divergent or convergent cross flows," AIAA Journal, Vol. 5, No. 9, p. 1570-1579.
- Moore, Jr., R. W., and Richardson, D. L. (1955) "Skewed boundary layer flow near the end walls of a compressor cascade," Trans. ASME, Vol. 79, November 1957, No. 8, see also: MIT Gas Turbine Lab Report 33, 1955.

- Nash, J. (1968) "A finite difference method for the calculation of incompressible boundary layers in two dimensions," Aerospace Sciences Laboratory, Lockheed-Georgia Company.
- Nash, J. (1969) "The calculation of three-dimensional turbulent boundary layers in incompressible flow," JFM 37, p. 625-642.
- Nash, J. (1971) "An explicit scheme for calculation of three-dimensional turbulent boundary layers," ASME Paper 71-FE-19.
- Parr, O. (1963) "Flow in the three-dimensional boundary layer on a spinning body of revolution," AIAA Journal, Vol. 2, No. 2, 1964, p. 361 and Ingenier-Archiv., Vol. 32, pp. 393-413.
- Pierce, F. (1966) "The law of the wake and plane of symmetry flows in three-dimensional turbulent boundary layers," TASME, Ser. D, Vol. 88.
- Prandtl, L. (1944) "On boundary layers in three-dimensional flow," Reps. and Trans. No. 64, British M.A.P. .
- Reynolds, W. (1970) "Computation of turbulent flows, state-of-the-art, 1970," Stanford University, Department of Mechanical Engineering, Report MD-27.
- Sandborn, V. (1970) "Boundary layer separation and reattachment," Paper presented at symposium "Fluid Mechanics and Design of Turbomachinery" at Pennsylvania State University, Aug. 31 - Sept. 3, 1970.
- Shanebrook, J. and Eichelbrenner, E. (1966) "An approximate method of treating the three-dimensional, laminar, incompressible boundary layer equations when cross flow is small," ASME Paper 66WA/FE-34.
- Smith, P. D. (1966) "Calculation methods for three-dimensional turbulent boundary layers," Aeronautical Research Council A.R.C. 28 586 F.M. 3792 (Superseded by A.R.C. - R/M - 3523).
- Stain, W. C. (1961) "The three-dimensional turbulent boundary layer on a rotating disc," Aerophysics Dept., Mississippi State University, Research Report No. 35.
- Swamy, N. V. (1969) "Turbulent boundary layer on a yawed flat plate," Aerodynamische Versuchsanstalt, Gottingen, Report 69-A-44.
- Townsend, A. (1960) "Equilibrium layers and wall turbulence," JFM 11, p. 97-120.
- Townsend, A. (1970) "Entrainment and the structure of turbulent flow," JFM 41, p. 13-46.

Wakhaloo, C. L. (1968) "Three-dimensional turbulent boundary layer on the end wall of a compressor cascade," Doctoral Dissertation, Liverpool University, UK.

Wheeler, A. and Johnston J. (1971) "A compilation of data for three-dimensional, incompressible turbulent boundary layers," to be published.



## APPENDIX A

### THE COMPUTER PROGRAM

A general computer program has been prepared which will accept any shear stress model considered in the present study. Nine different decks have been produced however, three for infinite swept wings, three for the Johnston Step flow and three for the plane of symmetry flows. In each group of three, one uses the Bradshaw model, another the Nash model and the third either the eddy viscosity or mixing length models. Although the time required to change a program from one shear stress model to another is not long (changes and debugging take less than a day), different decks for each shear stress model was considered convenient. This appendix contains a description of the Bradshaw method only. The differences in the other programs are not major and would be readily apparent to an experienced programmer.

Table A.1 contains a list of the variables used in the computer program. Table A.2 is a list of input variables showing the input format and Table A.3 is some sample output. Table A.4 is a complete listing of the Bradshaw model computer program.

Table A.1 Variables Used in Computer Program

This table gives the equivalence between variables used in the computer program and the nomenclature used elsewhere in this report which are shown in quotes " ". As a general rule, the prefix D on a computer program variable indicates differentiation with respect to  $x$  and a last letter P on a program variable name indicates differentiation with respect to  $y$ . For example

$$DU = \partial U / \partial x$$

$$UP = \partial U / \partial y .$$

Most of the subscripted variables have the subscript varying in the  $y$  direction and the first value (subscript = 1) is at the first mesh point away from the wall. Subscripted variables which deviate from this rule are noted in the list of variables.

Table A-1 (Cont'd) SIMPLE VARIABLES

AVUTAU	Average value of " $Q_{\tau}$ ", $(UTAU + UTAUO)2.0$
BETA	Value of " $\beta$ " at first mesh point
BETAW	Angle of limiting wall streamline " $\gamma_w$ "
BETOLD	$\gamma$ at first mesh point from previous x-step
C	" $\phi$ " in Equation 3.10
COSS	Cosine of " $\psi$ ", free-stream velocity angle
DBETDX	" $\partial\gamma_1/\partial x$ ", rate of change of $\gamma_1$ with "x", Equation 2.36
DELRAT	" $\delta$ "/" $\delta_{995}$ "
DELTA	Maximum "y" value of calculations at each x-step
DELTAx	" $\delta_1$ ", displacement thickness
DELTAz	" $\delta_2$ "
DPDR	" $dP/dx$ ", pressure gradient
DUTAU	" $\partial Q_{\tau}/\partial x$ ", see Equation 2.36
DX	" $\Delta x$ ", "x" increment
DX1	"x" increments where UINF and DUINF read in
D995	" $\delta_{995}$ ", boundary layer thickness
EPS	Eddy viscosity " $\epsilon$ "
H	"H", shape factor
H1	Inlet "H"
I	Index or counter
ITER	Number of iterations. Determine if Equation 3.2 or 3.3 used
IUNIT	Number of "x"-values where printout required
J	Index or Counter
K	$NY + 2$

Table A-1 (Cont'd)

KD995	Lower index of $y$ in interval where $\delta_{995}$ falls
KL	= 1, part of an obsolete procedure
L	Index or Counter
LX	Number of UINF and DUINF values read in
ND	DELRAT = $1.4 + 0.1 \cdot ND$ , determines width of $y$ -grid
NIT	Number of iterations, 1 or 2
NPRINT	Printout required every NPRINT $x$ -step
NU	" $\nu$ " kinematic viscosity
NY	"N", number of $y$ -grid points
OMEGA	= 0.0, part of obsolete feature
PA	Johnston's "A", Equation 1.21b
PEPS	Tangent of " $\beta_w$ "
PHI1	Inlet " $\psi$ ", swirl or sweep angle
PI	Coles' $\Pi$
PRNT	= 1 in printout required, = 0 otherwise
PSIO	" $\psi$ ", free stream velocity direction
QINF1	" $Q_\infty$ ", free stream velocity magnitude
R	"R", radius of vaneless diffuser
RI	"R", at starting " $x$ "
RML	" $\ell$ ", mixing length
SINS	sine of " $\psi$ "
TAUM	" $\tau_{\max}$ ", maximum shear stress in $y$ direction
TAU1	" $\tau$ " at first mesh point away from wall
THETAX	" $\theta_{11}$ ", momentum thickness
THETAZ	" $\theta_{22}$ "

Table A-1 (Cont'd)

THETXZ	" $\theta_{12}$ "
THETZX	" $\theta_{21}$ "
THETI	" $\theta_{11}$ " at starting "x"
TW	" $\tau_w$ ", wall shear stress
T1	Variable used in synthetic initial crossflow velocity profile
T2	Variable used in synthetic initial crossflow velocity profile
UTAU	" $Q_\tau$ ", shear velocity
UTAUO	" $Q_\tau$ " at previous x-station
UTS	" $U_{\tau s}$ " square root of component of $\tau_w$ in streamwise direction, Equation 3.14
UVW	" $\tau_{w,x}$ " "x"-component of wall shear stress
X	"x" coordinate direction
VWV	" $\tau_{w,z}$ " z-component of wall shear stress
XI	"x" at start of calculation
XL	"x" at end of calculation
X1	Value of "x" where first UINF and DUINF values given
YCON	"C" in Equation 3.10
YFIRST	Use in calculation of YCON
YN	Number of y points
YSCALE	Scale factor of "y" in reading in starting velocity profiles. $Y = Y_{\text{input}} * YSCALE$

Table A-1 (Cont'd)

SUBSCRIPTED VARIABLES<sup>+</sup>

ANGVEL	Velocity angle = $\tan^{-1} "W"/"U"$ , ANGVEL(1) is wall value
ANGVLN	New value of ANGVEL, used in interpolation, ANGVLN(1) is wall value
ANGVLP	$\partial(\text{ANGVEL})/\partial Y$ , ANGVLP(1) is value at first mesh point
DU	" $\partial U/\partial x$ "
DUINF	" $\partial Q/\partial x$ ", array in x-direction
DUV	" $\partial \tau_x/\partial x$ "
DVW	" $\partial \tau_z/\partial x$ "
DW	" $\partial W/\partial x$ "
GUV	" $G\tau_x$ ", part of diffusion term in Equation 2.19
GVW	" $G\tau_z$ ", part of diffusion term in Equation 2.20
Q	"Q", velocity magnitude
QN	"Q", new value used in interpolation
QP	" $\partial Q/\partial y$ "
TAU	" $\tau$ ", magnitude of shear stress
U	"U", "x" component of velocity
UU	" $U^2$ ", used in evaluating integral parameters
UINF	" $Q_\infty$ ", free stream velocity, array in "x"-direction
UN	"U", new value, used to evaluate QN and ANGVLN
UP	" $\partial U/\partial y$ "
US	" $U_s$ ", streamwise component of velocity
UV	" $\tau_x$ ", x-component of shear stress
UVN	Same as UV, new value used for VCXN

<sup>+</sup>Except as noted, all arrays are in y-direction and have their first value at first mesh point away from wall.

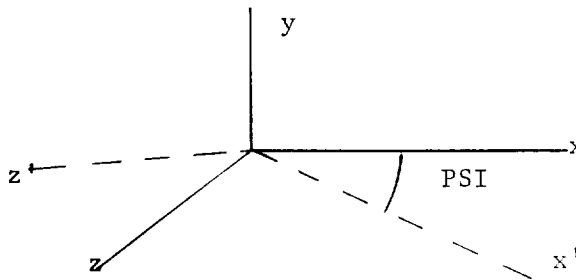
Table A-1 (Cont'd)

UVP	" $\partial\tau_x/\partial y$ "
UVS	" $\tau_s$ ", streamwise component of shear stress
V	"V", velocity normal to wall
VCX	" $\tau_x$ ", same as UV except first value is wall value
VCXN	Same as VCX, new value used for interpolation
VCY	" $\tau_z$ ", same as VW except first value is wall value
VCYN	Same as VCY, new value used for interpolation
VW	" $\tau_z$ ", z-component of shear stress
VWN	Same as VW, new value used for VCYN
VWP	" $\partial\tau_z/\partial y$ "
VWS	" $\tau_c$ "
W	"W", z-component of velocity
WN	"W", new value use for QN and ANGVLN
WP	" $\partial W/\partial y$ "
WS	" $W_s$ ", streamwise component of velocity
WU	"W U", used in integral parameter evaluation
WW	" $W^2$ ", used in integral parameter evaluation
XF	Values of "x" where UINF, DUINF read in
XPRINT	Values of "x" where printout desired
Y	"y"
YØ	"y", old value used for interpolation
Y2	"y", same as Y except first value is wall value
Y2N	Same as Y2, new value used for interpolation

Table A.2 - Input Data Format

This table contains the format of the input cards to run the computer program. The following are special notes concerning the use of the program.

1. For infinite wing flows, the initial  $R$  should be assigned a value of  $1.0 \text{ E} + 08$  or larger.
2. For two dimensional flows, the initial values of  $\text{PSI}$ ,  $\text{BETAW}$  and  $A$  should be 0.0
3. The values of  $U$  and  $W$  on card 10 (and continuation cards) are in an  $x'z'y$  coordinate system which is rotated about the  $y$ -axis an angle  $\text{PSI}$  ( $\psi$ ) relative to the  $x$ -axis.



4. All inputs of angles are in degrees.
5. The unit system used is not important but must be consistent, i.e., if  $NU$  is given in  $\text{ft}^2/\text{sec}$ , velocities must be in  $\text{ft}/\text{sec}$  and distances in feet.

Card 1 - column 2-80, A 79 letter title

Card 2 - Column 1-10 Initial  $x$   
11-20 Final  $x$   
21-30 Initial free stream velocity  
31-40 Initial shape factor,  $H$

Table A.2 (Cont'd)

41-50 Initial momentum thickness,  $\theta_{11}$   
 51-60 Initial shear velocity,  $Q_\tau$   
 61-70 Kinematic viscosity,  $\nu$

Card 3 - column 1-10 Radius at initial  $x$   
 11-20  $\psi$  at initial  $x$   
 21-30 Angular velocity ( $= 0$ )  
 31-40  $\beta_w$  at initial  $x$   
 41-50 Boundary layer thickness at  $x$  initial  
 51-60 'A' in Johnston triangular profile model  
 (Eq. 1.21b)

Card 4 - column 1-10 Value of  $x$  where first UINF, DUINF value given  
 11-20 Increment of  $x$  where UINF, DUINF given  
 21-25 Integer number of UINF, DUINF values

Card 5 7F10.3 format UINF values  
 Use additional cards as required

Card 6 7F10.3 format DUINF values  
 Use additional cards as required

Card 7 - column 1-2 Integer number  $y$  points  
 3-4 Integer  $x$  stations between printout  
 5-6 = 01 synthetic profile, = 00 experimental profiles  
 7-8 Number of specific  $x$  values where printout desired  
 9-10 Number of iterations (usually 2)  
 11-12 ND where  $\text{DELTA}/D995 = (1.4 + 0.1 \cdot \text{ND})$

Card 8 7F10.3 format, values of  $x$  where printout desired  
 in increasing value, must be greater than  $x$  initial  
 Use additional cards as required (max. 20  $x$  values)

Table A.2 (Cont'd)

Card 9     - column    1-10   YSCALE, normalizing value for  $y$  in experi-  
                                         mental starting profiles

Card 10    - column    1-10   Y/YSCALE  
                         11-20   U/QINF  
                         21-30   W/QINF

Use additional cards as required

RESULTS AT XSTATION 5 WITH R = 1.60 X = 0.1892  
D95 = 0.023584 DELTA = 0.033017 DELTAX = 0.004474  
THETA = 0.002911 DELTAZ = 0.001281 THETAZ = 0.000104  
THETAZ = 0.000939 THETAZ = 0.000342 H = 1.5370  
BETA = 11.894 PSI = 44.886 UTAU = 1.7587  
QINF = 36.099 RTHETA = 618.14 CF = 0.00475

Y/D955	U/QINF	W/QINF	V/QINF	UV/QISO	VW/QISO	Y	Y+
0.03008	0.47426	0.09838	0.00101	-0.00222	-0.00040	0.00071	7.3
0.06781	0.57010	0.11114	0.00225	-0.00222	-0.00016	0.00160	16.5
0.11220	0.63056	0.11072	0.00329	-0.00212	0.00012	0.00267	27.6
0.16625	0.67446	0.10698	0.00450	-0.00211	0.00032	0.00392	40.6
0.22695	0.71184	0.09897	0.00608	-0.00175	0.00045	0.00535	55.4
0.29531	0.74941	0.08800	0.00784	-0.00159	0.00047	0.00696	72.1
0.37133	0.78809	0.07702	0.00953	-0.00142	0.00042	0.00876	90.6
0.45500	0.82544	0.06652	0.01097	-0.00138	0.00044	0.01073	111.0
0.54633	0.86843	0.05103	0.01244	-0.00136	0.00053	0.01288	133.3
0.64531	0.91132	0.03287	0.01404	-0.00114	0.00051	0.01522	157.4
0.75195	0.94613	0.01739	0.01549	-0.00087	0.00038	0.01773	183.5
0.86625	0.97482	0.00607	0.01670	-0.00063	0.00023	0.02043	211.4
0.98820	0.99440	0.00025	0.01753	-0.00032	0.00008	0.02331	241.1
1.11781	1.00046	-0.00054	0.01787	-0.00007	0.00000	0.02636	272.7
1.25508	1.00001	0.00001	0.01785	0.00001	-0.00001	0.02960	306.2
1.40000	1.00000	0.00000	0.01775	0.00000	0.00000	0.03302	341.6
MOMENTUM INTEGRAL CHECK							
LHS=	-0.142E-01	RHS=	-0.158E-01				

Table A.3 Sample Output

Table A.4 Bradshaw Model

## Computer Program Listing

C THREE DIMENSIONAL TURBULENT BOUNDARY LAYER PREDICTION USING THE	5.
C BRADSHAW METHOD	6.
C THIS PROGRAM CAN BE USED TO PREDICT THE GROWTH OF THE THREE-DIMENSIONAL	7.
C TURBULENT BOUNDARY LAYERS IN 'INFINITE WINGS' AND AXIALLY SYMMETRIC	8.
C RADIAL VANELESS DIFFUSERS IF THE EXTERNAL PRESSURE FIELD IS KNOWN	9.
C THE INPUT DATA IS AS FOLLOWS	10.
C CARD 1 - COLUMN 2-80, A 79 LETTER TITLE	11.
C CARD 2 - COLUMN 1-10 INITIAL X	12.
C 11-20 FINAL X	13.
C 21-30 INITIAL FREE STREAM VELOCITY	14.
C 31-40 INITIAL SHAPE FACTOR H	15.
C 41-50 INITIAL MOMENTUM THICKNESS THET11	16.
C 51-60 INITIAL SHEAR VELOCITY, UTAU	17.
C 61-70 KINEMATIC VISCOSITY, NU	18.
C CARD 3 - COLUMN 1-10 RADIUS AT INITIAL X	19.
C 11-20 PSI AT INITIAL X	20.
C 21-30 ANGULAR VELOCITY(=0.0)	21.
C 31-40 BETAW AT INITIAL X	22.
C 41-50 BOUNDARY LAYER THICKNESS AT INITIAL X	23.
C 51-60 'A' IN JOHNSTON TRIANGULAR CROSSFLOW MODEL	24.
C CARD 4 - COLUMN 1-10 VALUE OF X WHERE FIRST UINF, DUINF VALUE GIVEN	25.
C 11-20 INCREMENT OF X WHERE UINF, DUINF VALUES GIVEN	26.
C 21-25 INTEGER NUMBER OF UINF, DUINF VALUES, MOVE TO	27.
C RIGHT SIDE OF INTERVAL, E.G. 00013	28.
C CARD 5 PUNCH SUCCESSIVE UINF VALUES IN COLUMNS 1-10, 11-20, 21-30,	29.
C 31-40, 41-50, 51-60, 61-70	30.
C USE ADDITIONAL CARDS AS REQUIRED	31.
C CARD 6 - PUNCH DUINF VALUES IN SAME FORMAT AS UINF VALUES. USE	32.
C ADDITIONAL CARDS AS REQUIRED	33.
C CARD 7 - COLUMN 1- 2 INTEGER NUMBER OF Y POINTS	34.
C 3- 4 INTEGER NUMBER OF X-STATIONS BETWEEN PRINTOUT	35.
C 5- 6 =01 SYNTHETIC PROFILE, =00 EXPERIMENTAL	36.
C STARTING VELOCITY PROFILE	37.
C 7- 8 NUMBER OF SPECIFIC X-STATIONS WHERE PRINTOUT	38.
C REQUIRED	39.
C 9-10 NUMBER OF ITERATIONS, USUALLY 02	40.
C 11-12 ND, WHERE $\Delta/D_{995} = (1.4 + 0.1 \cdot ND)$	41.
C CARD 8 - SUCCESSIVE VALUES OF X WHERE PRINTOUT REQUIRED IN INCREAS-	42.
C ING VALUE, MUST BE GREATER THAN X INITIAL	43.
C MAXIMUM 20 X VALUES	44.
C CARD 9 - COLUMN 1-10 YSCALE, NORMALIZING VALUE FOR Y IN EXPERIMENTAL	45.
C STARTING VELOCITY PROFILES. THIS AND SUCCESS-	46.
C IVE CARDS NOT REQUIRED WITH SYNTHETIC START	47.
C CARD 10 - COLUMN 1-10 Y/YSCALE	48.
C 11-20 U/QINF1	49.
C 21-30 W/QINF1	50.
C THE VALUES OF U AND W READ IN ARE IN A COORDINATE SYSTEM ROTATED	51.
C ABOUT THE Y-AXIS BY PSI INITIAL RELATIVE TO THE X-AXIS	52.
C ON CARD 10 IT IS ALSO POSSIBLE TO READ $\tau_{ux}/QINF1^{**2}$ AND $\tau_{w7}$	53.
C $QINF1^{**2}$ IN COLUMNS 31-40 AND 41-50 RESPECTIVELY. IF THIS IS DONE,	54.
C STATEMENT 22 MUST BE MOVED SO THAT IT IMMEDIATELY FOLLOWS STATEMENT 40	55.
C INSTEAD OF BEING THE SECOND STATEMENT AFTER STATEMENT 21	56.
C DIMENSION TITLE(20), Y(43), U(43), W(43), Q(43), QP(43),	57.
C 1UV(43), VW(43), UVS(43), VWS(43), US(43), WS(43), WW(43), WU(43),	58.
C 2UU(43), UP(43), WP(43), VWP(43), UVP(43), YD(43), VN(43), DU(43),	59.

```

3DW(43),DUV(43),DVW(43),UN(43),WN(43),UVN(43),VWN(43) 60.
4,V(43), QN(43),XPRINT(20),ANGVEL(44),ANGVLN(44),ANGVLP(43), 61.
5 GUV(43),GVW(43),TAU(43) 62.
6,XF(50),UINF(50),DUINF(50),Y2(44),VCX(44),VCY(44) 63.
7,Y2N(45),VCXN(45),VCYN(45) 64.
EQUIVALENCE(VCX(1),UVW),(VCX(2),UV(1)),(VCY(1),VWW),(VCY(2),VW(1)) 65.
1,(Y2(2),Y(1)),(Y2N(2),Y0(1)),(VCXN(2),UVN(1)),(VCYN(2),VWN(1)) 66.
REAL NU,NUOUT 67.
INTEGER XSTAT,PRNT 68.
Y2(1)=0.0 69.
Y2N(1)=0.0 70.
C**** 71.
C INPUT TITLE,GEOMETRY,INLET CONDITIONS AND RUN PARAMETERS 72.
C**** 73.
1 READ(5,4) TITLE 74.
PRNT=1 75.
4 FORMAT(20A4) 76.
READ(5,5)XI,XL,QINF1,H1,THET1,UTAU,NU,RI,PHI1,OMEGA,ANGVLN(1) 77.
1,DELTA,PA 78.
REAC(5,798)X1,DX1,LX 79.
798 FORMAT(2F10.3,I5) 80.
READ(5,5) (UINF(I),I=1,LX) 81.
READ(5,5) (DUINF(I),I=1,LX) 82.
XF(1)=X1 83.
DO 797 I=2,LX 84.
797 XF(I)=XF(I-1)+DX1 85.
5 FORMAT(7F10.3) 86.
READ(5,6)NY,NPRINT,IT,IUNIT,NIT,ND 87.
DELRAT=1.4+0.1*FLOAT(ND) 88.
IF(IUNIT.GT.0) READ(5,5)(XPRINT(I),I=1,IUNIT) 89.
6 FORMAT(6I2) 90.
C**** 91.
C WRITE OUT HEADINGS 92.
C**** 93.
WRITE(6,8) TITLE 94.
8 FORMAT(1H1,19X,20A4) 95.
WRITE(6,9)RI,UTAU,ANGVLN(1),PHI1,QINF1,H1,THET1,NU 96.
9 FORMAT(19X,49H BRADSWHAW 3D BOUNDARY LAYER PREDICTION 97.
1/20X,' INSIDE RADIUS =',F10.3,2X,' INITIAL UTAU =',F10.5/20X, 98.
2' INITIAL BETAW =',F10.6,2X,' SWIRL ANGLE =',F10.3/20X, 99.
3' INLET VELOCITY=',F10.3,2X,' INLET H =',F10.3 /20X, 100.
4' INLET THETA =',F10.5,' NU',12X,'=',F10.7//) 101.
DELTAX=H1*THET1 102.
PHI1=PHI1*3.14159/180.0 103.
ANGVLN(1)=ANGVLN(1)*3.14159/180.+PHI1 104.
UTS=UTAU*SQRT(COS(ANGVLN(1)-PHI1)) 105.
UTAU0=UTAU 106.
XSTAT=1 107.
R=RI 108.
C=0.3 109.
K=NY+2 110.
X=XI 111.
DX=0. 112.
DUTAU=0. 113.
CBETDX=0. 114.
C**** 115.
C READ IN VELOCITY PROFILES 116.
C**** 117.
COSS=COS(PHI1) 118.
SINS=SIN(PHI1) 119.

```

	IF(IT.EQ.1)GO TO 20	120.
	READ(5,18) YSCALE	121.
	READ(5,18)(Y(I),UN(I),WN(I),UV(I),VW(I) ,I=1,NY )	122.
18	FORMAT(5E10.3)	123.
	DO 17 I=1,2	124.
	UN(NY+I)=UN(NY)	125.
	WN(NY+I)=WN(NY)	126.
	UV(NY+I)=0.	127.
	VW(NY+I)=0.	128.
17	Y(NY+I)=Y(NY)+(Y(NY)-Y(NY-1))*FLOAT(I)	129.
	DO 19 I=1,K	130.
	Y(I)=Y(I)*YSCALE	131.
	UN(I)=UN(I)*QINF1	132.
	WN(I)=WN(I)*QINF1	133.
	UV(I)=-UV(I)*QINF1**2	134.
	VW(I)=-VW(I)*QINF1**2	135.
	ANGVLN(I+1)=ATAN(WN(I)/UN(I)) +PHI1	136.
	UVN(I)=UV(I)*COS(PHI1)-VW(I)*SIN(PHI1)	137.
	VWN(I)=UV(I)*SIN(PHI1)+VW(I)*COS(PHI1)	138.
19	QN(I)=SQRT(UN(I)**2+WN(I)**2)	139.
	GO TO 22	140.
	C****	141.
	C SYNTHETIC PROFILES	142.
	C****	143.
	C USE COLES LAW OF WALL-WAKE TO COMPUTE INITIAL STREAMWISE VELOCITY PROF	144.
20	CALL SYNQP(F1,THET1,QINF1,NY,NU,Y,US,UTS ,DELTA)	145.
	C USE JOHNSTON TRIANGULAR MCDL TO COMPUTE INITIAL CROSSFLOW VELOCITY	146.
	PEPS=SIN(ANGVLN(1)-PHI1)/COS(ANGVLN(1)-PHI1)	147.
	DO 23 I=1,K	148.
	T1=PEPS*US(I)/US(NY)	149.
	T2=PA*(1.-US(I)/US(NY))	150.
	T1=AMIN1(T1,T2)	151.
23	WS (I)=T1*US(NY)	152.
	DO 21 I=1,K	153.
	QN(I)=SQRT(US(I)**2+WS(I)**2)	154.
21	ANGVLN(I+1)=ATAN(WS(I)/US(I))+PHI1	155.
	BETOLD=ANGVLN(2)	156.
22	CONTINUE	157.
	C CALCULATE Y DERIVATIVES OF STARTING PROFILES	158.
	QP(1)=((QN(1)-QN(2))/ALOG(Y(1)/Y(2)))/Y(1)	159.
	ANGVLP(1)=DERIV(ANGVLN,Y2,2)	160.
	DO 29 I=2,NY	161.
	IF((Y(I)*UTAL/NU).GT.200) GO TO 28	162.
	QP(I)=((QN(I-1)-QN(I+1))/ALOG(Y(I-1)/Y(I+1)))/Y(I)	163.
	GO TO 30	164.
28	QP(I)=DERIV(QN,Y,I)	165.
30	ANGVLP(I)=DERIV(ANGVLN, Y2,I+1)	166.
29	CONTINUE	167.
	C CALCULATE INITIAL SHEAR STRESS PROFILES USING A MIXING LENGTH	168.
	DO 31 I=1,NY	169.
	UP(I)=QP(I)*COS(ANGVLN(I+1))-QN(I)*SIN(ANGVLN(I+1))*ANGVLP(I)	170.
31	WP(I)=QP(I)*SIN(ANGVLN(I+1))+QN(I)*COS(ANGVLN(I+1))*ANGVLP(I)	171.
	NUOUT=0.016*QN(NY)*DELTA	172.
	INNER=1	173.
	RML=0.	174.
	DO 40 I=1,NY	175.
	RML=AMAX1(RML,FLOOR(Y(I)/DELTA)*DELTA)	176.
	IF(RML/DELTA.GT..079)RML=.079*DELTA	177.
	EPS=(RML**2)*SQRT(UP(I)**2+WP(I)**2)	178.
33	UVN(I)=-UP(I)*EPS	179.

	VWN(I)=-WP(I)*EPS	180.
40	CONTINUE	181.
	DO 35 I=1,2	182.
	UVN(NY+I)=0.0	183.
35	VWN(NY+I)=0.0	184.
	VCXN(1)=-UTAU**2*COS(ANGVLN(1))	185.
	VCYN(1)=-UTAU**2*SIN(ANGVLN(1))	186.
	DPDR=DPDRF(X,UINF,DUINF,XF,LX)	187.
	D995=DELTA	188.
	C START REPEATING PART OF CALCULATIONS.(ALL PREVIOUS STATEMENTS	189.
	C CONCERNED INPUT OR INITIALIZATION	190.
44	CONTINUE	191.
	IF((XSTAT/NPRINT)*NPRINT-XSTAT.EQ.0) PRNT=1	192.
C	FIND D995	193.
	DO 501 I=1,K	194.
	KD995=I-1	195.
	IF(ABS(1.0-QN(I)/QN(K)).LE.0.005) GO TO 511	196.
501	CONTINUE	197.
511	D995=Y(KD995)+(Y(KD995+1)-Y(KD995))*(0.995*QN(K)-QN(KD995))/	198.
	1(QN(KD995+1)-QN(KD995))	199.
	DELTA=D995*DELTA	200.
C	ESTIMATE COLES PI	201.
	PI=0.2*(QN(NY)/UTAU-(2.5*ALOG(D995*UTAU/NU)+5.1))	202.
C	ESTIMATE THE X GRADIENT OF UTAU	203.
	IF(DX/D995.GT.0.001)DUTAU=((UTAU-UTAU0)/DX+DUTAU)/2.	204.
C	ESTIMATE THE X GRADIENT OF THE VELOCITY DIRECTION AT THE FIRST	205.
C	MESH POINT	206.
	IF(DX/D995.GT.0.001)DBETDX=((ANGVLN(2)-BETOLD)/DX+DBETDX)/2.0	207.
C****		208.
C	SET Y GRID AND INTERPOLATE VALUES	209.
C****		210.
C	PUT OLD Y IN OLD Y STORE	211.
	DO 75 I=1,K	212.
C	SUBTRACT VELOCITY COMPUTED BY LAW OF WALL WAKE FROM Q PROFILE	213.
C	FOR INTERPOLATION	214.
	QN(I)=QN(I)-UWAKE(Y(I),UTAU,PI,D995,NU)	215.
75	YQ(I)=Y(I)	216.
C	SET Y GRID	217.
	YN=FLOAT(NY)	218.
	YFIRST=DELTA*(C/YN+(1.-C)*(1./YN)**2)	219.
	AVUTAU=0.5*(UTAU+UTAU0)	220.
	YCON=30.*NU/AVUTAU -YFIRST	221.
	DO 100 I=1,K	222.
100	Y(I)=DELTA*(C*FLOAT(I)/YN+(1.-C)*(FLOAT(I)/YN)**2)+YCON	223.
C	INTERPOLATE TO FIND VALUES OF U ETC. ON NEW Y GRID	224.
	M=1	225.
	DO 110 I=1,K	226.
	DO 86 J=1,K	227.
	L=J	228.
	IF(Y(I).LT.YQ(J)) GO TO 101	229.
86	CONTINUE	230.
101	L=L-1	231.
87	CALL INT(Y(I),Q(I),YQ,QN,K,L,2)	232.
C	ADD BACK VALUE OF VELOCITY COMPUTED BY LAW OF WALL WAKE AFTER	233.
C	INTERPOLATION	234.
	Q(I)=Q(I)+UWAKE(Y(I),UTAU,PI,D995,NU)	235.
88	CALL INT(Y(I),UV(I),Y2N,VCXN,K+1,L+1,2)	236.
	CALL INT(Y(I),VW(I),Y2N,VCYN,K+1,L+1,2)	237.
	CALL INT(Y(I),ANGVEL(I+1),Y2N,ANGVLN,K+1,L+1,2)	238.
	U(I)=Q(I)*CCS(ANGVEL(I+1))	239.

W(I)=Q(I)*SIN(ANGVEL(I+1))	240.
110 CCNTINUE	241.
UTAU0=UTAU	242.
BETOLD=ANGVEL(2)	243.
DO 206 ITER=1,NIT	244.
C CALCULATE MAXIMUM SHEAR STRESS	245.
CALL MAXSHR(K ,UV,VW,TAU,TAUM)	246.
C****	247.
CPREDICTION OF U,W ETC. AT FIRST MESH POINT	248.
C****	249.
CALL GFCALC(UV,VW,Q(NY),K,Y,D995,GUV,GVW,TAUM)	250.
C CALCULATE SHEAR STRESS GRADIENTS AT FIRST MESH POINT	251.
TAU1=TAU(1)	252.
UTAU=WSF(Q(1),Y(1),TAU1,UTAU,NU)	253.
C FIND BETAW BY TAYLOR SERIES EXTRAPOLATION FROM OUTER POINTS	254.
ANGVEL(1)=ANGVEL(2)-Y(1)*(ANGVEL(3)-ANGVEL(2))/(Y(2)-Y(1))	255.
1+0.5*(Y(1)**2)*((ANGVEL(4)-ANGVEL(3))/(Y(3)-Y(2))-(ANGVEL(3)-	256.
2*ANGVEL(2))/(Y(2)-Y(1)))/(0.5*(Y(3)-Y(1)))	257.
TW=UTAU**2	258.
UVW=-TW*COS(ANGVEL(1))	259.
VW=-TW*SIN(ANGVEL(1))	260.
UVP(1)=DERIV(VCX,Y2,2)	261.
VWP(1)=DERIV(VCY,Y2,2)	262.
DO 144 I=1,K	263.
IF(UV(I).GT.0.)VW(I)=0.	264.
IF(UV(I).GT.0.) UV(I)=0.	265.
C SUBTRACT LAW OF WALL VELOCITY FROM Q FOR DIFFERENTIATION	266.
144 Q(I)=Q(I)-UTAU*(2.5*ALOG(Y(I)*UTAU/NU)+5.)	267.
C CALCULATE VELOCITY GRADIENTS AT FIRST MESH POINT	268.
QP(1)=(Q(2)-Q(1))/(Y(2)-Y(1))+2.5*UTAU/Y(1)	269.
ANGVLP(1)=DERIV(ANGVEL,Y2,2)	270.
C CALCULATE Y DERIVATIVES OF U,W,UV,VW: NAMELY UP,WP,UVP, AND VWP	271.
145 DO 148 I=2,NY	272.
ANGVLP(I)=DERIV(ANGVEL,Y2,I+1)	273.
UVP(I)=DERIV(UV,Y,I)	274.
VWP(I)=DERIV(VW,Y,I)	275.
148 QP(I)=DERIV(Q,Y,I)+2.5*UTAU/Y(I)	276.
DO 149 I=1,K	277.
149 Q(I)=Q(I)+UTAU*(2.5*ALOG(Y(I)*UTAU/NU)+5.)	278.
DO 150 I=1,NY	279.
UP(I)=QP(I)*COS(ANGVEL(I+1))-Q(I)*SIN(ANGVEL(I+1))*ANGVLP(I)	280.
WP(I)=QP(I)*SIN(ANGVEL(I+1))+Q(I)*COS(ANGVEL(I+1))*ANGVLP(I)	281.
150 CONTINUE	282.
C ESTIMATE NORMAL VELOCITY V AT FIRST MESH POINT	284.
V(1)=-COS(ANGVEL(2))*(405.*NU*UTAU/UTAU+298.*NU/R)	285.
1+SIN(ANGVEL(2))*DBETDX*296.5*NU	286.
CALL VCALC(NY,U,W,V,Y,R,DPDR,UVP,OMEGA)	287.
C FORCE PRINTOUT IF ORDINARY SEPARATION HAS OCCURED	288.
IF(ABS(ANGVEL(1)).GT.1.5703) PRNT=1	289.
IF(ITER.GT.1) GO TO 111	290.
IF(PRNT.NE.1) GO TO 111	291.
C****	292.
C CALCULATION OF INTEGRAL PARAMETERS	293.
C****	294.
C CALCULATE THE STREAMWISE AND CROSSFLOW COMPONENTS OF VELOCITY	295.
PSIO=ANGVEL(NY+1)	296.
BETA=ANGVEL(2)-ANGVEL(NY+1)	297.
BETAW=ANGVEL(1)	298.
COSS=COS(PSIO)	299.

SINS=SIN(PSIO)	300.
DO 50 I=1,K	301.
UVS(I)=UV(I)*COSS+VW(I)*SINS	302.
VWS(I)=-UV(I)*SINS+VW(I)*COSS	303.
US(I)=U(I)*CCSS+W(I)*SINS	304.
WS(I)=-U(I)*SINS+W(I)*COSS	305.
WU(I)=US(I)*WS(I)	306.
WW(I)=WS(I)**2	307.
UU(I)=US(I)**2	308.
50 CONTINUE	309.
C CALCULATE THE PARAMETERS	310.
KL=1	311.
DELTA=DXF(NY,US,Y,UTAU,KL,BETA,Q,NU)	312.
109 THETA=THXF(NY,UU,Y,UTAU,KL,BETA,DELTA,US,Q,NU)	313.
DELTAZ= DZF(NY,WS,Y,UTAU,KL,BETA,US,Q,NU)	314.
THETAZ= THZF(NY,WW,Y,UTAU,KL,BETA,US,Q,NU)	315.
THETZX= THZXF(NY,WU,Y,UTAU,KL,BETA,US,Q,NU)	316.
THETXZ=DELTAZ-THETZX	317.
H=DELTA/THETA	318.
C****	319.
C PRINTOUT RESULTS	320.
C****	321.
65 CALL SPRINT(US,WS,UVS,VWS,NY,DELTA,D995,DELTA,THETA,THETAZ,THETZX,THETXZ,H,BETA,XSTAT,R,IUNIT,V,Y,UTAU,PSIO,2,X,NU)	322.
IF(ABS(ANGVEL(1)).GT.1.5703) GO TO 1	323.
IF(X.GE.XL) GO TO 1	324.
66 PRNT=0	325.
111 CONTINUE	326.
C CALCULATE THE XSTEP	327.
IF(ITER.EQ.2) GO TO 61	328.
DX=XSTEP(NY,V,U,TAU,Y,TAUM,D995,ANGVEL(1))	329.
IF(TW/TAUM.LT..1) DX=DX/5.	330.
C MODIFY DX IF A DESIRED X PRINTOUT STATION OCCURS IN NEXT DX INTERVAL	331.
IF(IUNIT.EQ.0) GO TO 61	332.
DO 118 I=1,IUNIT	333.
IF(X+DX.LT.XPRINT(I)) GO TO 118	334.
DX=XPRINT(I)-X	335.
XPRINT(I)=2.*XL	336.
PRNT=1	337.
118 CONTINUE	338.
61 CONTINUE	339.
C CALCULATE X DERIVATIVES OF U,W,UV,VW: NAMELY DU,DW,DUV,DVW	340.
DO 200 I=1,NY	341.
DU(I)=DUF(I,DPDR,R,UP,V,UP,U,OMEGA)	342.
DW(I)=DWF(I,R,VWP,W,V,WP,U,OMEGA)	343.
DUV(I)=DUVF(I,D995,UV,UP,U,UP,GUV,V,Y,TAU,TAUM)	344.
DVW(I)=DVWF(I,D995,VW,VWP,U,WP,GVW,V,Y,TAU,TAUM)	345.
200 CONTINUE	346.
IF(ITER.EQ.2) GO TO 300	347.
DO 205 I=1,NY	348.
UN(I)=U(I)	349.
WN(I)=W(I)	350.
UVN(I)=UV(I)	351.
VWN(I)=VW(I)	352.
C ESTIMATE VALUES OF U,W,UV,VW AT MIDDLE OF DX INTERVAL	353.
U(I)=U(I)+DU(I)*DX/2.	354.
W(I)=W(I)+DW(I)*DX/2.	355.
Q(I)=SQRT(U(I)**2+W(I)**2)	356.
ANGVEL(I+1)=ATAN(W(I)/U(I))	357.
	358.
	359.

	UV(I)=UV(I)+DUV(I)*DX/2.	360.
205	VW(I)=VW(I)+DVW(I)*DX/2.	361.
	DO 204 I=1,2	362.
	U(NY+I)=U(NY)	363.
	Q(NY+I)=Q(NY)	364.
	ANGVEL(NY+I+1)=ANGVEL(NY+1)	365.
204	W(NY+I)=W(NY)	366.
	DPDR=DPDRF(X+DX/2.,UINF,DUINF,XF,LX)	367.
206	CONTINUE	368.
	C CALCULATE U,W,UV,VW, AT NEW XSTATION	369.
	C EXTRAPOLATE U,W,UV,VW TO X+DX	370.
300	DO 240 I=1,NY	371.
	UN(I)=UN(I)+DX*DU(I)	372.
	WN(I)=WN(I)+DX*DW(I)	373.
	QN(I)=SQRT(UN(I)**2+WN(I)**2)	374.
	ANGVLN(I+1)=ATAN(WN(I)/UN(I))	375.
	UVN(I)=UVN(I)+DX*DUV(I)	376.
	VWN(I)=VWN(I)+DX*DVW(I)	377.
240	CONTINUE	378.
	DPDR=DPDRF(X+DX,UINF,DUINF,XF,LX)	379.
	TAU1=SQRT(UVN(1)**2+VWN(1)**2)	380.
	UTAU=WSF(QN(1),Y(1),TAU1,UTAU,NU)	381.
	ANGVLN(1)=ANGVLN(2)-Y(1)*((ANGVLN(3)-ANGVLN(2))/(Y(2)-Y(1))	382.
	1+0.5*(Y(1)**2)*((ANGVLN(4)-ANGVLN(3))/(Y(3)-Y(2))-(ANGVLN(3)-	383.
	2ANGVLN(2))/(Y(2)-Y(1)))/(0.5*(Y(3)-Y(1)))	384.
	VCXN(1)=-UTAU**2*COS(ANGVLN(1))	385.
	VCYN(1)=-UTAU**2*SIN(ANGVLN(1))	386.
763	DO 460 I=1,2	387.
	UN(NY+I)=UN(NY)	388.
	WN(NY+I)=WN(NY)	389.
	QN(NY+I)=QN(NY)	390.
	ANGVLN(I+1+NY)=ANGVLN(NY+1)	391.
	UVN(NY+I)=0.0	392.
460	VWN(NY+I)=0.0	393.
	XSTAT=XSTAT+1	394.
	IF(X.GE.XL) PRNT=1	395.
	X=X+DX	396.
	R=R+DX	397.
	IF(C.LE.0.31) GO TO 600	398.
	C=0.3	399.
	GO TO 601	400.
600	C=0.45	401.
601	CONTINUE	402.
	GO TO 44	403.
	RETURN	404.
	END	405.
	FUNCTION DPDRF(X,UINF,DUINF,XF,LX)	406.
	C THIS SUBROUTINE COMPUTES -UINF*DUINF FROM INPUT VALUES	407.
	DIMENSION UINF( 50),DUINF( 50),XF( 50)	408.
	CALL INT(X,U,XF,UINF,LX,0,2)	409.
	CALL INT(X,CU,XF,DUINF,LX,0,2)	410.
	DPDRF=-U*DU	411.
	RETURN	412.
	END	413.
	SUBROUTINE SPRINT(US,WS,UVS,VWS,NY,DELTA,D995,DELTAX,THETAX,	414.
	C THIS SUBROUTINE PRINTS OUT RESULTS	415.
	1DELTAX,THETAZ,THETZX,THETXZ,H,BETA,XSTAT,R,IUNIT,V,Y,UTAU,PSIO	416.
	2,X,VISC)	417.
	DIMENSION US( 23),WS( 23),UVS( 23),VWS( 23),V( 23),Y( 23),YP( 43),	418.
1	UX( 43),WX( 43),VX( 43),UVX( 43),VWX( 43),YX( 43)	419.

```

RTHETA=THETAX*US(NY)/VISC 420.
INTEGER XSTAT 421.
CF=2.0*(UTAU/US(NY))**2 422.
PSIOP=PSIO*180./3.14159 423.
PSIOP=PSIO*180./3.14159 424.
BETAP=(BETA-PSIO)*180./3.14159 425.
WRITE(6,20) XSTAT,R,X 426.
20 FORMAT(20H1RESULTS AT XSTATION,14,9H WITH R =, F10.2,' X =',F10.4) 427.
WRITE(6,30) D995,DELTA,DELTAZ,THETAX,DELTAZ,THETAZ,THETZX,THETXZ, 428.
1H,BETAP,PSIOP,UTAU,US(NY),RTHETA,CF 429.
30 FORMAT(' D995 =',F10.6,' DELTA =',F10.6,' DELTAZ =',F10.6/ 430.
1' THETAX =',F10.6,' DELTAZ =',F10.6,' THETAZ =',F10.6/ 431.
2' THETZX =',F10.6,' THETXZ =',F10.6,' H =',F10.4/ 432.
3' BETA =',F10.3,' PSI =',F10.3,' UTAU =',F10.4 433.
4/' QINF =',F10.3,' RTHETA =',F10.2,' CF =',F10.5//) 434.
K=NY+2 435.
USQ=US(K)**2 436.
DO 40 I=1,NY 437.
YP(I)=Y(I)*UTAU/VISC 438.
YX(I)=Y(I)/D995 439.
VX(I)=V(I)/US(K) 440.
UVX(I)=UVS(I)/USQ 441.
VWX(I)=VWS(I)/USQ 442.
WX(I)=WS(I)/US(K) 443.
40 UX(I)=US(I)/US(K) 444.
WRITE(6,50) 445.
50 FORMAT(' Y/D995 U/QINF W/QINF V/QINF UV/QISQ VH/QISQ' 446.
1,' Y ',' Y+') 447.
WRITE(6,60)(YX(I),UX(I),WX(I),VX(I),UVX(I),VWX(I),Y(I),YP(I), 448.
1I=1,NY) 449.
60 FORMAT(7F9.5,F9.1) 450.
C COMPUTE MOMENTUM INTEGRAL BALANCE IN X DIRECTION 451.
C=COS(PSIO) 452.
S=SIN(PSIO) 453.
UINF=US(NY) 454.
IF(XSTAT.GT.1) GO TO 80 455.
S10=(UINF**2)*(-THETAX*C**2-2.*THETZX*C*S+THETAZ*S**2+DELTAZ*C*S) 456.
S20=(UINF**2)*(-THETAX*(C**2-S**2)-4.*THETZX*C*S+(S**2-C**2)* 457.
1THETAZ+DELTAZ*C*S+DELTAZ*S**2)/R 458.
ST2=0. 459.
ST3=0. 460.
RHS=0. 461.
X0=X 462.
S30=-UINF*C 463.
S40=UINF*(C*DELTAZ+S*DELTAZ) 464.
S50=-0.5*(UINF**2)*(CF*COS(BETA)) 465.
80 CONTINUE 466.
S1=(UINF**2)*(-THETAX*C**2-2.*THETZX*C*S+THETAZ*S**2+DELTAZ*C*S) 467.
S2=(UINF**2)*(-THETAX*(C**2-S**2)-4.*THETZX*C*S+(S**2-C**2)* 468.
1THETAZ+DELTAZ*C*S+DELTAZ*S**2)/R 469.
ST2=ST2+0.5*(S2+S20)*(X-X0) 470.
S3=-UINF*C 471.
S5=-0.5*(UINF**2)*(CF*COS(BETA)) 472.
S4=UINF*(C*DELTAZ+S*DELTAZ) 473.
ST3=ST3+0.5*(S4+S40)*(S3-S30) 474.
XLHS=(S1-S10)+ST2+ST3 475.
RHS=0.5*(S5+S50)*(X-X0) +RHS 476.
S20=S2 477.
S30=S3 478.
S40=S4 479.

```

```

S50=S5 480.
X0=X 481.
WRITE(6,90)XLHS,RHS 482.
90 FORMAT(' MOMENTUM INTEGRAL CHECK'/' LHS=',F14.3,' RHS=',E14.3) 483.
IF(H.GT.3.0) STOP 484.
RETURN 485.
END 486.
FUNCTION XSTEP(NY,V,U,TAU,Y,TAUM,D995,PSII) 487.
C THIS SUBROUTINE ESTIMATES X-STEP FROM CHARACTERISTICS 488.
DIMENSION V(23),U(23),TAU(23),Y(23) 489.
TANC=0.0 490.
DO 20 I=1,NY 491.
B=0.15*TAUM*GORD(Y(I)/D995)/U(NY) 492.
20 TANC=AMAX1(TANC,ABS((V(I)+B+(B**2+0.3*TAU(I))**0.5)/U(I))) 493.
XSTEP=AMIN1(Y(1),Y(2)-Y(1))*1./TANC 494.
RETURN 495.
END 496.
FUNCTION DZF(NY,WS,Y,UTAU,KL,BETA,US,Q,VISC) 497.
C THIS COMPUTES DELTA2 498.
DIMENSION WS(100),Y(100),US(100),Q(100) 499.
A=SIN(BETA)*(Y(KL)*(Q(KL)-2.5*UTAU)-33.5*VISC)/US(NY) 500.
B=AITEG(WS,Y,KL,NY)/US(NY+2) 501.
DZF=A+B 502.
RETURN 503.
END 504.
FUNCTION THZXF(NY,WU,Y,UTAU,KL,BETA,US,Q,VISC) 505.
C THIS COMPUTE THETA21 506.
DIMENSION WU(100),Y(100),US(100),Q(100) 507.
A=((UTAU*2.5*Y(KL)*(0.4*Q(KL)**2/UTAU-2.0*Q(KL)+2.0*UTAU*2.5)- 508.
1420.*UTAU*VISC)/Q(NY)**2)*(COS(BETA)*SIN(BETA)) 509.
B=AITEG(WU,Y,KL,NY)/US(NY+2)**2 510.
THZXF=A+B 511.
RETURN 512.
END 513.
FUNCTION THZF(NY,WW,Y,UTAU,KL,BETA,US,Q,VISC) 514.
C THIS COMPUTES THETA22 515.
DIMENSION WW(100),Y(100),US(100),Q(100) 516.
A=((UTAU*2.5*Y(KL)*(0.4*Q(KL)**2/UTAU-2.0*Q(KL)+2.0*UTAU*2.5)- 517.
1420.*UTAU*VISC)/Q(NY)**2)*(SIN(BETA))**2 518.
B=AITEG(WW,Y,KL,NY)/US(NY+2)**2 519.
THZF=A+B 520.
RETURN 521.
END 522.
FUNCTION WSF(U,Y,TAU1,UTAU,NU) 523.
C THIS COMPUTES QTAU,THE MAGNITUDE OF THE SHEAR VELOCITY 524.
REAL NU 525.
UTAUN=UTAU 526.
5 F=1.-(UTAUN**2/TAU1)**0.25 527.
R=U-2.5*(UTAUN*(ALOG(Y*UTAUN/NU)+2.))+2.0*(TAU1)**0.5*F) 528.
IF (ABS(R/U).LE.0.0001)GO TO 10 529.
DR=-2.5*(ALOG(Y*UTAUN/NU)+3. ) 530.
UTAUN=UTAUN-R/DR 531.
GO TO 5 532.
10 WSF=UTAUN 533.
RETURN 534.
END 535.
FUNCTION AITEG(Y,X,L,M) 536.
C THIS IS A UTILITY INTEGRATING ROUTINE 537.
DIMENSION Y(23),X(23) 538.
S=0.0 539.

```

```

      K=L+1
      Z=(Y(K)-Y(K-1))/(X(K)-X(K-1))
10    C=(Z+(Y(K)-Y(K+1))/(X(K+1)-X(K)))/(X(K-1)-X(K+1))
      B=Z-C*(X(K-1)+X(K))
      A=Y(K-1)-(B+C*X(K-1))*X(K-1)
      S=S+A*(X(K)-X(K-1))+0.5*B*(X(K)**2-X(K-1)**2)+C*(X(K)**3-X(K-1)**3
1) /3.0
      IF(K.EQ.M) GO TO 20
      K=K+1
      GO TO 10
20    AINTEG=S
      RETURN
      END
      FUNCTION DERIV(Y,X,I)
C THIS IS A UTILITY DIFFERENTIATING ROUTINE
      DIMENSION Y( 23),X( 23)
      Z=(Y(I)-Y(I-1))/(X(I)-X(I-1))
      C=(Z+(Y(I)-Y(I+1))/(X(I+1)-X(I)))/(X(I-1)-X(I+1))
      B=Z-C*(X(I-1)+X(I))
      DERIV=B+X(I)*2.0*C
      RETURN
      END
      SUBROUTINE SYNQP(H,THETA,QINF,NY,NU,Y,Q,UTAU,DELTA)
C THIS SUBROUTINE GENERATES THE STREAMWISE STARTING VELOCITY
C PROFILE USING THE LAW OF THE WALL-WAKE
      REAL Q( 23),Y( 23),NU
C USE CURVE FIT TO FIND COLES PI
      DELS=H*THETA
      A=-2./(1.-1.0/H)
      B=0.4*DELS*QINF/NU
      N=0
      PI=0.0
10    F=ALOG(B/(1.+PI))+2.0+2.0*PI+A*(1.+1.6*PI+0.761*PI**2)/(1.+PI)
      N=N+1
      IF(N.GE.100) STOP
      IF(F.LE.0.0001)GO TO 20
      DF=-1.0/(1.+PI)+2.+A*(1.6+2.*0.761*PI-(1.+1.6*PI+0.761*PI**2)/
1) (1.+PI))/(1.+PI)
      PI=PI-0.8*F/DF
      GO TO 10
20    CONTINUE
      UTAU=0.4*(1.-1./H)*(1.+PI)*QINF/(2.*(1.+1.6*PI+0.761*PI**2))
      DELTA=0.4*DELS*QINF/((1.+PI)*UTAU)
      K=NY+2
      YN=NY
      DO 50 I=1,K
      Y(I)=DELTA*(0.25*FLOAT(I)/YN+0.75*(FLOAT(I)/YN)**2)
      Q(I)=QINF +UTAU*(2.5*ALOG(Y(I)/DELTA)-2.5*PI*(1.0+COS(3.1415*Y(I)
1) /DELTA)))
50    CONTINUE
      DO 55 I=1,2
55    Q(K-2+I)=Q(NY)
      WRITE (6,80) (Y(I),Q(I),I=1,K)
80    FORMAT(20X,'SYNTHETIC VELOCITY PROFILE'/23X,' Y ', ' Q '
1) /(20X,F10.5,F10.2))
      WRITE(6,81) PI
81    FORMAT(25X,'COLES PI=',F10.3)
      RETURN
      END
      FUNCTION DUF(I,DPDR,R,UVP,W,V,UP,U,OMEGA)

```

```

C THIS EVALUATES DU/DX FROM X-MOMENTUM
  DIMENSION UVP(23 ),W(23 ),V( 23 ),UP( 23 ),U( 23 )
  DUF=(-DPDR-UVPI)+W(I)**2/R-V(I)*UP(I)+2.*OMEGA*W(I)+R*OMEGA**2)
  1/U(I)
  RETURN
  END
  FUNCTION DWF(I,R,VWP,W,V,WP,U,OMEGA)
C THIS EVALUATES DW/DX FROM Z MOMENTUM
  DIMENSION VWP(23 ),W(23 ),V(23 ),WP(23 ),U(23 )
  DWF=(-U(I)*W(I)/R-V(I)*WP(I)-VWP(I)-2.*OMEGA*U(I))/U(I)
  RETURN
  END
  SUBROUTINE VCALC(NY,U,W,V,Y,R,DPDR,UPV,OMEGA)
C CALCULATES THE NORMAL VELOCITY V EXCEPT FOR V(1)
  DIMENSION U( 23 ),W( 23 ),V( 23 ),Y( 23 ),UPV( 23 ),XIG( 43 )
  K=NY+2
  DO 50 I=1,NY
    XIG(I)=0.0
    XIG(I)=(UPV(I)+DPDR-(U(I)**2+W(I)**2)/R-2.*OMEGA*W(I)-R*OMEGA**2)
    1/U(I)**2
  50 CONTINUE
    XIG(NY+1)=XIG(NY)
    DO 100 I=2,NY
      V(I)= U(I)*AINTG(XIG,Y,I-1,I)+V(I-1)*U(I)/U(I-1)
  100 CONTINUE
    RETURN
    END
    FUNCTION DXF(NY,US,Y,UTAU,KL,BETA,Q,VISC)
C CALCULATES DELTA 1
  DIMENSION US( 23 ),Y( 23 ),Q( 23 )
  UT=UTAU*SQRT(COS(BETA))
  A= (Y(KL)*(US(KL)-2.5*UT )-33.5*VISC)/US(NY)
  B=AINTG(US,Y,KL,NY)/US(NY+2)
  DXF=Y(NY)-(A+B)
  RETURN
  END
  FUNCTION THXF(NY,UU,Y,UTAU,KL,BETA,DELTAX,US,Q,VISC)
C CALCULATES THETA11
  DIMENSION UU( 23 ),Y( 23 ),Q( 23 ),US( 23 )
  A=((UTAU*2.5*Y(KL)*(0.4*Q(KL)**2/UTAU-2.0*Q(KL)+2.0*UTAU*2.5)-
  1420.*UTAU*VISC)/UU(NY+2))*(COS(BETA))**2
  B=AINTG(UU,Y,KL,NY) /US(NY+2)**2
  THXF=Y(NY)-DELTAX-(A+B)
  RETURN
  END
  SUBROUTINE INT(XV,YV,X,Y,M,N,L)
C A UTILITY INTERPOLATION ROUTINE
  DIMENSION X( 23 ),Y( 23 )
  K=N
  IF(XV.GT.X(2))GO TO 40
  YV=Y(1) +(Y(2)-Y(1))*(XV-X(1))/(X(2)-X(1))
  GO TO 100
  40 IF(XV.GE.X(M-1)) GO TO 59
  IF(K.NE.0) GO TO 55
  DO 50 I=1,M
    K=I-1
    IF(X(I).GT.XV) GO TO 55
  50 CONTINUE
  55 CONTINUE
    IF(K.LT.M-4) GO TO 57

```

	K=K+1	660.
	GO TO 60	661.
57	YV=0.0	662.
	DO 58 I=1,L	663.
	Z=(Y(K)-Y(K-1))/(X(K)-X(K-1))	664.
	C=(Z+(Y(K)-Y(K+1))/(X(K+1)-X(K)))/(X(K-1)-X(K+1))	665.
	B=Z-C*(X(K-1)+X(K))	666.
	A=Y(K-1)-(B+C*X(K-1))*X(K-1)	667.
	K=K+1	668.
58	YV=(A+(B+C*XV)*XV)/FLOAT(L)+YV	669.
	GO TO 100	670.
59	K=M	671.
60	YV=Y(K-1) +(Y(K)-Y(K-1))*(XV-X(K-1))/(X(K)-X(K-1))	672.
100	CONTINUE	673.
	RETURN	674.
	END	675.
	FUNCTION RLORD(Z)	676.
C CALCULATES BRADSHAW'S L		677.
	RLORD=.4*Z	678.
	IF(Z-.18)1103,1104,1104	679.
1104	IF(Z-1.1)1105,1106,1106	680.
1105	RLORD=.095-.055*(2.*Z-1.)*2	681.
	GO TO 1103	682.
1106	RLORD=.016*EXP(-10.*(Z-1.1))	683.
1103	RETURN	684.
	END	685.
	FUNCTION GORD(Z)	686.
C CALCULATES BRADSHAW'S G(NORMALIZED)		687.
	IF(Z-.63)1107,1108,1108	688.
1107	GORD=17.5*Z**1.86	689.
	GO TO 1109	690.
1108	IF(Z-.89)1110,1111,1111	691.
1110	GORD=90.9*Z-49.75	692.
	GO TO 1109	693.
1111	GORD=18.7*Z+14.85	694.
1109	RETURN	695.
	END	696.
	FUNCTION DUVE(I,D995,UV,UVP,U,UP,GUV,V,Y,TAU,TAUM)	697.
C CALCULATES -DTAU/DX FROM X SHEAR STRESS EQUATION		698.
	DIMENSION U( 23),UP( 23),UV( 23),UVP( 23),V( 23),GUV( 23),TAU( 23)	699.
	1,Y( 23)	700.
	IF(I.EQ.1) GO TO 2	701.
	GUV=DERIV(GUV,Y,I)	702.
	GO TO 3	703.
2	GUV=(GUV(I+1)-GUV(I))/(Y(I+1)-Y(I))	704.
3	DUVE=(-V(I)*UVP(I)+0.3*(-TAU(I)*UP(I)-UV(I)*SQRT(TAU(I))	705.
	1/(RLORD(Y(I)/D995)*D995)-SQRT(TAUM) *GUV))/U(I)	706.
	RETURN	707.
	END	708.
	FUNCTION DVWF(I,D995,VW,VWP,U,WP,GVW,V,Y,TAU,TAUM)	709.
C CALCULATES DTAU/DX FROM Z SHEAR STRESS EQUATION		710.
	DIMENSION U( 23),WP( 23),VW( 23),VWP( 23),V( 23),GVW( 23),TAU( 23)	711.
	1,Y( 23)	712.
	IF(I.EQ.1) GO TO 2	713.
	GVW=DERIV(GVW,Y,I)	714.
	GO TO 3	715.
2	GVW=(GVW(I+1)-GVW(I))/(Y(I+1)-Y(I))	716.
3	DVWF=(-V(I)*VWP(I)+0.3*(-TAU(I)*WP(I)-VW(I)*SQRT(TAU(I))	717.
	1/(PLORD(Y(I)/D995)*D995)-SQRT(TAUM) *GVW))/U(I)	718.
	RETURN	719.

```

END 720.
SUBROUTINE MAXSHR(NY,UV,VW,TAU,TAUM) 721.
C CALCULATES MAXIMUM TAU AND TAU FROM TAUZ AND TAUZ 722.
DIMENSION UV( 23),VW( 23),TAU( 23) 723.
TAUM=0.0 724.
DO 10 I=1,NY 725.
TAU(I)=SQRT(UV(I)**2+VW(I)**2) 726.
TAUM=AMAX1(TAUM,TAU(I)) 727.
10 CONTINUE 728.
RETURN 729.
END 730.
SUBROUTINE GFCALC(UV,VW,QINF,K,Y,D995,GUV,GVW,TAUM) 731.
C CALCULATES G*TAUX AND G*TAUZ 732.
DIMENSION UV( 23),VW( 23),Y( 23),GUV( 23),GVW( 23) 733.
DO 130 I=1,K 734.
GUV(I)=GORD(Y(I)/D995)*(TAUM)**0.5/QINF 735.
GVW(I)=GUV(I)*VW(I) 736.
GUV(I)=GUV(I)*UV(I) 737.
130 CONTINUE 738.
RETURN 739.
END 740.
FUNCTION UWAKE(Y,UTAU,PI,D995,NU) 741.
C CALCULATES VELOCITY ACCORDING TO COLES LAW OF WALL-WAKE 742.
REAL NU 743.
Y1=Y 744.
IF(Y1.GT.D995)Y1=D995 745.
UWAKE=UTAU*(2.5*ALOG(Y1*UTAU/NU)+5.+2.5*PI*(1.-COS(3.1416*Y1/D995) 746.
1)) 747.
RETURN 748.
END 749.
$DATA 750.
GARDGW B-50.6 VANELESS DIFFUSER 751.
.18 1.01 40.5 1.5 .004218 1.77 .00017 752.
1.585 49.6 0. 16.1 .0304 .425 753.
-.005 .1 00012 754.
44. 42.2 40.3 38.4 36.7 35.2 33.9 755.
32.7 31.9 31.2 30.8 30.7 756.
-17.6 -18.04 -18.81 -18.5 -15.4 -14.23 -11.92 757.
-10. -7.27 -5.21 -1.93 -.434 758.
1503010502 759.
.1303 .36 .53 .71 .85 1.01 760.
$STOP 761.
/* 762.

```

## APPENDIX B

### METHODS FOR ESTIMATING THE WALL SHEAR STRESS DIRECTION

As mentioned in chapter 2, it is generally more accurate to extrapolate the velocity direction to the wall rather than the shear stress direction. Hence, most of the methods investigated are of the velocity extrapolation type.

It is rather difficult to make a direct evaluation of the empirical functions used to extrapolate the wall shear stress direction because very few of the experimental velocity profiles which are available are accurate in the region close to the wall. Hence, the wall conditions are evaluated by such criteria as reliability, ease of application and effect on overall predictions of the mean velocity field.

#### Method 1

This method simply approximates the wall shear stress direction as being the same as the velocity direction at the first mesh point. As Figure B.1 indicates, this can significantly underestimate the wall shear stress angle. On Figure B.1, the solid dots represent the approximate locations of the first three computational mesh points.

#### Method 2

In this method,  $\beta_w$  is obtained by linear extrapolation of the velocity angle from the first two computed mesh points. In the data shown in Figure B.1, this method appears to work quite well. In some data sets, a curvature exists in the  $\beta$  versus  $y$  curve and it was felt that Method 2 might in some cases cause errors. Hence, other methods were tried.

### Method 3

Method 3 is based on a suggestion of Nash (personal communication) in which it is proposed to fit a cubic of the form

$$W = A + BU + CU^2 + DU^3 \quad (B.1)$$

to the computed values of  $U$  and  $W$  at the wall and the first two mesh points. The fourth condition required to evaluate the constants is:

$$\frac{\partial^2 W}{\partial U^2} = \frac{-v \sin \gamma_w \frac{dP}{dx}}{\tau_w \cos^3 \gamma_w} \quad (B.2)$$

This expression is derived from the momentum equations Equation 1.9 and 1.10 when the limit as  $y$  approaches zero is taken. This expression indicates that in any situation with a pressure gradient, if there is any skewing, the polar plot of  $W$  versus  $U$  is curved next to the wall. Cham (1968) also concluded this.

The wall shear stress direction is found by differentiating Equation B.1 and evaluating it at  $U = 0$ .

$$\left( \frac{\partial W}{\partial U} \right)_{\text{wall}} = \tan \gamma_w$$

Method 3 did not work well - in fact in some cases no suitable cubic could be found. This is because the requirement imposed by Equation B.2 is too severe for a simple cubic to satisfy if the cubic also satisfies the requirements at the first two mesh points. This method was dropped from further consideration.

### Method 4

In this method, which is what Nash actually suggested, the cubic is fitted to the polar plot ( $W_s$  vs  $U_s$ ) rather than to  $U$  and  $W$  directly. This method is more difficult to apply but is not expected to function significantly differently from Method 3.

### Method 5

Method 5 assumes that a parabola can be fitted to the tangent of the velocity angle  $\gamma$  at the first two mesh points.

$$\tan\gamma = A + B\gamma + C\gamma^2 \quad (\text{B.3})$$

Equation B.2 is also used to evaluate the constants. This method appeared to have similar problems to Method 3. The difficulty with Methods 3, 4, and 5 all seem to be related to the fact that in real flows,  $\partial^2 w / \partial U^2$  changes very rapidly near the wall, and this variation cannot be represented by the simple functions tried here. This difficulty is illustrated in Figure B.2.

### Method 6

Method 6 is based on the two-dimensional method of Bradshaw. The  $x$  component is obtained from:

$$\tau_{x_{\text{wall}}} = \tau_{x_1} + 0.5 \frac{dp}{dx} \quad (\text{B.4})$$

This expression is an approximation of the  $x$  momentum equation. The factor 0.5 is used to compensate for the convective terms. The wall shear stress magnitude is computed as discussed in Chapter 2. The direction of the wall shear stress is thus computed from

$$\cos\gamma_w = \tau_{x_{\text{wall}}} / \tau_{\text{wall}} \quad (\text{B.5})$$

The results of this method were similar to those of Method 2, however in some cases, at low momentum thickness Reynolds numbers, where the distance between the wall and the first mesh point is as great as 0.18995, some oscillations in the computed wall shear stress direction appeared. Method 2 was considered to be preferable.

### Method 7

This method is an attempt to improve on Method 6 by approximating the convective terms directly. Using the continuity equation (Equation 1.8) and the momentum equations (Equations 1.9 and 1.10) the following expressions can be obtained.

$$\frac{\partial U^2}{\partial x} + \frac{\partial UV}{\partial y} = - \frac{dP}{dx} + \frac{\partial \tau_x}{\partial y} \quad (B.6)$$

$$\frac{\partial UW}{\partial x} + \frac{\partial VW}{\partial y} = \frac{\partial \tau_z}{\partial y} \quad (B.7)$$

Rearranging and integrating from the wall to the first mesh point, one obtains

$$\tau_x - \tau_{x_w} = U_1 V_1 + y_1 \frac{dP}{dx} + \int_0^{y_1} \frac{\partial U^2}{\partial x} dy \quad (B.8)$$

$$\tau_z - \tau_{z_w} = W_1 V_1 + \int_0^{y_1} \frac{\partial UW}{\partial x} dy \quad (B.9)$$

Thus  $\tau_{x_w}$  and  $\tau_{z_w}$  can be found if the definite integrals can be evaluated. However,  $V_1$  is not known accurately (in fact, when this method was actually tried, the approximation for  $V_1$  was not as good as is described in Chapter 2). Furthermore, the definite integrals could only be evaluated by assuming a functional form for the velocity profiles. This is in fact what Bradshaw did for Method 6 and it is not felt that Method 7 would offer any obvious advantage over Method 6. Method 7 is, however, more difficult to apply.

### Method 8

This is the method which is actually described in Chapter 2. Method 8 is a slight variation of Method 2. If the  $\beta$  versus  $y$  curve has a curvature in the region of the first three mesh points, this curvature

is continued in the curve which extrapolates the velocity direction to the wall. In some cases this method should be a better approximation than Method 2.

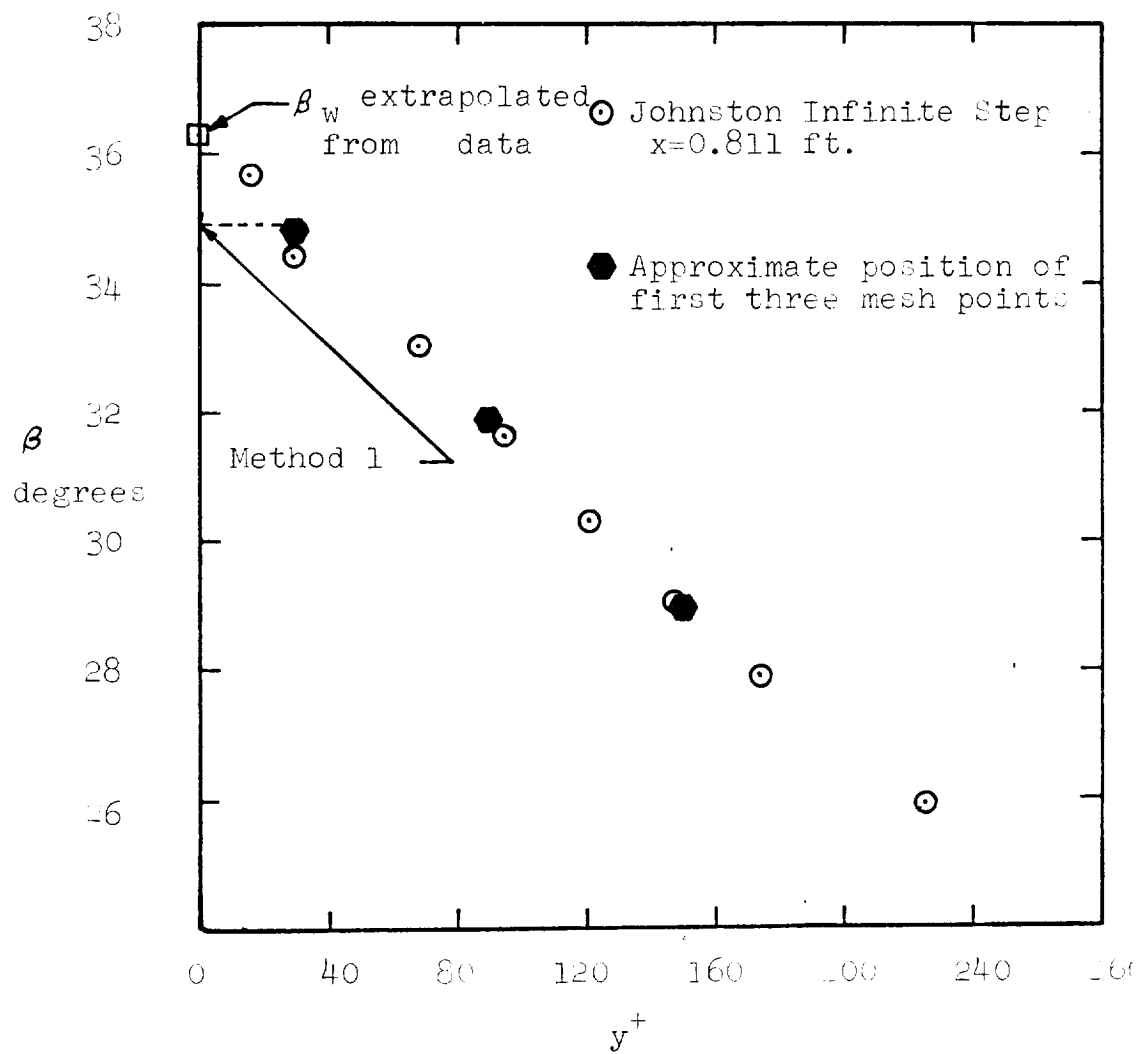


Figure B.1 Extrapolation of  $\beta_w$

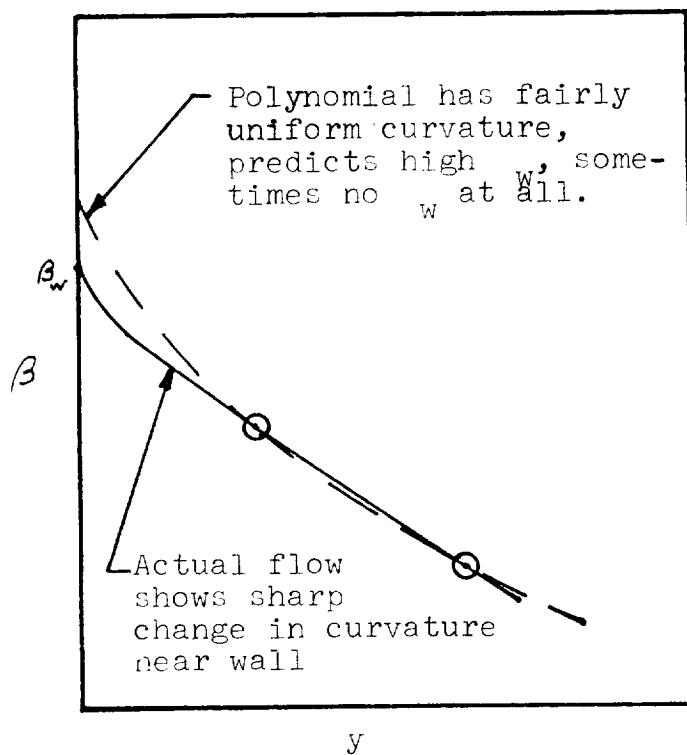


Figure B.2  $\beta$  vs.  $y$  Near Wall

## APPENDIX C

### ATTEMPTS TO COMPUTE ROTATING DISC FLOWS

In the present research program, an unsuccessful attempt was made to predict the rotating disc flows of Cham. In his rotating disc experiments, a simple circular disc was rotated about its axis in free air (see Figure 1.2(e)). Since the no slip boundary condition holds at the surface of the disc, the fluid close to the disc is forced to rotate. This effect in turn generates centrifugal forces within the rotating fluid which tend to drive the flow radially outward. In our attempt at prediction, a coordinate system fixed to the surface of the disc was used and thus Coriolis acceleration terms were included in the momentum equations. The  $x$  direction was oriented in the radial direction, but because  $U$ , which is a divisor in the momentum and shear stress equations in the form of Equation 3.2, is always zero in the free stream, difficulties were encountered. Division by  $U$  is a consequence of the explicit method used. It need not occur in an implicit forward differencing method and Cooper (1971) successfully computed the rotating disc flows of Cham using a modification implicit eddy viscosity method of Cebeci and Smith (Kline et. al. 1969). To circumvent the problem, in our work an artificial radial flow of  $U \neq 0$  was superimposed on the free-stream and an attempt was made to establish the limit as this radial flow was reduced to zero. Unfortunately, when the imposed radial flow became small, the number of  $x$ -steps became immense (on the order of 1000) and various numerical inaccuracies accumulated and destroyed the predictions. It was then realized that this class of flows could not be properly treated with our present numerical technique and further efforts were abandoned for the time being.

## APPENDIX D

### SUGGESTED IMPROVEMENTS IN THE COMPUTER PROGRAM

Although the numerical method used in the present study works reasonably well and is considered to be adequate for the situations considered, a number of desirable improvements are now evident.

a. Difficulties arise from Equation 3.10, the function which distributes the mesh points in the  $y$  direction. The first problem concerns the constant  $C$  which fixes the first mesh point at a  $y^+$  of 30. As discussed in Chapter 4, at low Reynolds numbers, it was felt desirable to keep the first point at this value of  $y^+$  and take the consequent limitations in accuracy. At high Reynolds numbers, this restriction is not needed. At momentum Reynolds numbers higher than about 20,000, the first mesh point will be much closer to the wall than the first mesh point is to the second mesh point. This is undesirable from the standpoint of differentiating and interpolating on the computed profiles. Furthermore, it causes a small  $x$ -step (see Equation 3.12) which increases computer time and at the same time increases errors due to roundoff, truncation and interpolation. Thus it is recommended that the  $y^+$  at the first mesh point be allowed to increase with Reynolds number such that the first mesh point is about the same distance from the wall as the second mesh point is from the first. It should be pointed out that Equation 2.36 will have to be reworked so that  $V_1$  is a function of  $y^+$ .

The second problem concerns the two alternate  $y$ -grids used. Due to the fact that the value of  $y$  at the first mesh point changes very little at alternate  $x$ -stations, it turns out that the grids computed by Equation 3.10 with two different values of  $\phi$  are often not very

different and the advantage of interpolation is lost. This can increase the chance of instabilities. On the other hand, Equation 3.10 will always produce alternate grids which are essentially the same in the outer part of the flow. This is desirable since interpolation has been found unnecessary in this region and interpolation errors can effect the location of  $\delta_{995}$  and result in surprisingly large effects on the calculations. (This was discovered when an alternate grid was used which was exactly interspaced between the previous grid.) Thus, it is recommended that a function be developed which will distribute the points on two alternate grids and will produce a considerable change in distribution of points in the inner part of the turbulent region and very little in the outer part regardless of the location of the first mesh point.

b. As mentioned above, the value of  $\delta_{995}$  is very sensitive to interpolation errors in the outer part of the flow. In the part of the flow around  $y = \delta_{995}$ ,  $\partial U / \partial y$  is small and consequently  $\partial y / \partial U$  is very large. This sensitivity of  $\delta_{995}$  produces a rather large change in the calculations when a small number of mesh points (10 for example) are used with the Nash and Bradshaw methods. In the Nash and Bradshaw methods  $\delta_{995}$  is a parameter in the calculation of the shear stress in the outer part of the flow. It is recommended that the dissipation length and diffusion functions be normalized on an integral property of the boundary layer (like  $\theta_{11}$  or  $\delta_1$ ) to avoid this problem.